Creep of natural rubber vulcanizates.

Wilcock, A. D.

Award date:
1975

Awarding institution:
University of Bath

CREEP OF NATURAL RUBBER VULCANIZATES

Submitted by A. D. Wilcock

for the degree of Ph.D.

of the University of Bath

1975

A. D. Wilcock.

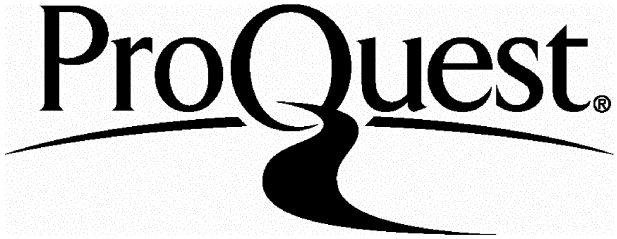

ABSTRACT

A study of creep at temperatures within the rubbery plateau region is presented. Creep and stress-relaxation are reviewed and such relevant factors as crystallisation and surface cracking during creep are considered. Creep is determined by both physical (viscoelastic) and chemical mechanisms. "Physical creep" is manifested by semi-logarithmic, creep $\propto$ log (time), or log-log kinetics whereas "chemical creep" follows a generally linear law, creep $\propto$ time. These relationships are examined in terms of their relevance to data extrapolation beyond the experimental time scale.

The semi-logarithmic relationship implies that the apparent activation energy for creep increases in proportion to creep strain and a tentative explanation of why this may be so is suggested. It is considered that such creep kinetics may be attributed to the slow breakdown and re-organisation of regions of short range order in the rubber. This activation energy approach is used to interelate creep data with tensile stress-strain data at different strain rates.

The physical creep of carbon black filled vulcanizates did not follow semi-logarithmic kinetics except at short times, $<10,000$ minutes, and the rates exceeded that of their gum equivalent by a factor of ~ 2. It is suggested that this arises from instability of reinforcement and the phenomenon is discussed with reference to stress-softening and scragging. Various techniques,

including dilatometry and electron microscopy showed that carbon black/matrix debonding did not occur even after 60,000 minutes under load.

The observed activation energy, ~ 129 KJ mol^{-1}, for the "chemical creep" of conventional sulphur cured vulcanizates, gum and reinforced, is discussed in terms of possible mechanistic processes particularly oxidation and sulphur diffusion. A model for the diffusion of oxygen into rubber is presented which suggests a maximum penetration depth of 2 to 10 mm at 20°C. This penetration depth decreases with increasing temperature.

Acknowledgements

I would like to express my gratitude to Professor C. R. Tottle of Bath University for useful discussion and advice, to Mr. R. Dove of Avon Rubber Co. Ltd. for his help in sample preparation and to Mr. D. V. Badami and Dr. M. A. Hepworth of TBA Industrial Products Ltd. for providing typing facilities.

CONTENTS

SYMBOLS

a_T	Logarithmic time shift factor
a	Accelerator concentration
a & A	Constants
b & B	Constants
B	Permeability coefficient
c	Logarithmic creep rate
C_w	% wt concentration
C	Constant
	Concentration
d	Constant
D	Diffusion coefficient
E	Modulus
h	Half thickness of a rubber sheet
h_1, h_2, h_3	Critical depths of oxygen penetration into rubber
H_f	Enthalpy of formation
k	Boltzmans constant
K, K_1, K_2	Decay constants
K_v	Rate of reaction of oxygen with rubber; vol O_2/unit time/unit volume of rubber.
K_3	Rate of reformation of broken chains
K^1	Chemical creep rate
l_c	Average length of a network chain
L	Specimen length
M	Constant
n	Network chain density
n_s	Number of sulphur atoms per crosslink
N	Crosslink concentration
N_R	Free radical concentration due to broken crosslinks
P	Gas partial pressure
Q	Activation Energy
R	Gas constant
R.H.	Relative humidity
s	Logarithmic stress-relaxation rate

t	Time
T	Temperature
v	Volume of gas
V	Volume fraction
w	Mass of a network chain
X	Crosslink concentration
x	Distance
α, β	Constants
γ	Activation volume or domain volume
Δ	Deviation of chemical creep from a linear relationship with time
ε	Strain
ε_1, ε_t	Strain at 1 and t minutes under load
ε_c	Creep strain, i.e. $\varepsilon - \varepsilon_1$
ε_g	Average strain in the gum phase of filled vulcanizate
θ	Angle
λ	Elongation ratio
ν	Concentration of domains
ρ	Density of rubber
σ	Stress
τ	Time or relaxation time

CHAPTER 1

INTRODUCTION

1.1 Commercial Considerations

The use of rubber components for load bearing applications has enjoyed increasing prominence in recent years. This is exemplified by the advent of transverse engined motor cars utilizing rubber cone, hydrolastic and pneumatic suspension systems and by the increasing use of rubber mountings, supports and bearings in the sphere of civil engineering. It is not surprising therefore, that much attention has been devoted to those engineering factors which influence the service life of such components. Particular interest has centred on stress analysis, on heat build up during cyclic loading, on fatigue and environmental factors such as ozone cracking and more recently on creep and stress-relaxation. Indeed, A. E. Moulton[1], inventor of a number of rubber based suspension systems, has pointed out that creep resistance is a major limiting factor in the design of rubber components which are subjected to continuous applied stress. This investigation was instigated by Avon Rubber Company Limited of Melksham, Wiltshire, who are interested in obtaining an awareness of the creep limitations of rubber components in service. In particular, at the time this research was started they hoped to start manufacturing bridge bearings, design considerations

for which would include limited vertical creep. Avon themselves have measured creep rates at various temperatures for certain specific rubber mixes which could be used for this application. Meanwhile this report discusses results obtained for simple mix recipe's in order to elucidate the mechanisms of creep deformation.

Despite the development of synthetic elastomers natural rubber has retained a position of prime commercial importance because of its properties, availability and price. In particular it has good strength, creep resistance and low hysterisis which make it suitable for many engineering applications. Of the synthetic polymers styrene butadiene, cis-polyisoprene and polybutadiene rubbers are used in large quantities. Although the cheapest, styrene butadiene rubber has poor creep resistance and high hysterisis and is unsuitable for components requiring dimensional stability under load or low dynamic heating. Cis-polyisoprene is often regarded to be inferior to natural rubber in terms of strength and tear resistance. This leaves polybutadiene rubber as the main competitor to natural rubber for stressed applications but as yet the latter is favoured, particularly in Britain. The work to be presented in this thesis has been devoted to natural rubber with this in mind. Lack of consistency between individual batches of natural rubber has been minimized by using standard Malaysian grade SMR5CV.

1.2 The Creep Problem

Present industrial creep design practice is based

on short duration tests with extrapolation to long times. It is important, therefore, in the first instance to establish the validity of the extrapolation procedures. Much short term stress-relaxation work has been published from the 1940's onwards and some creep work from the 1960's onwards and this will be described later. There has however been only limited discussion regarding the shape of creep curves, creep = function (time).

For commercial reasons the rubber industry is somewhat secretive about mix formulations but it is generally accepted that conventional sulphur plus accelerator cures are by far the most widely used. Mix additions of carbon black, non-reinforcing fillers, processing oils and of cheapening polymer such as styrene butadiene rubber are the rule rather than the exception. Clearly, therefore, creep resistance depends on the extent and type of these additions and this is important in regard to product profitability. Nevertheless these factors are poorly understood and a more comprehensive appraisal would be useful in the development of mix practice. The simplification that rubbers remain fixed in character throughout the duration of a creep experiment is usually implicit in the analyses of results so far published. In fact loss of volatiles, internal and physical changes and a continuation of the vulcanization/reversion process may have an influence, which if significant, would add complexity to data extrapolation procedures. Finally little is known about the effect of cycling stress,

temperature and humidity although Gent[19] has suggested that stress cycling has an easily predictable influence. Figure 1.1 sums up the factors affecting creep.

1.3 Vulcanization

The most widely used vulcanization procedures are elaborations of the original method of heating rubber with sulphur discovered by Goodyear in 1839. Despite extensive research sulphur based vulcanizates still have the best balance of physical and chemical properties.[2] The process involves heating a mechanically plastized mix of rubber, sulphur, curing agents and other ingredients. Elemental sulphur can be replaced by organic sulphur donating agents such as the thiurams or alternatively non sulphur vulcanizates can be prepared using organic peroxides or radiation to promote crosslinking.

The type of crosslink formed and the cleanliness of the system are known to have a great influence on creep. Polysulphide crosslinks are produced by conventional sulphur plus accelerator cures; the average bond length diminishes as vulcanization proceeds[3]. Monosulphidic crosslinking is achieved using sulphur donating agents with no elemental sulphur whilst carbon crosslinks are produced from peroxide cures. Figure 1.2 indicates the relative stability of these crosslinks.

Vulcanization is usually carried out at 140°C to 200°C until optimum crosslinking, strength and stiffness are achieved. During the process both cross-

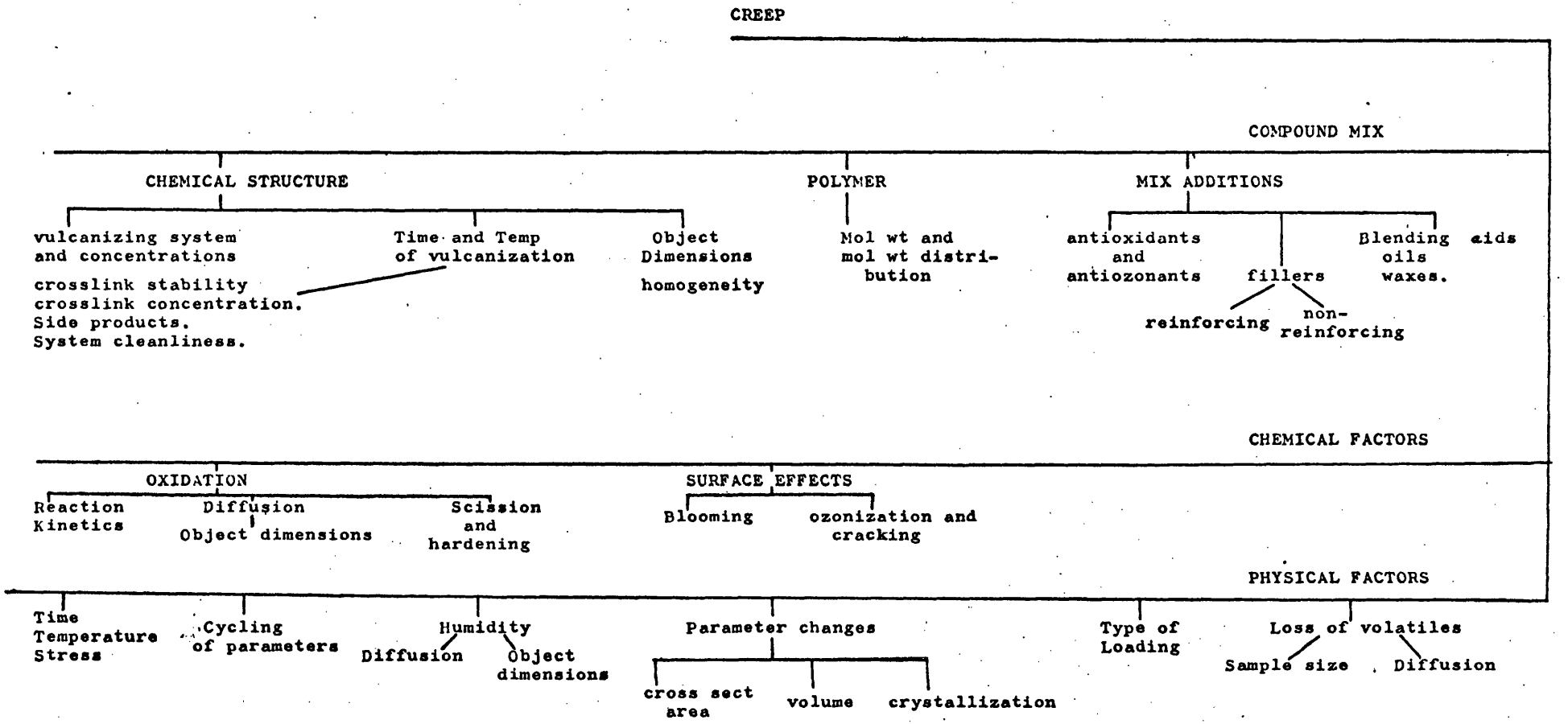

Figure 1.1 Factors affecting creep

C - C (C - C link. $E_f \sim$ 350 KJ mol^{-1})

C - S - C (monosulphide link. $E_f \sim$ 285 KJ mol^{-1})

C - S - S - C (Disulphide link. $E_f \sim$ 270 KJ mol^{-1})

C - S - S_x - S - C (Polysulphide link. $E_f <$ 270 KJ mol^{-1})

Figure 1.2 Types of crosslink in order of stability and their energies of formation. See Reference 2.

linking and thermal crosslink breakdown occur, the former being dominant initially when the curing agent concentrations are highest. The softening which occurs once optimum cure is passed is known as reversion and clearly this must influence creep response at elevated temperatures.

1.4 The Statistical Theory of Rubber-elasticity

This fundamental theory forms the basis of the understanding of secondary creep and stress relaxation and is a necessary precursor to their discussion. Extensive reviews are available,[4-7]. Fixed crosslinks introduced into a rubber during vulcanization prevent long range relative translations of adjacent molecules. A pertubation of the macro-network by external stress alters the distribution of inter-crosslink distances and consequently the freedom of individual network chains to adopt different configurations. This may be interpreted in terms of a reduction of entropy for the system which can be computed statistically. Thermodynamic considerations permit the calculation of external stress directly from the rate of change of entropy with strain since the internal energy of rubbery networks is approximately independent of strain. For simple uniaxial tension this leads to:-

$$\sigma = nkT\ (\lambda - \lambda^{-2}) \qquad 1.1$$

σ = stress

n = no. of network chains per unit volume

k = Boltemans constant

T = Temperature

λ = Elongation ratio

i.e. sample length/original length.

In practice this is an acceptable approximation to real behaviour at moderate strains and this is illustrated in Figure 1.3 which shows data for vulcanizate 'A' (see Chapter 2) at various temperatures.

The Mooney-Rivlin equation[7-9] is a better approximation for the rubber stress-strain curve but is less convenient in analytical situations. This suggests:

$$\sigma = 2 (C_1 + C_2 \lambda^{-1}) (\lambda - \lambda^{-2}) \quad - 1.2$$

C_1 is analogous to 'nkT' of equation 1.1. The interpretation of C_2 is at present subject to debate.

1.5 The Stress-Relaxation Technique

In a stress relaxation experiment a tensile sample is extended to a predetermined strain and the stress monitored over a period of time. Much of the original work in this field is due to A. V. Tobolsky and co-workers; Figure 1.4 shows a typical family of relaxation curves obtained by them for a gum vulcanizate over a range of temperatures at 50% strain[10]. Equation 1.1 suggests that stress and temperature are proportional, other things being equal, and so for comparison the stress levels for each temperature have been 'reduced', in this case to 25°C. This involves multiplying actual stresses by a factor T_o/T where T_o is some arbitrary selected temperature. Figure 1.5 is a cross plot taken

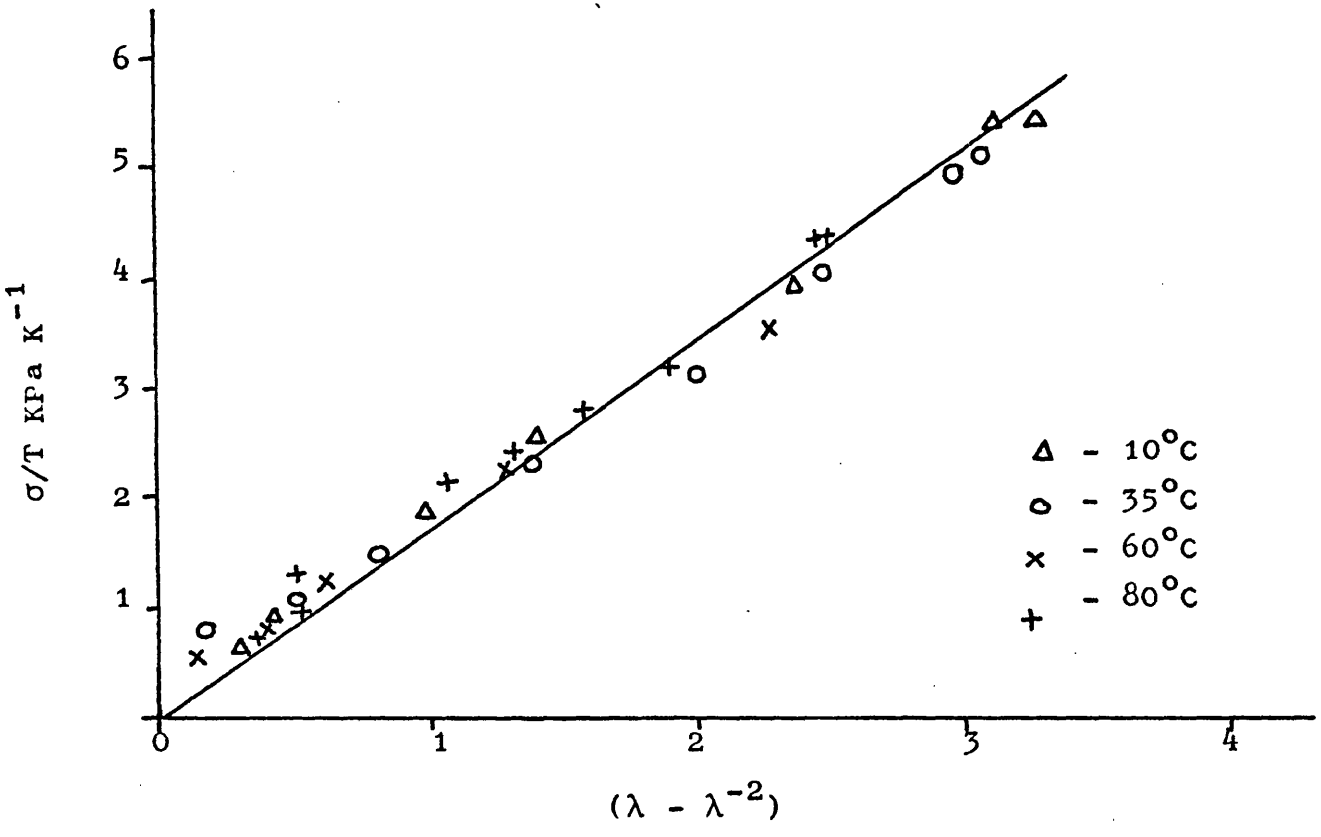

Figure 1.3 Tensile data for vulcanizate 'A' plotted according to Equation 1.1. Points represent isochronal data taken 1 minute after loading.

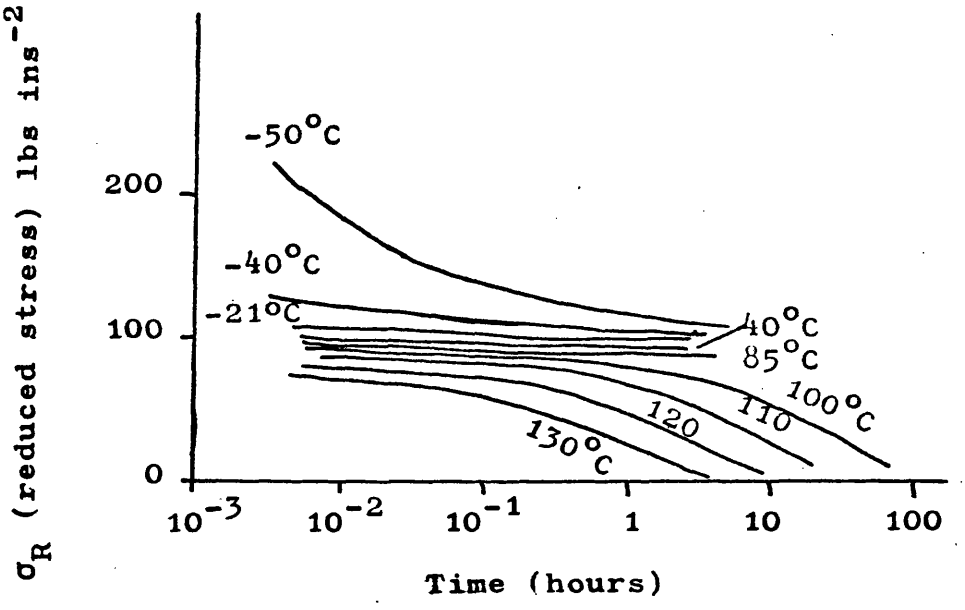

Figure 1.4 Reduced stress as a function of time at various temperatures. Vulcanized N.R. at 50% strain. See Reference 10.

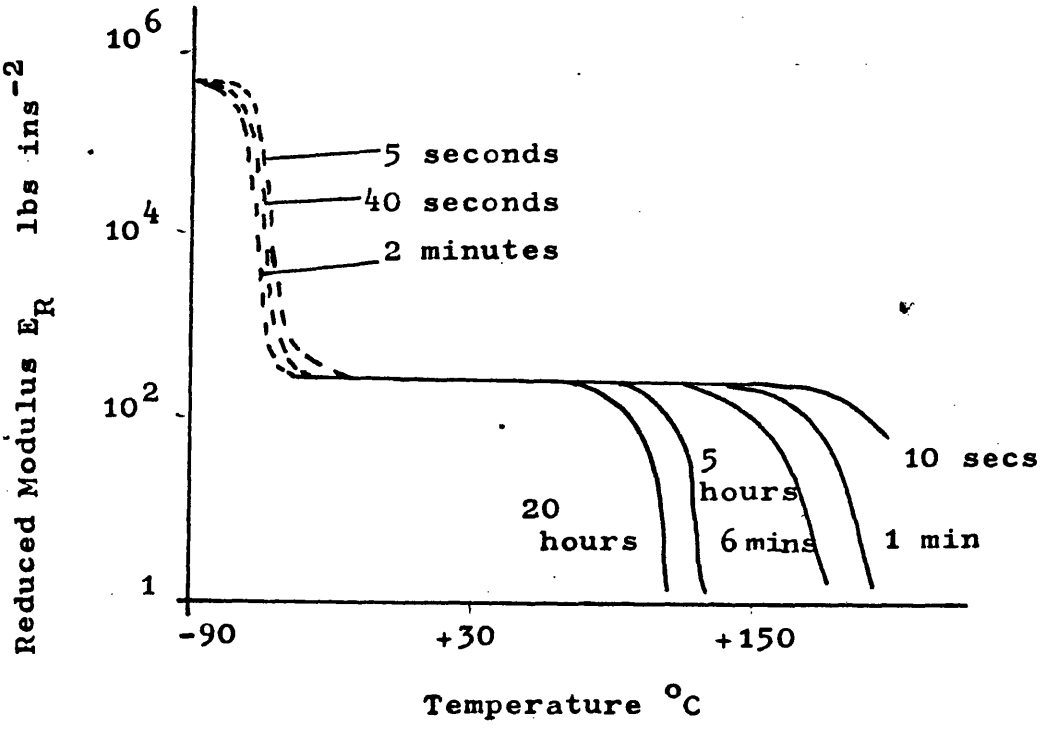

Figure 1.5 Reduced modulus as a function of temperature for various times. See Reference 10.

from Figure 1.4.

Figures 1.4 and 1.5 indicate three distinct temperature regions of present interest - high and low temperature regions of rapid stress decay and an intermediate region of comparative stability. It is thought that in the low temperature region, - 30°C and below, stiffening of the rubber occurs as a result of weak physical bonding between network chains. These bonds are however unstable and constantly break and reform and this leads to a reversible dynamic equilibrium which is manifested by stress decay. The high temperature region of instability is associated with heat ageing, a process of network degradation resulting from chemical reactions. This involves the 'cutting' or scission of crosslinks or network chains and concurrent creation of others. Again this leads to a decay of stress with time. The scission process is markedly influenced by the presence of oxygen. In the intermediate temperature range physical bonds are so weak that they relax before the first stress reading whilst the primary bond scission reaction is too slow to be significant within the experimental time scale. The present work is, however, devoted to this 'rubbery plateau' region since it covers the range of service temperatures for practical components.

If only for the sake of clarity, the low temperature relaxation process will be referred to as primary or physical relaxation and the high temperature process as secondary or chemical relaxation.

1.6 Viscoelastic Theory

Viscoelastic behaviour can be represented by well known mathematical models involving combinations of springs and dashpots to represent idealy elastic and idealy viscous components of material response[11]. Figure 1.6, for example, shows a model suitable for the discussion of creep. By resolving forces along the stress axis it can be shown that this will deform according to:

$$\varepsilon_t = \frac{\sigma}{E} \sum_{i=1}^{I} \left[1 - \exp - \frac{t}{\tau_i} \right] \qquad 1.3a$$

ε_t = strain at time 't'

E = Elastic modulus

where τ_i is the relaxation time of the i'th element in the model. If a large number of elements having a distribution of 'τ', $F(\tau)$, is assumed then

$$\varepsilon_t = \frac{\sigma}{E} \int_{-\infty}^{+\infty} F(\tau) \left[1 - \exp - \frac{t}{\tau} \right] d\tau \qquad 1.3b$$

Relaxation spectra for real materials can only be obtained indirectly by examination of experimental data. The model is of limited technological value therefore and as Tobolsky has pointed out[10], any data can be fitted to a sufficiently complicated distribution of relaxation times. Analagous concepts involving distribution functions may however be obtained by treating viscoelasticity in terms of various molecular mechanisms.

Consideration of the dashpot and spring model suggests a qualitative analogy for the effect of temperature on viscoelasticity. Reducing dashpot

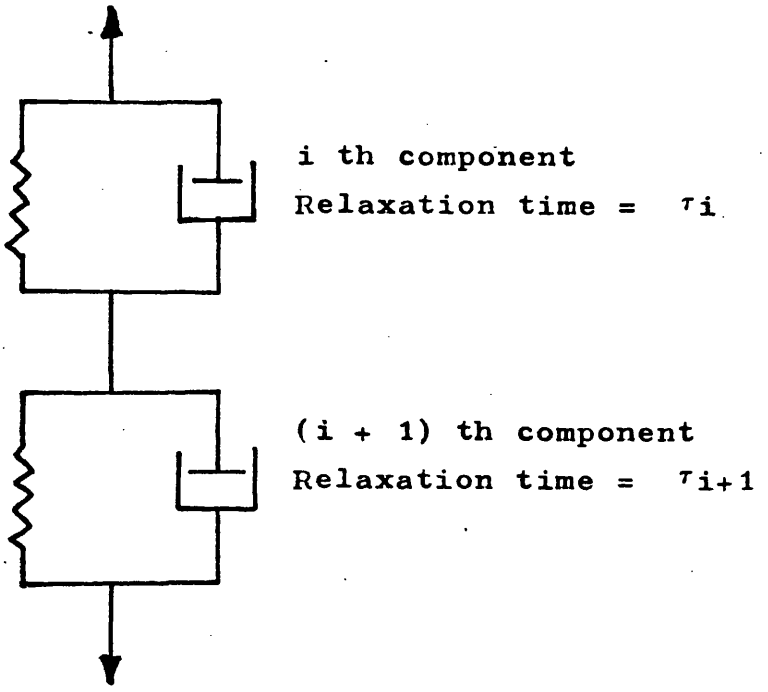

Figure 1.6 A dashpot and spring model suitable for the analysis of creep.

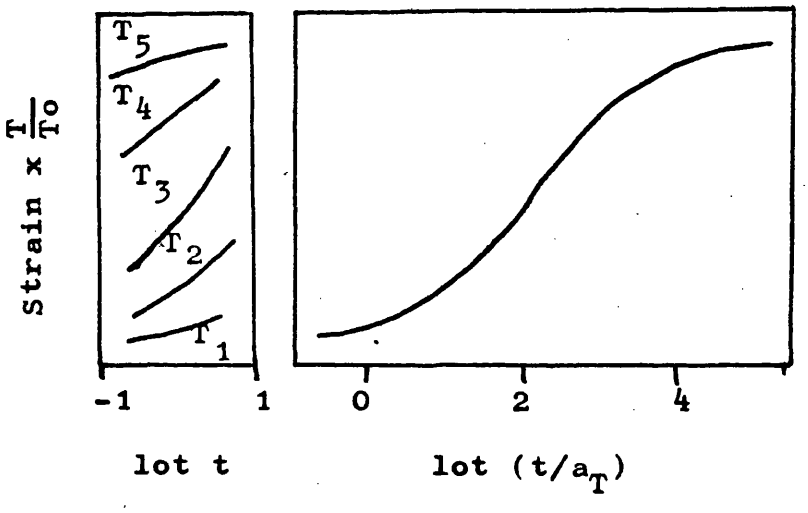

Figure 1.7 A schematic illustration of the time-temperature superposition principal for the case of creep data.

viscosity with increasing temperature allows more rapid response to applied stress, i.e. relaxation times decrease with increasing temperature. At very low temperatures, just above the glass transition therefore, creep deformation should be very slow as a result of long relaxation times. At higher temperatures, just below the rubbery plateau, creep should again be slow since relaxation times here are so short that the viscoelastic process is almost complete before the first strain measurement is made. Indeed, it is in the transition region between these two temperature extremes where viscoelastic behaviour is most prominant. Further, it can be argued that all relaxation times ' τ ' have the same temperature dependence [12,14]. Consequently, changes in temperature merely modify the time scale of viscoelastic response since in equations, such as 1.3, relaxation times always appear as a ratio with time. This implies that viscoelastic response data at different temperatures can be interelated and leads to the concept of time temperature equivalence. The relaxation spectrum for creep will cover a smaller range of times, for example, at some temperature T that at a lower reference temperature T_s and a function a_T may be defined.

$$a_T = \frac{\tau \text{ at temperature } T}{\tau \text{ at temperature } T_s}$$

If physical observations are plotted in terms of logarithmic time this means that data at different temperatures should be identical but shifted some

distance a_T with respect to each other. This is the basis of the time-temperature superposition principal first proposed by Leaderman[13] as a means of extrapolating data beyond the experimental time scale. Figure 1.7 shows a schematic illustration for the case of creep data. Hypothetical creep curves at different temperatures are shown on the left. These are reduced, as described earlier, to some arbitrary reference temperature to compensate for the effect of temperature on modulus. The mastercurve on the right has been synthesised by shifting individual curves along the 'log t' axis and represents, in this case, an extrapolation for data at temperature T_1 over an extended time period. Williams, Landel and Ferry[14] have shown that if a correct choice is made for T_s then a_T is a function of general applicability to all amorphous polymers. They proposed

$$\log a_T = -8.86\ (T-T_s)\ (101.6 + T-T_s)^{-1}$$

where T_s is usually some 45°C to 55°C higher than the glass transition.

Tobolsky, his co-workers and others[10,15,17 & 34] have successfully superposed creep and stress-relaxation data for gum vulcanizates of styrene butadiene rubber for results obtained in the temperature range -60°C to -15°C and have obtained good agreement for the shift factor a_T for the two cases. Other workers[16] have shown that a plot of log a_T against reciprocal temperature may yield a straight line over limited regions indicating an Arrhenius type energy barrier. Unfortunately the time-temperature superposition principal

is not convenient for the analysis of present creep data since this has been collected in the rubbery plateau region where relaxation is very slow. In Figure 1.7 for example the creep curves have been drawn well separated along the ordinate whereas in the present work initial elongations over a wide range of temperature were almost identical for any given stress, see Figure 1.3. Furthermore, present physical creep curves do not show marked curvature when plotted against logarithmic time and are therefore impossible to superpose. This will be discussed in greater detail in Chapter 5.

1.7 Physical Creep and Stress-Relaxation

In keeping with many polymers the physical creep and stress-relaxation of vulcanized rubbers generally vary in proportion to the logarithm of time under load, certainly in the rubbery plateau region.[18-30] In the case of creep therefore

$$\Delta\varepsilon \propto \log (t/t_o)$$

$\Delta\varepsilon$ = change in strain measured from some arbitrary starting time t_o.

Creep strain is normally expressed, however, as a fraction of the initial strain measured for convenience at 't_o' equal to 1 or 10 units. This automatically compensates for the temperature-modulus effect and also for slight differences in initial elongation (stress). Although a starting time of 10 minutes is recommended by British Standards[31], present work will be expressed in terms of the strain at 1 minute and this is in accordance with current practice in the publications of

MRPRA.* Hence the strain at any time 't' may be defined by:-

$$\varepsilon_t = \varepsilon_1 + c\varepsilon_1 \log_{10} t \qquad - \ 1.4$$

ε_1 = strain at 1 minute

c = logarithmic creep rate.

Similarly, the stress relaxation response may be represented by:-

$$\sigma_t = \sigma_1 - s\sigma_1 \log_{10} t \qquad - \ 1.5$$

σ_1 = stress at 1 minute

s = logarithmic stress relaxation rate.

A thoroughly satisfying theoretical interpretation of these relationships is not available[32] although they may be fitted to a derived distribution of relaxation times. As Gent has pointed out, the observed linearity with logarithmic time must fail at both very long and very short times. At long times an equilibrium deformation must be achieved in the absence of structural failure whilst at short times the curves must extrapolate backwards to some reasonable value of initial strain rather than to minus infinity. It is worthwhile pointing out, however, that there is little published data extending beyond 10^4 minutes and indeed much of the established understanding has developed from experiments of less than 10^3 and even 10^2 minutes duration.

Consideration of the Boltzmann superposition principle suggests that stress relaxation rates 's' should be independent of strain if it is assumed that vulcanized

*Malaysian rubber producers research association.

rubbers follow linear viscoelastic behaviour. Some experimental evidence[10,19,20,23] shows that this is a reasonable approximation for moderate strains up to perhaps 200%. At higher strains relaxation rates increase and Gent[20] has attributed this to the onset of stress induced crystallization. He compared relaxation rates with crystallinity measurements on natural rubber at various extensions and also showed that the effect was absent in butyl and styrene butadiene rubbers which do not crystallize. By contrast, Figure 1.8 shows the effect of extension on stress relaxation rates of peroxide and conventional vulcanizates of natural rubber with different crosslink densities.[24,25] It shows that relaxation rates are not necessarily independent of extension even at low extensions but it should be noted that the ordinate of this graph covers only a one percent range and that the vulcanizates have low relaxation rates of 2% per decade or less.

Gent has proposed a method by which creep and stress-relaxation rates may be interelated. Using the definitions:

$$c = (1/\varepsilon_1)\,(d\varepsilon/d \log_{10} t)_\sigma$$

$$s = (1/\sigma_1)\,(d\sigma/d \log_{10} t)_\varepsilon$$

he derived:-

$$s/c = (\varepsilon_1/\sigma_1)\,(d\sigma/d\varepsilon)_t \qquad - 1.6$$

Figure 1.8 indicates that creep and stress relaxation rates are smaller for vulcanizates with higher crosslink densities, i.e. higher moduli. This is in agreement with Gent[12,23] who compared stress relaxation

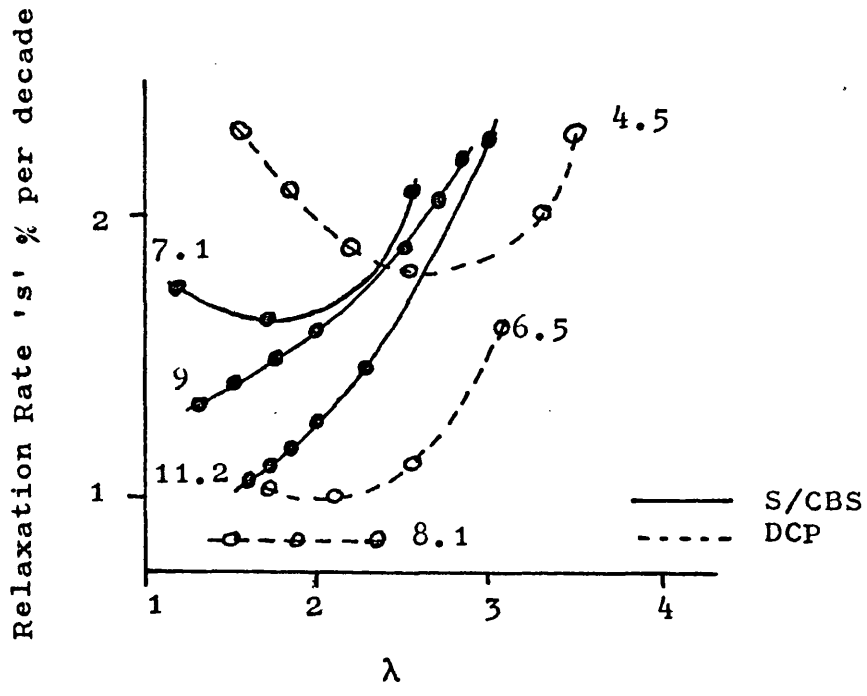

Figure 1.8 Dependence of stress relaxation rates on extension for natural Rubber vulcanizates of various degrees of crosslinking. The 100% modulus is indicated against each curve in Kg cm^{-2}. See Reference (24 and 25).

rates with crosslink density. He further suggested however that relaxation rates are independent of the type of curing system but this is in contradiction with Figure 1.8 which indicates that peroxide vulcanizates show improved creep resistance over conventional vulcanizates when compared at similar moduli. Farlie[28] has proposed that extra-network material is particularly important in determining creep response and more recently creep resistant vulcanizates have been developed[33] from deprotinized natural rubber by avoiding insoluble by-products normally produced by conventional curing systems. That differences exist between the creep behaviour of different types of vulcanizate of similar crosslink density is now well accepted.

1.8 Chemical Creep and Stress-Relaxation

Relaxation processes in rubber resulting from thermal and oxidative ageing have been introduced earlier. The subject has been christened "chemorheology" since it is the study of flow involving permanent changes in the molecular network due to the cleavage and creation of primary bonds. Two reviews of the subject[35] and [36,37] present the background work carried out in the USA and Britain respectively.

Tobolsky[38] observed the chemical relaxation phenomenon during a study of vulcanized rubbers at elevated temperatures. He attributed the process to the progressive rupture of chemical bonds as a result of the presence of molecular oxygen. This was supported by concurrent investigations of elevated temperature creep

by Wohlstenholme [39] who came to similar conclusions. Tobolsky further observed that the relaxation rate was independent of oxygen pressure in the range between that present in ordinary air atmosphere and in a commercial nitrogen atmosphere. These conclusions have been well corroberated and are now almost universally accepted for non sulphur cured vulcanizates. Indeed many workers have compared relaxation rates in air with those for vacuum or dry purified nitrogen atmospheres [40-51]. In particular Berry and Watson [52] have followed the relaxation of peroxide cured vulcanizates in cycled air/vacuum conditions and have shown the relaxation rate in vacuum to be about 1/400 of that in air. Reduction of oxygen partial pressure from atmospheric to 2 torr had no effect. By contrast the relaxation of polysulphide containing rubbers in vacuum was not negligible.

The reaction mechanisms of oxygen with rubber have been studied by means of model experiments on simple olefins, rubber solutions, organic sulphides and vulcanizates [53]. Deterioration of rubber by reaction with oxygen to form peroxide intermediates has been recognised for fifty years and it is known that simple olefins combine with oxygen at the α - methylinic bonds. Simple kinetic studies to elucidate the mechanisms have suggested the following generalisations:-

(I) Hydroperoxides are formed but not in quantitative yields.

(II) The reaction is autocatalytic.

(III) Oxidation proceeds by a free radical mechanism and is therefore catalysed by free radical

producing substances such as peroxides, azo compounds and ultra violet light. It is inhibited by active reactants for free radicals such as some antioxidants.

(IV) The rate is largely insensitive to oxygen concentration but depends on olefinic structure. The greater the mobility of the α - methylinic bond the greater the rate.

A multistep reaction mechanism has been established in which the first step involving molecular oxygen is generally not rate controlling. The mechanisms by which scission of crosslinks or of main chains occurs as a result of oxidation are not understood but the term scission efficiency has been defined:-

$$SE = \frac{\text{no. of molecules of } O_2 \text{ absorbed}}{\text{no. of scissions produced}} \quad - \quad 1.7$$

It can be estimated from measurements of oxygen absorption and network degradation. The latter is usually assessed by means of stress relaxation or from changes in swelling (modulus). Ingeneral the scission efficiency decreases as the test temperature is increased; i.e. less oxygen is required at higher temperatures to produce the same amount of network degradation. Scission efficiencies of sulphur based vulcanizates are somewhat lower than for non sulphur cures, although this follows partially from the fact that a large proportion of the relaxation in air for these structures is not due to oxidation. The high stress relaxation rates observed for these vulcanizates cannot therefore be interpreted

directly in terms of high rates of oxygen induced scission.

Investigations [54-57] of oxygen absorption by natural rubber vulcanizates have shown that the type of cure and in particular the type of crosslink formed has a great influence. In general, the shorter the cross-links formed the greater the resistance to oxidation although slight variations may occur depending on test temperature and on the presence or absence of natural and added antioxidants. Odd results have been produced from purified samples when the natural antioxidants are removed. The susceptibility of various cure systems to oxidation is therefore:-

unaccelerated sulphur cure > accelerated sulphur cure > TMTD or EV cure > Peroxide cure.

Note that sulphur vulcanizates not only absorb oxygen at a faster rate but have apparently lower scission efficiencies.

1.9 Chemical Stress-Relaxation Curves

A number of attempts have been made to interpret the shapes of stress relaxation curves in order to elucidate the mechanisms, in particular to distinguish between crosslink scission and main chain scission. The kinetic theory of rubber elasticity, as presented earlier, Eqn. 1.1,

$$\sigma = nkT\ (\lambda - \lambda^{-2})$$

suggests that at high temperatures, where the visco-elastic response is rapid, changes in stress at constant elongation should reflect changes in chain density 'n'.

Indeed it is common practice to relate 'σ' and 'n' directly; the validity of this will be discussed later.

Investigations by Berry and Watson [36, 52] include examples of this type of approach. They started from the Flory end correction equation

$$n = 2X - F$$

where X = crosslink concentration

F = concentration of free chain ends.

from which they suggested that network degradation by means of crosslink scission would lead to:-

$$\frac{n_t}{n_o} = \frac{2X_t - F_o}{2X_o - F_o} = \left[\frac{X_t}{X_o} - \frac{F}{2X_o}\right]\left[1 - \frac{F}{2X_o}\right]^{-1}$$

where the subscripts refer to times 'o' and 't' respectively.

For first order scission of one type of crosslink therefore

$$-dX/dt = KX$$

gives $$\frac{n}{n_o} = \frac{\sigma}{\sigma_o} = \left[\exp -Kt - \frac{F}{2X_o}\right]\left[1 - \frac{F}{2X_o}\right]^{-1}$$

$$\simeq \exp - K.t$$

since $F \ll 2X_o$

Similarly for the first order scission of two types of crosslink

$$\frac{n}{n_o} = \frac{\sigma}{\sigma_o} = \left[A_1 \exp -K_1 t + A_2 \exp -K_2 t - \frac{F}{2X_o}\right]\left[1 - \frac{F}{2X_o}\right]^{-1}$$

$$\simeq A_1 \exp - K_1 t + A_2 \exp - K_2 t$$

OR, assuming autocatalytic scission of crosslinks for example:-

$$-dX/dt = K_1 + K_2 (X_o - X)$$

and $$\frac{n}{n_o} = \frac{\sigma}{\sigma_o} = \left[1 - (K_1 \exp K_2 t - 1)(K_2 X_o)^{-1} - \frac{F}{2X_o}\right]\left[1-\frac{F}{2X_o}\right]$$

$$\simeq (1 - K_1 K_2 t)$$

for $K_2 t << 1.0$

Other equations for first order scission and for autocatalytic scission of main chains can be developed assuming that the susceptibility to scission of an individual chain is proportional to the number of scissionable bonds it contains. A comparison of such equations with experimental data led Berry and Watson to conclude that peroxide and sulphur vulcanizates degrade by oxidative scission of one type and more than one type of crosslink respectively. At the time of writing however the concensus of opinion is that peroxide vulcanizates degrade by scission of the main chains and this exemplifies the difficulties of interpreting stress relaxation curves.

By contrast with Berry and Watson, Tobolsky maintains [35] that it is impossible to distinguish between chain scission and crosslink scission purely from stress relaxation kinetics. He has shown that if reasonable assumptions are made for the kinetics of either process an exponential decay can be derived for both.

$$\sigma_t/\sigma_o = \exp - Kt \qquad - 1.8$$

$$\text{where } K = K_o \exp - Q/RT \qquad - 1.9$$

He has used this approach in much of his work. From other considerations, however, he has proposed that chain scission must be an important factor in the oxidative process. This follows from the fact that

different polymers vulcanized with the same curing agents show vastly different oxidation resistance. By comparison the difference in stress relaxation resistance between sulphur and peroxide vulcanizates of the same polymer, NR or SBR say, is a factor of only four [59]. The fact that unvulcanized gum rubbers show oxidative degradation lends support to the idea of chain scission.

Examinations of the effect of initial crosslink density on stress relaxation have been pursued with the intention of deducing the mechanisms. If one assumes a first order scission of crosslinks for example where $-dX/dt = KX$ then the stress relaxation rates $(d \ln \sigma/dt)$ should be unaffected by crosslink density. By comparison, for a first order scission of main chains the rate at which chains are broken would be proportional to the concentration of uncut chains and the number of monomer units in each chain. In this case, the relative stress relaxation rate $\frac{1}{\sigma_o} d \ln \sigma/dt$ should be initially independent of crosslink density. From such considerations Tobolsky [35,42] has proposed that radiation and peroxide cured vulcanizates degrade by scission in the main chain and this is supported by more recent work [60]. Similar work suggests that TMTD vulcanizates show both main chain and crosslink scission [42,61,50]. Sulphur vulcanizates are thought to show main chain plus crosslink scission [62,63] or chain scission plus sulphur bond interchange [50,53]. In conclusion therefore, present opinion is that main chain scission predominates in networks

containing C-C crosslinks whilst bond interchange and crosslink scission are important in networks containing polysulphide bonds.

Relaxation processes involving multiple mechanisms such as are discussed above should show non-exponential stress relaxation behaviour. Instead, a bi-mechanistic process might well follow [50,61,63]:-

$$\sigma/\sigma_o = A_1 \exp - K_1 t + A_2 \exp - K_2 t \qquad - \quad 1.10$$

for example.

This suggests that with increasing time the extent of stress decay would become progressively less than that predicted for a single process, i.e. an exponential extrapolation. It is of interest to point out however that since the rate constants K_1 and K_2 depend on temperature there could well be a range of temperature where $K_1 \simeq K_2$, assuming a difference in activation energies for the two processes. Alternatively at extremes of temperature one of the two processes could completely dominate the relaxation behaviour. This would lead to a simple exponential decay of stress with time. Early work by Tobolsky et al, for example, on sulphur vulcanizates was carried out mainly at 130°C and simple exponential decay was observed. By comparison other work suggesting bi-mechanistic processes tends to have been done at lower temperatures; 80°C [52], 100°C [50] and 110°C [61,63].

1.10 The Influence of Bond Reformation during Chemical Stress-Relaxation

It is well known that new crosslinks can form during the ageing of rubber networks. This results from the reformation of broken bonds, from a continuation of the vulcanizing process and as a result of sulphur bond interchange. The technique of continuous and intermittent stress relaxation is used to detect such crosslinking [35]. Here two samples are used, one held at the test elongation as in a normal stress relaxation experiment, the other held unstrained but for short periods intermittently to assess the modulus and hence total crosslink density. In general it is assumed that new crosslinks formed in the permanently elongated sample do not contribute to the stress since they are not deformed. On the other hand, new crosslinks formed in the intermittently elongated sample do contribute to the measured modulus (stress). A comparison of the two stress-time curves so obtained enables estimates to be made of the extent of concurrent crosslinking. Tobolsky [64] has suggested a two network theory, using this concept, in which two interpenetrating but independent chain networks are considered to exist - one with say n_o chains remaining from the original network and one with n_n new chains generated at the test elongation. This idea can be used to predict the extent of permanent set expected after releasing the permanently elongated sample from the test elongation. One simply sets up an equation based on a stress-strain

law, for example:-

$$n_o\left[\frac{L_s}{L_o} - \frac{L_o^2}{L_s^2}\right] = n_n\left[\frac{L_s}{L_T} - \frac{L_T^2}{L_s}\right] \qquad 1.11$$

where L_s = set length

L_o = original length

L_T = stress relaxation test length.

- so calculating the intermediate length where the new and old networks are in equilibrium. A modification of the continuous and intermittent technique has been suggested [65] to obtain the same results from a single sample whilst other workers [44] have suggested varying the ratio of elongated to relaxed times in the case of the intermittent sample.

The concept of the two network theory has been subjected to a detailed analysis since its inception. It is generally agreed [66,67] that the formation of additional crosslinks in a strained primary network without concurrent scission of the original structure will result in a "composite" elastomer obeying the two network theory. This has been verified experimentally [68]. By comparison however, the simultaneous scission and formation of crosslinks in a state of strain is not considered to follow this simple model since the original network imposes a "memory" on the new one [69]. Although new chains formed by crosslinking the original network are considered to be initially unstressed, they become stressed as scission occurs in adjacent stressed chains as a consequence of local network perturbations. New chains become progressively integrated into the original network with increasing degradation. Mathe-

matical interpretations have been developed for the case where new bonds are considered degradable [67,70] and for the case where new links are considered to be stable [71] and again these ideas have some experimental justification [68,72]. According to this concept, the rate of stress relaxation should become increasingly slower than that expected for a simple decay process as the secondary network develops. Flory, for example, [67] has suggested for the case where the total crosslink density remains constant:-

$$K.t = (-\ln \sigma/\sigma_o) + \frac{\left[-\ln \frac{\sigma}{\sigma_o}\right]^2}{2.2} + \frac{\left[-\ln \frac{\sigma}{\sigma_o}\right]^3}{3.3} + \frac{\left[-\ln \frac{\sigma}{\sigma_o}\right]^4}{4.4} \qquad - 1.12$$

which compares with $K.t = -\ln(\sigma/\sigma_o)$ when the secondary network contribution is neglected. This means that the two network theory is a good approximation for relatively small extents of stress decay where $K.t << 1.0$. More recently Fricker [73] has proposed a dynamical theory of assymptotic relaxation and has suggested

$$\sigma \propto t^{-\frac{1}{2}} \qquad - 1.13$$

There is some doubt [67] as to the applicability of the Flory theory to relaxation resulting from sulphur bond interchange. A typical mechanism for this process may involve the creation of "hybrid" chains where the newly created chain consists of portions that were originally stressed and stress free [67,74]:-

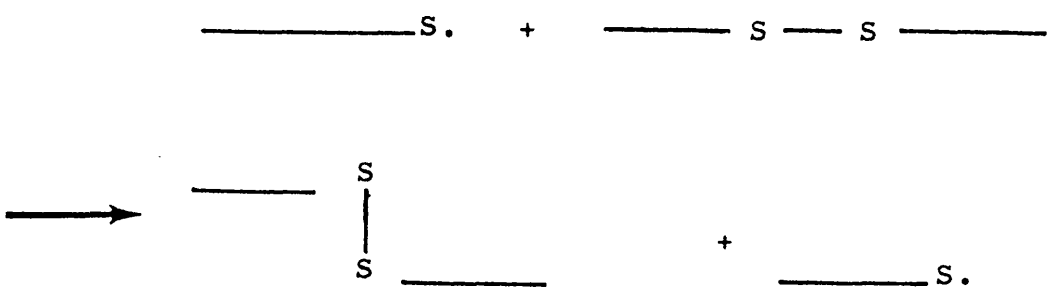

Here one would intuitively expect an initial exponential time law for the stress decay since each new chain would, on average inherit some constant fraction of the stress maintained by its environmental network at the time of its creation. As a result, the occurance of a single interchange event does not reduce the stress in a chain to zero, as is assumed for chain scission, but rather to some fraction of the original stress. Nevertheless, some mitigation of stress relaxation at longer times by redistribution of chain "tensions" as envisaged by Flory is still possible. Finally it should be pointed out that the stress decay law of equation 1.12 assumes a constant total crosslink concentration. In practice, the secondary network contribution to the total stress would depend on the ratio of crosslinking rate to scission rate.

A neat investigation of the extent of secondary crosslinking has been carried out by Minoura and Kamagata [75] using TMTD and conventional vulcanizates. The rate of link formation was assumed to be proportional to the concentration of residual accelerator whilst the rate of scission was assumed to obey first order kinetics hence ~

$$\frac{dn_{Total}}{dt} = K_1 a - K_2 n$$

where a = accelerator concentration

From this they derived

$$\frac{n_{Total}}{n_o} = A_1 \exp - K_1 t + A_2 \exp - K_2 t.$$

This approach deserves more attention, especially for polysulphidic rubbers where it might prove useful in distinguishing between continued vulcanization and secondary crosslinking resulting from bond interchange, crosslink reformation and oxidative hardening.

1.11 The Influence of Vulcanizate Structure on Chemical Relaxation

The stress relaxation behaviour of rubber networks is markedly influenced by the type and relative concentrations of crosslink present.

Radiation and peroxide vulcanizates, whilst of little commercial importance, are chemically the simplest obtainable, containing only relatively stable carbon-carbon crosslinks. The oxidative ageing is markedly influenced by purity, purified samples extracted before vulcanization showing autocatalytic kinetics [75]. This is markedly affected by small concentrations of conventional antioxidants [36,57,63], the rate of stress decay being inversely proportional to the inhibitor concentration [45]. Conversly, small concentrations of free radicals such as peroxide radicals themselves accelerate the process [43,70]. As discussed earlier, Berry and Watson [52] suggested that crosslink scission

was predominantly responsible for oxidative degradation in peroxide vulcanizates but the present concensus of opinion is in agreement with Tobolsky et al. Carbon-carbon crosslinks are extremely stable [47] and scission occurs mainly in the network chains. If one assumes, for example, that scission occurs with equal readiness in the c-c bonds of the crosslinks and of the main chains, the scission of chains must predominate since these contain a far higher number of scission sites [42]. Little secondary crosslinking takes place during the stress relaxation of peroxide vulcanizates and this reflects in good resistance to compression set [79]. Negligible relaxation occurs in vacuum.

Next in descending order of chemical simplicity are the vulcanizates containing monosulphidic and disulphidic crosslinks as prepared by curing with sulphur donating agents such as the thiurams. These show not disimilar behaviour to peroxide vulcanizates, exhibiting negligible relaxation in vacuum, little secondary crosslinking and autocatalytic oxidation kinetics when purified [36]. Degradation is thought to occur by a bi-mechanistic process involving the scission of both network chains and crosslinks [36,42,61,80]. The good ageing resistance of these vulcanizates is partially due to the presence of zinc dimethyldithiocarbamate, a powerful antioxidant produced as a side product during cure [36,58]. The removal of this by extraction explains the consequently poorer autocatalytic rate law.

Relaxation characteristics of conventionally cured sulphur plus accelerator vulcanizates are the least well understood, mix proportions and cure conditions being important. Crosslink structures range from monosulphidic to long polysulphidic chains up to S_8, the result of splitting a single sulphur ring. In general, shorter links result from high accelerator to sulphur ratios and from extended curing times, a structure similar to the TMTD type being produced in extreme cases [2,3]. Extensive relaxation occurs in vacuum, the kinetics are not autocatalytic and extensive secondary crosslinking takes place [35,36,49,57]. Approximately exponential stress decay is observed [35,36,52,82] although bi-mechanistic processes involving a double exponential decay have been considered more recently [50,63,83]. Activation energies in the range 100-150 KJ mol^{-1} have been observed [35,36,44,84,85]. Intermittent stress relaxation measurements show little change with time indicating that crosslinking and scission rates are approximately equal. Conventionally cured vulcanizates differ too in that their ageing resistance is not improved by the addition of normal antioxidants such as the dithiocarbamates; in fact some evidence suggest that these aggravate stress decay [37]. Phenolic based antioxidants are used instead. Prolonged cure times and increased accelerator to sulphur ratios mitigate against stress relaxation and this has been attributed to the breakdown of long polysulphide bonds with subsequent reformation of shorter ones during cure. Indeed, stress relaxation rates have been correlated with sulphur

content and more specifically with the distribution of sulphur bond lengths [44,80,82,86,87]. Furthermore, vulcanizates containing long polysulphide bonds show more rapid oxygen absorption [55-57, 88,89]. Work by Tobolsky et al on sulphur cured rubbers is summarized in his book [35]. Stress relaxation in these vulcanizates, he says, occurs through the interchange of di, tri and tetrasulphide linkages with each other or with mercaptan groups.

Unaccelerated sulphur vulcanizates contain predominantly long sulphide linkages and so exhibit relaxation behaviour comparable with the extreme case of a conventional cure. Prolonged curing is not so effective in correcting this.

Recent developments in compounding practice include the development of efficiently vulcanized (E.V.) rubbers using high accelerator to sulphur ratios or mixtures of sulphur donating agents and sulphur. These produce a good compromise between the good ageing resistance of TMTD cures and the good mechanical properties of conventional cures. [78,81,89,90]

1.12 Discussion

In view of the commercial factors outlined in section 1.1 the present work has been devoted primarily to sulphur plus accelerator cured vulcanizates of natural rubber although some work has been carried out on peroxide cured samples for comparison. The relative importance of primary and secondary components in determining stress

relaxation at intermediate temperatures where both occur at comparable rates has been discussed by Thirion and Chasset [76] and by Tobolsky [77]. Both agree that oxidative reactions participate in the relaxation process down to room temperatures where viscoelasticity was once thought to be the sole mechanism. In the present work primary and secondary creep components will be considered seperately using the method of Gent (see Chapter 2) to distinguish between them.

The literature survey presented in this introductory chapter is by no means complete and indeed the most relevant published papers will be discussed later along with the present work. Nevertheless, it is clear that the chemical stress-relaxation process has been well investigated previously; the application of the derived theories to secondary creep will be considered in Chapter 4. In particular, this will culminate in a discussion of the relative importance of oxidative ageing and sulphur bond lability in determining secondary creep response. Absorption and diffusion of oxygen as rate limiting mechanisms in the secondary creep process have received very little attention. A simple model for the influence of specimen size, temperature and diffusion rates on oxygen adsorption will be presented in Chapter 3.

The logarithmic law for primary creep as is observed in the rubbery plateau region is as yet unexplained. Further, this linearity with logarithmic time precludes the application of the WLF time -

temperature superposition principle to data collected in this commercially important temperature range. These factors will be considered in Chapter 5, together with a possible theory for physical creep based on activation energy concepts.

The influence of carbon black on primary and secondary creep will be discussed in Chapters 6 and 4 respectively. Again this is another area which has received little attention in previous publications.

REFERENCES; CHAPTER 1

1. A. E. Moulton "The Moulton Suspension Systems." Use of Rubber in Engineering. Proc of the (1966) Conference. Ch 14 pp 182-193. Pub. McLaren & Son, London. Ed. P. W. Allen, P. B. Lindley and A. R. Payne.

2. L. Bateman, C. G. Moore, M. Porter and B. Saville "The Physics and Chemistry of Rubberlike Substances." Ch. 15 Ed. L. Bateman Pub. McLaren & Son, London. Wiley, N. Y. (1963).

3. W. Hoffman "Vulcanization and Vulcanizing Agents." McLaren & Son, London (1967).

4. L. R. G. Treloar The Physics of Rubber Elasticity. 2nd Edition. Oxford Clarendon Press (1958).

5. P. J. Flory "Principles of Polymer Chemistry." Ch. 11. Cornell Univ. Press N. Y. (1953).

6. L. R. G. Treloar Contemporary Physics 12 (1), pp 35-56 (1971).

7. L. R. G. Treloar Rep prog phys 36 (7), pp 755-826 (1973).

8. R. S. Rivlin and D. W. Saunders Phil Trans Roy Soc A243, pp 251-88 (1951).

9. L. Mullins and A. G. Thomas "The Physics and Chemistry of Rubberlike Substances." Ch. 7 Ed. L. Bateman Pub. McLaren & Son, London. Wiley, N. Y. (1963).

10. A. V. Tobolsky and R. D. Andrews J. Chem phys 13 (1), pp 3-27 (1945).

11. J. D. Ferry "Viscoelastic Properties of Polymers." Wiley, N. Y. & London (1961).

12. A. N. Gent and P. Mason "The Physics and Chemistry of Rubberlike Substances." Ch. 8 Ed L. Bateman Pub. McLaren & Son, London. Wiley, N. Y. (1963).

13. H. Leaderman "Elastic and Creep Properties of Filamentous Materials and Other High Polymers." Pub. The Textile Foundation Washington (1943).

14. M. L. Williams, R. F. Landel and J. D. Ferry J Am chem soc 77, p 3701 (1955).

15. J. R. Bischoff, E. Castiff and A. V. Tobolsky J Am chem soc 74, pp 3378-81 (1952).

16. P. I. Vincent "Physics of Plastics" Ch. 2 Pub. The Plastics Institute (1965). Ed. P. D. Ritchie.

17. A. V. Tobolsky "Polymer Science and Materials." Ch. 10 Ed. A. V. Tobolsky and H. F. Mark (1971).

18. P. Phillips Proc physical soc of London 19 (4), pp 491-511 (1905).

19. A. N. Gent J. App polym Sci 6 (22), pp 433-441 (1962).

20. A. N. Gent Rubb Chem and Technol 36 (3), pp 697-708 (1963).

21. L. A. Wood Rubb Chem and Technol 43, pp 1482-90 (1970).

22. D. J. Plazek J. Polym Sci 4, pp 745-763 (1966).

23. A. N. Gent Cahiers Group Francais De Rheologie 5, pp 241-51 (1960).

24. C. J. Derham, E. Southern and A. G. Thomas N. R. Technology. Rubb Dev Supp (1970) No. 7.

25. C. J. Derham, E Southern and A. G. Thomas Int Rubb Conference, Moscow (1969).

26. C. J. Derham MRPRA 3rd Rubber in Engineering Conference London (1973).

27. C. J. Derham, G. J. Lake and A. G. Thomas J. Rubb Inst., Malaya. 22 (2), pp 191-200 (1969).

28. E. D. Farlie J. App polym Sci 14, pp 1127-41 (1970).

29. G. M. Martin, F. L. Roth and R. D. Stiehler Trans Inst Rubb Industry 32 (6), pp 189-203 (1956).

30. C. J. Derham and P. B. Lindley
Proc 5th Int Conf on fluid sealing. Warwick (1971).
Pub. The British Hyromechanics Research
Association, Cranfield.

31. British Standards 903 part A15 (1958).

32. W. N. Findley S.P.E. Journal 16, pp 57-65 (1960).

33. J. F. Smith MRPRA 3rd Rubber in Engineering
Conference, London (1973).

34. F. S. Conant, G. L. Hall and W. J. Lyons
J. App phys 21 (6), pp 499-504 (1950).

35. A. V. Tobolsky "Properties and Structure of
Polymers." Ch. 5
Pub. Wiley, N. Y. (1962).

36. J. R. Dunn and J. Scanlon
"The Chemistry and Physics of Rubberlike
Substances." Ch. 18. Ed. L. Bateman.
Pub. McLaren & Son, London. Wiley, N. Y. (1963).

37. L. Bateman, J. I. Cunneen, C. G. Moore, L. Mullins and
A. G. Thomas
"The Chemistry and Physics of Rubberlike
Substances." Ch. 19. Ed. L. Bateman.
Pub. McLaren & Son, London. Wiley, N. Y. (1963).

38. A. V. Tobolsky, I. B. Prettyman and J. H. Dillon
J. App phys 15 (4), pp 380-95 (1944).

39. M. Mooney, W. E. Wolstenholme and D. S. Villars
J. App phys 15, pp 324-37 (1944).

40. W. C. Schneider Ph D Thesis Princeton University
(1944).

41. A. V. Tobolsky J. App phys 27, p 673 (1956).

42. Y. Takahashi and A. V. Tobolsky
Polymer J 2 (4), pp 457-67 (1971).

43. J. R. Dunn, J. Scanlon and W. F. Watson.
Trans Far Soc. 55, pp 667-75 (1959).

44. K. H. Hillmer and W. Scheele
Rubb Chem and Technol 43 (4), pp 788-98 (1970).

45. J. R. Dunn, J. Scanlon and W. F. Watson
Trans Far Soc. 54, pp 730-39 (1958).

46. S. Baxter and M. A. A. Wilson
Polymer 4, p 163 (1963).

47. M. T. Shaw and A. V. Tobolsky
Rubb Chem and Technol 44 (3), pp 579-86 (1971).

48. P. F. Lyons, T. C. P. Lee and A. V. Tobolsky
Rubb Chem and Technol 39, p 1634 (1966).

49. A. N. Gent J. App polym Sci 6 (22) pp 442-448 (1962).

50. K. Murakami and S. Tamura
J. Polym Sci, polym letters Ed.
11 (5), pp 317-21 (1973).

51. D. B. Jaroszynska Proc Int Rubb Conf, Brighton (1967) pp 59-68
Pub. Inst Rubb Ind.

52. J. P. Berry and W. F. Watson
J. Polym Sci 18, pp 201-13 (1955).

53. D. Barnard, L. Bateman, J. I. Cunneen and J. F. Smith
"The Chemistry and Physics of Rubberlike Substances." Ch. 17
Ed. L. Bateman
Pub. McLaren & Son, London. Wiley, N. Y. (1963).

54. D. Barnard, M. E. Cain, J. I. Cunneen and T. H. Houseman
Rubb Chem and Technol 45 (2), pp 381-401 (1972).

55. C. L. M. Bell and J. I. Cunneen
J. App polym Sci 11, pp 2201-2214 (1967).

56. E. T. McDonel and J. R. Shelton
J. Chem Eng Data 4, pp 360-366 (1959).

57. J. I. Cunneen Rubb Chem and Technol 41 (1), pp 182-208 (1968).

58. W. P. Fletcher and S. G. Fogg
Rubb J. and int Plastics Jan 4th, p 16 (1958).

59. A. Mercurio and A. V. Tobolsky
J. Polym Sci 36, pp 467-473 (1959).

60. S. Tamura and K. Murakami
J. App polym Sci 16, pp 1149-54 (1972).

61. K. Murakami, S. Tamura and N. Katsuta
J. Polym Sci, polym letters Edn.
10, pp 619-623 (1972).

62. M. M. Horikx J. Polym Sci 19, pp 445-54 (1956).

63. S. Baxter and H. A. Vodden
Polymer 4, pp 145-54 (1963).

64. R. D. Andrews and A. V. Tobolsky
J. App physics 17, p 352 (1946).

65. S. Ore J. App polym Sci 11 (6), pp 318-21 (1959).

66. J. P. Berry, J. Scanlon and W. F. Watson
Trans Far Soc 52, p 1137 (1956).

67. P. J. Flory Trans Far Soc 56 (5), pp 722-43 (1960).

68. D. K. Thomas Polymer 7 (3), pp 125-33 (1966).

69. J. Scanlon and W. F. Watson
Trans Far Soc 54, pp 740-50 (1958).

70. H. S. Fricker Proc Roy Soc, London A335, pp 267-287 (1973).

71. J. Scanlon Trans Far Soc 57, pp 839-45 (1961).

72. D. S. Cambell Brit Polym J. 5, pp 55-66 (1973).

73. H. S. Fricker Proc Roy Soc, London A335, pp 289-300 (1973).

74. A. V. Tobolsky and W. J. McKnight
"Polymeric Sulphur and Related Polymers."
Ch. 4 Pub. Interscience. N. Y. (1965).

75. Y. Minoura and K. Kamagata
Polymer 10 (11), pp 852-58 (1969).

76. P. Thirion and R. Chasset
Rubb Chem and Technol 37, pp 617-26 (1964).

77. G. Steiner and A. V. Tobolsky
Rubb Chem and Technol 43 (5), pp 1036-39 (1970).

78. G. M. Doyle, R. E. Humpheries and R. M. Russel
J. App polym Sci 15, pp 1855-68, (1971).

79. G. M. Bristow NR - Technology, Rubb Dev Supplement No. 1 (1970).

80. A. V. Tobolsky, W. J. McKnight and M. Takahashi
Rubb Chem and Technol 39, pp 524-29 (1966).

81. P. M. Lewis Natural Rubb Technol 4 (3), pp 52-62 (1973).

82. B. A. Dogadkin and Z. N. Tarasova
Rubb Chem and Technol 27, pp 883-98 (1954).

83. K. Murakami and S. Tamura
J. Polym Sci, polymer letters Ed.
11 (8), pp 529-31 (1973).

84. K. Murakami, S. Tamura and T. Kusano
Reports on progress in polymer physics, Japan
12, pp 287-88 (1969).

85. T. Kusano and K. Murakami
J. Polym Sci 10, pp 2823-31 (1972).

86. A. Y. Coran Rubb Chem and Technol 37 (3),
pp 673-78 (1964).

87. J. H. Farmer and J. E. Stuckey
J. Inst Rubb Indust 5 (5), pp 200-203 (1971).

88. B. N. Leyland and T. J. Meyrick
J. Inst Rubb Indust. 3 (2), pp 60-65 (1969).

89. E. J. Blackman and E. B. McCall
Rubb Chem and Technol 43 (3), pp 651-63 (1970).

90. M. Porter Natural Rubb Technol 4 (4), pp 76-90
(1973).

CHAPTER 2

INTRODUCTION TO THE CREEP WORK

2.1 Specimen Preparation

Specimens were prepared by Avon Rubber Company of Melksham to specifications provided. Several vulcanizates have been tested and the recipe's are shown in Figure 2.1. In all cases a cure time of 40 minutes at 140°C was used. As far as possible the same batch of natural rubber was used whenever more than one vulcanizate was prepared at a time. It will be noted that many of the vulcanizates are variations on the basic recipe 'A' and in particular 'B' is identical to 'A' but for the absence of antioxidant.

Creep samples [33] as illustrated in Figure 2.2 were stamped from moulded sheets. The gauge marks were drawn using biro; cathetometer readings were taken at tangents to the circles indicated.

2.2 Description of the Equipment

Creep testing was carried out in a climatic cabinet (see Figure 2.3) built specially for the purpose by Fisons Scientific Apparatus Ltd., Loughborough. It has been described briefly elsewhere[1]. This facilitates, within limits, independent control of temperature and humidity. The forced airflow in the cabinet is circulated around cooling coils and heating elements. Humidity is controlled by wet and

	A	B	C	C2	D	E	F	G	H	I	J	K	L	M
Natural Rubber (SMR 5CV)	100	100	100	100	100	100	100	100	100	100	100	100	100	100
Stearic Acid	2	2				2	2	2	2	2	2	2	2	2
Zinc Oxide	5	5				5	5	5	5	5	5	5	5	5
Nonox ZA[1]	1.5				1.5	1.5	1.5	1.5	1.5	1.5	1.5	1.5	1.5	1.5
CBS[2]	0.6	0.6				0.6	0.6	0.6	0.6	0.6	0.6	0.6	0.6	0.6
Sulphur	2.5	2.5				2.5	2.5	2.5	2.5	2.5	2.5	2.5	2.5	2.5
DCP[3]			3	3										
H.S.-HAF black						30					10	50		
L.S.-HAF black							30							
L.S.-SRF black								30						
L.S.-F.T black									30					
N.S.-SAF black										30			10	50

Figure 2.1 Composition of Vulcanizates

1. 4 - isopropylamino - diphenylamine. Antioxidant.
2. N - Cyclohexyl benzothiazole - 2 - Sulphenamide. Accelerator.
3. Dicumyl Peroxide. Curing agent.

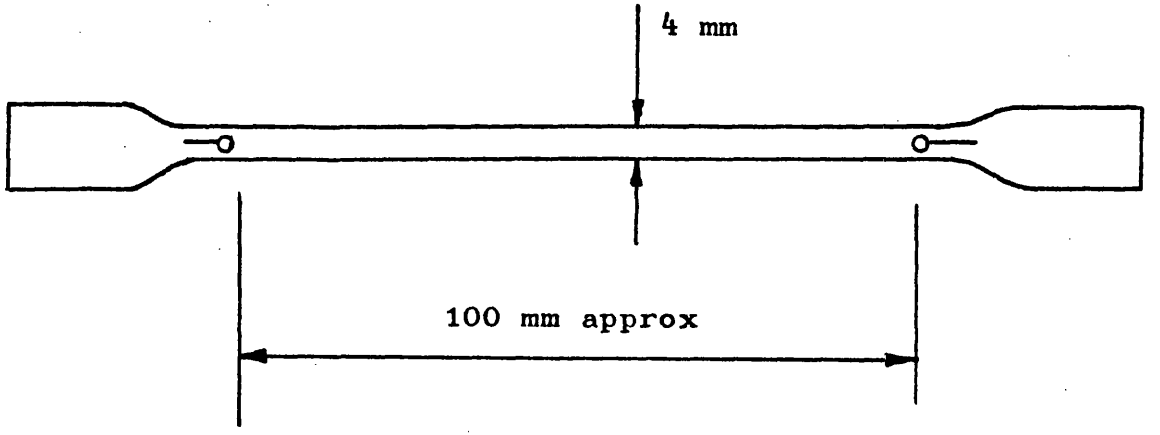

Figure 2.2 Illustration of specimen shape.
Thickness 1.7 to 2.1 mm.
Notice the gauge marks. Cathetometer readings were taken tangentially to the circles.

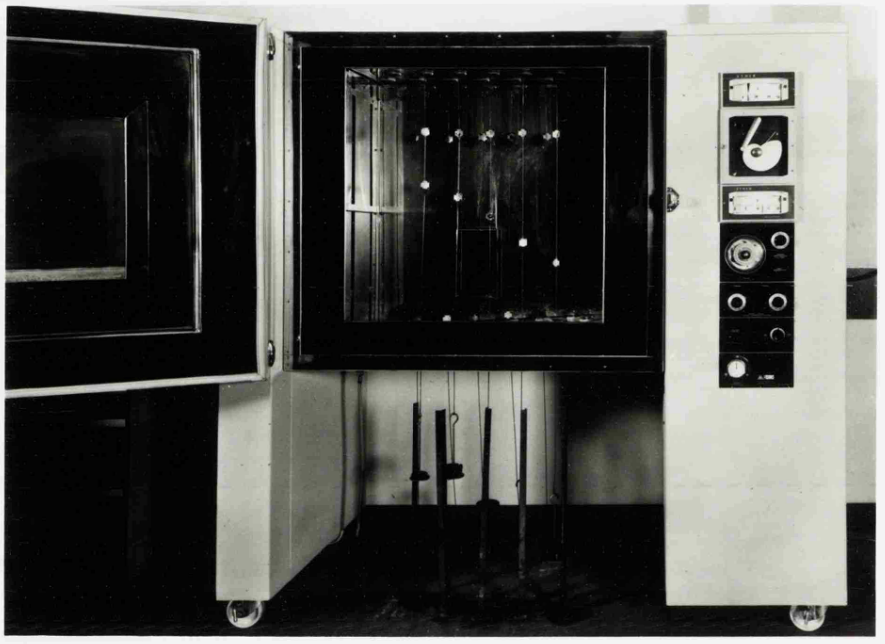

Fig 2.3 The Fisons Climatic Cabinet.
Note specimens and grips. The loading weights can be seen below the cabinet where they are prevented from rotating by the vertical strips.

dry resistance thermometers positioned in the airflow, the depression of the wet thermometer being used to activate either water injectors or refrigerent circulation to the cooling coils. In the latter case water vapour from the air condenses onto the coils and runs out of the cabinet via a pipe in the base. The cooling action is balanced by a corresponding heat input from the heating elements which are in turn controlled by means of a separate dry resistance thermometer. Alternatively the system can be used as an oven cum refrigerator with a continuous temperature range from sub zero upwards. Temperature stability and temperature variation throughout the cabinet are excellent, there being less than 1/2°C discrepancy from the set value in any position by comparison with independent thermistor readings. The maximum wet bulb depression setting is 20°C with the control system supplied and this limits the minimum obtainable humidity at higher temperatures. The cabinet manufacturers do not recommend the use of the humidity control system at temperatures in excess of 80°C. In practice however its use at temperatures much higher than this is prevented by the cooling effect of the de-humidifier coupled with the limited power of the heating coils. Approximate ranges of operating conditions for the cabinet are indicated in Figure 2.4.

Initial specimen length and subsequent extension were followed by intermittent cathetometer readings taken through a triple glazed window in the door of

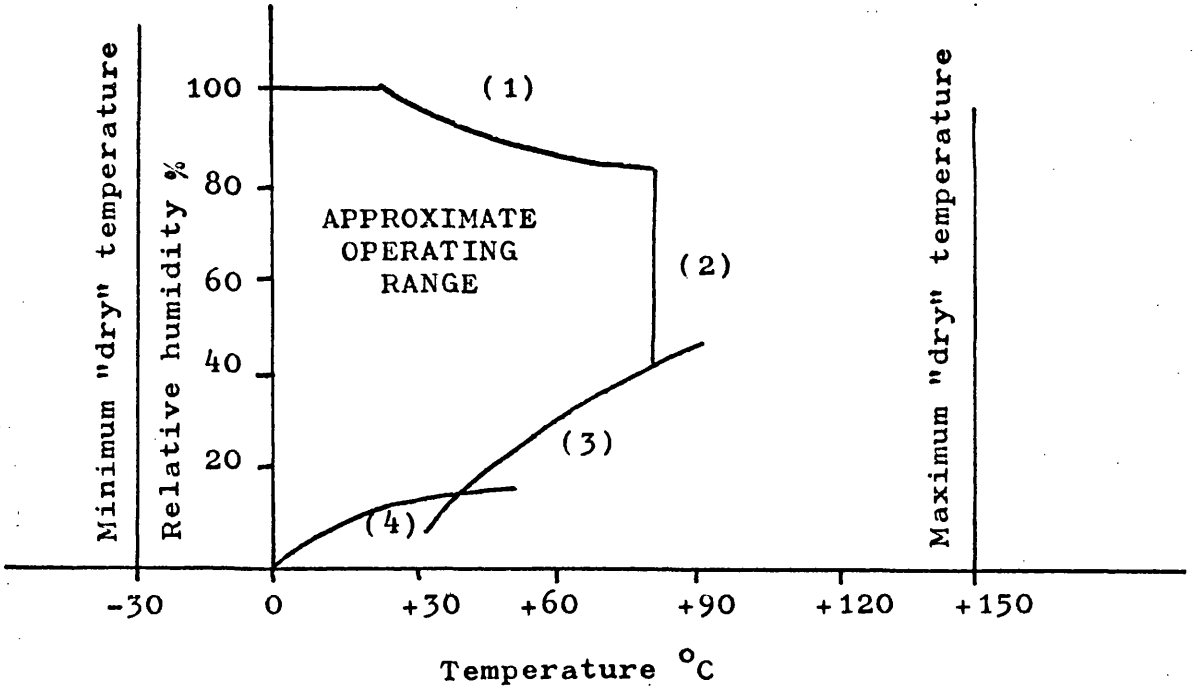

Figure 2.4 Approximate range of operation for the Fisons climatic cabinet (1) Maximum humidity limited by water injectors. (2) Maximum temperature with humidity control in use limited to 80°C, (3) Minimum humidity limited by the 20°C maximum wet bulb depression setting. (4) Minimum humidity limited by dehumidifier.

the cabinet. The cathetometer sits via three adjustable legs onto a heavy table and is set to the vertical by means of spirit levels. In turn each leg of the table is independently adjustable to prevent rocking. The cathetometer vernier is graduated in steps of 0.05 mm but in practice accuracy is limited by eyesight, by the clarity of the markings on the specimen and by the stability of the cathetometer and specimen throughout an experiment. Accurate determinations of initial strain, creep strain and creep as a fraction of initial elongation can be made despite deviations from the vertical of either cathetometer or specimen. This follows from the fact that these functions are ratio's in which both numerator and denominator are equally affected by misalignment of the system. By comparison, however, a relative displacement of the cathetometer and specimen within the duration of an experiment can sometimes introduce unacceptable errors. Consider the simple case depicted in Figure 2.5 in which it is assumed that both specimen and cathetometer were originally parallel but become displaced by a relative angle 'θ' in the plane of the paper as shown. For a typical case where the specimen gauge length under load may be up to 300 mm one can show that θ must not exceed about 1^{o} if measureable inaccurancies, i.e. 0.1 mm, are to be avoided. Since this is in the same order as the sensitivity of the spirit levels and since re-alignment in the other vertical plane is equally detrimental it is essential for best results to ensure that neither

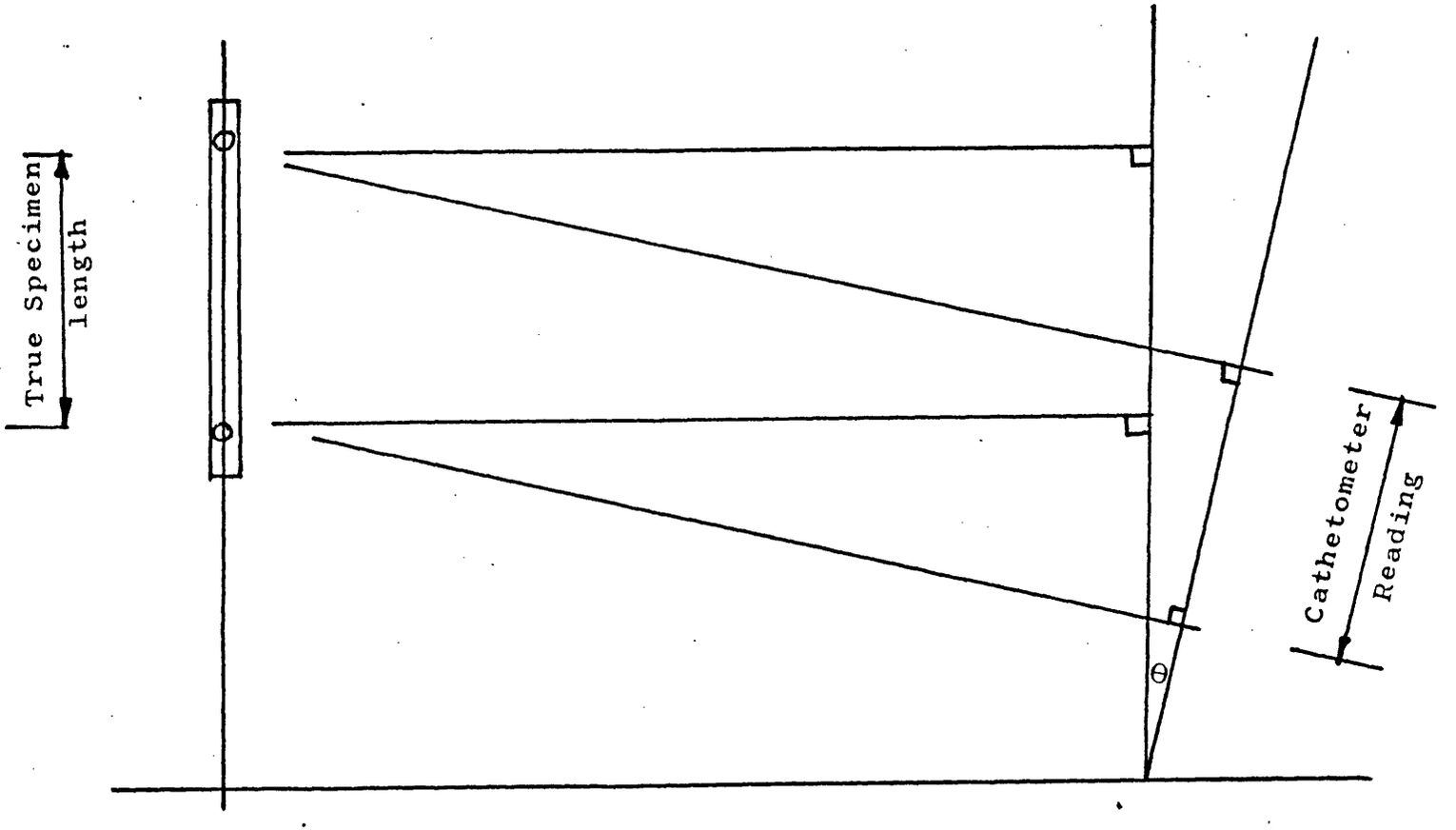

Figure 2.5 Effect of Misalignment of Cathetometer and Specimen.

the cabinet containing the specimens nor the cathetometer are moved during the duration of an experiment. This is particularly so for tests at low stress where any inaccuracy represents a larger proportion of the initial extension in which terms the creep is expressed.

2.3 Creep Testing Procedure

Specimens were generally subjected to the test "climate" for some 24 hours prior to loading during which time they were freely suspended from the upper loading grips in the cabinet. This was intended to provide some time for an equilibrium to be established between the rubber and the atmosphere, particularly with regard to humidity. The specimen gauge length was then determined using the cathetometer. The cabinet door was opened and the lower loading grips, their weight supported from below where they protrude through the cabinet base, were attached. The door was then reclosed and a further hour allowed for specimen reconditioning before applying the creep loads onto the lower grips. Each specimen-load assembly was prevented from rotating and oscillating by a vertical strip of L-section steel sheet placed in the slot of each loading weight; this can be seen in Figure 2.3. Every effort was made to apply loads gently to prevent over-straining and hence stress cycling the specimen. This means that loading was not instantaneous. In practice each load was carefully lowered to the point where it was fully supported by the specimen over a period of some five seconds.

Specimen gauge lengths were measured, using top and bottom gauge marks, one minute after the start of loading and at random intervals thereafter.

2.4 Creep-Time Relationships

Consideration has been given to a number of creep-time relationships which have been proposed for polymers and elastomers. For a review of these the reader is referred to Findley W.N. [2,3]. In addition C.S. Kim [4] has obtained straight line plots of $(\lambda-\lambda^{-2})$ against time for polybutadiene rubbers under ambient room conditions. His results were for thin samples over long periods of time when viscoelastic, chemical and surface cracking processes would all be important. In the present work however the relationships proposed by A. N. Gent and adopted generally by MRPRA, as described in Chapter 1, have proved most useful. Some partial success has also been achieved using a log-log relationship and this will be outlined briefly here.

Assuming that the creep-time relationship obeys a simple function;

$$\varepsilon_c = A\sigma^a \varepsilon^b t^c f(T) \qquad - 2.1$$

ε_c = creep strain

σ = stress

ε = strain

t = time

a,b&c = constants

T = Temperature

one might expect a log-log relationship between creep

and time since creep experiments are conducted at constant stress and temperature. This would follow if b = o or if $\varepsilon_c \ll \varepsilon$. Creep data for vulcanizate 'A' has been inspected in this fashion, see Figures 2.6 to 2.8. At 80°C such curves have three distinct regions - a decelerating initial region, a centre linear portion and an accelerating final region. At lower temperatures only the first two of these are observed within the experimental time scale. These curves are typical of a whole range of results but the extent of the linear portion varies and in extreme cases, as shown, the curves become sigmoidal. The gradients of the centre linear portion are indicated at 10°C and 60°C respectively in Figures 2.9 and 2.10 respectively. From the different dependences on stress one might infer two different dominating mechanisms - a viscoelastic process at the lower temperature and an oxidative or labile sulphur crosslink process at 60°C perhaps. A major difficulty with this type of plot, in fact, is that of relating the portions of the curves to specific mechanisms. Consider the curves at 10°C for example which suggest a change in dominating mechanism after about 100 minutes under load where the curves become linear. The whole curve must however represent a low temperature viscoelastic process and indeed the same results can be plotted as single straight lines over the entire time scale on a semi-log plot. It can be misleading to interpret changes in the character of a curve as representing changes in dominant mechanism since the point of inflection depends on the type of plot. The converse

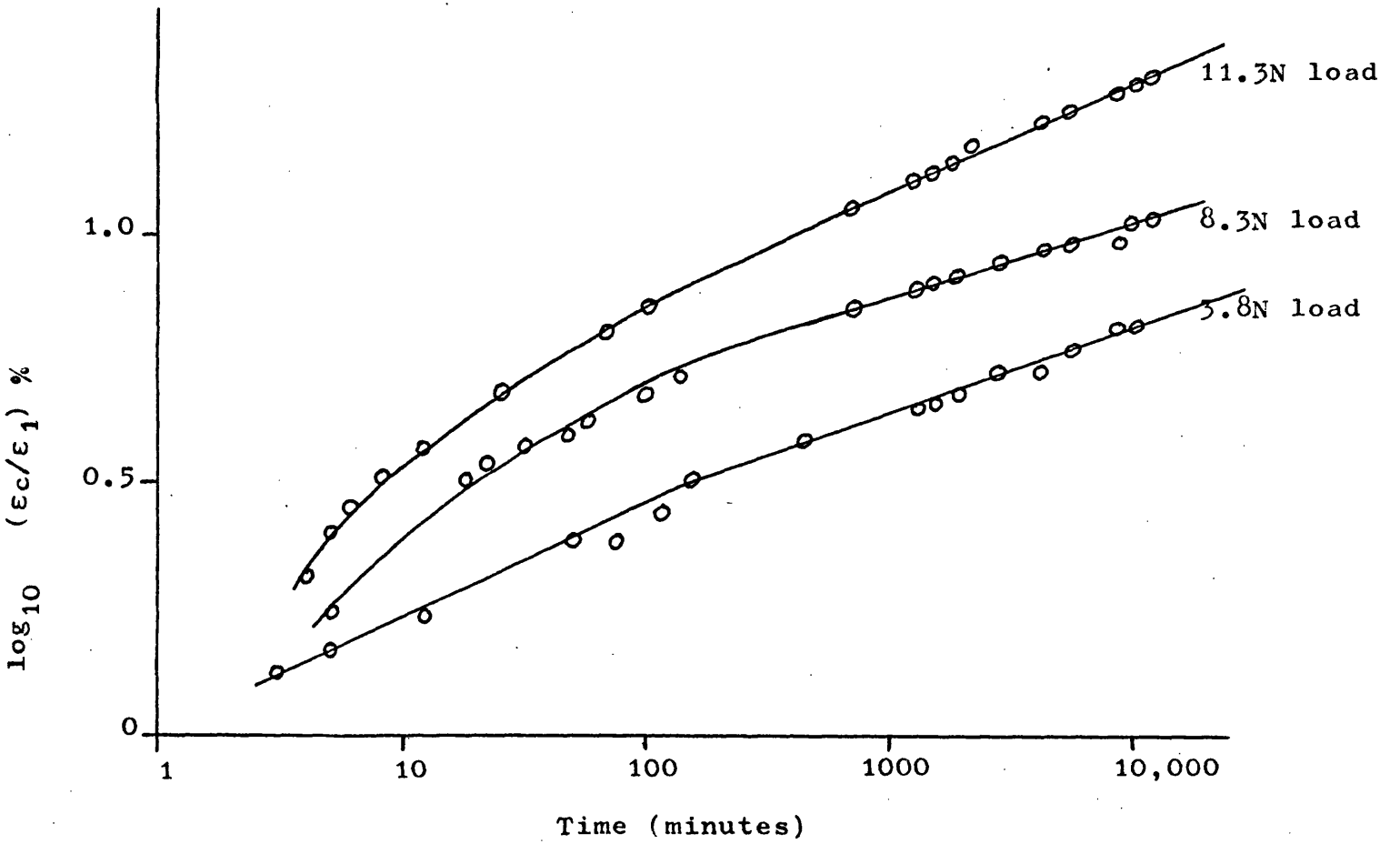

Figure 2.6 Log-Log plots of the creep of vulcanizate 'A' at 10°C. 40% relative humidity.

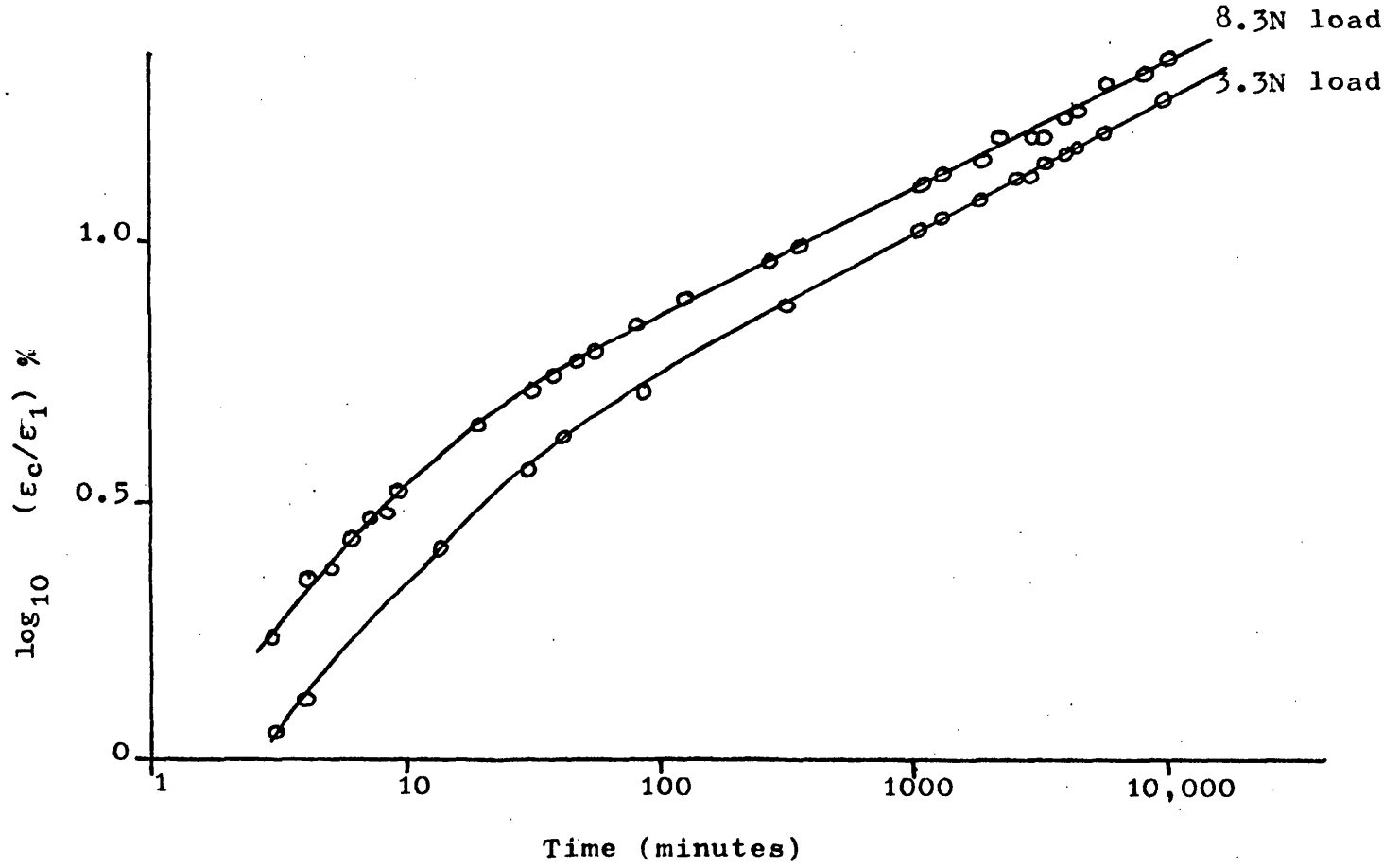

Figure 2.7 Log-Log plots of the creep of vulcanizate 'A' at 60°C and 40% R.H.

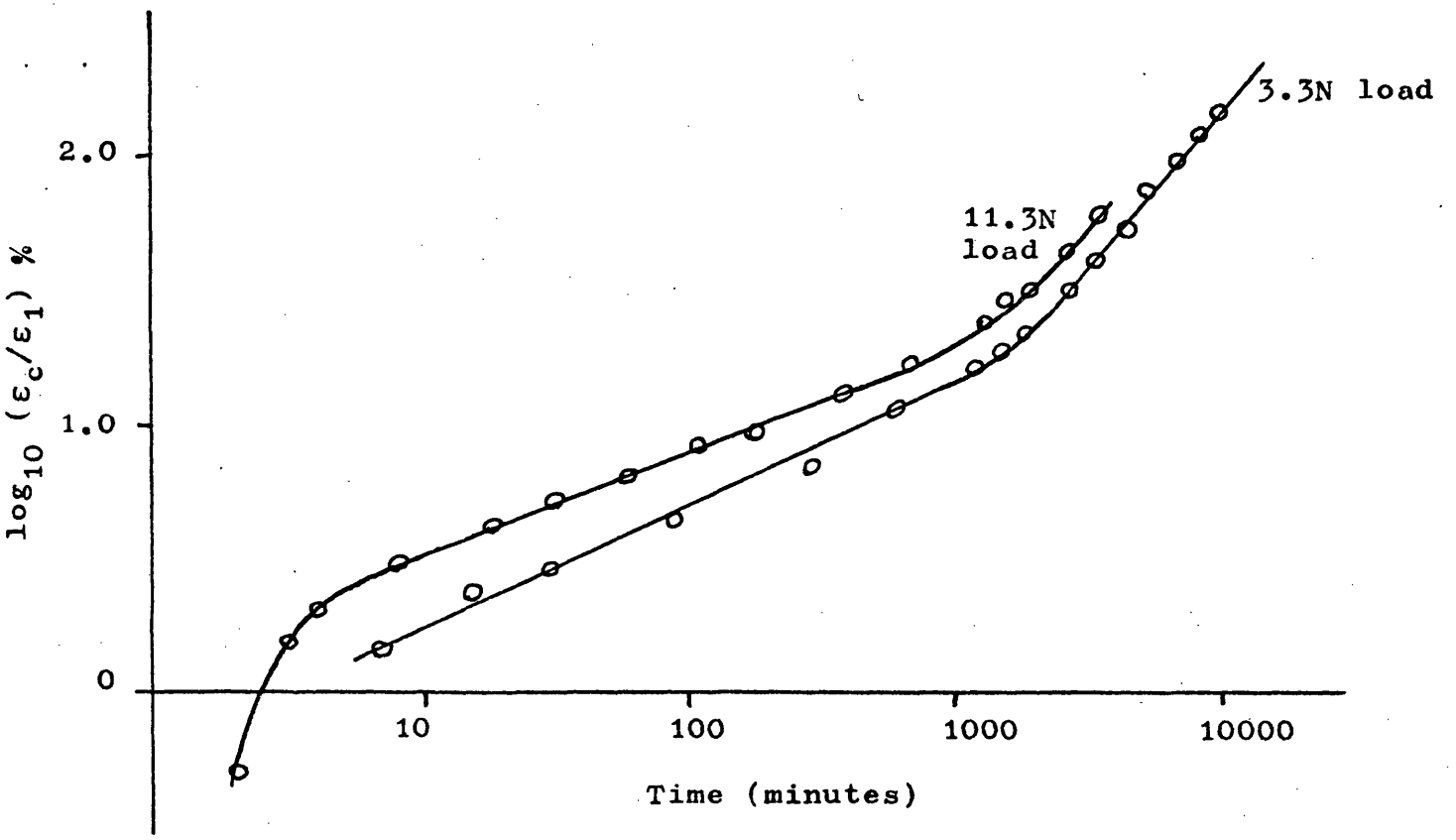

Figure 2.8 Log-Log plots of the creep of vulcanizate 'A' at 80°C and 40% relative humidity.

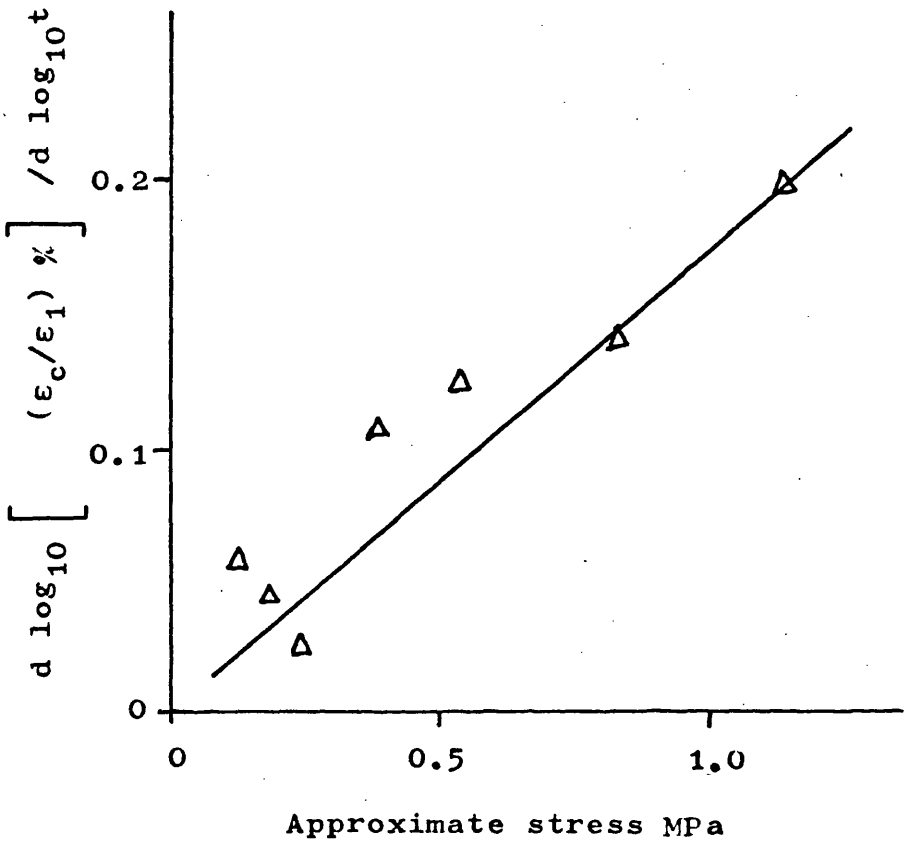

Figure 2.9 Measured gradients of the Log-Log creep curves for vulcanizate 'A' at 10°C and 40% relative humidity as a function of applied stress.

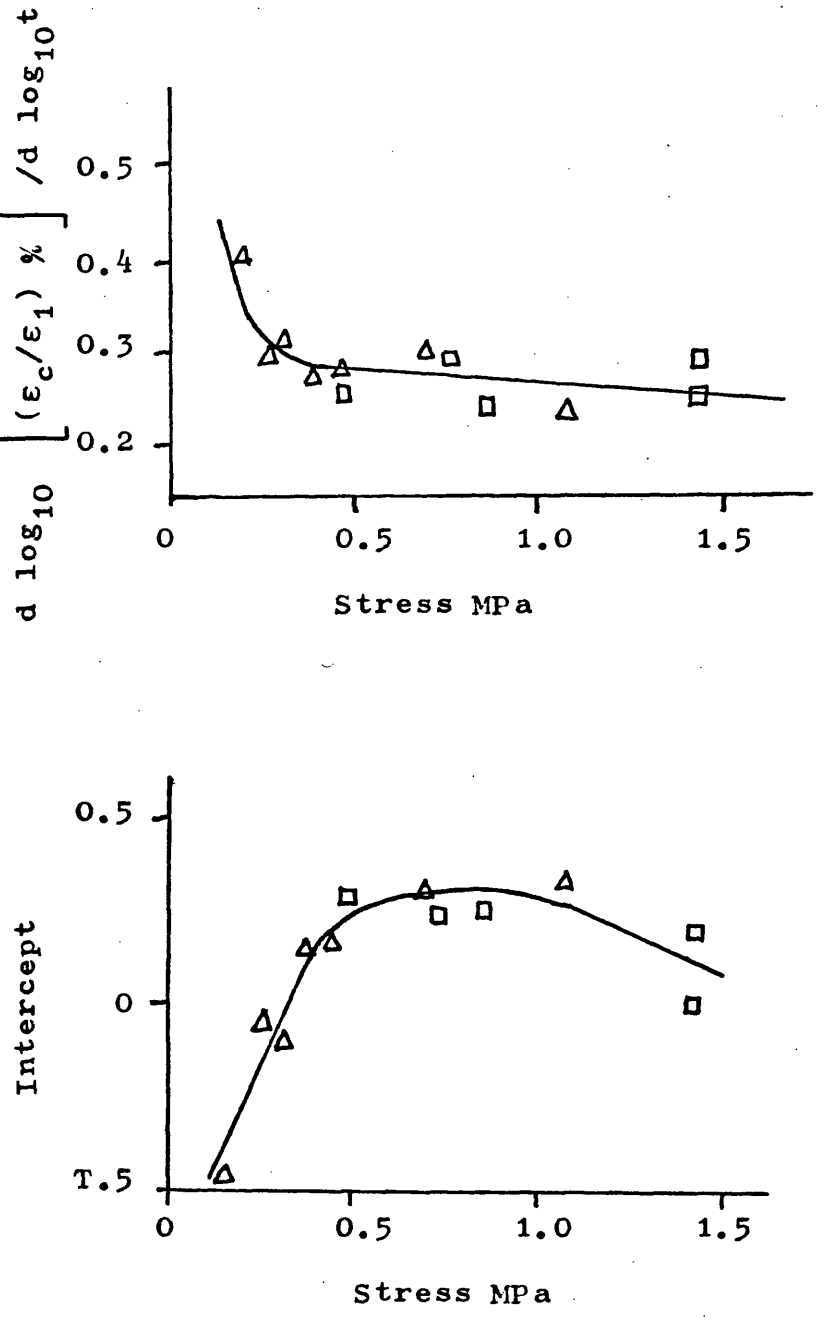

Figure 2.10 Measured gradients and intercepts of Log-Log creep plots for vulcanizate 'A' at 60°C as a function of applied stress.

Δ - 40% relative humidity

□ - oven humidity

may also apply. This comment is of particular importance with regard to the creep of rubbers since the subject has received limited investigation. Figure 2.11 shows a log-log plot for vulcanizate 'C' for comparison and it too has the same general trends. Although this type of plot will not be considered further it is suggested that it may merit some attention with a view to extrapolating data beyond the experimental time scale at low temperatures,(see Chapter 6). This follows from the fact that at moderate temperatures the linear portions of each curve make an excellent fit with observed results at long time periods.

The analysis of creep curves as proposed by Gent and which has been described in Chapter 1 has received the closest attention. In this approach the total creep curve is divided into two components:-

a) An initial region which varies with the logarithm of time and which is associated with viscoelastic behaviour and lower temperatures.

b) A secondary region which varies linearly with time and which is associated with chemical activity in the rubber. This is strongly activated by increasing temperature and becomes dominant at longer times.

The relative contributions of oxidative ageing and sulphur bond lability to this secondary process can however be readily determined. Figures 2.12 to 2.16 show typical results for vulcanizate 'A' represented in this way. Figure 2.12 indicates the difficulty of making

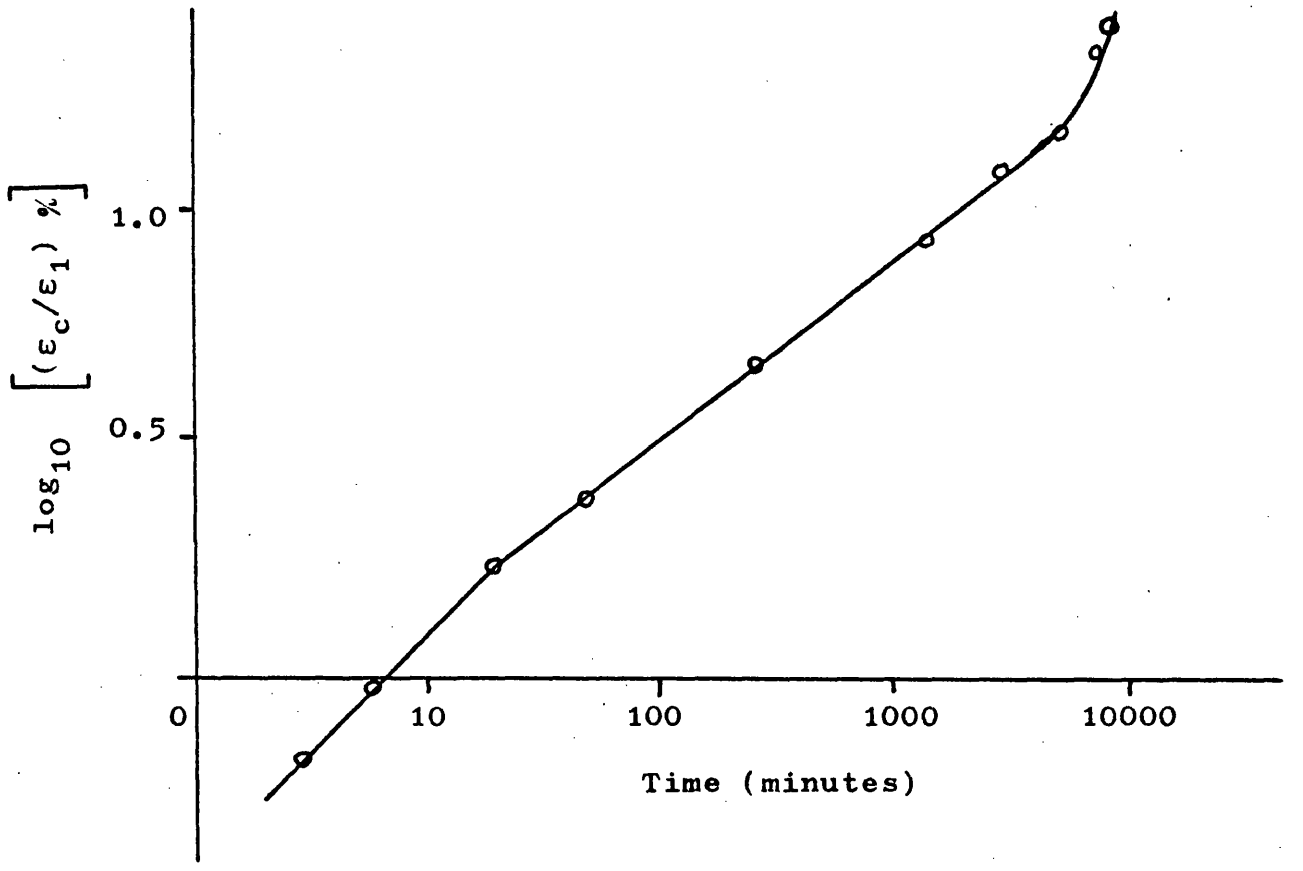

Figure 2.11 Log-Log plot of the creep of vulcanizate 'C' at 80°C and 'oven' humidity.

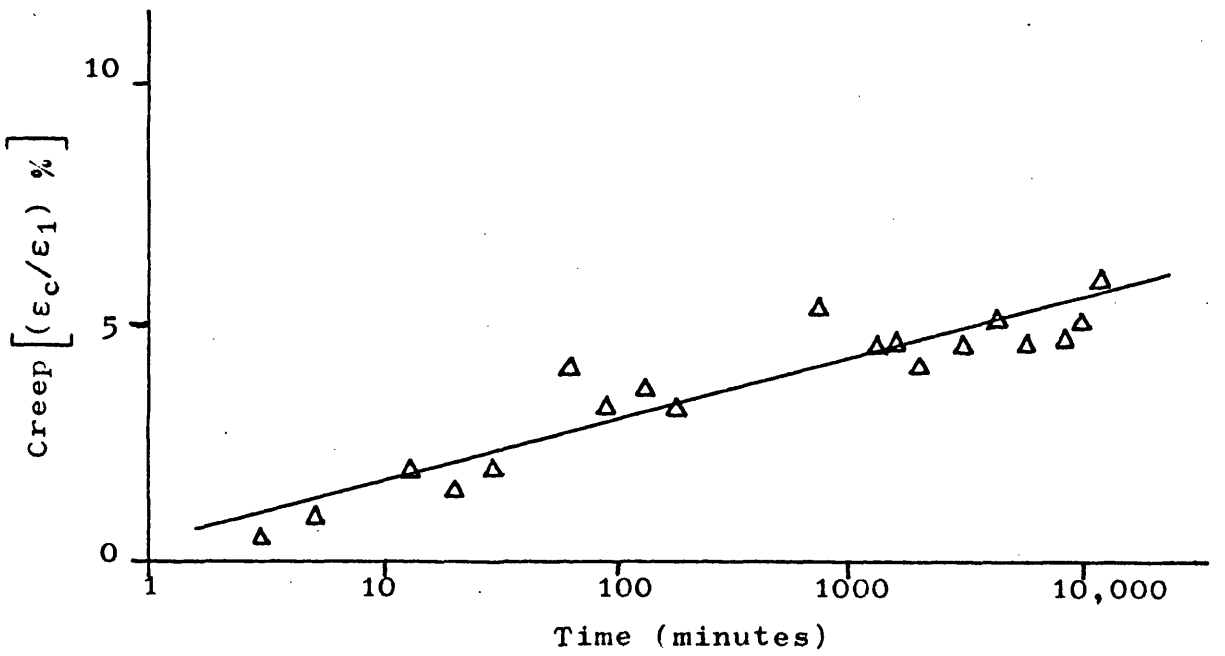

Figure 2.12 Creep of vulcanizate 'A' at 10°C and 40% relative humidity. Applied stress = 180 KPa.

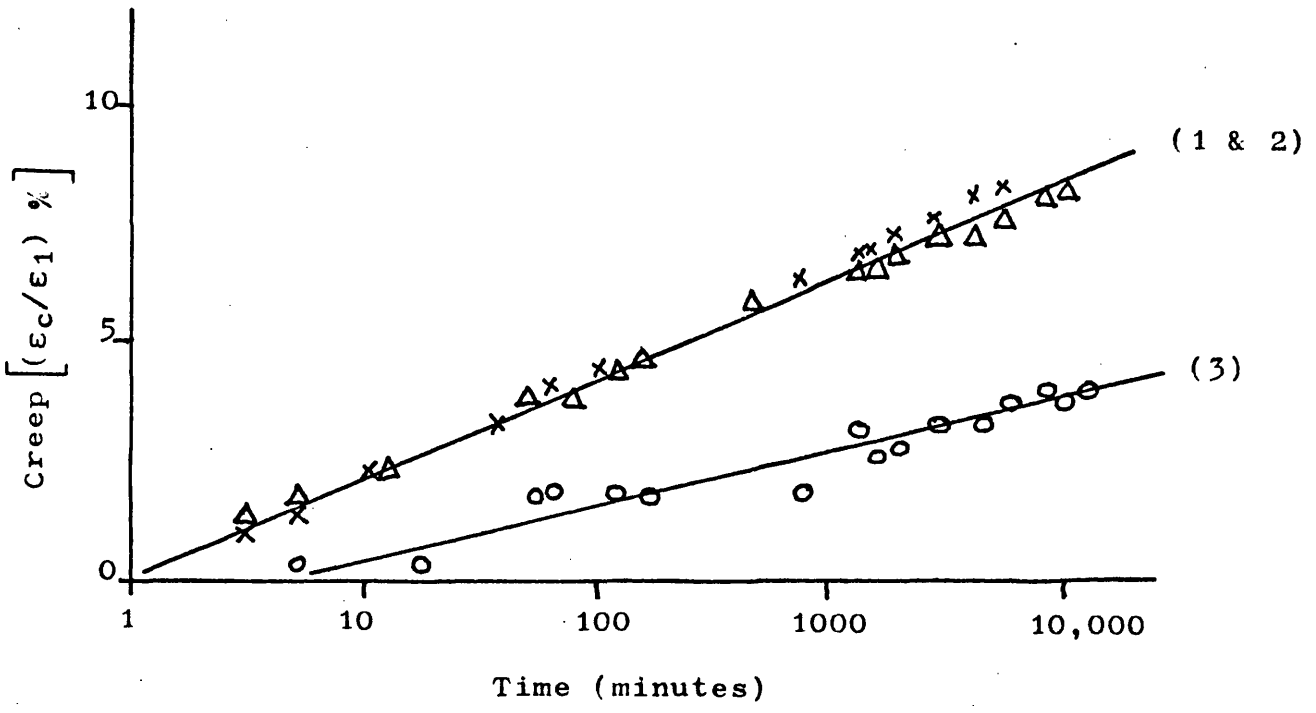

Figure 2.13 Creep curves for vulcanizate 'A' at 10°C and 40% relative humidity.

Applied stress:- (1) Δ 528 KPa

(2) × 725 KPa

(3) o 320 KPa

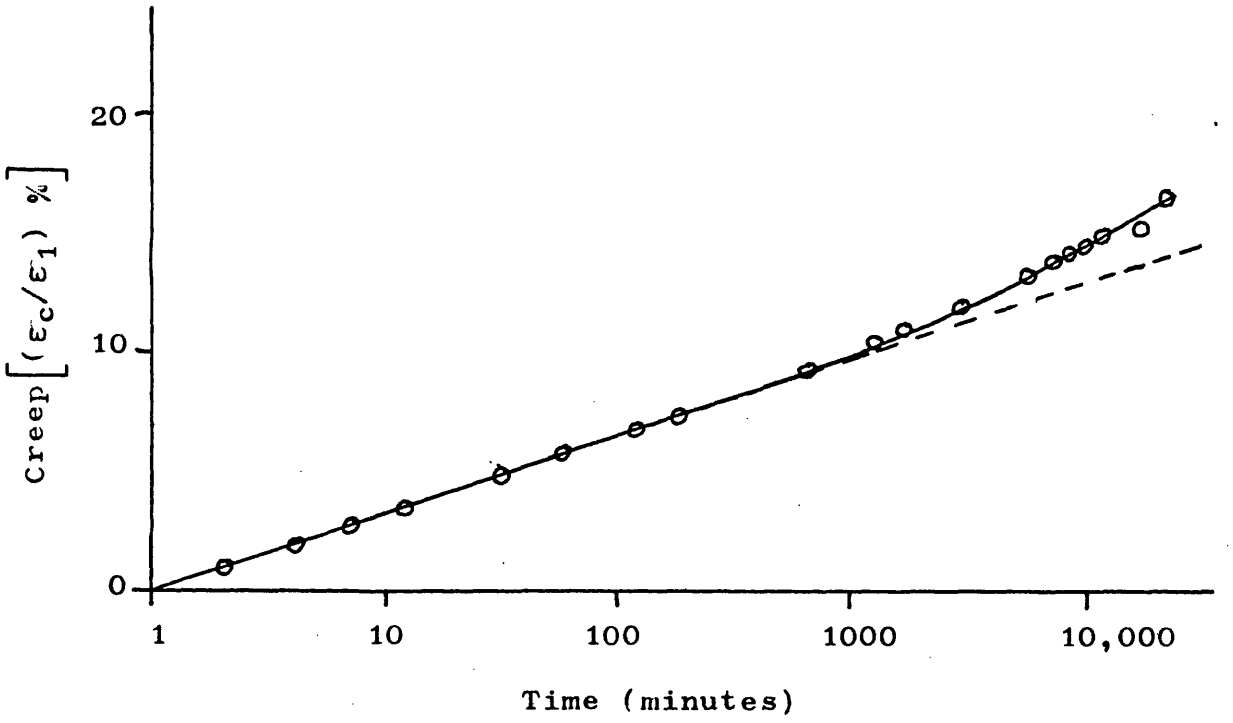

Figure 2.14 Creep of vulcanizate 'A' at 35°C and 40% relative humidity
Applied stress = 1530 KPa.

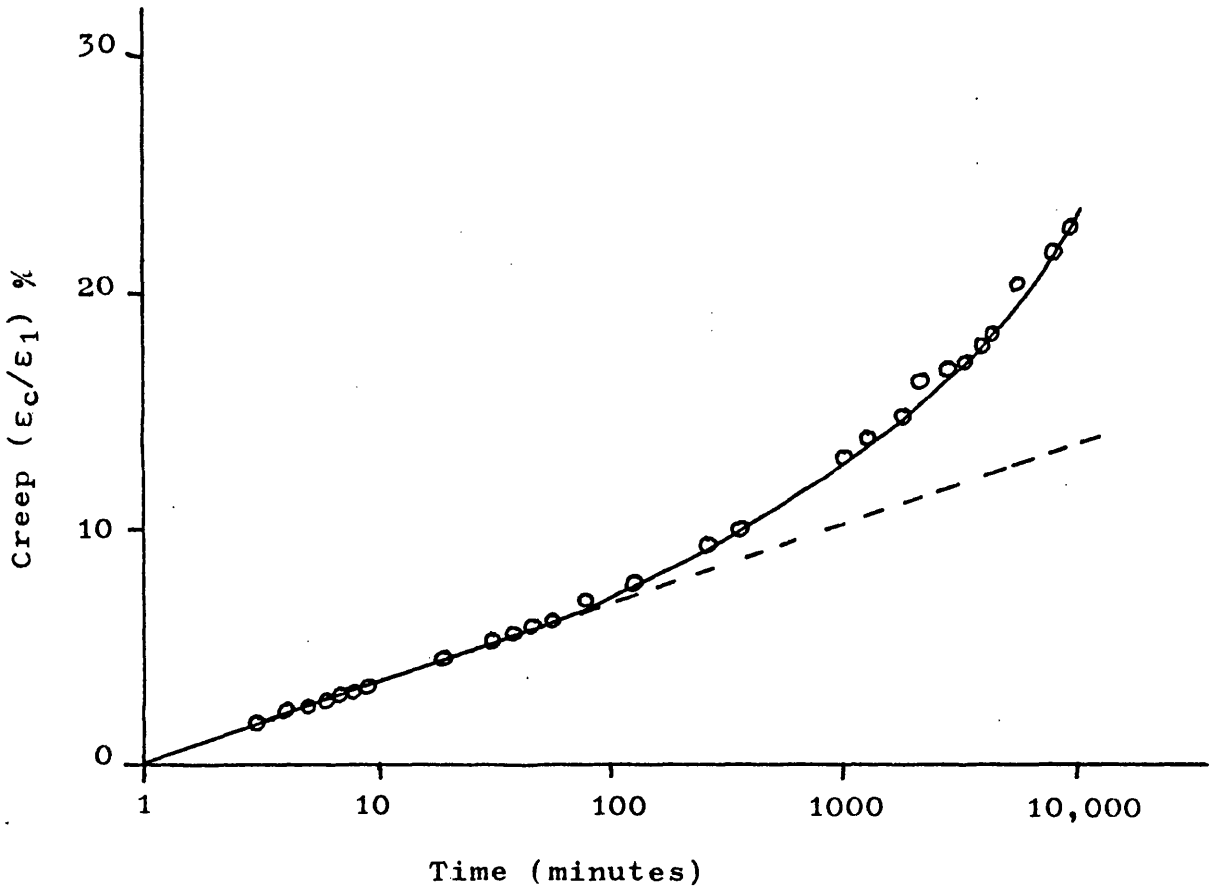

Figure 2.15 Creep of vulcanizate 'A' at 60°C and 40% relative humidity. Applied stress = 1170 KPa.

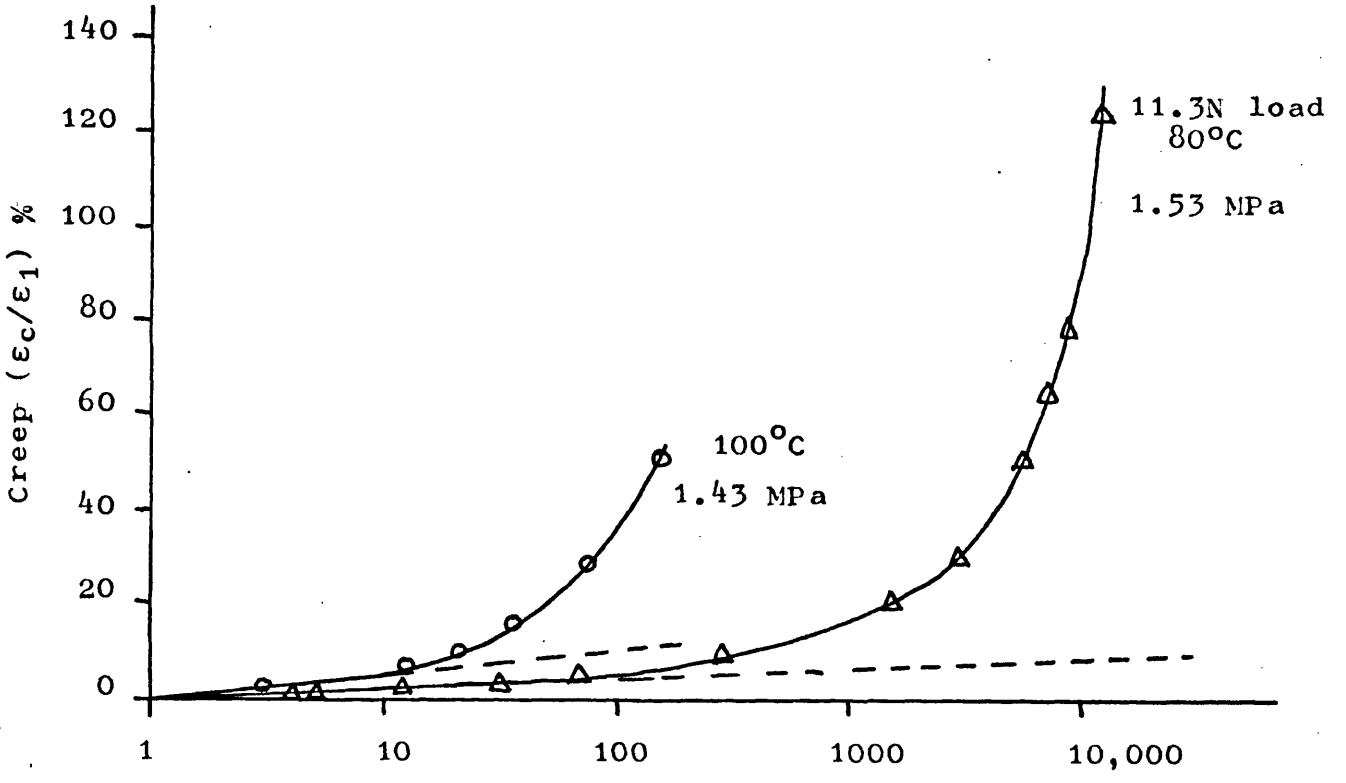

Figure 2.16 Creep curves for vulcanizate 'A' at 40% relative humidity.

accurate creep elongation measurements at low stress and low temperature; the initial elongation of this sample was approximately 11% and the total creep deflection only 0.65 mm over a period of 10^4 minutes. Other curves for moderate stresses are indicated for samples at 10°C in Figure 2.13 where the semi-logarithmic law is seen to hold over long periods. Samples 1 and 2 on this figure are for quite different stresses but the response appears to be almost identical: this results from the use of the $(\varepsilon_c/\varepsilon_1)$ ratio as the ordinate. The onset of a secondary creep process is marked by a breakway from the straight line relationship and an examination of Figures 2.14 to 2.16 indicates that this is greatly influenced by temperature. Indeed, this is particularly clear in Figure 2.17 where the extent of this secondary process is shown as a function of time for various temperatures. The secondary contribution is estimated by deducting the extrapolated logarithmic line from the total creep.

A more detailed discussion of primary and secondary creep contributions as determined from the Gent type analysis will be presented in subsequent chapters.

2.5 The Influence of Humidity on Logarithmic Creep

Derham et al [5-10] have shown that ambient humidity has an influence on the rate of physical creep and stress-relaxation of elastomers, an increase in humidity causing an increase in creep rate, much of their work has been done by following the creep of thin samples immersed in aqueous solutions of certain salts having

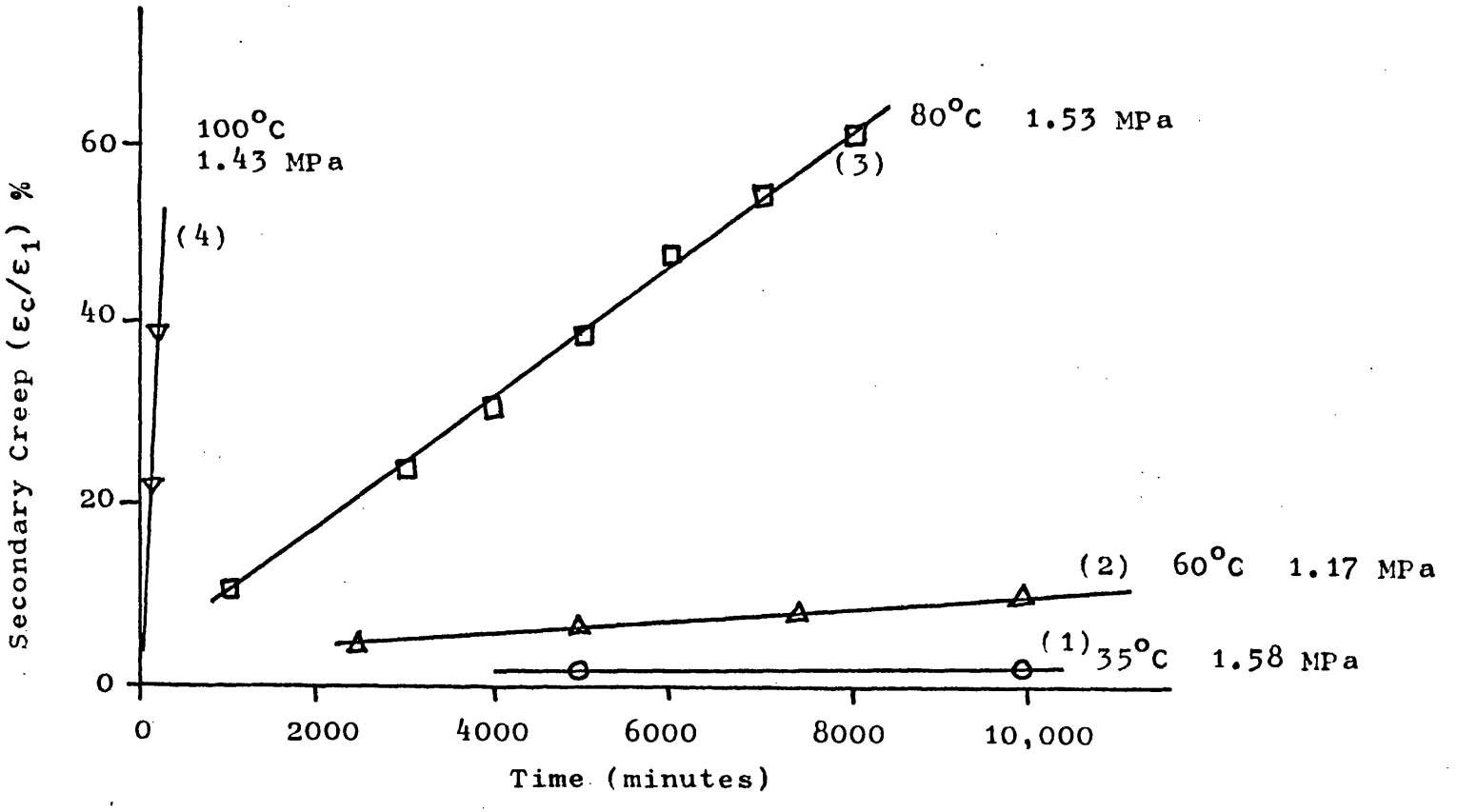

Figure 2.17 Secondary creep for vulcanizate 'A' at various temperatures.

pre-determined vapour pressures. This is theoretically equivalent to subjecting the samples to a gas, eg air, containing water vapour at the same vapour pressure. These workers have also indicated that the modulus of rubber is affected by humidity, a decrease of 5% in modulus being observed as a result of a 80% increase in relative humidity. This is important when creep or stress-relaxation tests are carried out on thin laboratory specimens since a variation of humidity during the duration of an experiment would produce spurious results: the change in elongation resulting from a change in modulus would be misinterpreted as part of the creep response. For thick samples and many industrial products having large cross-sectional areas however the low permeability rate of water in rubber would preclude a significant effect on the creep.

The absorption of water by rubber has been reviewed by Van Amerongen [11] and Barrie [12]. The solubility of water in rubber obeys Henry's law up to an applied relative humidity of about 75% above which the solubility increases disproportionately with humidity. As a result, the one dimensional equation for diffusion into a semi infinite solid can be strictly applied only for absorption from relatively non-saturated atmospheres, i.e. $< 75\%$ saturated. Nevertheless, some simple estimates of the infusion process at $25^{o}C$ will now be considered if only to obtain a general impression of the magnitudes involved. The one dimensional equation can be written [13]:-

$$\frac{C\ (x,t)}{C_o} = 1 - \frac{2}{\sqrt{\pi}} \int_o^{x/2\sqrt{Dt}} \exp - y^2\ dy$$

t = time

D = Diffusion Constant

x = distance from the surface

C(x,t) Concentration of the diffusing species at time t and position x

C_o = Concentration at the surface

It is assumed that C_o remains constant for all t and that C(x,t) = 0 at t = 0 for x > 0. The integral in this equation is the well known error function and the relationship may be re-written:-

$$\frac{C(x,t)}{C_o} = 1 - \text{Erf}\ \left(\frac{x}{2\sqrt{Dt}}\right) \qquad - 2.2$$

Furthermore, the error function values can be obtained directly from tables or may be derived from tables of the better known normal curve which are readily available in most books on statistics. Figure 2.18 has been so derived from equation 2.2 taking $D = 7.8 \times 10^{-13}\ m^2\ sec^{-1}$ (see Appendix 2A) and indicates the long periods associated with the penetration of water into comparatively thin sections, i.e. < 2 cms. Clearly, large industrial products such as bridge bearings would be unaffected by high applied humidities over many years. By comparison the penetration of water into thin laboratory samples is relatively rapid. Consider the samples used in the present experimental programme which had a cross

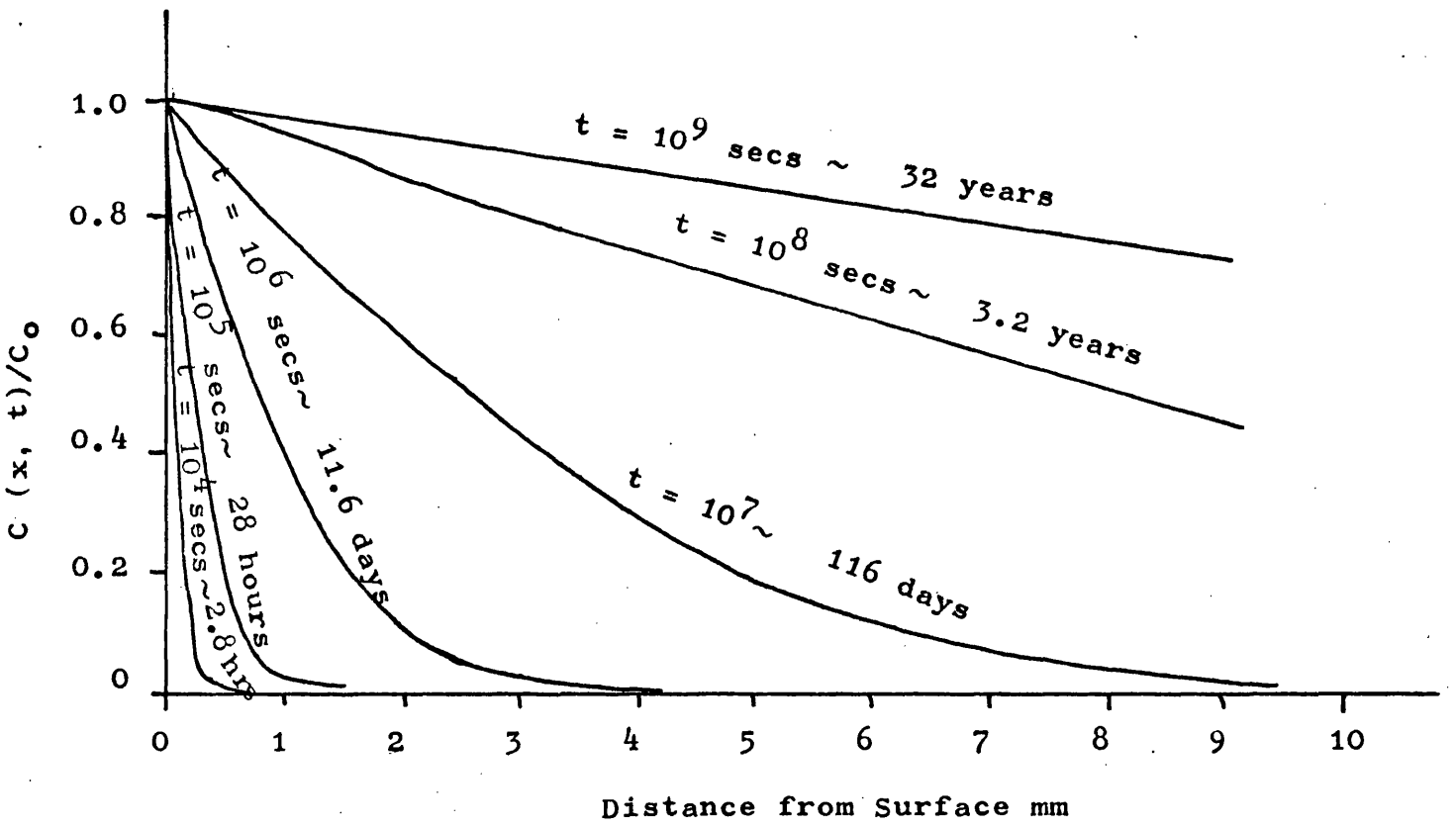

Figure 2.18 Penetration of water into a soft vulcanizate of natural rubber as a function of time and distance. Calculated according to equation 2.2.

section of approximately 4 mm x 2 mm: the maximum distance of any point from the closest surface would be 1 mm. Figure 2.18 shows that the concentration of water at a depth $x = 1$ mm begins to increase after a period of about 10^5 secs, i.e. $\simeq$ 1 day, from the application of water vapour at the surface. Equation 2.2 can therefore be applied to these samples for times up to 10^5 seconds only; beyond that time the rate of concentration increase $(dc/dt)_{x,t}$ at any point x would be more rapid than Figure 2.18 implies. This follows from the fact that water at the sample centreline $x = h$ say is no longer transported to greater distances of x and is therefore not being continuously removed from the zone $o > x > h$. In the present work samples were prepared some one to three months prior to testing during which time they were stored at ambient room conditions. It may be considered therefore that at the beginning of a test they would have been in equilibrium with room humidity; atmospheric relative humidities in the British Isles are usually in the range 70% to 90% [14]. In view of this, experiments at room temperature and below were generally carried out at "oven humidity"; i.e. no attempt was made to control the humidity within the environmental cabinet. At temperatures below 25°C the diffusion constant D would be smaller than that used to derive Figure 2.18 and periodsof several days would have been required for an equilibrium to be achieved. The activation energy for diffusion of water in soft vulcanized rubber is quoted by Barrer [13] as 11.8

KJ mol^{-1}. At higher temperatures creep experiments have been performed both at oven humidity and 40% relative humidity; Figures 2.19 and 2.20 indicate some typical results for vulcanizates 'A' and 'B'. It was found that the logarithmic creep rates for these were indistinguishable which is not surprising in view of the fact that both had the same composition but for the inclusion of antioxidant in 'A'. It is clear from these figures that a transition in creep behaviour occurs in the temperature range 0 to 20°C, a minimum creep rate being observed at about 10 to 15°C. Further it is evident that the creep rate appears to be influenced by humidity for temperatures above this transition zone only. This may not be so however since the test relative humidity of 40% at 20°C is low in comparison to atmospheric humidities whereas at elevated temperatures it represents a high vapour pressure of water. Saturated vapour pressures can be estimated [15] from the formula

$$\log_{10} V.P = \frac{AT}{B + T} + C$$

where VP = saturated vapour pressure in millibars

A = 7.5

B = 237.3

C = 0.78571

T = Temperature in °C.

This suggests for example that the vapour pressure of water corresponding to 40% relative humidity at 35°C is approximately 6/5 times higher than that associated

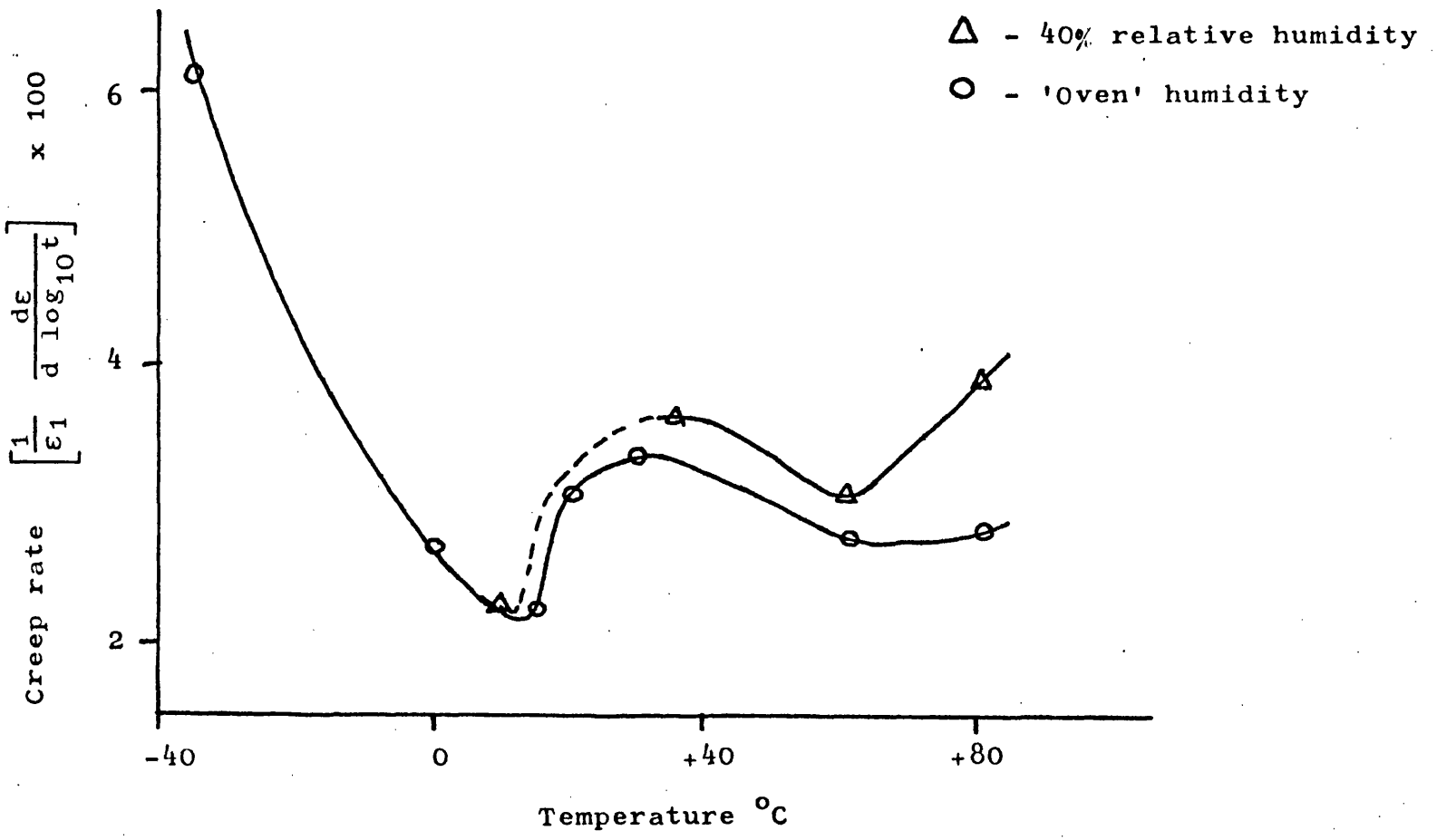

Figure 2.19 Logarithmic creep rates for vulcanizates 'A' and 'B'

Initial strain of ε_1 = 1.0

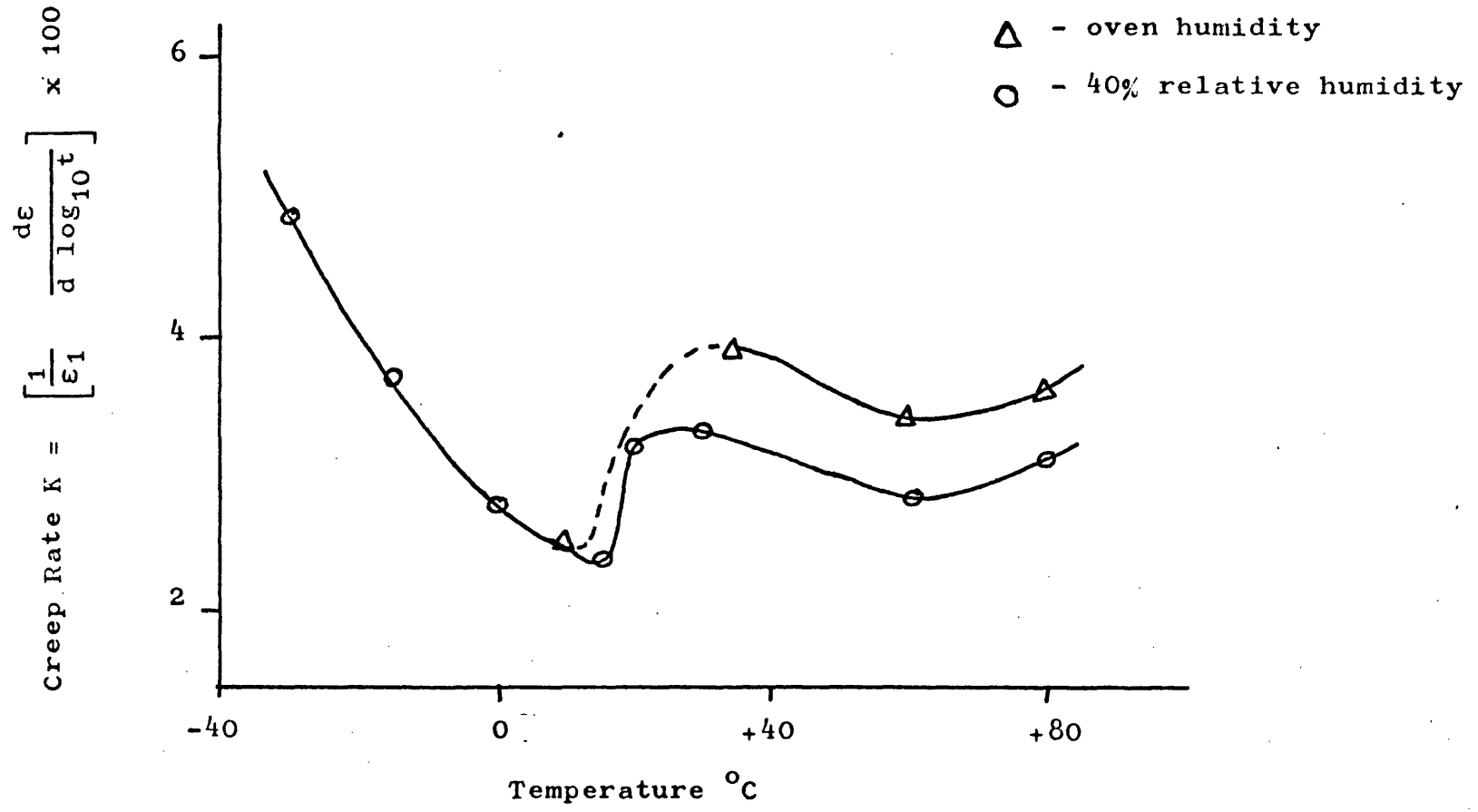

Figure 2.20 Logarithmic creep rates for vulcanizates 'A' and 'B'

Initial strain of ε_1 = 1.50.

with 80% relative humidity at 20°C.

There have been no recent accounts in the literature to explain the effect of humidity on the creep of rubbers but an interesting paper on water absorption has been published by Briggs et al [16]. They introduced abnormally high concentrations of water into rubber by boiling samples in a sealed tube at 160°C. An examination of cooling and heating curves of treated samples led them to propose that water in rubber can exist as droplets which in their case were of one to ten microns in diameter. This corresponded to approximately 10^8 droplets per mm^3 which in turn corresponded with the zinc oxide particle concentration. They suggested that water accumulates in pools around particles of hydrocarbon insoluble impurities, the driving force for absorption being the difference in vapour pressure between the internal solution and external water; i.e. osmosis. This driving force diminishes as absorption proceeds owing to the dilution of the internal solution. They suggested that a balance would be achieved when the osmotic pressure equals the hydrostatic pressure generated by dilution of the cavity and they analysed the situation from a simple mathematical model. This approach is consistent with the general theory of clustering of water in hydrophobic materials [12] and the solubility of water in rubber is known to have a strong dependence on the concentration of soluble or sparingly soluble impurity. Fedors [32] has recently

suggested a failure mechanism for elastomers based on the Briggs concept. He suggested that the osmotic pressure created around inclusions by the infusion of liquids may cause cavities to form and that these should grow to an equilibrium size or contribute to catastrophic failure. This would be particulary so if the inclusions were insoluble in the rubber and could not diffuse out. If similar criteria are applicable to humidity aggravated creep then one would expect that a decrease in water soluble impurity or an increase in modulus of the polymer phase would be mitigating factors. Some evidence for the first comment is derived from the fact that the creep of DCP vulcanizates of natural rubber, which contain no other curing additions such as zinc oxide, is comparatively independent of relative humidity [10].

The influence of water vapour on creep may be due to the formation of weak bonds between rubber molecules. Alternatively an examination of the osmotic pressure concept of water absorption leads to another possibility : consider a rubber sample that has been allowed to come to an equilibrium with the ambient humidity around it. The vapour pressure of water in each microcavity of the rubber would therefore be in equilibrium with the hydrostatic pressure generated in the rubber matrix around it. On application of an external load however the internal "hydrostatic pressure" in the rubber would be decreased and further infusion of water into the sample would follow. In turn this would

generate increased strain concentrations around each water droplet and thus increase the macroscopic creep rate. For this latter explanation the increase in creep rate with humidity would depend on continued infusion of water with time and this would reflect on a dependence on sample cross-section. A simple experiment could thus be performed to ellucidate this point although this has not been done during the present work.

2.6 The Effect of Crystallisation on Creep

Natural rubber is known to crystallise at low temperatures or on straining at moderate temperatures. The kinetics and general behaviour have been reviewed by Bekkedahl[26].

During the present experimental programme it was decided to examine logarithmic creep rates for the DCP vulcanizate 'C' as a function of temperature and applied stress. At low temperatures, however, it was found that samples became non-rubbery after conditioning for 24 hours prior to testing. A specimen conditioned overnight at -30°C for example showed only 5% strain when a stress of 820 KPa was applied and furthermore the subsequent creep was immeasureably small. This is equivalent to a modulus of 16.4 MPa although the observed 100% 1 minute modulus for this vulcanizate at 20°C was only 415 KPa. By comparison at 0°C the relationship between initial extension (1 minute) and applied stress was in agreement with normal rubbery behaviour. The subsequent creep response is illustrated in Figure 2.21 :

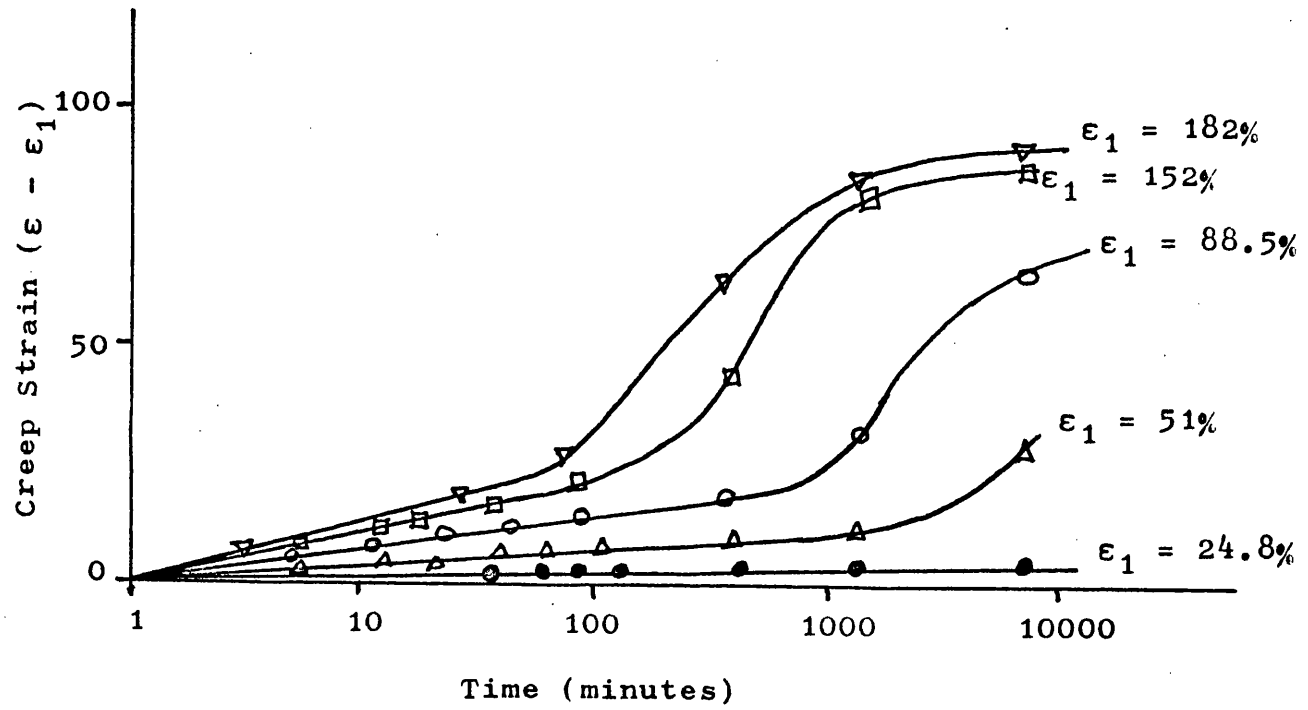

Figure 2.21 Creep response for vulcanizate 'C' at 0°C and oven humidity for various initial strains.

in general each curve represents conventional logarithmic creep followed by an acceleration at times dependent on the applied stress. At the highest stresses full sigmoidal behaviour was observed within the experimental time scale, the creep rate eventually decreasing to a very small value. At the lowest stress only logarithmic creep was observed within the experimental time scale. Examination of Figure 2.21 indicates that all five curves belong to a single family in which the time for the onset of breakaway creep decreases with applied stress. Further, an imaginative comparison of the curves suggests that the total extent of creep resulting from this breakaway process is not strongly influenced by stress.

Wood and Bullman [18] have previously reported breakaway creep behaviour of this type in DCP vulcanizates although they did not observe the decelerating part of the curves within their experimental time scale of about 10^4 minutes. This is not surprising in view of the fact that their test temperature was + 24°C and their initial elongations less than 100%. They observed that their specimens, originally transparent, became milky during the breakaway period and consequently attributed this behaviour to crystallisation of the rubber. The present work lends support to this conclusion; not only was the development of opacity in the samples observed after sufficiently long times at low temperatures but the full sigmoidal curves as shown are symptomatic of phase change kinetics as

described by the Avrami equation [19]. Other workers in this field [20,21] have employed the stress-relaxation technique to determine the development of crystallinity with time. In this case the specimen is held at constant elongation and the decay of stress with time can be related to the volume fraction of rubber transformed. In the creep case however the nucleation and growth of crystals has two mutually opposite effects:- a) an initial increase in strain due to a reduction in the concentration of elastically active chains and b) an increase in modulus resulting from the reinforcing action of crystallites which in turn reduces the rate of subsequent creep. Consequently the creep response resulting from a continuous process of precipitation and growth of nuclei as is envisaged for crystallisation in rubber [22-24] must be considered to be fundamentally complex. For this reason no attempt will be made to analyse the curves of Figure 2.21.

Breakaway creep of the type discussed above has not been observed in other gum vulcanizate examined during the present work within the experimental time scale. The gum vulcanizate 'A' has been tested down to $-30^{o}C$ for moderate periods and for times of 20,000 to 60,000 minutes at room temperature with no evidence of a sigmoidal addition to the logarithmic law. This is in accordance with the established facts that sulphur vulcanizates crystallise less readily than DCP vulcanizates [20] and that crystallisation is further repressed by an increase in cross link density [18,20]. Most of

the other vulcanizates in Figure 2.1 are based on vulcanizate 'A' which is a sulphur vulcanizate with a higher cross link density than 'C'. This is not conclusive proof however that crystallisation has not taken place undetected during creep tests. Gent[25] has suggested for example that the high stress relaxation rates he observed at high extensions for sulphur cured vulcanizates could be attributed to crystallisation. Further he proposed that the creep rate would not be equally adversly effected by this process although he did not prove the point by experiment. Finally Gent proposed that the influence of crystallisation on stress relaxation at room temperature was important only for extensions in excess of 200% whereas in the present work such high extensions have generally been avoided. The increase of creep rate with decreasing temperature for vulcanizate 'A' as shown in Figures 2.19 and 2.20 will be discussed later in this thesis in terms of viscoelasticity. A negligible contribution to the creep response of this vulcanizate from crystallisation will therefore be assumed implicitly and the above discussion is intended to give this some justification.

2.7 Other Contributory Factors

C.S. Kim [4] using thin films of filled polybutadiene has examined creep as a summation of viscoelastic, chemical and surface phenomena. Deformation was followed over time periods of 1000 hours and longer under ambient room conditions. Ultimate fracture was

attributed to crack initiation and propagation as a result of surface reaction with atmospheric ozone. He observed that the time to final fracture was independent of stress over a wide range of stress. This was explained in terms of the known insensitivity of chemical scission rates to stress at moderate elongations and also because of a crack interaction effect. At low stresses a few cracks nucleate and grow unimpeded to a critical length for instability whereas at high stresses many cracks nucleate and mutual stress relief due to interaction restrains any one fissure from becoming dominant. He discussed the effects of surface ozonization and oxidative ageing on youngs modulus and surface energy in terms of Griffith instability and stress concentration factors.

The surface reaction of ozone with rubber has been examined in detail at NRPRA. Andrews and Braden [27] have shown that the reacted layer increases in thickness with time as expected for a process of diffusion with simultaneous complete reaction. If the rubber is unstrained a fine pattern of etch pits, resolveable by electron microscopy, is formed whilst in the strained condition narrow fissures and cracks develop perpendicular to the stress direction. Raab [28] has suggested that the presence of such flaws reduce the time to failure under load in accordance with a viscoelastic process which implies that they would have an accelerative action on the creep response.

With the above factors in mind it was decided to examine the surface of rubber specimens before and after creep testing. Two stage replicas were taken from sample surfaces for examination by electron microscopy. Reasonable success has been achieved using an ordinary bex film replicating technique : bex film was softened by immersion in acetone and applied to the specimen. After drying for two days it was peeled off and a second stage coating of carbon applied to it by evaporation. The bex film was then disolved in acetone leaving the thin carbon film for examination. Shadowing was not employed.

Figure 2.22 shows the surface of vulcanizate 'B' in the as received condition although this appearance is typical of 'A', 'B' and 'C'. The crescent shaped features are difficult to explain but since they all point the same way they could perhaps represent small protrubrances on the specimen surface. Deposition of the second stage carbon film at an angle would then explain the crescent appearance. The interpretation of these pictures must be treated with some caution since the samples were moulded in ordinary steel moulds although these were generally well polished. By contrast Figure 2.23 shows the surface of a sample of vulcanizate 'B' after subjection to 100% strain for 72 hours at 100°C. The crescent features have completely disappeared and instead parallel cracks have developed normal to the strain direction. Similar behaviour has been observed for ozone cracking at room temperature [29].

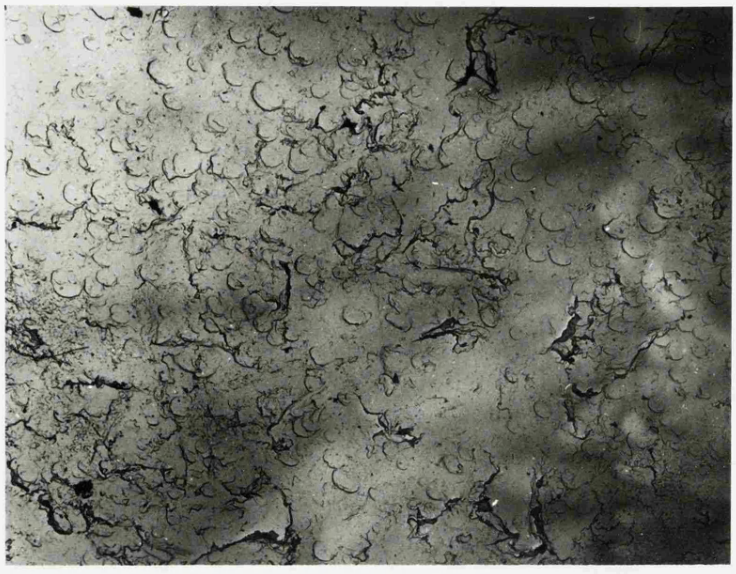

x 1K

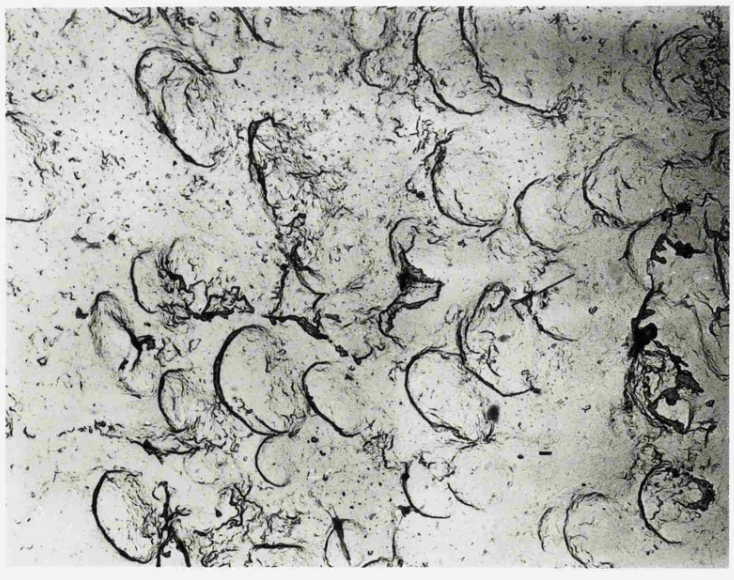

x 4K

Fig 2.22 Surface morphology of Vulcanizate 'B' as received. E-M replicas.

X 1.3K

Fig 2.23 Electron micrograph of a Vulcanizate 'B' specimen subjected to 100% elongation for 72 hours at 100°C

This interpretation of Figures 2.22 and 2.23 is supported by Figure 2.24 which shows a scanning electron micrograph of the surface of a vulcanizate 'A' specimen after heating in an air oven at 100°C for 24 hours. A nodular appearance is indicated although these are some four times larger than for virgin surfaces of the vulcanizate 'B' samples in Figure 2.22.

The high temperature cracking process need not necessarily be attributed to ozone but it will have similar consequences. Figure 2.25, for example, shows the fracture surfaces of two specimens of a commercial black filled rubber mix which failed after several days under creep conditions at 100°C and high applied stresses. Both indicate that failure was by a process of crack nucleation and growth followed by catastrophic failure. In this case however the cracks appear to be associated with voids. Similar two-stage fracture surfaces to these have been reported [30] for fatigue failure in synthetic rubbers.

No significant cracking has been observed for either vulcanizate 'A' or 'B' at room temperature and moderate applied stress ($\varepsilon \leq 200\%$) within the experimental time scale. It is concluded therefore that observed logarithmic creep rates are not significantly influenced by crack formation at low temperatures.

Re-examination of Figure 2.24 shows that the specimen surface has a nodular appearance and further that it is covered by an array of needle-like features.

x IK

Fig 2.24 S.E.M. micrograph of the surface of a Vulcanizate 'A' specimen after ageing for 24 hours at 100°C

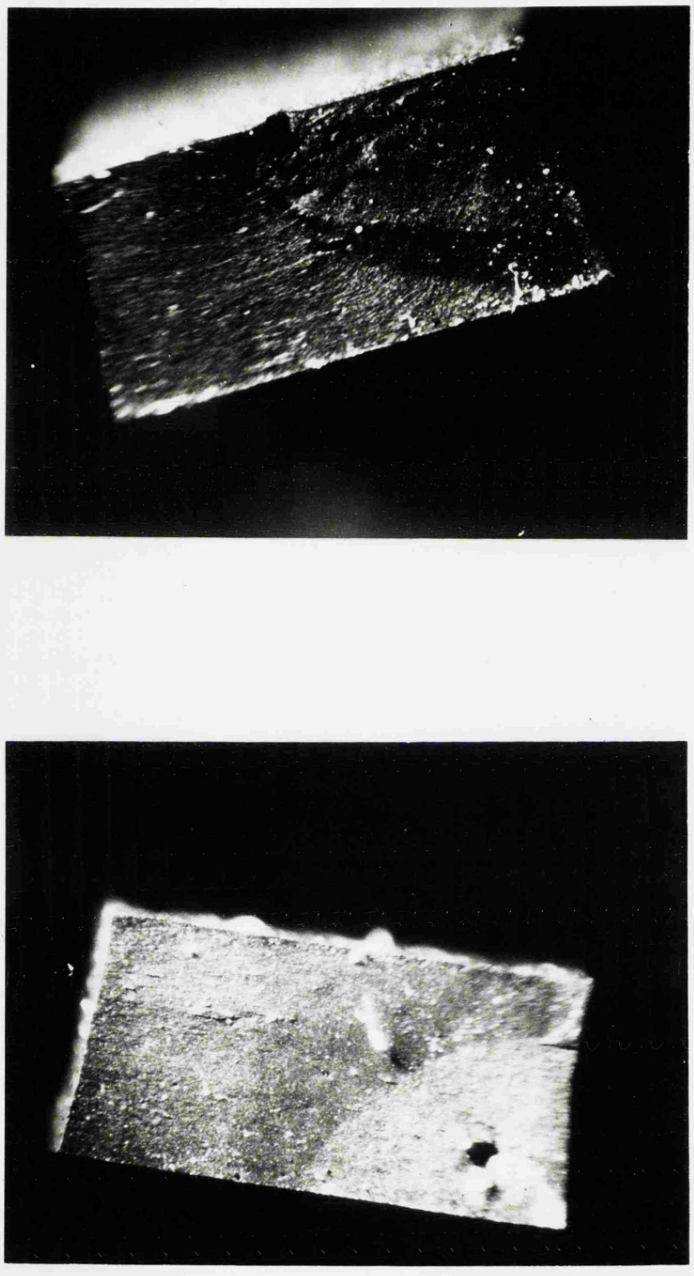

Fig 2.25 Optical fractographs of two commercial Vulcanizate samples which failed during creep at 100°C x 18

Cross-sections of rubber samples were prepared in order to investigate this further. Creep specimens as shown in Figure 2.2 were immersed in liquid nitrogen and fractured by bending. Replicas were prepared from the fracture surface and an example of a vulcanizate 'A' specimen is shown in Figure 2.26. This is relatively featureless but for a few small extracted particles which are probably of undissolved zinc oxide. The curved lines on this picture are thought to be fracture striations on the sample surface resulting from the method of preparation. Scanning electron microscope pictures of similarly prepared surfaces, with a Au-Pd coating, for specimens subjected to 24 hours and 72 hours creep at 100°C (ε_1 = 60%) are shown in Figure 27. These show a nodular appearance similar to that for the surfaces of oven treated specimens. This suggests that these nodules are characteristic of the rubber and not dependent on the method of specimen preparation. No clear evidence for void formation during creep has been observed during these micro-structural studies. Further it is thought that vulcanizates 'A' and 'B' are reasonably homogenious since no evidence of precipitates or excessive solid contents has been found. Figure 2.28 for example shows a replica taken from a commercial rubber mix. The lenticular shaped features are thought to be caused by a precipitation of blending oil during cooling of the rubber from the vulcanization temperature and the small particles are carbon black. Recent work at

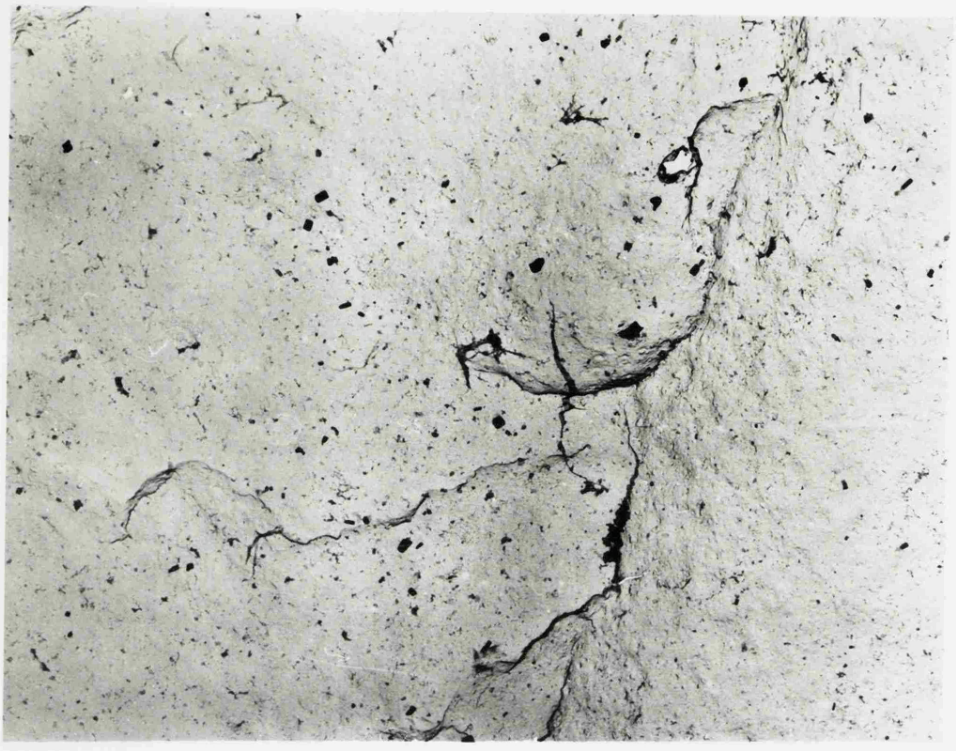

x 3K

Fig 2.26 Fracture cross-section of an as received vulcanizate 'A' specimen, E-M replica.

(a)

X 1K

(b)

X 500

Fig 2.27 S.E.M Fractographs of vulcanizate 'A' specimens after a) 24 hours b) 72 hours creep at 100°C and 60% strain.

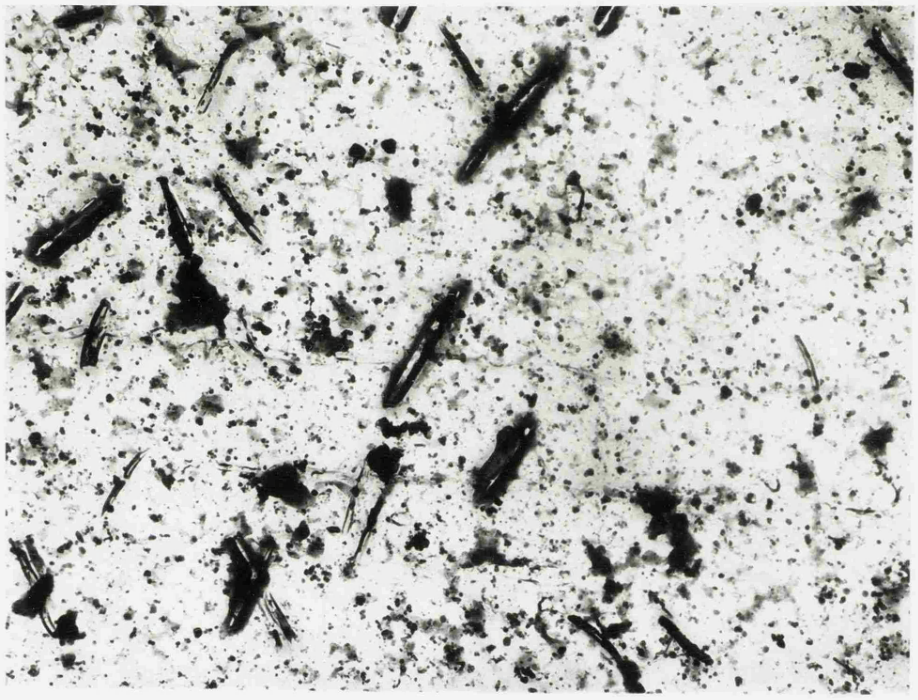

x 5K

Fig 2.28 E-M replica taken from a liquid nitrogen fractured cross-section of a commercial rubber vulcanizate.

MRPRA [31] has shown that insoluble precipitates, particularly zinc soaps, can cause reduced creep resistance.

Appendix 2A

Estimation of D, the diffusion coefficient of water in rubber at 25°C.

A value for D may be estimated from data on permeability and solubility as follows:-

$$D = B/S$$

B = Permeability constant

S = Solubility coefficient

For soft vulcanized rubber at 25°C Barrer [17] quotes values of B between 2×10^{-6} and 3×10^{-6}; his units are CM^3 at NTP sec^{-1} cm^{-3} for a 1 mm thick sample with an applied pressure equal to 1 cm of mercury. Taking an average value of 2.5×10^{-6} of these units and converting gives:-

$$B = 3.29 \times 10^{-13} \quad m^2 \quad sec^{-1} \quad at^{-1}$$

The solubility can be estimated from a graph shown in reference 11 which suggests that rubber disolves about 1% by weight of water at a relative humidity of 75%. At 25°C the saturated vapour pressure of water in air is approximately 24 mm of mercury [15]; i.e. about 24/760 or 3.16×10^{-2} atmospheres. Hence:-

$$S = \frac{\text{wt disolved}}{\text{applied pressure}} = \frac{1 \times 10^{-2}}{3.16 \times 10^{-2} \times 0.75} \quad \frac{gg^{-1}}{at}$$

i.e. $S = 4.22 \times 10^{-1} \quad at^{-1}$.

Using these results

$$D = B/S = \frac{3.29 \times 10^{-13}}{4.22 \times 10^{-1}} \qquad \frac{m^2\ sec^{-1}\ at^{-1}}{at^{-1}}$$

$$D = 7.8 \times 10^{-13} \quad m^2\ sec^{-1}.$$

REFERENCES; CHAPTER 2

1. Laboratory Equipment Digest 9 (11), p 99 (1971).

2. W. N. Findley SPE Journal 16, pp 57-65 (1960).

3. W. N. Findley SPE Journal 16, pp 192-96 and p 198 (1960).

4. C. S. Kim Rubb Chem and Technol 42 (4), pp 1095-1121 (1969).

5. C. J. Derham, G. J. Lake and A. G. Thomas J. Rubb Inst, Malaya 22 (2), pp 191-200 (1969).

6. C. J. Derham, E. Southern and A. G. Thomas NR Technology : Rubb dev supp (1970) No. 7.

7. C. J. Derham, E. Southern and A. G. Thomas Int Rubb Conference, Moscow (1969).

8. C. J. Derham Proc Int Rubb Conference, Brighton (1972).

9. C. J. Derham Proc 3rd MRPRA Rubber in Engineering Conference, London (1973).

10. C. J. Derham and P. B. Lindley Proc 5th Int Conference on fluid sealing. Warwick 1971.

11. G.J. Van Amerongen Rubb Chem and Technol 37 (5), pp 1065-1152 (1964).

12. J. A. Barrie "Diffusion In Polymers" Ch. 8 Ed. J. Crank and G. S. Park Pub. Academic Press (1968).

13. R. M. Barrer Trans Faraday Soc 35, pp 628-43 (1939).

14. "Averages of Humidity for the British Isles". Pub. HMSO (1962).

15. British Standard B.S. 1339 (1965).

16. G. J. Briggs, D. C. Edwards and E. B. Storey Rubb Chem and Technol 36 (3), p 621 (1963).

17. R. M. Barrer "Diffusion in and through Solids." Pub. CUP, Cambridge (1941).

18. L. A. Wood and G. W. Bullman
J. Polym Sci A2 10, pp 43-50 (1972).

19. J. W. Christian "The Theory of Transformations in Metals and Alloys." Chapters 1 and 12. Pergamon Press (1965).

20. A. N. Gent Rubb Chem and Technol 28 (1), pp 36-50 (1955).

21. D. Luch and G. S. Y. Yeh
J. Polym Sci, Polym letters Edn 11 (3), pp 467-86 (1973).

22. E. H. Andrews Proc Roy Soc. London A 277, pp 562-70 (1964).

23. A. N. Gent J. Polym Sci 18, pp 321-34 (1955).

24. D. Luch and G. S. Y. Yeh
J. App phys 43 (11), pp 4326-38 (1972).

25. A. N. Gent Rubb Chem and Technol 36 (3), pp 697-708 (1963).

26. N. Bekkedahl Rubb Chem and Technol 40 (3), pp XXV-XLVII (1967).

27. E. H. Andrews and M. Braden
J. Polym Sci 55, pp 787-98 (1966).

28. M. Raab J. Macromol Sci, phys. B5 (2), pp 285-92 (1971).

29. E. H. Andrews J. App Polym Sci 10, pp 47-64 (1966).

30. R. J. Eldred J. Polym Sci B 10 (5), pp 391-395 (1972).

31. J. Smith 3rd MRPRA Rubber in Engineering Conference London 1973.

32. R. F. Fedors J. Polym Sci, polym letters Ed 12 (2), pp 81-4 (1974).

33. British Standards BS 903 Part A15 (1958).

CHAPTER 3

THE INFLUENCE OF SAMPLE SIZE ON SECONDARY CREEP

3.1 Introduction

The prediction of long term creep behaviour from accelerated laboratory tests is a major object of creep research and the present work is no exception. The influence of oxygen diffusion on secondary creep, its temperature dependence and the effect of sample size are considered in this chapter.

Polysulphide crosslink lability and oxidative scission of crosslinks and network chains are regarded as the principle mechanisms of secondary creep deformation. Peroxide vulcanizates creep therefore as a result of oxidative network degradation only, in contrast to conventionally accelerated sulphur vulcanizates which contain a spectrum of crosslink lengths. Vulcanizate 'A' for example is known to contain monosulphide, disulphide and polysulphide crosslinks of which the latter are associated with the labile interchange process. Coran[1] for example, using stress-relaxation data, estimated that a vulcanizate similar in composition to 'A' contained approximately 40% polysulphide crosslinks. The same order of magnitude was observed by Farmer [2] who used both stress-relaxation and chemical probe techniques, although a discrepancy was observed between the two.

For most conventionally accelerated sulphur vulcanizates, therefore, creep occurs by a combination of oxidative network degradation and polysulphide crosslink interchange. Oxidative degradation may however be more important at low temperatures since scission efficiencies, as defined earlier, are known to decrease with decreasing temperature [3].

Clearly, oxidative degradation is important in determining secondary creep of all types of vulcanizate, even those containing high proportions of polysulphide crosslinks. This must be considered when estimating creep rates for engineering components at room or moderate temperature from the bahaviour of small laboratory samples at elevated temperature. The effect of limiting infusion of oxygen from the surface into bulk rubber requires examination. Carpenter [4] has discussed the significance of oxygen absorption data obtained from ageing experiments on laboratory sized specimens at elevated temperatures to the behaviour of large components at room temperature. He pointed out that the rate limiting process for oxygen absorption could be the rate of the oxygen-rubber reaction or the rate of diffusion of oxygen into rubber. Further, a sufficient difference in activation energies for these processes would result in each being rate limiting in different temperature ranges. An Arrhenius type plot of oxygen absorption rate and therefore of creep rate could thus have an inflection at some critical temperature. As a consequence, erronious estimates of

creep rate at temperatures below the inflection point would be obtained by extrapolation of data collected in an experimental temperature range above the inflection point. Shannin [5] observed that some rubbers become less permeable after ageing and deduced that this would inhibit continued infusion of oxygen. Cuthbert [6] and Derham [7,8] have suggested that large components are protected from oxygen by virtue of their bulk. In particular, Figure 3.1, taken from a recent paper [9], shows that the relaxation rate of a conventional sulphur vulcanizate at 110°C decreases with increasing sample thickness. The relaxation rate for a 7 mm thick sample appears to be about 40% of that for a sample of negligible thickness. The limiting relaxation rate as the sample thickness approaches infinity would depend, according to Coran, on the relative proportion of polysulphide crosslinks.

This chapter is devoted to an examination of the ideas of Carpenter and Derham with a view to estimating the effect of sample thickness from reaction rate and permeability data at various temperatures.

3.2 The Model

The effect of oxygen partial pressure on the stress-relaxation of di-cumyl peroxide cured natural rubber has been investigated by Berry and Watson [10]. They used very thin samples, 0.1 mm, in order to ensure that the infusion of oxygen from the surface did not become rate limiting. Experiments at 80°C on both

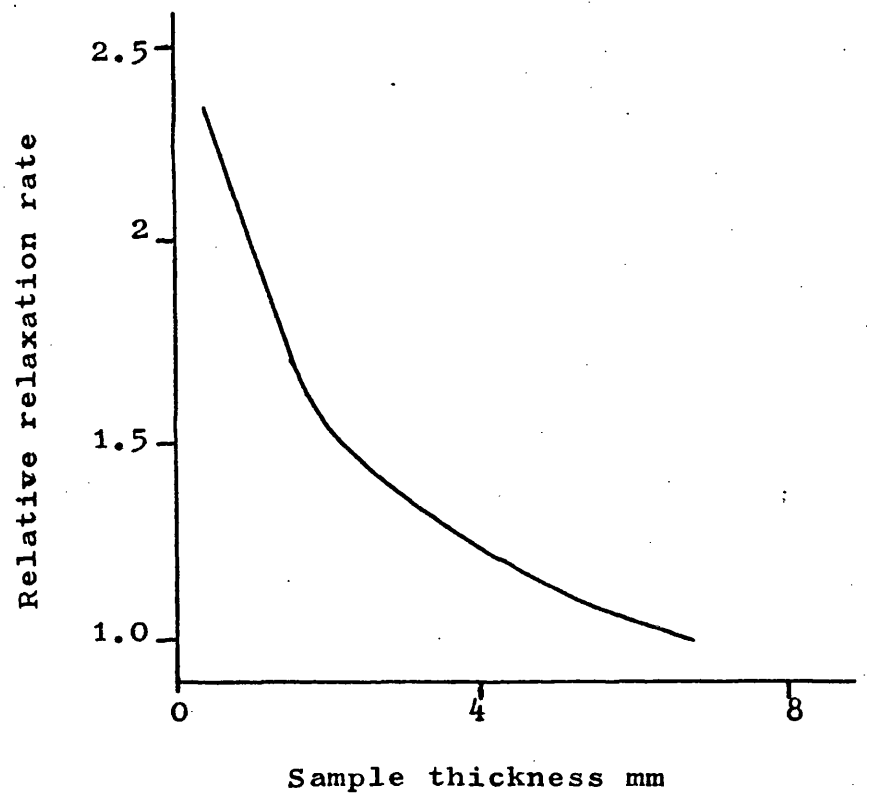

Figure 3.1 Influence of specimen thickness on the relaxation rate of a natural rubber vulcanizate at 110°C. After Derham[9].

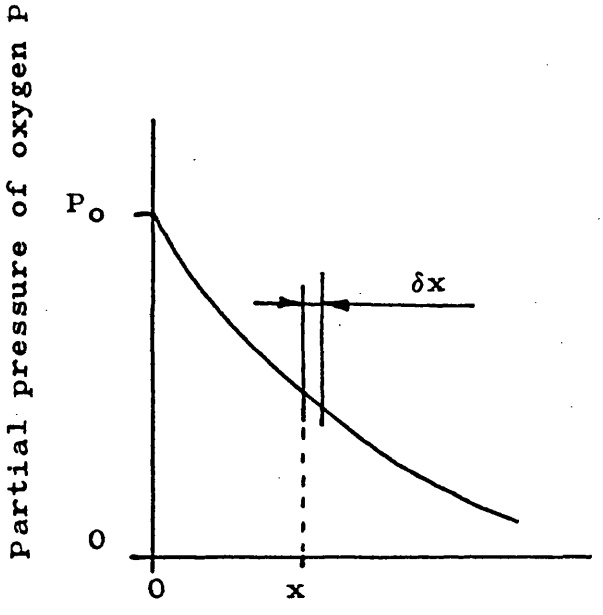

Figure 3.2 A hypothetical pressure profile for the diffusion of oxygen into rubber. 'P_o' is the partial pressure at the oxygen-rubber interface.

purified and antioxidant containing vulcanizates indicated that stress relaxation was independent of oxygen pressure in the range 2 torr to 600 torr. A further reduction in oxygen partial pressure down to 10^{-4} torr reduced the relaxation rate significantly. This reflects established work on the oxidation of polydienes in solution where the rate is independent of oxygen pressure above a limiting value (see Chapter 1). To explain this behaviour a multistep reaction mechanism has been proposed in which the first step involving molecular oxygen is not rate limiting [11]. By contrast at 100°C Berry and Watson found that the relaxation rate was affected by oxygen pressure, increasing by a factor of five in the range 1 torr to 100 torr. Further, they observed that the apparent activation energy for the process was 16.7 K cals mol^{-1} calculated from results at 80°C and 90°C and 10.7 K cals mol^{-1} calculated from results at 90°C and 100°C. They concluded that a change in dominating mechanism occured at about 90°C. Other work shows that the rate of oxidation at 100°C of natural rubber containing antioxidant increases with oxygen concentration. This is consistent with reaction initiation by direct attack of oxygen on the antioxidant [12]. In conclusion, the dependency of oxygen-rubber reaction rates on oxygen partial pressure are not clearly understood. Nevertheless, the behaviour of real vulcanizates probably fall between two extreme cases; either their rate of reaction with oxygen is independent of oxygen pressure above a

critical level or it is proportional to oxygen pressure.

According to diffusion theory, the flux of an element accross a given plane is proportional to its concentration gradient. In the case of gas therefore, since partial pressure is a measure of concentration, this may be expressed as:-

$$\frac{dv}{dt} = - B \frac{dP}{dx} \qquad - 3.1$$

where v = volume of oxygen at STP and B is a permeability constant. Figure 3.2 illustrates a hypothetical pressure profile, i.e. concentration profile, of oxygen diffusing into rubber. The distance from the oxygen-rubber interface is labelled 'x' and 'P_o' is the applied partial pressure of oxygen, usually 1/5 of an atmosphere, the partial concentration in air. Consider an element δx as indicated at a distance x from the surface. The rate of infusion of oxygen into the element is proportional to the pressure gradient, at x. Similarly the rate at which oxygen passes out of the element is proportional to the pressure gradient at $x + \delta x$. Oxygen is thus accumulated within the element at a rate proportional to the change in pressure gradient across it. More precisely, the rate of accumulation is:-

$$\left(\frac{dv}{dt}\right)_{STP} = + B \frac{d^2P}{dx^2} \delta x. \qquad - 3.2$$

per unit cross-section.

For simplicity, steady state conditions only are to be considered. The resulting calculation thus reflects

oxygen penetration after long exposure times. For the steady state situation, the rate of accumulation of oxygen in the segment δx equals its rate of reaction with the rubber within the segment.

$$\text{i.e.} \quad \left(\frac{dv}{dt}\right)_{STP} = K_v \, \delta x \quad \text{per unit cross-section.} \qquad - 3.3$$

where K_v is the rate of reaction of oxygen with rubber expressed in volume of oxygen at STP per unit volume of rubber per unit time. It is assumed that reacted oxygen is immobile and does not contribute to the pressure profile, i.e. that it is removed from the diffusion system. A comparison of equations 3.2 and 3.3 yields:-

$$\frac{d^2P}{dx^2} = \frac{K_v}{B} \qquad - 3.4$$

a) The pressure independent case.

For the extreme case where the rate of the oxygen-rubber reaction is independent of oxygen pressure, K'_v is a constant, K_o say. Assuming that the absorption of oxygen at the oxygen rubber interface is not rate limiting then equation 3.4 can be solved to give:-

$$h_c = (2 \, B \, P_o/K_o)^{1/2} = 1.414 \, (B \, P_o/K_o)^{1/2} \qquad - 3.5$$

See Appendix 3A

Here h_c represents the critical depth to which oxygen can penetrate into an infinite block before being totally consumed by reaction with rubber. Equation 3.5 is dimensionally correct and agrees with logical

considerations. Increased permeability and applied pressure are clearly consistent with increased penetration distance. Conversely, increased reaction rate limits the penetration distance because of more rapid removal of oxygen from the system. Since the rate of reaction, K_o, is constant over the whole penetration depth, h_c, then the total volume of oxygen absorbed by an infinite sheet per unit time is:-

$$Z = K_o h_c = 1.414 \ (K_o \ B \ P_o)^{1/2} \qquad - 3.6$$

where Z = absorption rate, volume of O_2 at STP per unit time per unit surface area.

Consider a freely suspended sheet of rubber surrounded by an oxygen containing atmosphere. Assume its length and width to be large in comparison with $2 h_c$ and in comparison with its thickness. Oxygen absorption would occur therefore primarly in the thickness direction. For sheets of thickness $2 h < 2 h_c$, oxygen penetrates to the sheet centre and the rate of absorption is therefore proportional to the sheet thickness. i.e. The absorption rate is K_o per unit volume of rubber or $2 K_o h$ per unit area of the sheet. Conversly, for sheets of thickness $2 h > 2 h_c$, oxygen penetrates only to a depth h_c from each of the sheet surfaces and the absorption rate is independent of thickness. The rate is in fact predicted by equation 3.6 and is $2.828 \ (K_o \ B \ P_o)^{1/2}$. The effect of thickness is summarized in Figure 3.3

b) The pressure proportional case.

The extreme case where the rate of the oxygen-rubber reaction is proportional to the partial pressure

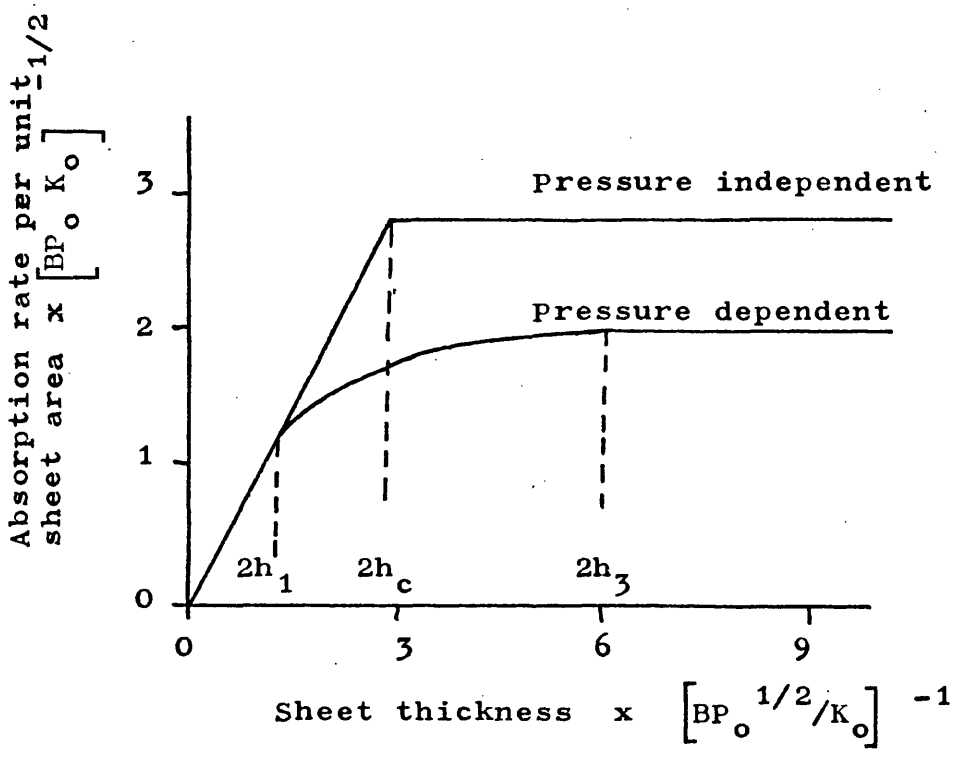

Figure 3.3 Calculated rates of oxygen absorption by a 'large' sheet of rubber as a function of sheet thickness.

h_c = maximum depth of oxygen penetration assuming that the oxygen-rubber reaction rate is independent of oxygen partial pressure.

h_3 = Same, but assuming that the oxygen-rubber reaction rate is proportional to oxygen partial pressure.

$2h_1$ = Maximum sheet thickness for which the absorption rate, per unit volume of rubber, is independent of sheet thickness. Again assuming reaction rate $\propto Po_2$.

of oxygen will now be considered. Here

$$K_v = \frac{K_o}{P_o} \cdot P \qquad - 3.7$$

where K_o is the reaction rate at a pressure P_o. This can be substituted into equation 3.4 to give

$$\frac{d^2P}{dx^2} - \left(\frac{K}{B\,P_o}\right) P = 0 \qquad - 3.8$$

In this case absorption by a large sheet of thickness 2 h will be considered directly. Equation 3.8 can then be solved, as detailed in Appendix 3B, yielding:-

$$2Z = 2\,(K_o\ BP_o)^{1/2}\ \text{Tanh}\ \left[h\left(\frac{K_o}{BP_o}\right)^{1/2}\right] \qquad - 3.9$$

where again Z is the rate of oxygen absorption in terms of volume at STP per unit surface area. This equation is similar in form to equation 3.6 for the pressure independent case, differing only by a factor. Figure 3.4 illustrates the dependence of Tanh (F) on F. Clearly Tanh (F) $\simeq$ F for small values of (F), indeed up to F $\simeq$ 0.6. Hence for $h\,(K_o/B\,P_o)^{1/2} < 0.6$, equation 3.9 can be modified to read

$$2Z = 2(K_o\ BP_o)^{1/2}\ h\ (K_o/BP_o)^{1/2}$$

$$= K_o h \qquad - 3.10$$

This is identical to the pressure independent case and implies that the rate of oxygen absorption is proportional to the sheet thickness for sheets up to a critical thickness $2h_1$ where

$$h_1 = 0.6\ (BP_o/K_o)^{1/2} \qquad - 3.11$$

i.e. The rate of oxygen absorption is not diffusion

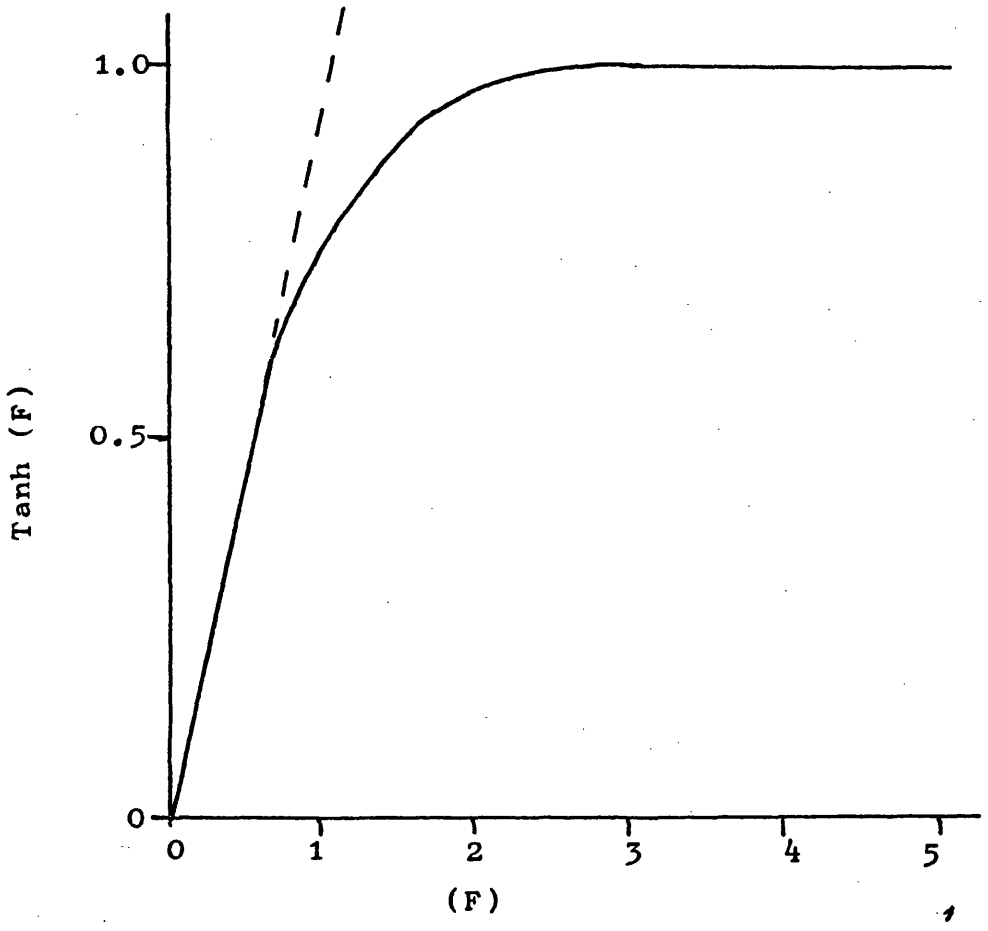

Figure 3.4 A comparison of (F) and Tanh (F)
Note that F $\simeq$ Tanh (F) for F $<$ 0.6
Tanh (F) = 0.995 at F = 3.0.

limited for sheets of thickness $2h < 2h_1$. This is in agreement with established data for a filled natural rubber containing an amine-type antioxidant at 100°C [12], where the rate of oxygen absorption per unit volume of rubber was extremely sensitive to applied pressure but almost independent of sample thickness within the range 0.013 ins (0.33 mm) to 0.039 ins (0.99 mm). Further, equation 3.11 is similar to equation 3.5 for the critical depth of oxygen penetration for the pressure independent case, again differing only by a factor. Other critical thicknesses can be derived from Figure 3.4. Tanh (F) varies within the limits $o < \text{Tanh } F < 1.0$. When F equals 3.0, tanh (F) equals 0.995 approximately which is very close to 1.0. According to equation 3.9 therefore, the rate of oxygen absorption by a sheet of half thickness $h\,(K_o/BP_o)^{1/2} = 3.0$ or $h = 3.0\,(BP_o/K_o)^{1/2}$ would be 99.5% of that for a sheet of infinite thickness. Consequently the maximum depth of oxygen penetration can be considered to be h_z where:-

$$h_3 = 3.0\,(BP_o/K_o)^{1/2} \qquad - 3.12$$

By comparison, a sheet of rubber of half thickness $2h_c$, the critical thickness for the pressure independent case, would absorb at a rate equal to 89% of that of an infinite block. This is obtained by substituting h_c as obtained from equation 3.5 into equation 3.9, i.e. $F = 1.414$. Again the effect of specimen thickness is summarized in Figure 3.3.

3.3 Experimental Details

Expressions have been derived for certain critical depths of oxygen penetration into rubber in terms of permeability and reaction rate. The experimental assessment of these quantities will now be described.

a) Measurement of Reaction Rates

This was achieved by oven ageing experiments. Dumbell shaped creep specimens, as illustrated in Figure 2.2 were stamped from rubber sheets of thickness 0.6 mm, 1.8 mm and 3.1 mm. Each specimen was threaded at one end with a short length of stainless steel wire bent into the shape of a hook by which means it was freely suspended in an air oven. The oven temperature was thermostatically controlled and monitored independently by intermittent thermistor readings. Air circulation within the oven was affected by means of a fan. The hole in the top of the oven, normally provided for the insertion of a mercury thermometer or other equipment was left clear in order to preclude changes in the oven air composition. The specimens were removed periodically and allowed to equilibriate with ambient room conditions for one hour. They were then weighed and reinserted into the oven. Sample weight was thus determined as a function of ageing time. A Mettler balance sensitive to $\pm 10^{-5}$ grms was used. The time lapse between removal from the oven and weighing was found to affect the result. In general, samples increased in weight with standing time, probably due to the absorption of water vapour from the atmosphere. The

rate of weight change, however, was negligible after one hour. Typical ageing curves for vulcanizates 'A' and 'B' are illustrated in Figure 3.5. Both show a rapid initial weight loss due to the evaporation of volatiles, principally absorbed water, remnants of the curing system and low molecular weight constituents of the rubber. In particular, initial weight losses for vulcanizate 'A' exceed those for 'B' by about 1% due, presumably, to the volatalisation of antioxidant and products of the antioxidant-oxygen reaction. i.e. Vulcanizates 'A' and 'B' are identical in composition but for the addition of 1.5 pphr antioxidant to 'A'. It is not proposed to discuss the shape of the ageing curves in terms of oxidation mechanisms, the involvements of autocatalytic kinetics and the effect of inhibitors. The major portion of the ageing curves, however, especially at lower temperatures, show an approximately linear increase of weight with time. This is attributed to the absorption of oxygen from the surrounding atmosphere. For thin samples the rate of absorption equals the rate of reaction of oxygen with rubber. This includes reaction with the rubber network and with extra network material including inhibitors. At ageing temperatures over 100°C the rate of oxygen absorption decreased towards the end of the experimental time scale. This is more evident at high temperatures and specimens aged at 120°C never show their full absorption potential because of the formation of a hard, brittle, impervious layer at the specimen

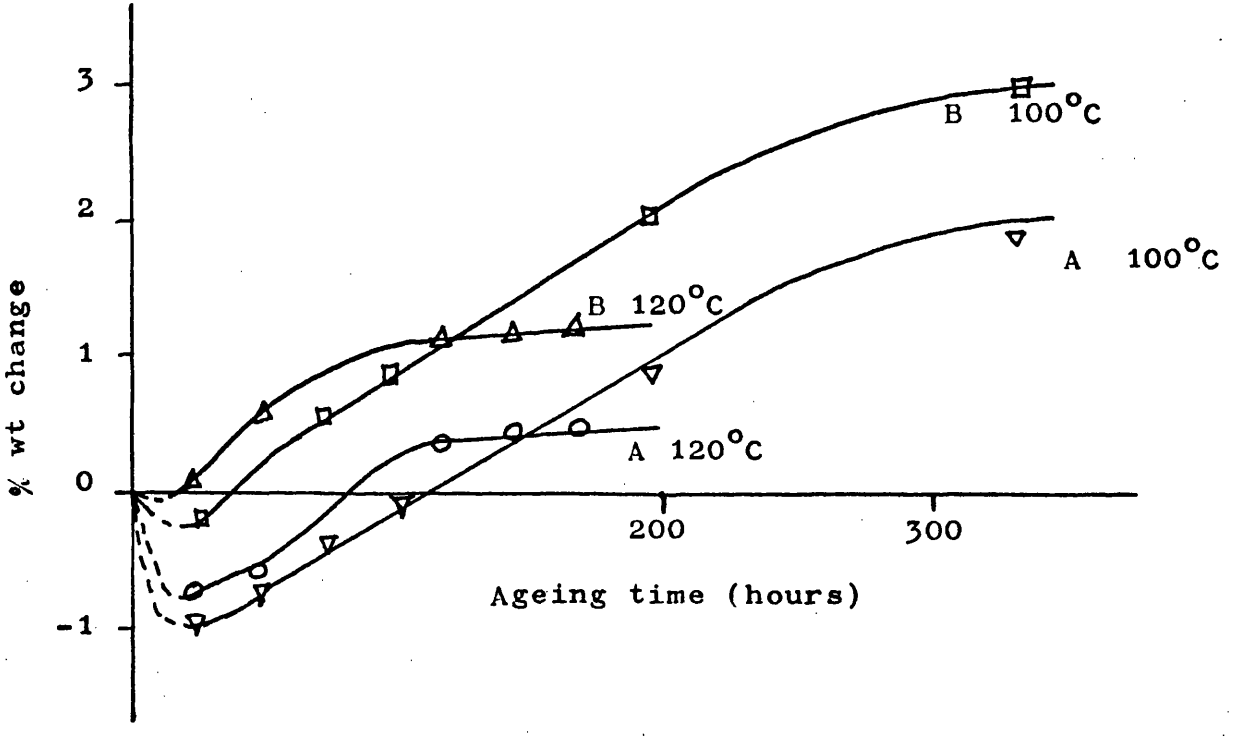

Figure 3.5 Observed weight changes during ageing. Vulcanizates 'A' and 'B' at 100°C and 120°C as shown. Specimen thickness ~1.8 mm.

surface. Continued infusion of oxygen is thus prohibited. This is illustrated in Figure 3.6 which shows fractured cross sections of two vulcanizate 'B' specimens aged at 120°C for 200 hours. It shows hard, brittle and darkened surface layers approximately 0.5 mm thick, surrounding soft rubbery interiors. Further inspection of Figure 3.5 shows that the ageing curves for vulcanizates 'A' and 'B' are very similar, being for the most part vertically displaced from each other according to the relative extents of initial weight loss. Indeed it is proposed that both vulcanizates absorb oxygen at approximately the same rate. Further that this rate is independent of time prior to hard layer formation, the initial non linearity of the curves being a result of two competing processes - oxygen absorption and volatile loss. For experimental convenience most subsequent ageing tests were carried out using vulcanizate 'B' only so that the linear portions of the curves were observed more clearly at shorter times due to the lower initial weight loss.

In order to assess the influence of stretching the rubber on oxygen absorption rate, a metal frame was constructed in which specimens could be held at constant elongation during ageing tests. Results are indicated in Figure 3.7. Within experimental error, the linear rate of weight gain for 1.8 mm thick specimens at 80°C was independent of elongation for the range of strain 0% to 130%. This implies that the rate is not limited by absorption at the surface for specimens of

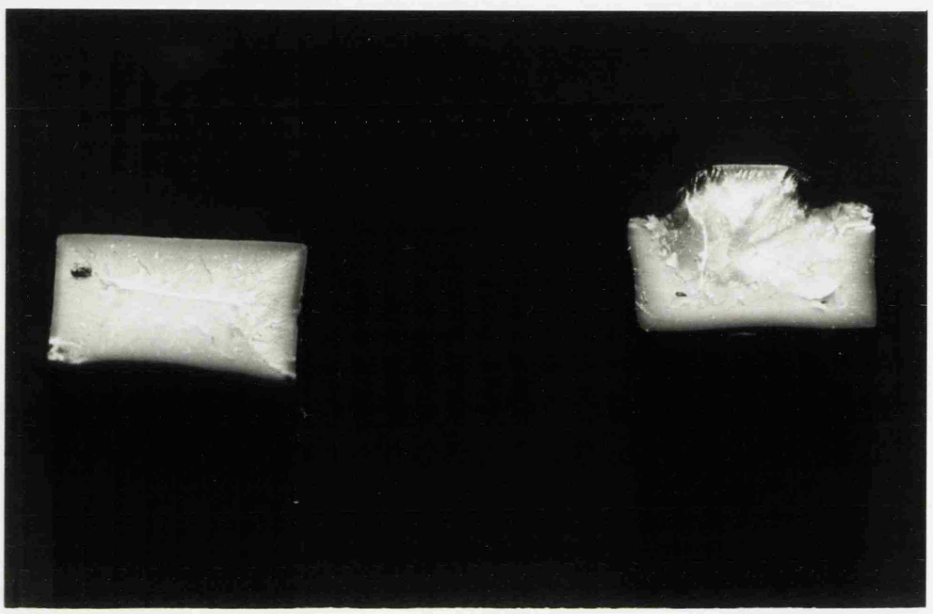

X 8

Fig 3.6 Fractured cross-sections of two vulcanizate 'B' samples after ageing for 200 hours at 120°C. Note the darkened hard layer at the surfaces.

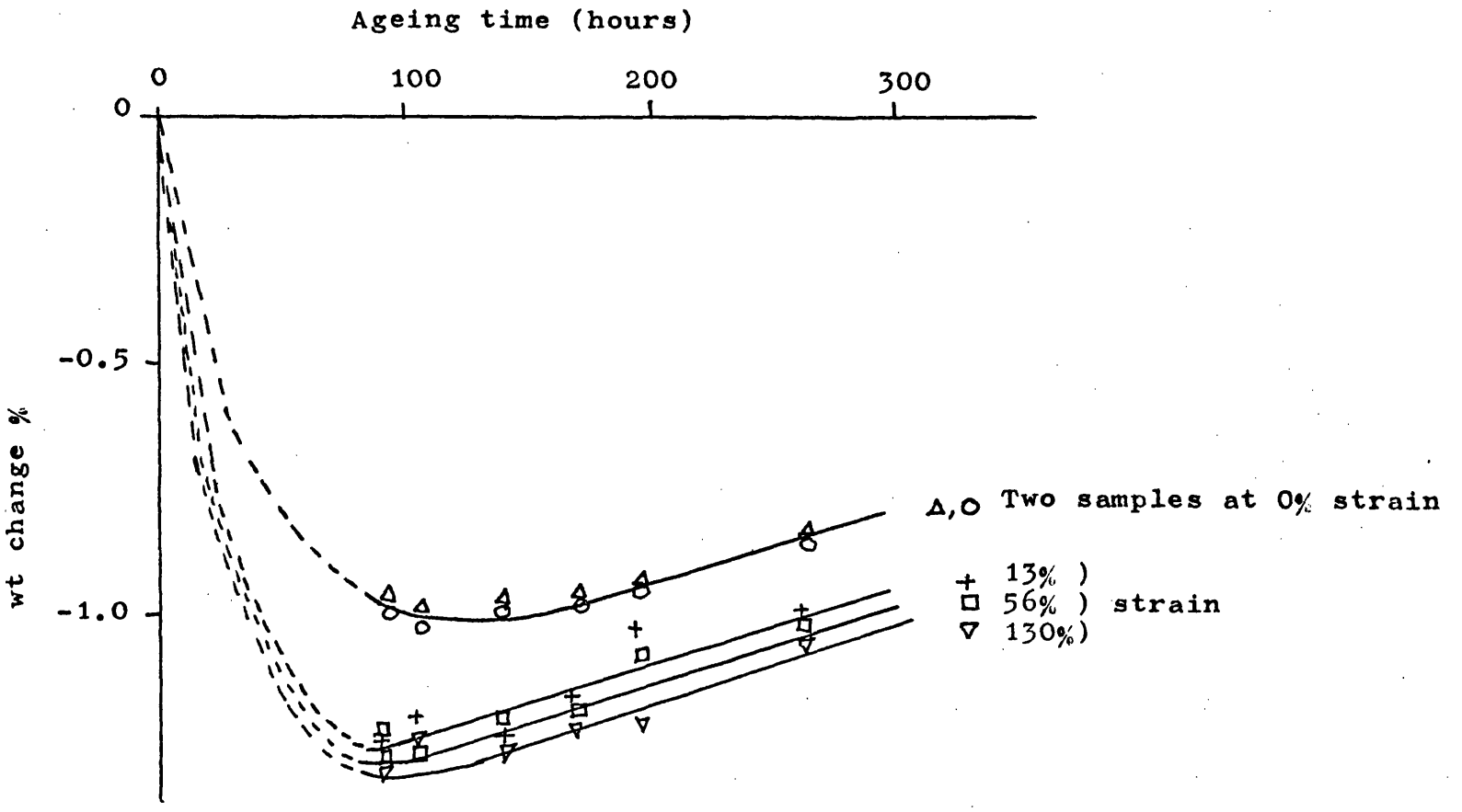

Figure 3.7 The influence of imposed strain on the ageing behaviour of vulcanizate 'A' at 80°C. Unstretched specimen thickness ~1.8 mm.

this thickness and at this temperature since surface area increase with elongation according to the square root of the elongation ratio. In this case an increase of 52% in area at a strain of 130%. Similarly, inward diffusion of oxygen into the sample cannot be rate limiting since specimen thickness and hence maximum diffusion distance decrease with elongation. In this case, at a strain of 130%, specimen thickness is reduced to 66% of that of an unstretched specimen. By comparison, consideration of the effect of strain on the initial weight loss process suggests that the rate of loss of volatiles is dependent on their diffusion to the surface. Finally, strain in the molecular chain network does not appear to have a significant effect on the rate of reaction of oxygen with rubber. Reaction rate measurements obtained for unstretched samples are therefore applicable to rubber components strained under conditions of creep or stress-relaxation.

No meaningful ageing results were obtained for the peroxide vulcanizate 'c' which showed continued weight loss over extended periods. This is illustrated in Figure 3.8. During ageing, these specimens degraded, became increasingly less rubbery and were eventually unable to support their own weight. Both weight loss and degradation were accelerated by increasing temperature. Mass spectroscopic analysis indicated that the volatiles responsible for the weight losswere predominantly breakdown fractions of dicumyl peroxide.

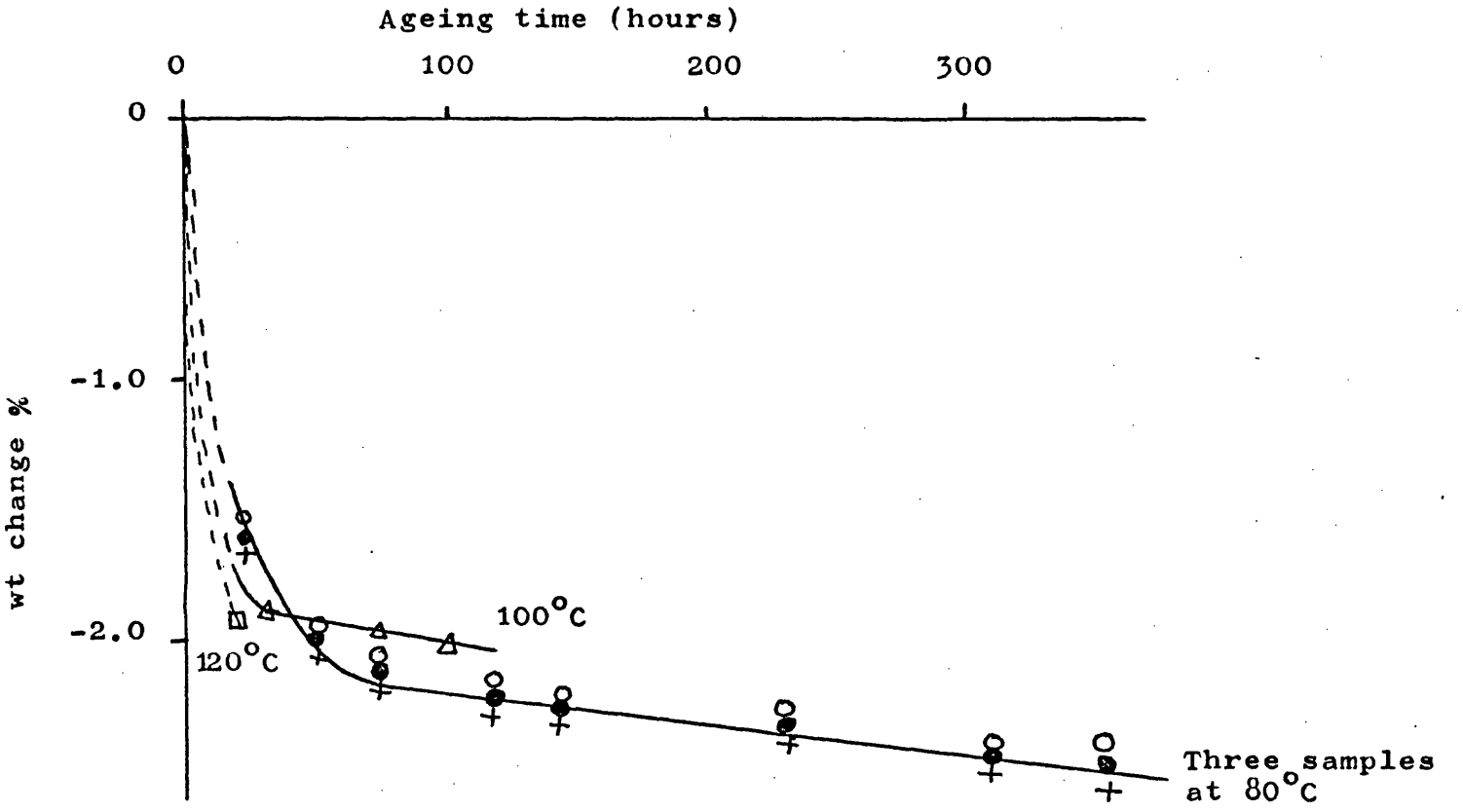

Figure 3.8 Ageing curves for the DCP vulcanizate 'C' at temperatures shown. Sample thickness ~ 1.8 mm.

Typical ageing curves for vulcanizate 'B' are shown in Figure 3.9. All show an approximately linear increase of weight with time over an extensive range, a 2.5% weight gain being observed within the experimental time scale for the sample at 100°C for example. This represents about 15 years ageing time at room temperature and weight gains in excess of 2.5% may be possible. The curve at 111°C shows how the rate of oxidation is suddenly reduced by the onset of hard film formation at the oxygen rubber interface after 180 hours ageing time. Film formation at 130°C (not shown) was so rapid that both the rate and extent of oxidation were significantly depressed. This behaviour therefore results in an upper limit for the experimental temperature range. Conversly, at low temperatures the rate of absorption is too slow to provide reliable weight gain measurements and the weighing accuracy thus determines the lowest experimental temperature. The sample aged at 77°C for example showed a weight gain of only 0.1%. Since its initial weight was about 1.0 grm this represents a total weight gain of 1 mg over a period of 300 hours. Within the permissible experimental temperature range of about 40°C the rate of oxygen absorption, as determined from the linear portion of each curve, increased with increasing temperature. To illustrate this the derived rate constants were plotted in an Arrhenius fashion as shown in Figure 3.10. Within experimental error this indicates a straight line plot and represents an activation energy of about 75 KJ mol^{-1}. Although three thicknesses of sample, ranging from

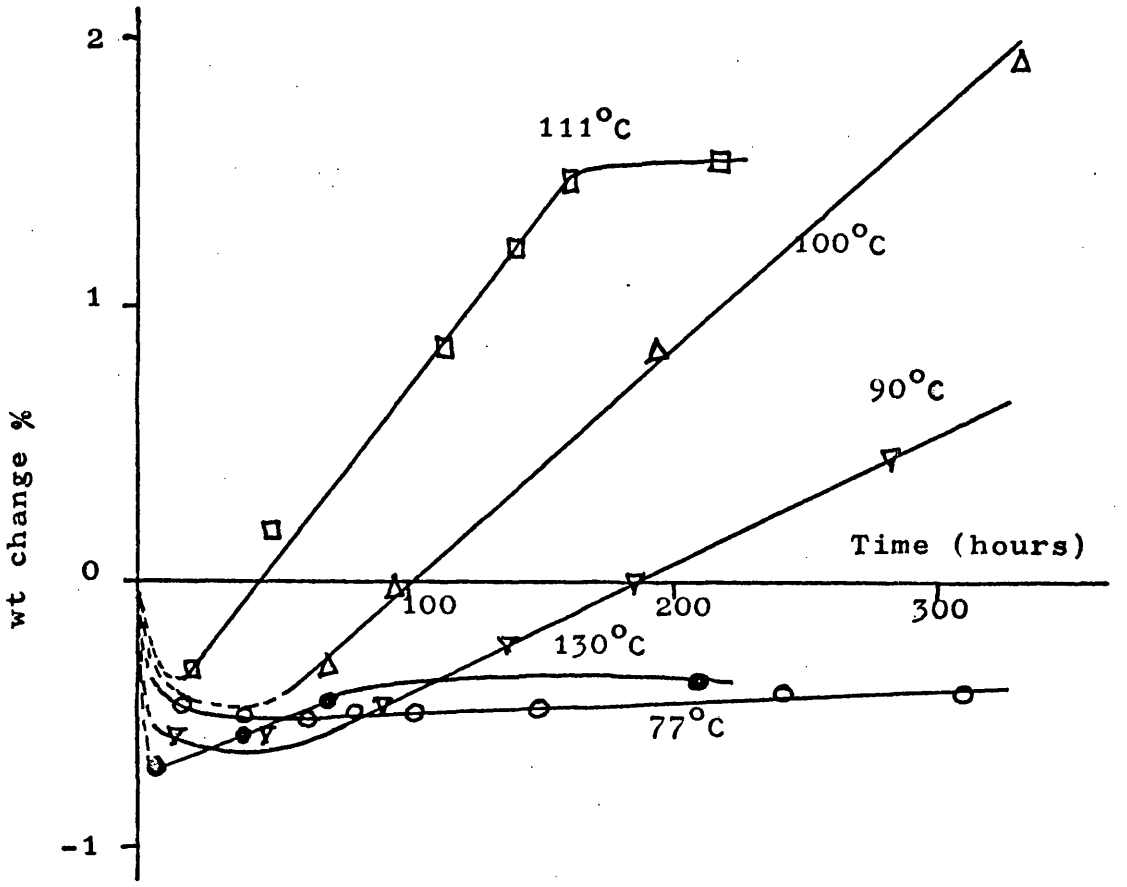

Figure 3.9 Ageing curves for vulcanizate 'B' at the temperatures shown. Sample thickness ~ 1.8 mm.

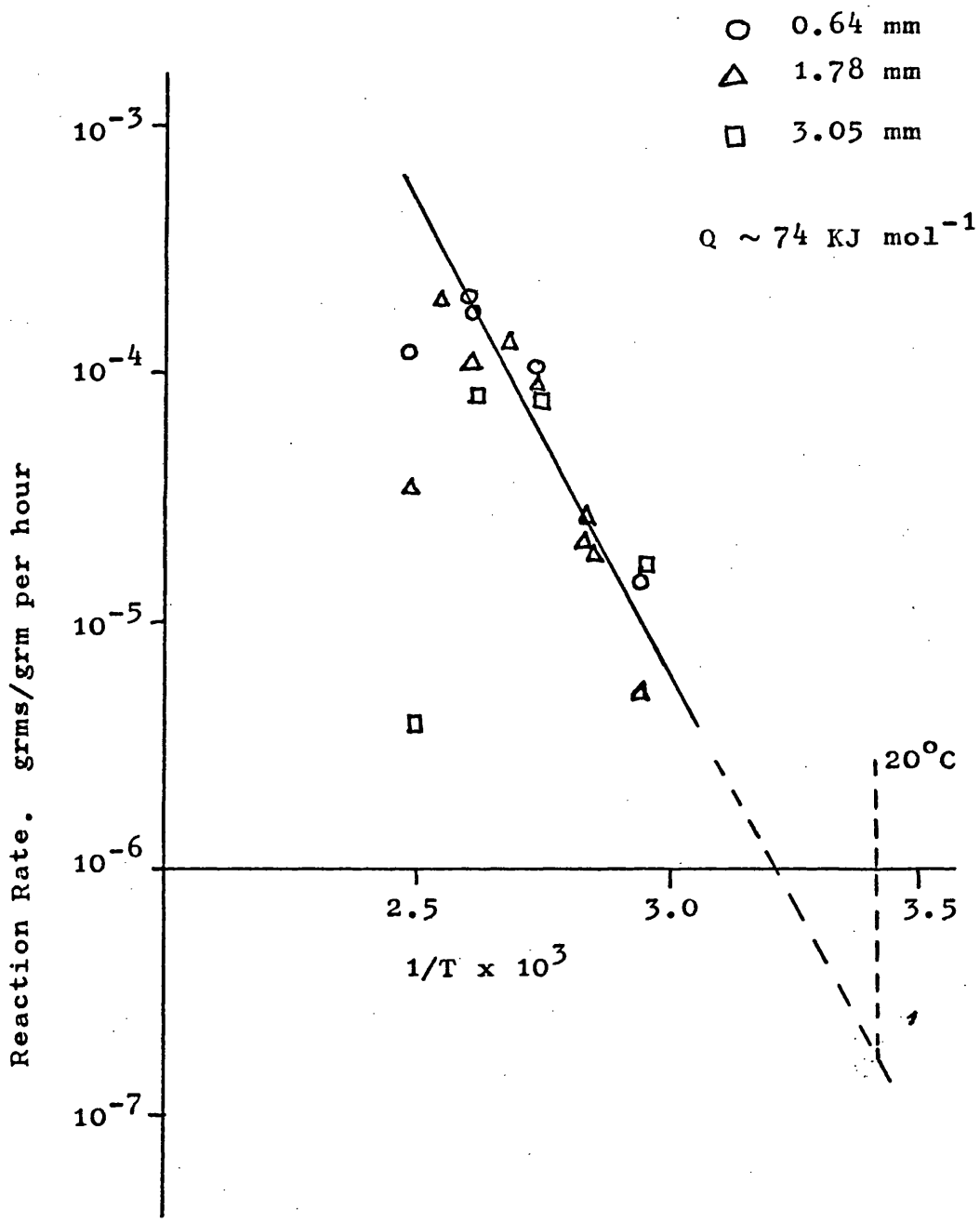

Figure 3.10 Influence of temperature and sample thickness on observed oxygen absorption rates for vulcanizate 'B'.

0.6 mm to 3.1 mm, were used all points are reasonably consistent and this suggests that neither oxygen adsorption nor diffusion were rate limiting and this is in agreement with the stretching experiment described earlier. This implies that the critical thickness, 2 h_c, for which oxygen diffusion would be rate limiting is in excess of 3 mm in this temperature range. The depression of measured absorption rates at temperatures in excess of 110°C due to hard film formation is clearly indicated in Figure 3.10 although a possible contribution to this from the onset of diffusion limitation cannot be discerned. For the purposes of calculating critical sample thicknesses, the reaction rate K_o will be estimated from the solid line in Figure 3.10.

b) Measurement of Permeability Rates

The permeability of air in rubber was assessed using a standard variable volume cell as shown in Figure 3.11. Its use and application have been reviewed by Stancell [13]. Transport of gas through the membrane results in a volume increase on the low pressure side of the cell and this is monitored from the position of a liquid drop in a precision bore capillary. Initially during each experiment the rate of gas transmission increases with time as the concentration of the diffusing species builds up in the membrane. Eventually an equilibrium concentration profile is established in the sample and steady state flow is observed. This is used to calculate the permeability coefficient.

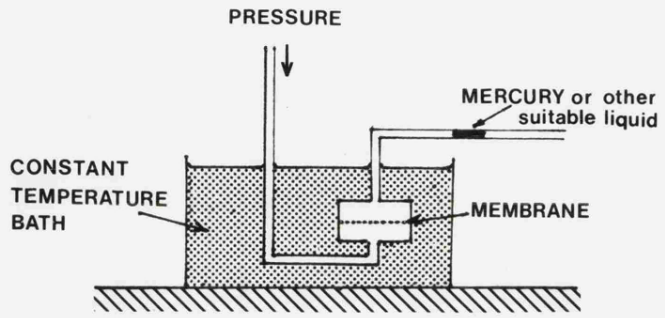

Fig 11a Schematic view of permeability equipment.

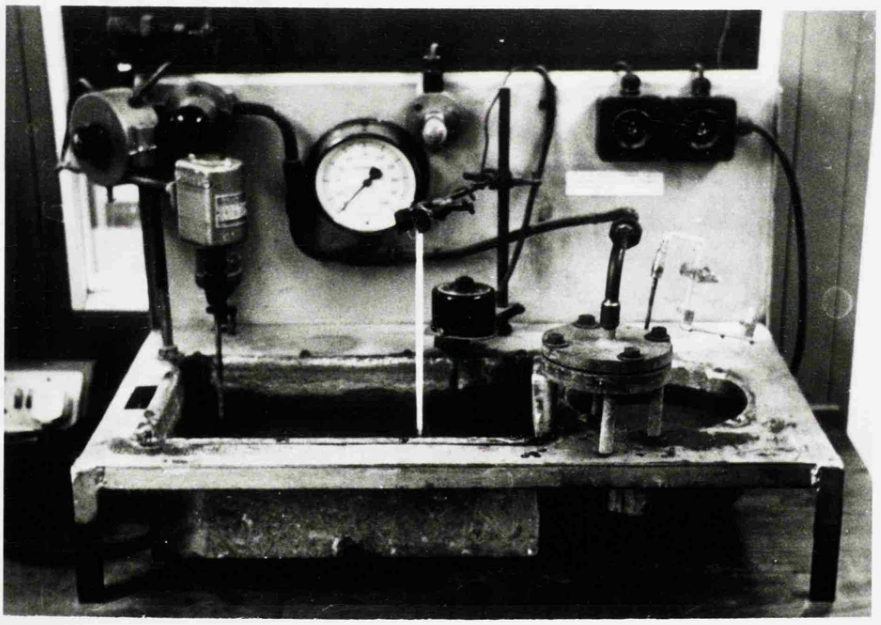

Fig 11b Actual equipment showing cell, pressure gauge, capillary and constant temperature bath.

The present work was carried out on a permeability rig at the research laboratories of Avon Rubber Company. On advice from British Oxygen Co. air was used as the diffusing species rather than pure oxygen to avoid the risk of explosion. Rubber membranes of between 0.5 mm and 0.7 mm thickness were subjected to air under 18 MNm^{-2} (60 lb/in^2) pressure and equilibrium rates were determined at room temperature, 45°C and 65°C. Attenuation of oxygen transmission by absorption in the membrane will be neglected since for this applied pressure and these temperatures, the critical distance for complete absorption proves to be some eight to sixty times greater than the membrane thickness. (see later). Furthermore the diffusion of the nitrogen content of the air is not affected by chemical reactions.

Experimental data is presented in an Arrhenius fashion in Figure 3.12. Vulcanizate 'C' has a lower modulus and therefore a lower crosslink density than vulcanizates 'A' and 'B'. Its higher permeability is a result of greater ease of movement of gas molecules within the more open macromolecular "lattice". Vulcanizates 'A' and 'B' show almost identical behaviour. Data obtained at the highest temperature show some tendency to fall below the level expected from an extrapolation of the two lower temperature results. This may be due to experimental error or to increased absorption of oxygen in the membrane at higher temperatures. The error in assuming a linear Arrhenius plot does not however appear to be very great. An activation energy of 40

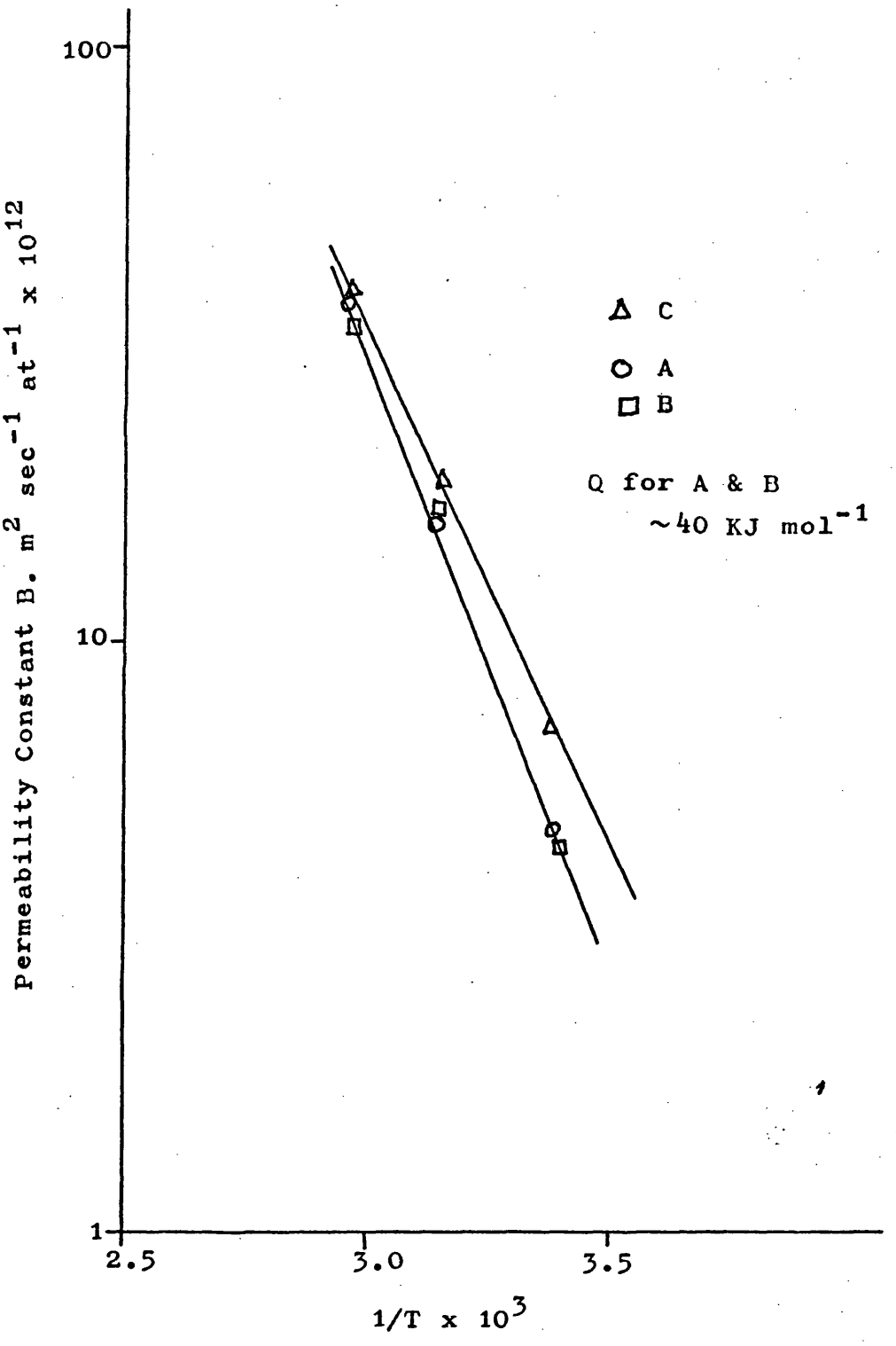

Figure 3.12 Arrhenius plots for measured values of the permeability of air in vulcanizates 'A', 'B' and 'C'.

KJ mol^{-1} can be derived and this is in reasonable agreement with literature values for oxygen and nitrogen. Diffusion constants and activation energies of diffusion for gases in rubbers are closely related to the size of the diffusing molecule and consequently oxygen and nitrogen are very close being consecutive elements in the atomic table. Amerongen [14] quotes 8.3 K cals mol^{-1} (35 KJ mol^{-1}) and 8.7 K cals mol^{-1} (37 KJ mol^{-1}) for the activation energies for diffusion of oxygen and nitrogen in natural rubber respectively. The solubility of both oxygen and nitrogen in natural rubber appears to be little effected by temperature. The solubility of oxygen at 25°C is quoted at 0.112 ccs/cc in comparison with 0.010 ccs/cc at 50°C. Similarly for nitrogen, quoted solubilities are 0.055 and 0.057 ccs/cc at 25°C and 50°C respectively. Since permeability equals the product of solubility and diffusivity it may be concluded that the activation energies for permeation and diffusion are very close. Further because the activation energies for permeation of nitrogen and oxygen are very similar, then the ratio of permeability rates for oxygen and nitrogen will be almost independent of temperature.

With the above points in mind it is proposed to establish an estimate for the permeability of oxygen in vulcanizates 'A' and 'B' and hence deduce critical depths of oxygen penetration according to the formulae presented earlier. It is assumed that the activation energies for permeation of oxygen and nitrogen are

equal and that their relative rates are independent of temperature. Barrer [15] found that the ratio B_{O_2}/B_{N_2} was 2.75 at 25°C in agreement with their differences in solubility. This ratio has not been seriously contradicted in later work; a value of 2.82 can be evaluated from a relatively recent review for example [16]. The permeability rate for air can thus be evaluated:-

$$B_{air} = 1/5\ B_{O_2} + 4/5\ B_{N_2}$$

taking air to consist of 20% oxygen and 80% nitrogen.

$$B_{air} = 1/5\ B_{O_2} + \frac{4}{5 \times 2.75}\ B_{O_2}$$

$$= 0.491\ B_{O_2}$$

$$\text{OR } B_{O_2} \simeq 2\ B_{air}$$

Permeability rates for oxygen in vulcanizates 'A' and 'B' will be taken to be twice that indicated from the relevant solid line in Figure 3.12.

3.4 Calculation and Interpretation of Critical penetration depths

Critical penetration depths h_1, h_c and h_3 have been defined earlier. According to equations 3.11, 3.6 and 3.12 they equal 0.6 h_o, 1.414 h_o and 3.0 h_o respectively where:-

$$h_o = (BP_o/K_o)^{1/2} \qquad - 3.13$$

h_o can be calculated taking P_o = 1/5 atmosphere, K_o from Figure 3.10 and B from twice the value for air as shown in Figure 3.12. Furthermore, h_o varies in an Arrhenius manner with temperature as do both B and K_o. From equation 3.13:-

$$2 \ln h_o = \ln B + \ln P - \ln K_o$$

But $B = B' \text{ Exp} - (Q_B/RT)$

$K_o = K_o' \text{ Exp} - (Q_K/RT)$

where Q_B and Q_K are the activation energies for permeation and reaction respectively.

Hence:-

$$2 \ln h_o = \ln P + \ln B' - (Q_B/RT) - \ln K_o' + (Q_K/RT)$$

$$2 \ln h_o = \ln (B'/K_o') + \ln P + \frac{1}{RT}(Q_K - Q_B)$$

$$\text{OR} \quad ho = \text{const.Exp} - \left(\frac{Q_B - Q_K}{RT}\right)$$

-3.14

Since Q_K exceeds Q_B, h_o decreases with increasing temperature. Calculated critical penetration depths are presented in Figure 3.13 for vulcanizates 'A' and 'B'.

To simplify the discussion of penetration depths reference will be made to the quantity h_c only. This is reasonable since h_c represents the maximum penetration depth for the "pressure independent" case or the half thickness of a large sheet that absorbs oxygen at a rate equal to 89% of an infinite block for the "pressure proportional" case. Real rubbers are assumed to fall between these extreme but not widely different cases. The effect of oxygen absorption on permeability measurements will be considered first. Since h_c decreases with increasing temperature, permeability measurements are increasingly influenced by oxygen absorption with increasing temperature. In

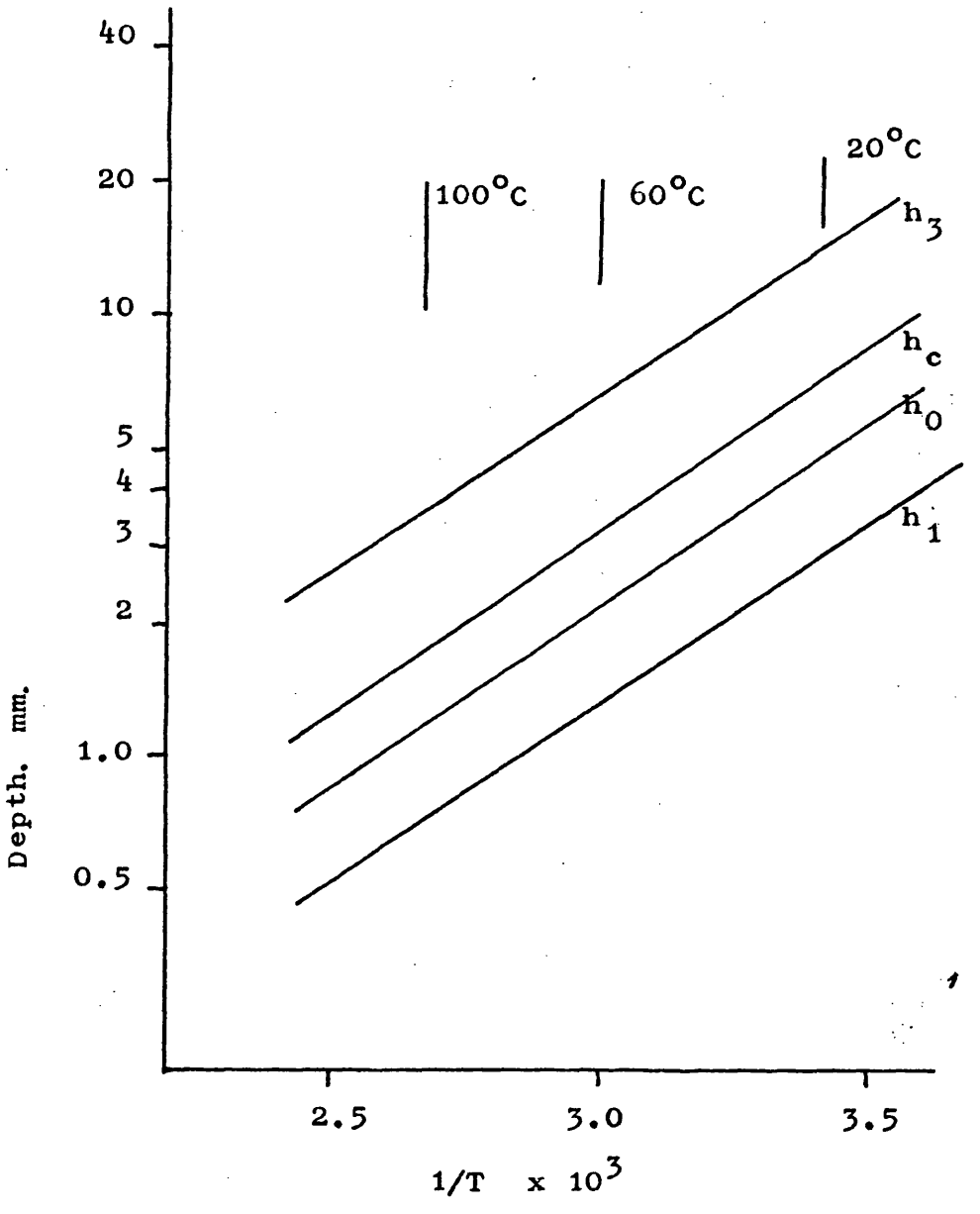

Figure 3.13 Calculated critical depths of oxygen penetration in vulcanizates 'A' and 'B' as a function of temperature.

the present work the highest temperature at which permeability data was obtained was 65°C, when, according to Figure 3.13 h_c equals 3 mm. The tests, however, were carried out with air at an applied pressure of four atmospheres and hence h_c would be $\sqrt{4}$ times as great, i.e. 6 mm. This compares with permeability sample thicknesses in the order of 0.5 to 0.7 mm. Clearly only $\simeq$0.6/6 or 10% of the oxygen content of the permeating gas is absorbed during transit through the membrane at this temperature. This represents an error of approximately 5% in the final result for the permeability of air and at lower temperatures the error is considerably less.

Consideration of equations 3.6 and 3.9 suggests a possible interpretation of the effect of temperature on ageing data. Extrapolation of ageing data obtained at elevated temperatures down to room or other service temperature may result in erronious estimates since h_c increases with decreasing temperature. Consider the "pressure independent" case applied to an ageing sample whose dimensions exceed 2 h_c at elevated temperature but less than 2 h_c at room temperature. The rate of oxygen absorption at elevated temperatures is given therefore by equation 3.8, $Z = \text{const } (K_o BP_o)^{1/2}$, and the observed activation energy for ageing would equal $(Q_K + Q_B)$. Below some critical temperature between the experimental range and room temperature, where 2 h_c equals the sample dimensions, oxygen absorption would no longer be influenced by diffusion and the activation

energy for ageing would be Q_K only. This would result in higher absorption rates at room temperature than would be expected from extrapolated data. The "pressure proportional" case is similar although more complex. In the present work, ageing data was obtained for specimens of 0.6, 1.8 and 3.1 mm thickness at temperatures up to 130°C. Reference to Figure 3.13 suggests that 2 h_c exceeds 3 mm for temperatures below 100°C which is in agreement with Figure 3.10 showing that absorption rate is unaffected by sample thickness up to 100°C. At higher temperatures absorption is presumably limited by diffusion factors for the thicker samples in addition to hard film formation.

A quantitative interpretation of the effect of oxygen penetration on creep behaviour can now be given. The absorption of oxygen is limited by diffusion when the specimen dimensions exceed some critical value between 2 h_1 and 2 h_c. At 110°C for example, oxygen absorption per unit volume of rubber decreases as the specimen thickness is increased beyond a critical value between 1.3 and 3.6 mm. A transition range of this order is suggested by Derhams creep data at 110°C presented in Figure 3.1. Furthermore, in the present work, creep experiments were performed on samples of unstretched thickness 1.7 to 1.85 mm. Oxygen absorption should not therefore have been limited by sample thickness up to at least 90°C and even higher for moderate applied strains. Bearing in mind the effect of temperature on creep rate (see Chapter 2) it is concluded

that all creep experiments were conducted within a range of parameters where oxygen penetration was not a limiting factor.

3.5 The Effect of Carbon Black Additions

Carbon black particles are relatively impermeable in comparison with rubbery vulcanizates, consequently carbon black filled vulcanizates are less permeable than their gum equivalents. Thirion [17] found that the reduction in permeability caused by the addition of non reinforcing fillers to a gum rubber was not strongly dependent on the type or size of particles so much as on the volume fraction present. His results correlated with an equation based on arguments of Carpenter and Twiss[18].

$$B_f/B_o = (1 + 1.3\ V_f)^{-1} \qquad 3.15$$

where B_o = permeability of a gum rubber

B_f = permeability of the filled rubber

V_f = Volume fraction of filler.

Figure 3.14 indicates the influence of LS-SRF black additions on the permeability of air in vulcanizate 'A'. Within experimental error the activation energy for permeation is independent of black content and consequently the ratio B_f/B_o is independent of temperature. B_f/B_o values derived from Figure 3.14 are compared with equation 3.15 in Figure 3.15a. The theoretical analysis slightly underestimates the decrease in permeability. An improvement in correlation may be possible using a fuller analysis as suggested by Carpenter

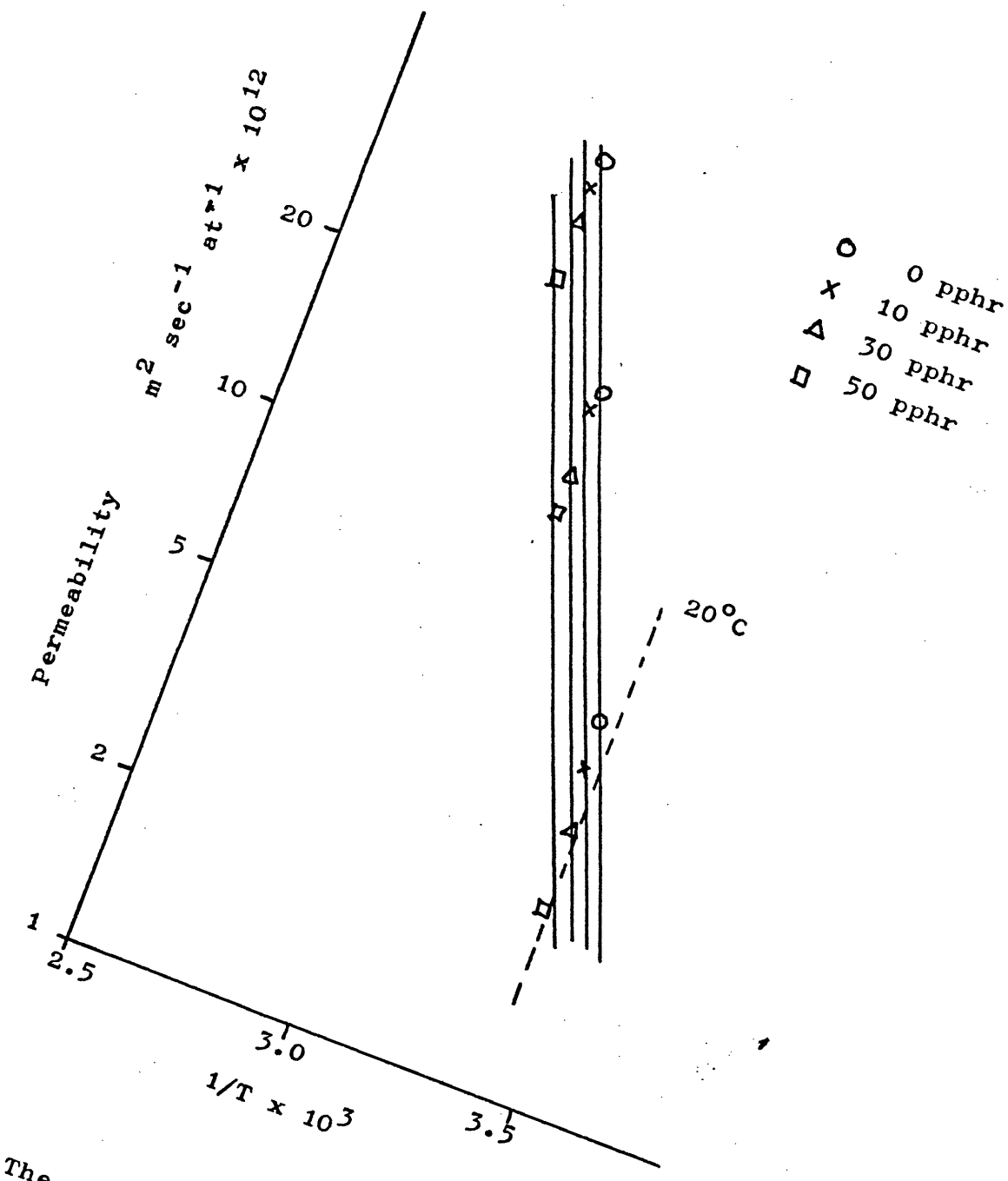

Figure 3.14 The influence of LS SRF carbon black additions to vulcanizate 'A' on its permeability to air.

black loading pphr	V_f	B_f/B_o Measured	B_f/B_o Calculated
0	0	1.0	1.0
10	0.04	0.88	0.95
30	0.11	0.75	0.88
50	0.17	0.65	0.79

Figure 3.15a Influence of filler content (LS SRF) on the permeability of vulcanizate 'A'. Comparison of measured data with that calculated according to Carpenter & Twiss.

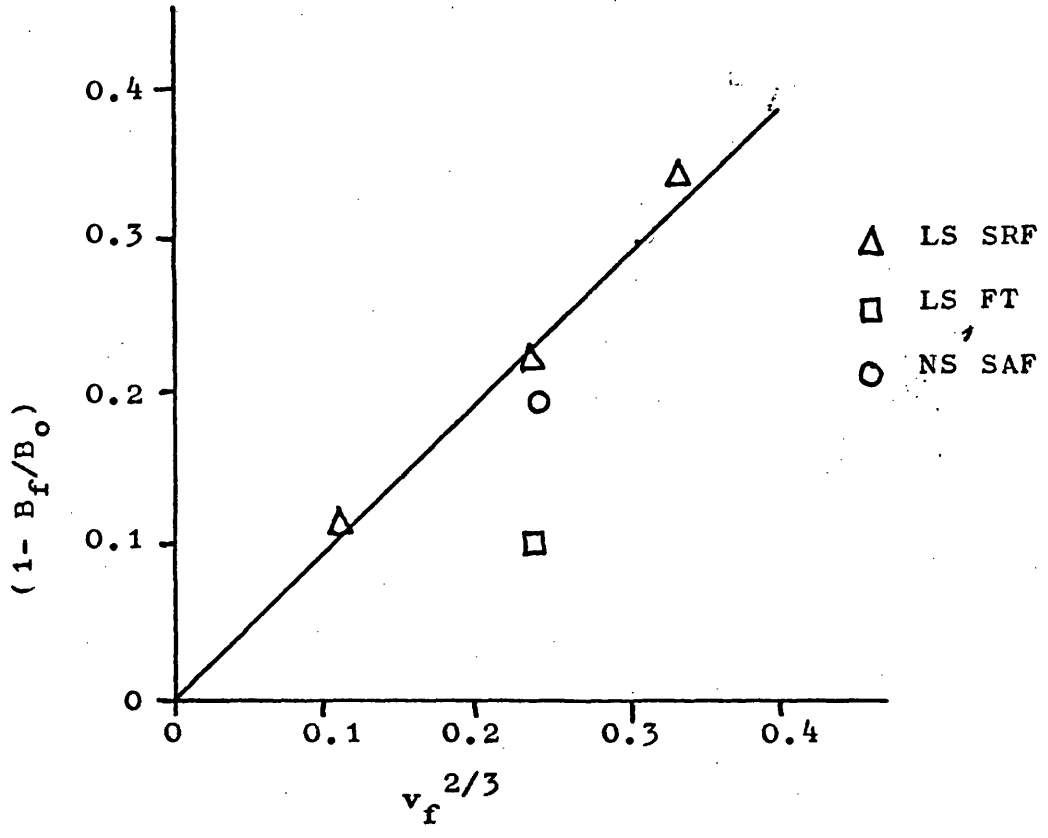

Figure 3.15b Influence of filler content on the permeability of vulcanizate 'A'. The solid line represents Equation 3.16 for α = 1.0.

and Twiss but for the present work a simple semi-quantitative approach is proposed. A method of calculating the reduction in cross-sectional area for diffusion due to the presence of non permeable particles is presented in Appendix 3C. This suggests

$$B_f/B_o = 1 - \alpha\, Vf^{2/3} \qquad 3.16$$

where α depends on the distribution and geometry of filler particles. One would expect α to be close to 1.0 since B_f/B_o should be zero for $V_f = 1.0$. Reasonable agreement between equation 3.16 and experimental results have been obtained for SRF and SAF carbon blacks added to vulcanizate 'A' see Figure 15b. These blacks have a medium, 600 Å, and small, 200 Å, particle size respectively. By comparison, samples containing 300 pphr of LS-FT black, of large particle size, 800 - 1500 Å, either do not fit in with the model or have a relatively small value for α. The single point for this black in Figure 15b has been repeatedly verified.

The complexity of possible reactions has led to conflicting conclusions on the role of carbon blacks in the thermal oxidation of elastomers. In general however, they act as mild antioxidants although mild pro-oxidant behaviour has been reported for some sulphur cured compounds [19]. The mechanisms of antioxidant behaviour are subject to debate but a contribution from purely physical considerations may be evaluated:- For inert carbon black particles the rate of oxygen pickup would be decreased by a factor determined by the volume fraction of rubber phase.

i.e. $K_f = K_o (1 - V_f)$ 3.17

where K_o and K_f are the reaction rates for the gum and filled rubbers respectively. Consequently the rate of oxygen absorption for samples of dimensions less than $2 h_c$ would be

$$Z_f = Z_o (1 - V_f) \quad 3.18$$

where Z_f and Z_o are the absorption rates per unit surface area of rubber for the filled and gum rubbers respectively. For larger samples the rate would be:-

$$Z_f = Z_o \left[(1 - \alpha V_f^{2/3}) (1 - V_f) \right]^{1/2} \quad 3.19$$

This is obtained from a comparison of equations 3.6, 3.9, 3.16 and 3.18. Similarly critical penetration depths may be estimated

$$h_f = h_g \left[\frac{1 - \alpha V_f^{2/3}}{1 - V_f} \right]^{1/2} \quad 3.20$$

where h_f and h_g are equivalent penetration depths in the filled and gum rubbers respectively. For inert impermeable fillers therefore, critical penetration depths, decrease with increasing filler content. Commercial compounds rarely contain over 30 volume percent of black however (approx 50 pphr). Insertion of $V_f = 0.3$ and $\alpha = 1.0$ into equation 3.20 suggests

$$h_f \simeq 0.9 h_g$$

According to this simple argument therefore, the penetration of oxygen into rubber is little affected by black additions. The chemical nature of carbon blacks and their role as antioxidants adds complexity to this basic model however.

6 Practical Aspects

A theory has been presented by means of which approximate estimates of oxygen absorption may be made. The deductions represent long term behaviour since steady state conditions have been considered. The model does not however simplify the interpretation of ageing behaviour as network changes result from only a proportion of absorbed oxygen. The possibility of reaction with antioxidants, extra-network material and fillers cannot be excluded. By comparison, network changes due to polysulphide crosslink lability may be unaffected by the presence or absence of oxygen.

Practical implications to engineering component design are obvious. At room temperature, for example, the influence of oxidative degradation may extend some 7 to 15 mm from the surface of vulcanizates 'A' and 'B'. See Figure 3.13. For large components such as bridge bearings and antivibration supports for buildings, the possibility of oxidative degradation in bulk rubber can be dismissed. Conversly, for small or thin components such as motor car tyres, small anti-vibration mountings, seals and belting, oxygen may penetrate to the component centre. In this case a better criterion for materials selection is provided by a comparison of absorption rate and design life. For intermediate sized components such as vechicle suspension systems, some allowance for oxidative degradation may be necessary.

APPENDIX 3A

Calculation of oxygen penetration depth I

The pressure independent case

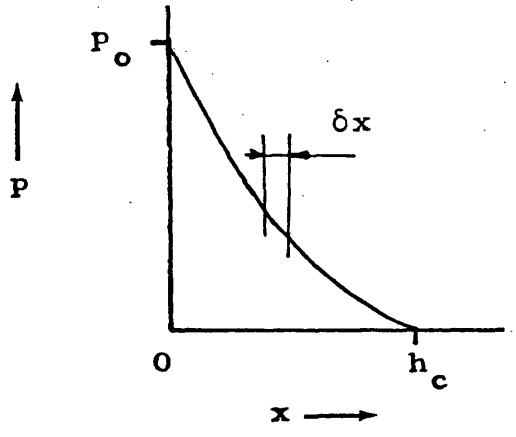

In the following derivation the rate of reaction of oxygen with rubber K_o ccs/cc per unit time is assumed to be independent of the oxygen partial pressure. The maximum depth of penetration is therefore h_c, as illustrated above. Steady state conditions are assumed.

The rate of influx of oxygen into the segment δx at x is:-

$$\left(\frac{dv}{dt}\right)_{IN} = - B \left(\frac{dP}{dx}\right)_x \qquad \text{per unit area}$$

and the rate of eflux at $(x + \delta x)$ is:-

$$\left(\frac{dV}{dt}\right)_{OUT} = - B \left(\frac{dP}{dx}\right)_{x+\delta x}$$

per unit area.

The rate of accumulation within the segment therefore is

$$\left(\frac{dV}{dt}\right)_{IN} - \left(\frac{dV}{dt}\right)_{OUT}$$

$$= - B \left(\frac{dP}{dx}\right)x - \left[- B \left[\left(\frac{dP}{dx}\right)x + \delta x \frac{d^2P}{dx^2}\right]\right]$$

$$= + B \frac{d^2P}{dx^2} \delta x$$

per unit cross section

This equals the rate at which oxygen reacts with the rubber within the segment, i.e. $K_o \delta x$ per unit cross sectional area.

Hence $$B \frac{d^2P}{dx^2} \cdot \delta x = K_o \delta x$$

or $$\frac{d^2P}{dx^2} = \frac{Ko}{B} \qquad 3A.1$$

Integration gives

$$\frac{dP}{dx} = \frac{Ko}{B} x + C_1 \qquad 3A.2$$

$$P = \frac{Ko}{2B} x^2 + C_1 x + C_2 \qquad 3A.3$$

where C_1 and C_2 are integration constants. At $x = o$ however $P = P_o$. Hence in Equation 3A.3

$$P_o = C_2 + C_1 O + \frac{Ko}{2B} O^2 \qquad 3A.4$$

or $C_2 = P_o$

Furthermore, the pressure gradient at $x = o$ determines the rate at which oxygen passes through the oxygen-rubber interface

$$\left(\frac{dV}{dt}\right)_{x = o} = - B \left(\frac{dp}{dx}\right)_{x = o} \qquad 3A.5$$

The rate at which oxygen is absorbed by the rubber however equals the rate at which the reaction occurs integrated over the whole penetration depth. Since the reaction rate, K_o, is independent of oxygen pressure this equals $Ko\ h_c$

Hence $$- B \left(\frac{dP}{dx}\right)_{x = o} = K_o h_c \qquad 3A.6$$

Comparison of equations 3A.5 and 3A.6 gives:-

$$\left(\frac{dP}{dx}\right)_{x=o} = -\frac{Ko\ hc}{B}$$

which can be substituted into equation 3A.2 to give:-

$$-\frac{K_o h_c}{B} = \frac{K_o}{B} 0 + C_1$$

$$\text{Or} \quad C_1 = -\frac{K_o h_c}{B} \qquad 3A.7$$

Substitution of relationships 3A.4 and 3A.7 into equation 3A.3 gives:-

$$P = P_o + \frac{K_o}{2B} x^2 - \frac{K_o h_c}{B} x \qquad 3A.8$$

But, at $x = h_c$ $P = 0$:-

$$0 = P_o + \frac{K_o}{2B} h_c^2 - \frac{K_o}{B} h_c^2$$

$$P_o = \frac{K_o}{2B} h_c^2$$

$$\text{Or} \quad h_c = \sqrt{\frac{2B\ P_o}{K_o}} \qquad 3A.9$$

The depth which oxygen can penetrate before being totally consumed by reaction with the rubber h_c, is given by equation 3A.9.

APPENDIX 3B

Calculation of oxygen penetration depth II

Here the rate of the oxygen-rubber reaction is considered to be proportional to the oxygen partial pressure. Steady state conditions are again assumed. In principle the analysis will be similar to that followed in Appendix A but equation 3A.1 is re-written as explained in the text to give:-

$$\frac{d^2P}{dx^2} = \frac{K_o}{B} \frac{P}{P_o}$$

This can be re-written:-

$$\frac{d^2P}{dx^2} - \alpha^2 P = 0 \qquad 3B.1$$

where $\alpha = (K_o/BP_o)^{1/2}$

Putting $P = A \text{ Exp } ax$

$$dP/dx = A\ a \text{ Exp } ax$$

$$d^2P/dx^2 = A\ a^2 \text{ Exp } ax$$

one obtains in equation 3B.1:-

$$A \text{ Exp } ax\ (a^2 - \alpha^2) = 0$$

$$a = \pm \alpha$$

Hence the general solution for equation 3B.1 is given by:-

$$P = A_1 \text{ Exp } - \alpha x + A_2 \text{ Exp } + \alpha x \qquad 3B.2$$

and $$\frac{dP}{dx} = \alpha\ A_2 \text{ Exp } \alpha x - \alpha\ A_1 \text{ Exp } - \alpha x \qquad 3B.3$$

Since $P = P_o$ at $x = o$, then in equation 3B.2 one obtains

$$P_o = (A_1 + A_2) \qquad 3B.4$$

and from equation 3B.3:-

$$\left(\frac{dP}{dx}\right)_{x = o} = \alpha\ (A_2 - A_1) \qquad 3B.5$$

Consider now the absorption of oxygen by a large sheet of rubber, thickness 2h. Ignoring edge effects, the rate of absorption at steady state is:-

$$2Z = 2\sum_{x=o}^{h} \frac{P}{P_o} K_o \delta x$$

Substituting into this the value for P obtained in equation 3B.2 one obtains:-

$$2Z = \frac{2 K_o}{P_o} \left[A_1 \int_o^h \text{Exp} - \alpha x \, dx + A_2 \int_o^h \text{Exp } \alpha x \, dx \right]$$

$$= \frac{2 Ko}{P_o} \left[- \frac{A_1}{\alpha} (\text{Exp} - \alpha x)_o^h + \frac{A2}{\alpha} (\text{Exp } \alpha x)_o^h \right]$$

i.e. $$2Z = \frac{2 K_o}{\alpha P_o} \left[- A_1 \text{ Exp} - \alpha h + A_2 \text{ Exp } \alpha h + A_1 - A_2 \right] \qquad 3B.6$$

The total absorption rate equals the rate at which oxygen passes the two planes at x = o i.e. The two gas-rubber interfaces at each side of the sheet. Hence:-

$$2Z = - 2B \left(\frac{dP}{dx}\right) x = o$$

From equation 3B.5 therefore

$$2Z = 2 \alpha B (A_1 - A_2) \qquad 3B.7$$

Comparing equations 3B.6 and 3B.7 gives:-

$$2\alpha B (A_1 - A_2) = \frac{2K_o}{\alpha P_o} \left[A_1 - A_2 + A_2 \text{ Exp } \alpha h - A_1 \text{ Exp} - \alpha h \right]$$

$$(A_1 - A_2) = \frac{2 K_o}{\alpha P_o \, 2 \alpha B} \left[A_1 - A_2 + A_2 \text{ Exp } \alpha h - A_1 \text{ Exp} - \alpha h \right]$$

But $\frac{2 K_o}{\alpha P_o} 2\alpha B = 1.0$ since $\alpha^2 = (K_o/BP_o)$.

Thus

$$A_2 \text{ Exp } \alpha h - A_1 \text{ Exp} - \alpha h = 0 \qquad 3B.8$$

From equation 3B.4

$$A_1 = P_o - A_2$$

and $A_2 = P_o - A_1$

Hence in Equation 3B.8

$$A_2 \text{ Exp } \alpha h - P_o \text{ Exp } - \alpha h + A_2 \text{ Exp } - \alpha h = 0$$

Or $A_2 (\text{Exp } \alpha h + \text{Exp } - \alpha h) = P_o \text{ Exp } - \alpha h$

$$A_2 = \frac{P_o \text{ Exp } - \alpha h}{2 \text{ Cosh } \alpha h}$$

Similarly

$$A_1 = \frac{P_o \text{ Exp } \alpha h}{2 \text{ Cosh } \alpha h}$$

Substituting these values for A_1 and A_2 into equation 3B.7

$$2Z = \frac{2 \alpha BP_o}{2} \left[\frac{\text{Exp } \alpha h}{\text{Cosh } \alpha h} - \frac{\text{Exp } - \alpha h}{\text{Cosh } \alpha h} \right]$$

$$= 2 \alpha BP_o \frac{\text{Sinh } \alpha h}{\text{Cosh } \alpha h}$$

$$= 2 \alpha BP_o \text{ Tanh } \alpha h$$

and since $\alpha = (K_o/BP_o)^{1/2}$

Then

$$2Z = 2 (K_o/BP_o)^{1/2} \text{ Tanh } \left[h \frac{K_o}{BP_o} \right]^{1/2} \qquad 3B.9$$

This is in agreement with a similar equation quoted by Carpenter[4] who deduced it from a complex diffusion analysis given by Daynes[20]. Carpenter did not give a proof.

APPENDIX 3C

A simple model for the effect of carbon black on Diffusivity

If one assumes carbon black particles to be relatively impermeable in comparison to the gum phase a simple model can be proposed. Consider the black particles to be perfectly spherical and to occupy positions at the corners of a simple cubic cell.

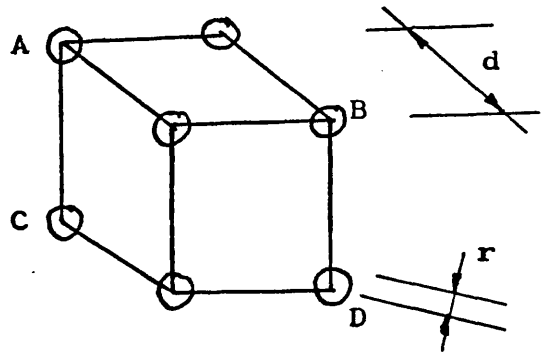

The black particles have a radius r and the cube edge is of length d as shown. Since eight unit cubes meet at a corner, each particle has one eighth of its volume in a single cube. As there are eight corners to each cube, however, eachcube contains 8 x 1/8 = 1 particle. The volume fraction of black particles V_f is therefore:-

$$V_f = \frac{4/3\ \pi\ r^3}{d^3} \qquad 3C.1$$

The area fraction of particles on any cube face, A_f, can be derived similarly

$$A_f = \pi r^2/d^2 \qquad 3C.2$$

But from Equation 3C.1

$$\frac{1}{d} = \left(\frac{3}{4\pi} V_f\right)^{1/3} \frac{1}{r}$$

Hence in Equation 3C.2

$$A_f = \pi r^2 \times \frac{1}{r^2} \left(\frac{3}{4\pi} V_f\right)^{2/3}$$

$$= \pi \left(\frac{3}{4\pi} V_f\right)^{2/3} = 1.2 \; V_f^{2/3}$$

For comparison the area fraction of particles on the plane ABDC as illustrated would be $0.85 \; V_f^{2/3}$. The area fraction on the cube face of a body centred cubic arrangement is $\pi \left(\frac{3}{8\pi} V_f\right)^{2/3} = 0.76 \; V_f^{2/3}$.

In general then

$$A_f = \alpha \; V_f^{2/3}$$

where α depends upon the spatial arrangement and orientation of particles.

Diffusing gas molecules are limited to an area $(1 - A_f)$ since the area A_f is occupied by non permeable particles. Observed permeability rates will be reduced by a factor therefore:-

$$B_f/B_o = (1 - A_f)/1 = 1 - A_f$$

$$\text{i.e. } B_f/B_o = 1 - \alpha \; V_f^{2/3} \qquad 3C.3$$

This oversimplified picture neglects two geometrical factors:-

a) That the average cross sectional area for diffusion exceeds A_f since the area increases and decreases repeatedly between and within planes throughout the hypothetical lattice.

b) That the path length for diffusion is increased since

molecules have to diffuse around successive particles. These have mutually opposite effects however and have not been considered.

For impermeable particles, the permeability, B_f, for a volume fraction of filler equal to 1.0 would be zero. This implies an expected value for α of 1.0.

REFERENCES; CHAPTER 3

1. A. Y. Coran — Rubb Chem and Technol 37 (3), pp 673-78 (1964).

2. J. H. Farmer and J. E. Stuckey — J. Inst rubb indust 5 (5), pp 200-3 (1971).

3. D. Barnard, L. Bateman, J. I. Cunneen and J. F. Smith — "The Chemistry and Physics of Rubberlike Substances." Ch. 17 Ed. L. Bateman Pub Wiley, N. Y. McLaren & Son, London (1963).

4. A. S. Carpenter — Ind Eng Chem 39, pp 187-94 (1947).

5. L. L. Shannin — Rubb Chem and Technol 29 (2), pp 602-6 (1956).

6. C. Cuthbert — "Use of Rubber in Engineering" Ed. P. W. Allen, P. B. Lindley and A. R. Payne Pub. McLaren & Son, London (1967).

7. C. J. Derham, G. J. Lake and A. G. Thomas — J. Rubb Res inst Malaya 22 (2), pp 191-200 (1969).

8. C. J. Derham, E. Southern and A. G. Thomas — Nat rubb technol, rubb dev supp (1970) No. 7.

9. C. J. Derham — MRPRA 3rd rubber in engineering conference. London (1973). Paper F.

10. J. P. Berry and W. F. Watson — J. Polym Sci 18, pp 201-213 (1955).

11. J. I. Cunneen — Rubb Chem and Technol 41 (1) pp 182-208 (1968).

12. J. R. Shelton — Rubb Chem and Technol 45 (2), pp 359-80 (1972).

13. A. F. Stancell — Polymer Sci and materials Ch. 12 Ed. A. V. Tobolsky and H. F. Mark Pub. Wiley Interscience N.Y. (1971).

14. G. J. Amerongen Rubb Chem and Technol 37 (5), p 1065 (1964).

15. R. M. Barrer Trans Far Soc 35, pp 628-643 (1939).

16. A. Lebovits Modern Plastics 43 (7) pages 139-42, 144, 146, 150, 194, 196, 198, 200, 202, 205, 206, 208, 210, 213 (1966).

17. P. Thirion Proc 3rd Rubber Tech Conference, London 1954 pp 334-350 Pub. Inst Rubb Indust.

18. A. S. Carpenter and D. F. Twiss Ind Eng Chem, Anal Edn 12, pp 99-108 (1940).

19. W. L. Hawkins and F. H. Winslow "Reinforcement of Elastomers," Ch. 17 Ed. G. Kraus Pub. Wiley, Interscience N. Y. (1965).

20. H. A. Daynes Proc Roy Soc, London A97, pp 286 -307 (1920).

CHAPTER 4

SECONDARY CREEP

4.1 Secondary Creep and its Relationship to Stress-Relaxation

The most extensive discussion of the secondary creep process published to date is by A. N. Gent[1]. Figure 4.1, taken from this paper indicates typical creep curves for TMTD vulcanizates at 60°C. A logarithmic rate law, consistent with physical creep, was observed at short times followed by a secondary process at later stages in the creep history. A comparison of this secondary contribution for DCP and TMTD vulcanizates in air and vacuum suggested that the process resulted from oxidation of the rubber network. This follows since the secondary creep in vacuum was negligible and in the case of TMTD vulcanizates the rate in air was increased after prior extraction to remove the antioxidant zinc dimethyldithiocarbamate. This conclusion is in agreement with earlier work by Wohlstenholme [2] who also observed a marked influence of oxygen on creep at elevated temperatures. Gent found that the secondary contribution to the total creep was proportional to the time under load and Figure 4.2 summarises some of his results. These curves are in accordance with expected chemical stabilities taking into account that the DCP sample was extracted and would therefore follow autocatalytic oxidation kinetics. By comparison, present work,

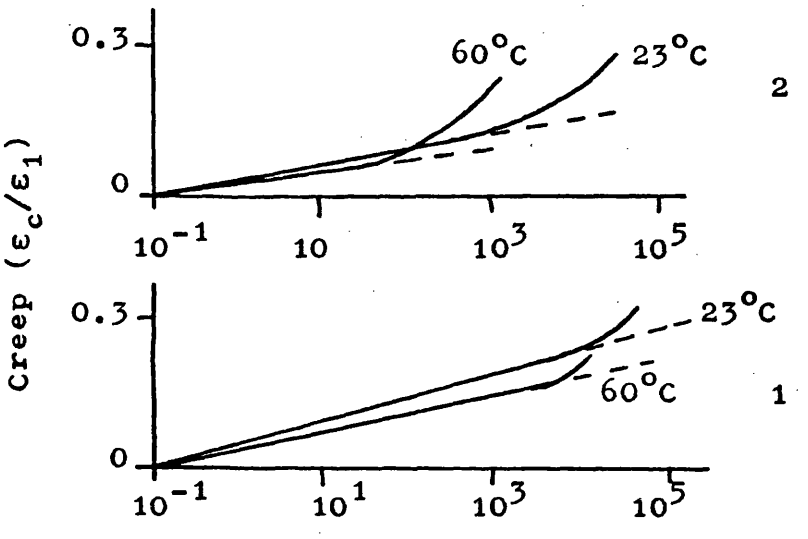

Figure 4.1 Creep curves at 23°C and 60°C for a TMTD vulcanizate before (1) and after (2) extraction. The ordinate represents the creep strain as a fraction of the initial strain at 1 minute under load. After A. N. Gent[1].

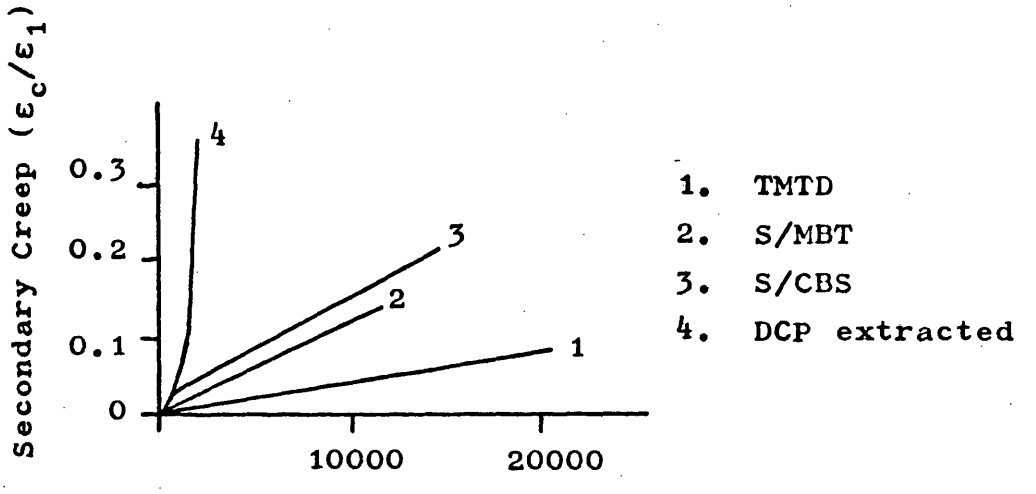

Figure 4.2 Secondary creep at 60°C for four different vulcanizates. After A. N. Gent[1].

Figure 4.3, indicates that DCP vulcanizates before extraction show superior creep resistance when compared at similar initial elongations. Gent further observed that recovery of secondary creep and the extent of permanent set were in accordance with stress-relaxation literature, indicating extensive secondary crosslinking/ bond interchange for sulphur cured vulcanizates and very little for peroxide vulcanizates. For sulphur cured rubbers the "permanent" set decreased with time if the samples were left at the test temperature after removal of the creep load and this suggests that secondary crosslinks, in these rubbers, like the primary ones, are chemically unstable. Permanent set for TMTD samples depended markedly on whether they had been extracted or not. As one might expect, residual curing agents in unextracted samples promote crosslinking and therefore favour high permanent set.

Tobolsky [3] has proposed that creep and stress relaxation are interelated processes; were it not for the onset of secondary crosslinking, he suggested, these would represent the same process and thus be deriveable one from another. Consider the kinetic theory of rubber elasticity, Equation 1.1:-

$$\sigma = nkT\ (\lambda - \lambda^{-2})$$

Hence, in a creep experiment where the stress and temperature remain constant and assuming no concurrent crosslinking.

$$n_1\ (\lambda_1 - \lambda_1^{-2}) = n_t\ (\lambda_t - \lambda_t^{-2}) \qquad 4.1$$

suffixes referring to time.

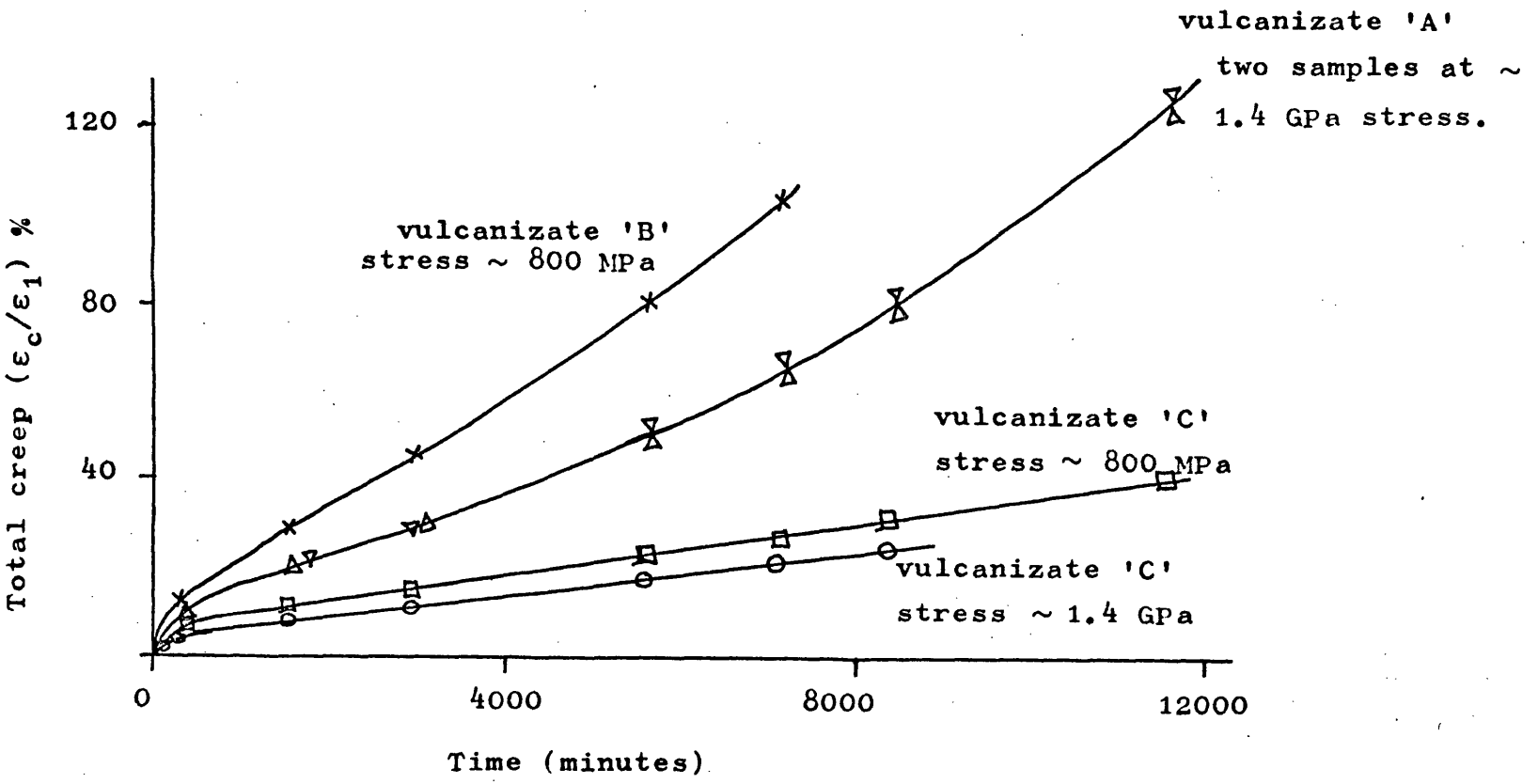

Figure 4.3 A comparison of creep curves for vulcanizates 'A' 'B' and 'C' at 80°C and oven humidity.

Figure 4.4 shows a comparison of creep and stress relaxation data based on this approach. The actual creep for the sulphur cured vulcanizate used in this experiment was less than stress relaxation predictions and this was attributed to the retarding influence of secondary crosslinking.

Stress relaxation characteristics of rubbers have been discussed in Chapter 1. Peroxide vulcanizates, having relatively stable crosslinks, are believed to relax by a first order scission of network chains with negligible concurrent crosslinking. As a result the expected stress-relaxation response is an exponential decay of stress with time:-

$$\sigma_t/\sigma_o = n_t/n_o = \text{Exp} - Kt$$

Hence, from Equation 4.1, one would expect the creep time relationship to obey:-

$$(\lambda_t - \lambda_t^{-2}) = (\lambda_o - \lambda_o^{-2}) \text{ Exp} + Kt \qquad 4.2$$

or, for small 'Kt'

$$(\lambda_t - \lambda_t^{-2}) = (\lambda_o - \lambda_o^{-2}) (1 + Kt) \qquad 4.3$$

Equation 4.3 is similar to that used by C. S. Kim [4] to describe the creep of polybutadiene at ambient temperature as mentioned in Chapter 2 and Figure 4.5 illustrates present data for the secondary creep of peroxide vulcanizate 'C'. At 100°C the creep strain falls below that suggested by Equation 4.2 and at even lower temperatures remains proportional to time for values of 'Kt' well in excess of that for which Equation 4.3 is a reasonable approximation. Permanent set for these and other peroxide samples was, within experimental error, less

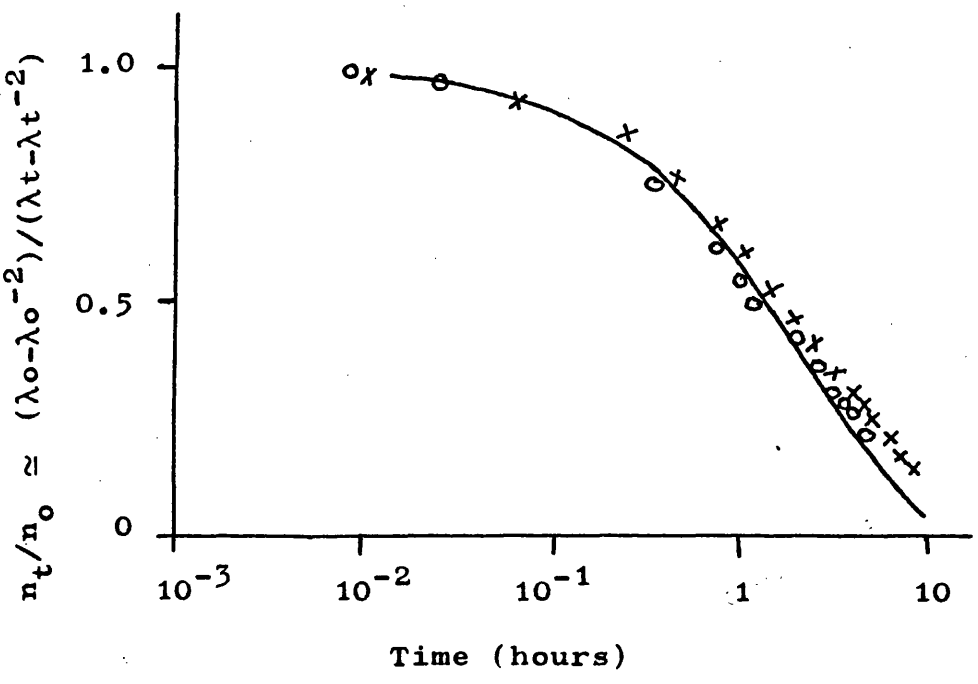

Figure 4.4 A comparison of stress relaxation and creep data for a sulphur cured vulcanizate at 120°C. The solid line represents stress relaxation data. Experimental points represent creep results at x~10-20% strain and 0 ~ 100% strain. After Tobolsky[3].

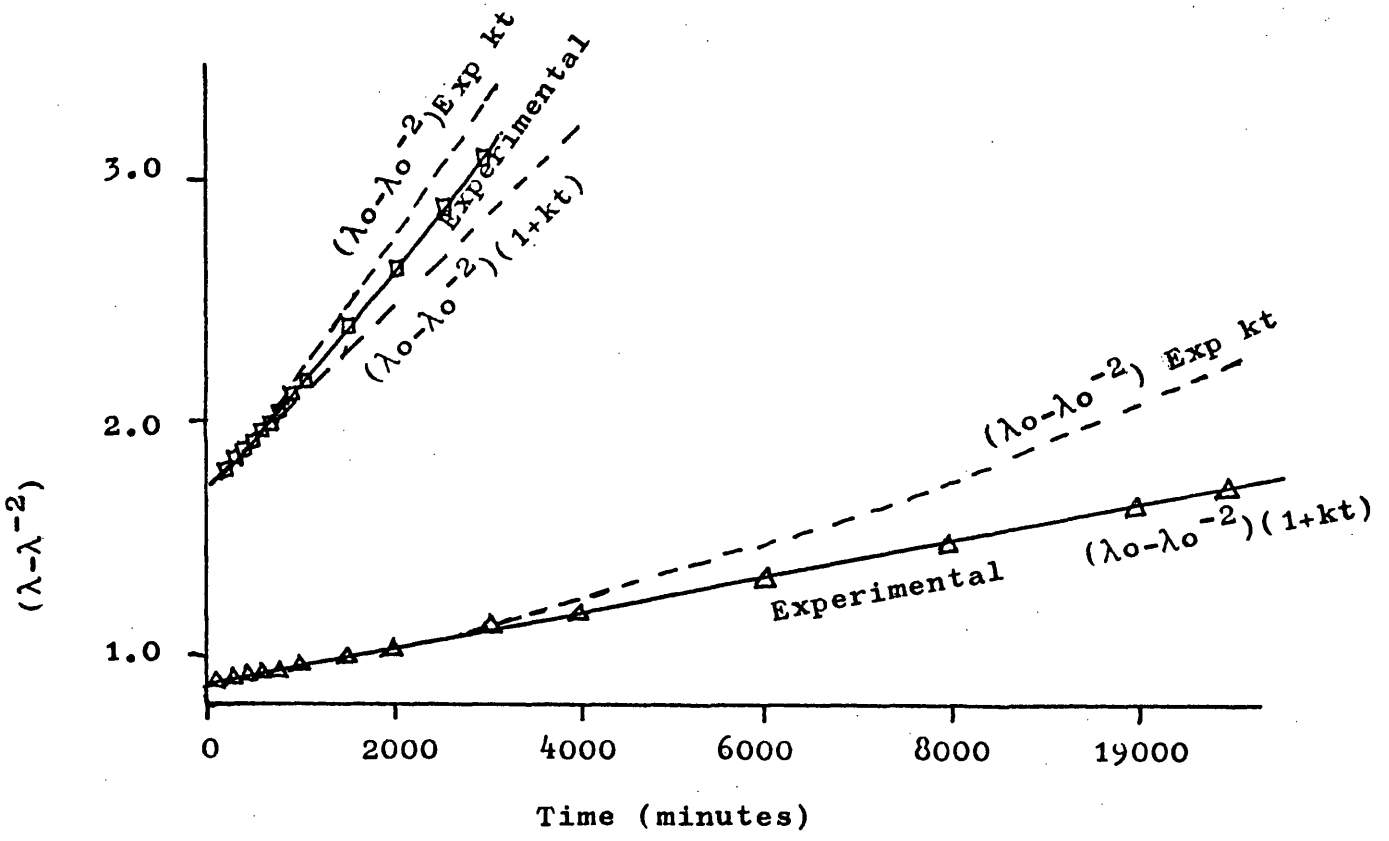

Figure 4.5 Secondary creep for peroxide vulcanizate 'C'

□ 100°C oven humidity

△ 80°C oven humidity

than 3% indicating that negligible crosslinking had occurred at the creep test elongation. This is in agreement with Gent [1]. The discrepancy between observed and expected creep response cannot therefore be attributed to the gradual transfer of stress to a secondary network. It should be borne in mind here however, that present creep work was carried out at temperatures generally below 100°C whilst stress relaxation theory has developed from experimental data obtained at temperatures above 100°C. Amongst the exceptions is some work by Thirion and Chasset [5] who have examined stress relaxation data for a peroxide vulcanizate down to moderate temperatures. They suggested that viscoelastic processes predominate at 30°C whilst ageing processes predominate at 100°C although they did not attempt a qualitative analysis. Tobolsky et al [6], by comparison, have proposed that oxidation reactions participate in the relaxation process down to ambient temperatures where visco-elasticity was once thought to be the sole mechanism. The present comparison of creep with stress-relaxation relies on the ability to separate viscoelastic and secondary contributions to the creep response as described in Chapter 2.

Stress relaxation rates are generally regarded as being independent of test elongation [7]. More recent work however, indicates this is not so for large strains and high temperatures [8]; critical values of $\varepsilon \simeq 1$ and 3 were observed at 100°C and 80°C respectively above which

the relaxation rate increased with strain. Gent has suggested [1], from work at 60°C, that secondary creep represents a fractional stress relaxation process which is independent of the degree of deformation. The mechanism, he says, is not stress activated but takes place equally readily and to equivalent extents over a wide range of deformation. Present creep data will be presented in the accepted way as a fraction of the initial extension, i.e.

$$\text{creep} = \frac{1}{(\lambda_1 - 1)} \quad (\lambda - \lambda_1) = \frac{\varepsilon_c}{\varepsilon_1}$$

where the subscript '1' refers to a time of 1 minute after loading and 'ε_c' is the increase in creep strain subsequent to a time of one minute under load.

$$\text{creep rate} = \frac{1}{\lambda_1 - 1} \quad \frac{d\lambda}{dt} = \frac{1}{\varepsilon_1} \quad \frac{d\varepsilon}{dt}$$

For moderate temperatures therefore, where the stress relaxation process is independent of strain and for small amounts of creep where Equation 4.3 is valid, K can be regarded as constant. Equation 4.3 may therefore be differentiated with respect to time to yield:-

$$\left(\frac{1}{\varepsilon_1} \quad \frac{d\varepsilon}{dt}\right) = \frac{K\ (\lambda_o - \lambda_o^{-2})}{(\lambda_o - 1)\ (1 + 2\lambda^{-3})} \qquad 4.4$$

Hence for small amounts of creep, where changes in $(1 + 2\lambda^{-3})^{-1}$ are small $d\varepsilon/dt$ should be a constant. This suggests that the "conventional" plot for secondary creep, where creep strain increases linearly with time, does in fact have some fundamental justification at least for small creep strains. Further, the effect of initial elongation (stress) on creep rate may be predicted, at

least semi-quantitatively, from Equation 4.4

$$\text{i.e. } \frac{1}{\varepsilon_1}\frac{d\varepsilon}{dt} \simeq \frac{K(\lambda_1 - \lambda_1^{-2})}{(\lambda_1 - 1)(1 + 2\lambda_1^{-3})} \qquad 4.5$$

This relationship is plotted graphically in Figure 4.6 which indicates that the creep rate should not be strongly influenced by applied stress. A maximum rate would be expected for initial strains of about 1.0.

4.2 Observations for the Conventional Vulcanizate 'A'

The secondary creep response observed for vulcanizate 'A' was not in general linear over the total experimental time scale. The discrepancy between the actual response and a linear relationship is to be examined in this section.

The creep of vulcanizate 'A' has been examined over a wide range of temperature and stress. Secondary creep contributions have been isolated and some typical curves are illustrated in Figures 4.7 to 4.11. Results at 35°C and 60°C at 40% relative humidity indicate an initially decelerating response; see Figures 4.7 and 4.8 respectively. At 60°C and 'oven' humidity this is less pronounced, Figure 4.9. At 80°C and 40% relative humidity the initial decelerating portion is extended into an initial sigmoidal response leading on to a linear relationship at longer times; Figure 4.10. By comparison, at 100°C, Figure 4.11, a linear relationship is established immediately and this may be due to the initial transients being small in comparison to the total creep, even at small times.

Discrepancies 'Δ' between the actual creep response and that expected for a linear relationship have been

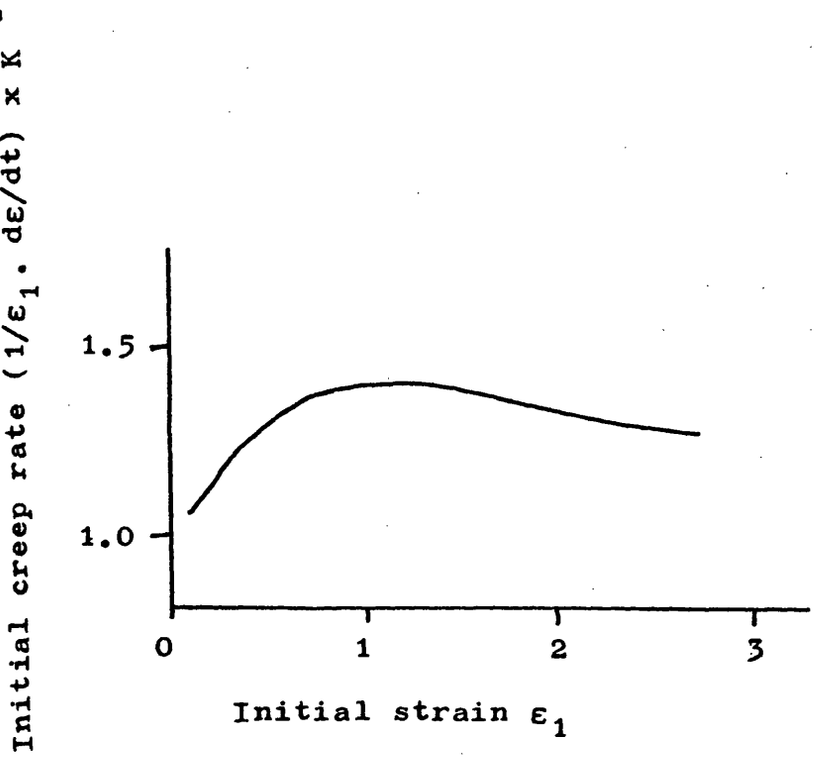

Figure 4.6 Initial creep rate as a function of initial strain according to equation 4.5. The creep rate is expressed in terms of 'K', the scission rate constant.

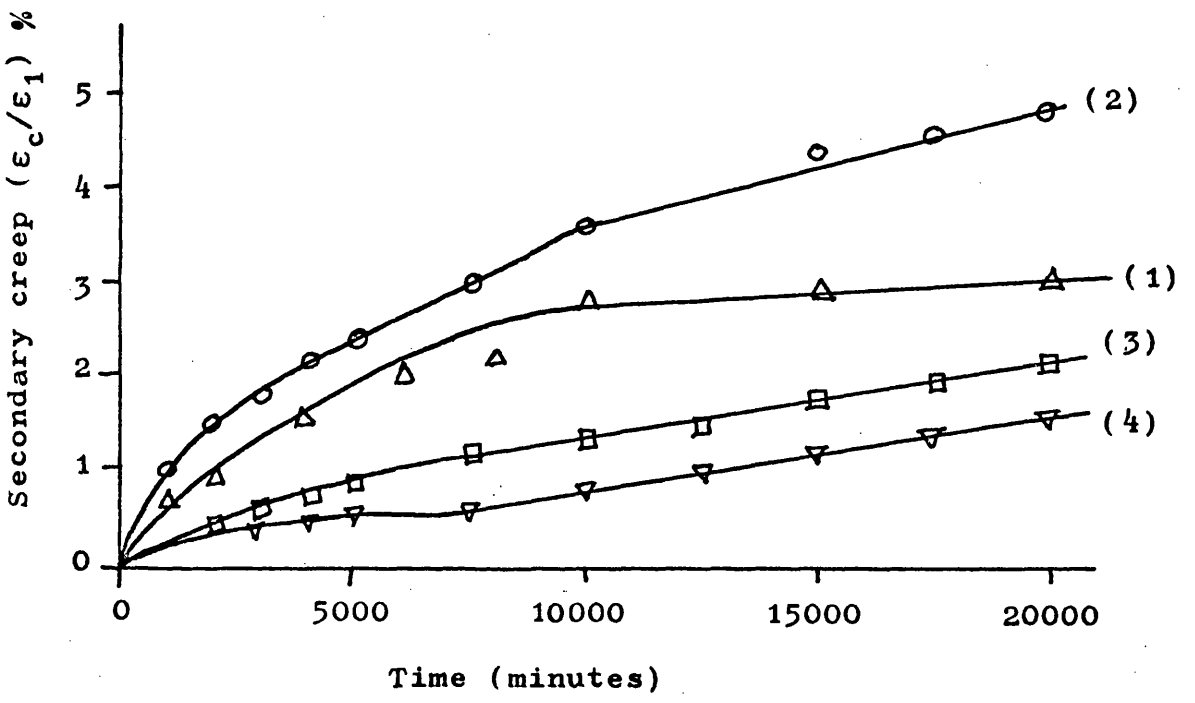

Figure 4.7 Secondary creep for vulcanizate 'A' at 35°C and 40% R.H.

	stress	ε_1
1.	243 KPa	0.153
2.	718 KPa	0.708
3.	1.26 MPa	1.63
4.	1.53 MPa	2.10

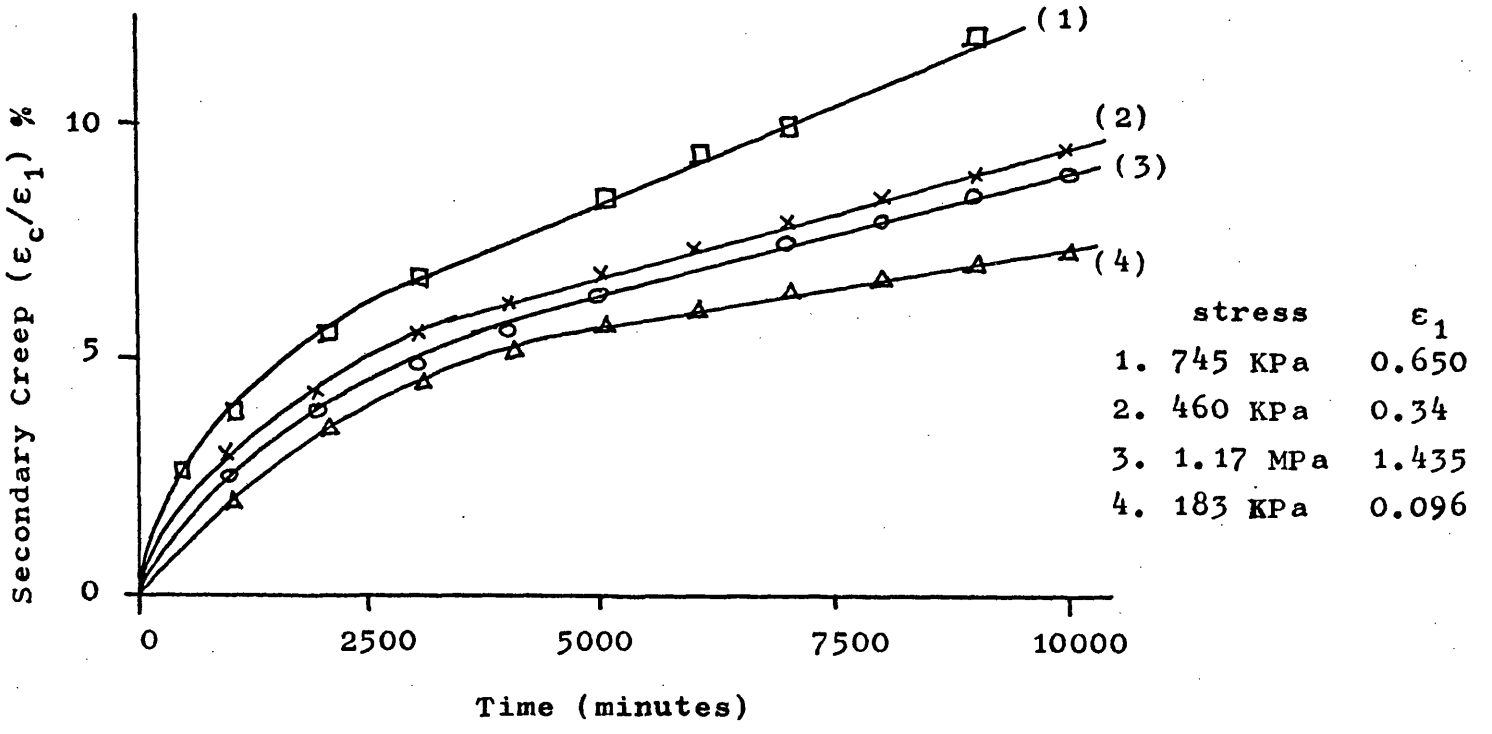

Figure 4.8 Secondary Creep for vulcanizate 'A' at 60°C and 40% R. Humidity

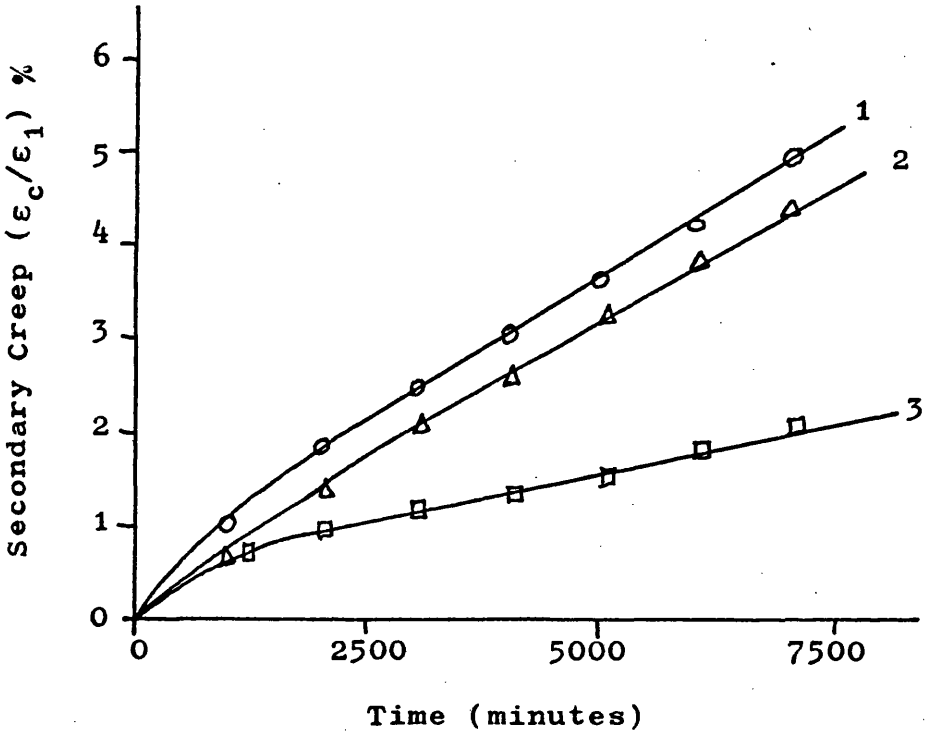

Figure 4.9 Secondary Creep for vulcanizate 'A' at 60°C and "oven humidity".

	stress	ε_1
1.	1.525 MPa	1.94
2.	840 KPa	0.72
3.	1.01 MPa	1.05

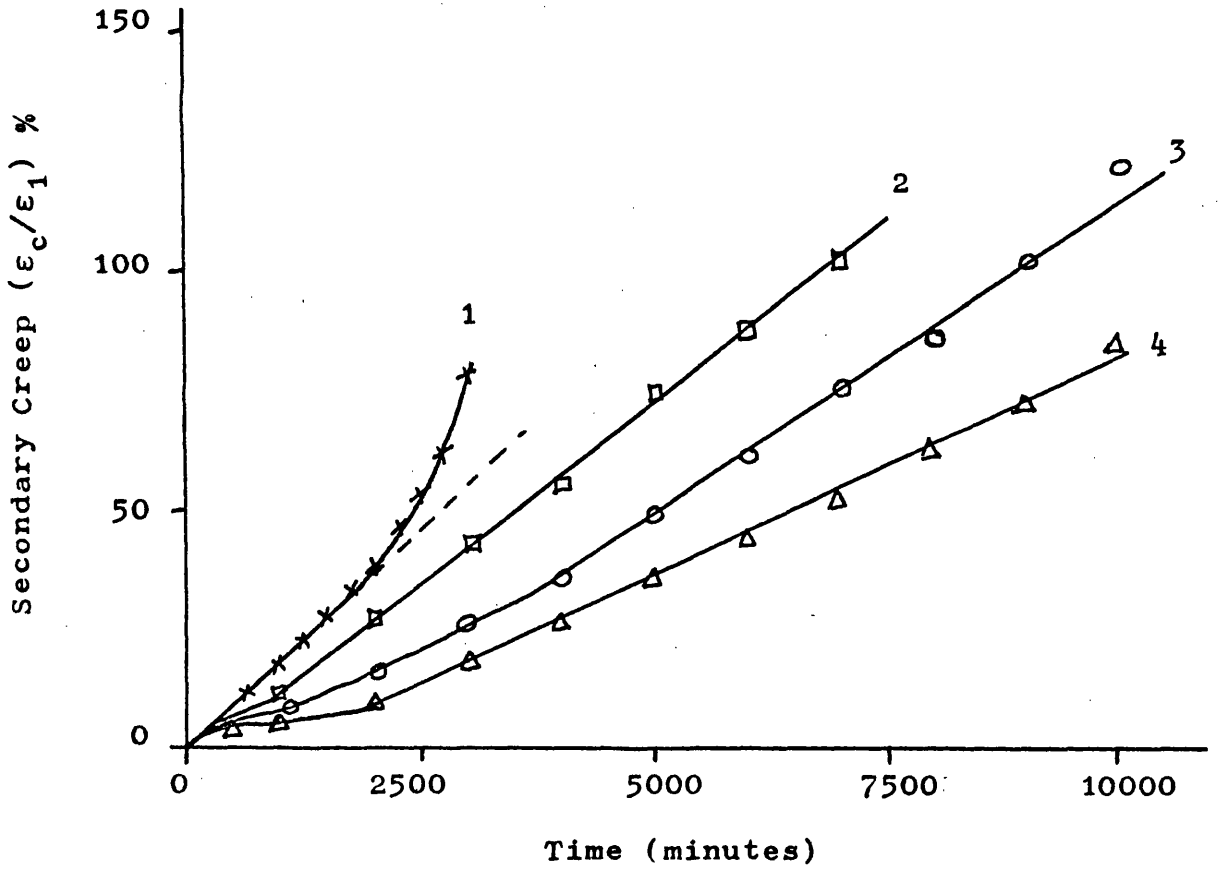

Figure 4.10 Secondary Creep of vulcanizate 'A' at 80°C and 40% R.H.

	stress	ε_1
1.	1.54 MPa	1.60
2.	1.12 MPa	1.07
3.	446 Kpa	0.234
4.	246 KPa	0.137

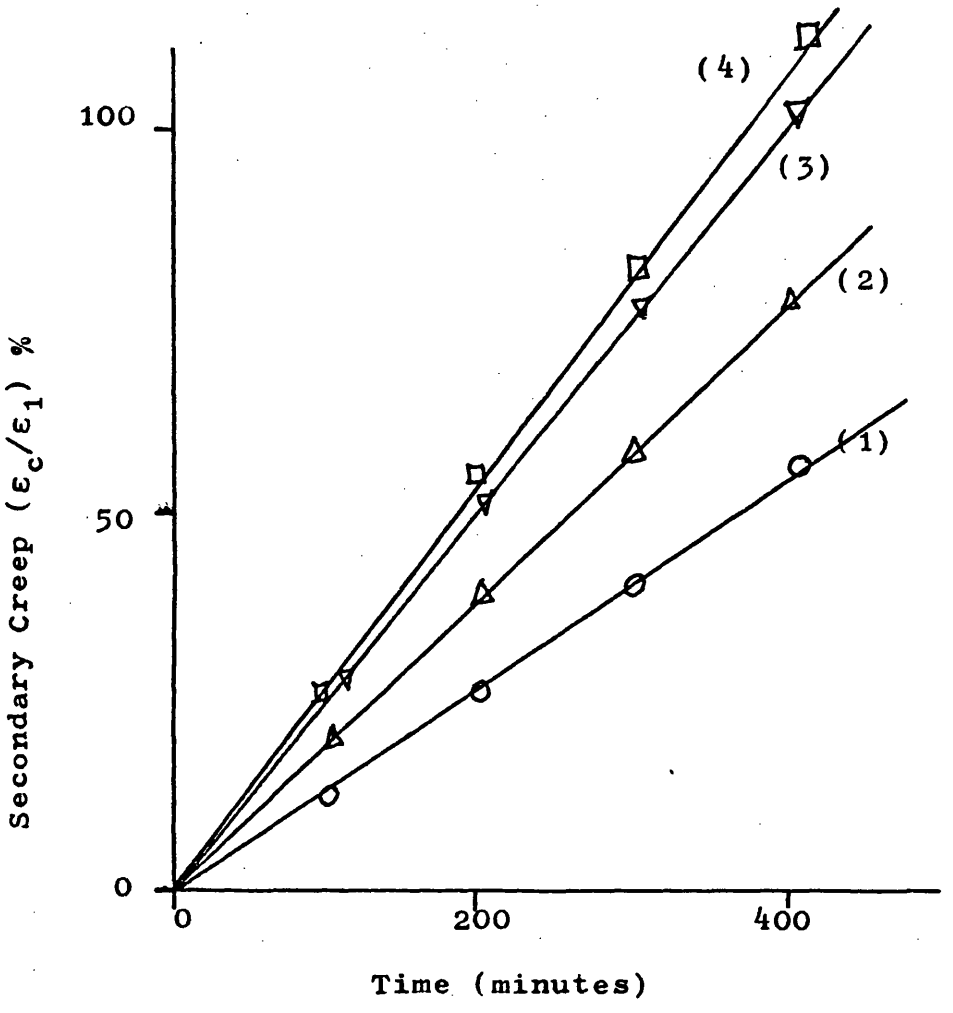

Figure 4.11 Secondary creep at 100°C and oven humidity for vulcanizate 'A'.

stress	ε_1
1) 410 KPa	0.222
2) 740 KPa	0.495
3) 1.06 MPa	0.70
4) 1.43 MPa	1.255

determined where:-

Δ = observed creep - $K't$

K' = linear creep rate derived from each curve at long times.

Although the extent of this discrepancy depends on stress and relative humidity it obeys a function of time which depends on temperature only

i.e. $\Delta = \Delta_\infty \; f(T)$

at constant temperature

where Δ_∞ is the maximum discrepancy observed at long times and which depends on temperature and humidity. This is illustrated in Figure 4.12 where estimated values for Δ have been plotted as a function of time. Results for each sample have been normalised by multiplying actual values by a factor N/Δ_∞ in each case so as to obtain a single composite curve. Note that the discrepancy contribution to the total creep at these temperatures has only a transient influence since it is complete at quite short times. By curve fitting it can be shown that at 35°C and 60°C the relationship between Δ and time can be represented by:-

$$\Delta = \Delta_\infty \left[1 - \text{Exp} - bt\right]$$

b = constant

For greater generality however the formula

$$\Delta = \Delta_\infty \left[1 - \text{Exp} - bt^d\right] \qquad 4.6$$

was examined initially. This can be manipulated to give

$$\log_{10}\left[-\ln\left(\frac{\Delta_\infty - \Delta}{\Delta_\infty}\right)\right] = \log_{10} b + d \log_{10} t.$$

Experimental results are shown in Figure 4.13, examination of which shows that the two straight plots have unit

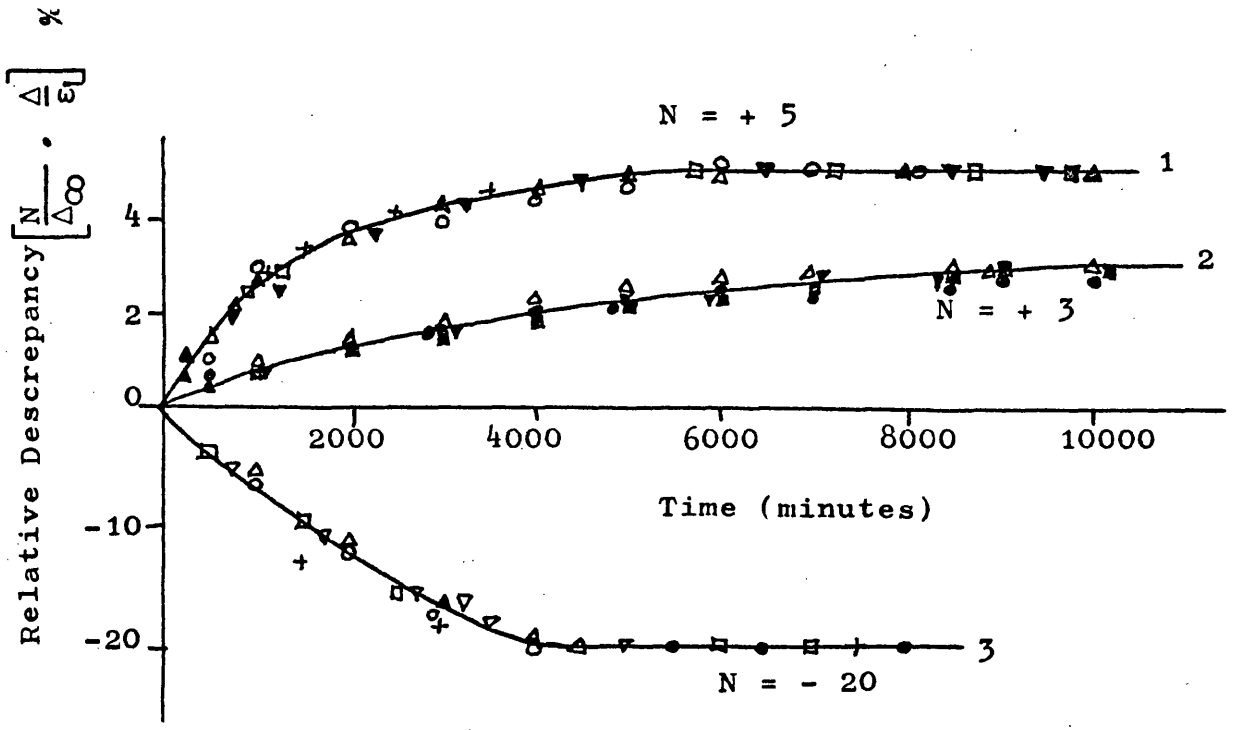

Figure 4.12 Normalised determinations of the discrepancy Δ as a function of time.
Note the change of scale at Δ = 0.

1) 60°C 40% R.H. ▲ ε_1 = 0.248, ○ ε_1 = 0.203, + ε_1 = 0.153, ▼ ε_1 = 1.435, □ ε_1 = 0.650

2) 35°C 40% R.H. ● ε_1 = 0.71, Δ 1.21, ■ 0.15, ▼ 0.20

3) 80°C 40% R.H. ● ε_1 = 0.86, Δ 0.624, □ 0.524, ▽ 0.234, + 0.137

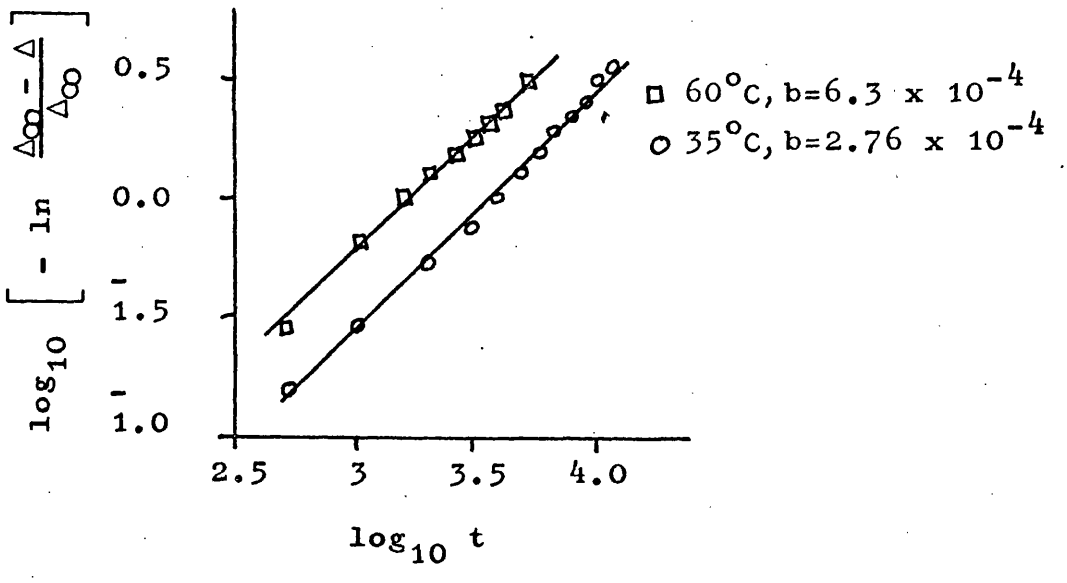

Figure 4.13 Examination of the 'discrepancy' Δ according to Equation 4.6 for results at 40% relative humidity.

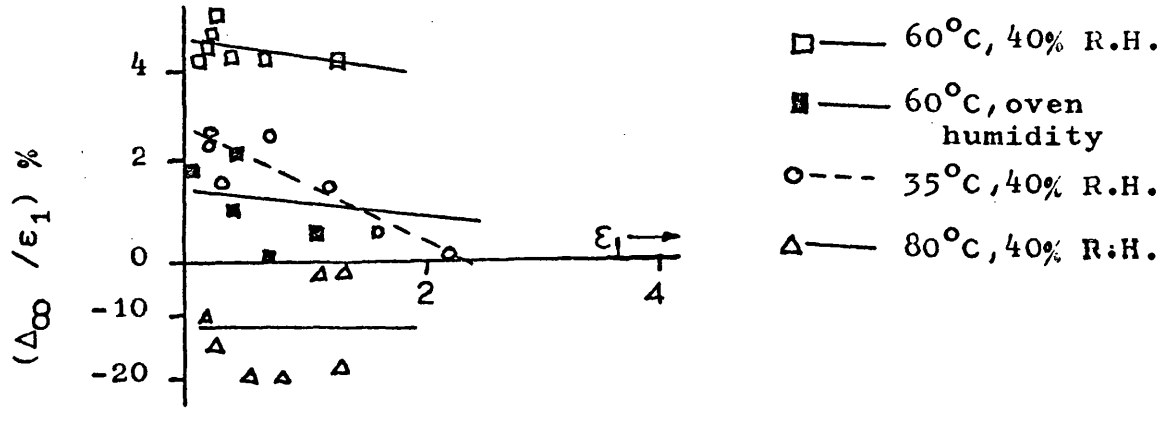

Figure 4.14 Maximum values, Δ_∞, for the discrepancy between actual and ideal creep curves. Note the change of scale at the origin.

gradient, so indicating that 'd' = 1.0. On the basis of these two results 'b' increases with temperature. Finally, observed values for Δ_∞ are shown in Figure 4.14; Δ_∞ decreases with applied stress (initial strain) and increases with increasing humidity for results at 35°C and 60°C.

4.3 The Initial Decelerating Response

The secondary creep response, as outlined above, is not in general linear over long periods of time. Whilst the post-sigmoidal acceleration observed at 80°C could possibly be examined in terms of a number of models, the decelerating response at shorter times and for more extensive periods at lower temperatures is more difficult to explain. This is to be examined more closely in this section.

The total secondary creep for vulcanizate 'A' observed within the experimental time scale, was only 2-5% and 8-10% of the initial deflection at 35°C and 80°C respectively. Consequently the approximations used in developing equations 4.3 and 4.5 may be regarded as valid in most cases and a linear variation of creep strain with time would be expected. This conclusion is equally applicable to situations involving bi-mechanistic decay processes; Equation 4.3 would simply require modification to read:-

$$(\lambda_t - \lambda_t^{-2}) = (\lambda_o - \lambda_o^{-2}) \left[1 + (A_1K_1 + A_2K_2)t \right]$$

and again the variation of $(\lambda_t - \lambda_t^{-2})$ and therefore of λ_t would be linearly proportional to time for small

deformations. Similarly, it can be shown from considerations of the quantities involved, for these small amounts of creep, that a progressive decrease of creep rate analagous to the mitigation of stress relaxation due to scission and recreation of network chains, as proposed by Flory, is not possible. (see Section 1.10). In the Flory equation

$$Kt = -\ln(\sigma/\sigma_o) + \frac{(-\ln \sigma/\sigma_o)}{2.2!}$$

terms higher than the first may be neglected for small 'Kt'. In the case of creep, however, the reformation of network chains has another and more important effect. Newly formed chains are progressively strained subsequent to the time of their formation because of continuing creep. A stress contribution from the secondary network is of ever increasing importance as a consequence. Green and Tobolsky [9], have examined this situation mathematically assuming a constant concentration of network chains, each broken chain being considered to reform in an unstrained position. New bonds, like the original network, were considered to decay by first order scission kinetics. This leads to *:-

$$\frac{\sigma}{E_o} = (\lambda - \lambda^{-2}) \text{ Exp } - Kt + K \text{ Exp } - Kt \int_o^t \left(\frac{\lambda}{\lambda_\tau^2} - \frac{\lambda_\tau}{\lambda^2}\right) \exp K\tau . d\tau$$

4.7

λ = elongation ratio at time t and for the purpose of the integral is a constant.

λ_τ = elongation ratio at time τ.

$\tau < t$.

K = decay constant

E_o = network modulus at zero time.

The two terms represent stress contributions from original and new networks respectively. An analytic solution to this equation, $\lambda = f(t)$ was not given but in the text it was suggested that λ should increase exponentially with time. Again therefore, for small amounts of creep, a linear creep-time relationship would be expected and this is supported by qualitative considerations of the proposed model. A creep strain of say 5% of the initial elongation suggests a reduction of a similar amount in the concentration of primary network chains. Approximately 5% of the total network would consist therefore of new chains and on average each of these would be strained by about 2.5% of the initial deflection. The partial contribution to the total stress from new chains, taking into account the shape of the rubber stress strain curve, would therefore be in the order of only 1/10% to 3/10% depending on the initial strain.

Some evidence suggests that the presence of oxygen has a great influence, not only on the degradation of elastomeric networks, but also on their formation. Tobolsky and Mercurio [10] for example observed oxidative hardening of SBR in the absence of vulcanizing agents

* This has been modified here so that 'σ' may be regarded as constant as is the case for creep. In the original analysis the stress was based on the instantaneous cross sectional area and therefore increased with strain.

whilst Studebaker and Beatty [11] have suggested that hardening is caused by oxygen and that it depends on similar factors to those which influence degradation, namely sulphur concentration and accelerator/sulphur ratio. Similar conclusions for natural rubber have been reported by Maisey and Scanlon [12] who suggested that secondary network formation depends on the extent of oxidation since antioxidant additions reduce both. For sulphur vulcanizates they proposed a bond interchange mechanism involving oxygen and this is supported by more recent evidence [13]. In the present work it was noticed that apparent increases in modulus were evident after a period of creep. The term 'apparent' is used here since obvious values for unstrained length and cross sectional area cannot be applied to samples which have been subjected to a period of network reorganisation at strains in the creep range. Nevertheless, experimental data is shown as a function of permanent set in Figure 4.15 for samples crept at 60°C and 80°C. Permanent set and modulus variations for samples crept at 35°C were too small to be measured. It appears, therefore, that secondary network formation may lead to a net increase in the chain concentration and this may be related to the presence of oxygen. Assuming that K_3 network chains form for every K_1 scissioned, where K_1 represents the decay constant, then equation 4.7 can be modified to compensate for an ever increasing network density. In this case

$$\frac{\sigma}{E_o} = (\lambda - \lambda^{-2}) \operatorname{Exp} - K_1 t + K_3 \operatorname{Exp} - K_1 t \int_o^t \left(\frac{\lambda}{\lambda_\tau^2} - \frac{\lambda_\tau}{\lambda^2}\right) \operatorname{Exp} K_3 \tau . \, d\tau .$$

and the actual creep response would depend on the ratio K_3/K_1. Even here, however, a significant contribution to the total stress from secondary network formation at the small creep strains observed for samples at 35°C is unlikely and this is supported by the lack of measureable permanent set. Furthermore, in comparison to Figure 4.14, if the decelerating creep response resulted from concurrent crosslinking it would be more prominant at higher initial strains where the ratio of tangent moduli for new and primary networks would be relatively higher. This follows from the shape of the rubber stress-strain curve.

In contrast to the two network theory and its subsequent re-examination by Flory and others, Tobolsky et al [14] have more recently proposed a mechanism of secondary network formation that can lead, in the absence of extensive simultaneous network degradation, to an increase in overall stress at constant elongation. They considered the crosslinking together of network chains already stressed. This was used to explain anomalous increases in stress observed during stress relaxation experiments on polybutadiene vulcanizates at 200°C in vacuum. Typical stress relaxation curves were, however, observed for the same rubber in air atmosphere where the degradative process completely masked this finer influence. Similar mechanisms may be important under air conditions at low temperatures, such as have been used in the present work, where oxidative degradation is slow.

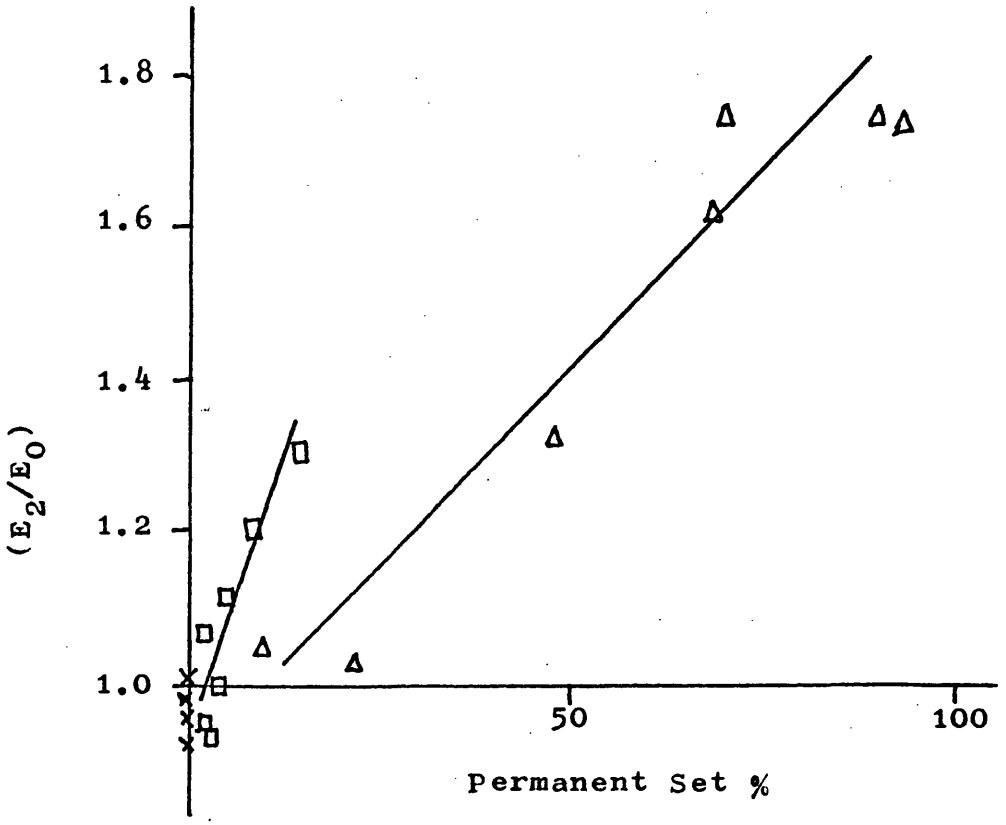

Figure 4.15 A comparison of rubbery moduli before, E_0, and after, E_2, creep testing as a function of permanent set. From results at 40% relative humidity.

Δ - 80°C

□ - 60°C

x - 10°C

The loss of volatiles by evaporation during the duration of creep experiments could have a great influence on rubbery modulus. C. S. Kim [15] has observed increases in modulus in the order of 25% for polybutadiene after ageing for 1.5 years at 27°C and has attributed this to losses of sol fraction by diffusion to the surface and subsequent evaporation. Effects of this magnitude are of obvious importance in determining creep response Nevertheless, the volatile loss from vulcanizate 'A' at temperatures as low as 35°C would be expected to be small, bearing in mind that only 1% loss occurs at temperatures in the range 80°C to 110°C, see section 3.3a. It is not considered therefore that the initial decelerating creep response can be explained solely in terms of network hardening resulting from gel fraction loss. This is further supported by the fact that the time discrepancy of the initial transient at any given temperature is not a function of elongation, see Figure 4.12, wheras volatile loss is accelerated by imposed extension, Figure 3.7.

Figure 4.14 indicates that the initial decelerating transient is greatly influenced by applied humidity and this may be examined in terms of the influence of humidity on network modulus and with respect to the time dependency of water adsorption or desorption. See section 2.5. Again, the fact that the time dependency of the decelerating response is not affected by imposed elongation (specimen thickness) suggests that the process cannot be attributed solely to a continued and slow infusion of water. Furthermore, it will be shown later that humidity

does not have a significant effect on the slope of the linear portion of secondary creep curves. Consider therefore the results obtained at 'oven humidity' at 60°C. During the duration of their creep history they would, if anything, desorb water and therefore their moduli would increase. This means that an accelerating initial creep response would be expected since the 'drying out' process would be more rapid during the early stages of creep. As a result the initially increasing network modulus would compensate for some of the creep elongation. Even so, these samples still showed a decelerating initial response. By comparison, it is not known whether the samples at 40% relative humidity would absorb or desorb water during the experimental duration. Clearly, an initial adsorption of water with its attendant reduction of network modulus would manifest itself as an initially rapid creep response. Again however, if this was the case, one would expect that the time dependency of this process would depend on applied elongation. In conclusion therefore the initial decelerating response cannot be solely attributed to a slow adsorption of water during the early stages of creep although this may make a contribution at high humidities. Nevertheless, the concentration of pre-absorbed water, as determined by test humidity and sample pre-conditioning time, does seem to influence the magnitude of this process.

Finally, it is of interest to note that Gent [1] has observed decelerating creep curves for a vulcanizate similar to 'A' at 60°C. The magnitude of the initial

curvature was more pronounced in the absence of oxygen. Further, he found that vulcanizates cured for only short times crept faster in vacuum than in air and proposed that in air weak polysulphide or other linkages were stabilised by the presence of oxygen. The possibility of a separate and rapid relaxation process to explain decelerating creep curves cannot be ignored.

4.4 The Influence of Carbon Black

Vulcanizates similar to 'A' but with 30 pphr carbon black additions have been prepared and tested. A single masterbatch of composition 'A' was used to prepare vulcanizates E, F, G, H and I, typical creep curves for which are shown in Figures 4.16 and 4.17. These are similar in shape to those for vulcanizate 'A' although the initial decelerating response is more pronounced and persists to higher temperatures. In contrast, slopes 'K' for linear portions observed at longer times were not significantly affected by the presence of black or by the type of black. Vulcanizate 'I' is an exception and consistently showed fractionally higher creep rates. It should be noted, however, that these samples were tested at similar stresses of about 1.4 MPa rather than at similar initial strains. As a result, the more highly reinforced vulcanizates showed lower initial elongations and therefore slower absolute creep rates. In this respect, vulcanizate 'I' had the highest modulus of the samples tested and one of the slowest absolute creep rates.

It is of interest to note that linear creep rates 'K' expressed in terms of initial strain, are almost

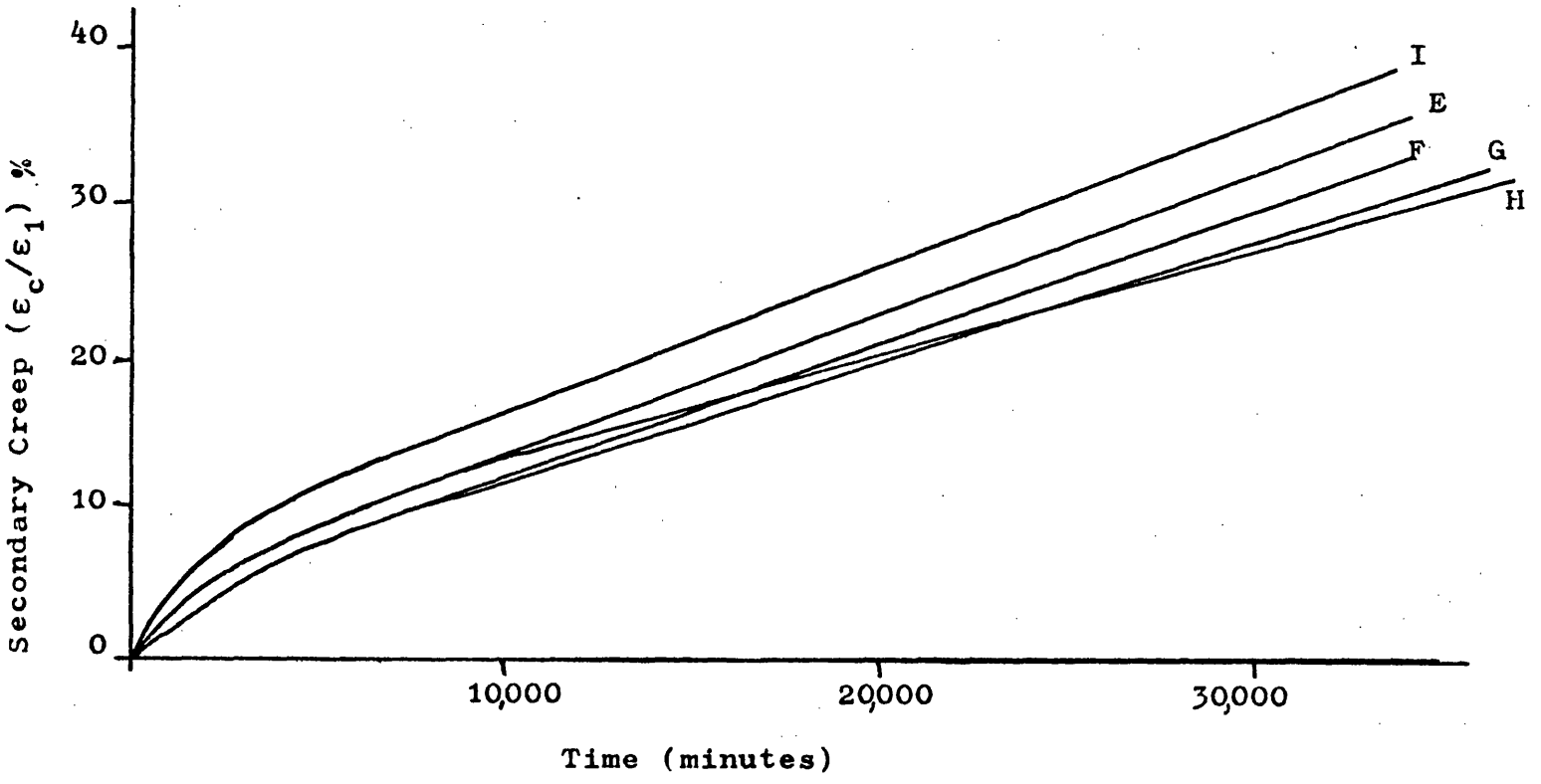

Figure 4.16 Secondary creep curves for vulcanizates E, F, G, H and I at 60°C and oven humidity.

ε_1 :- E 0.65, F 0.94, G 0.75, H 1.12, I 0.88

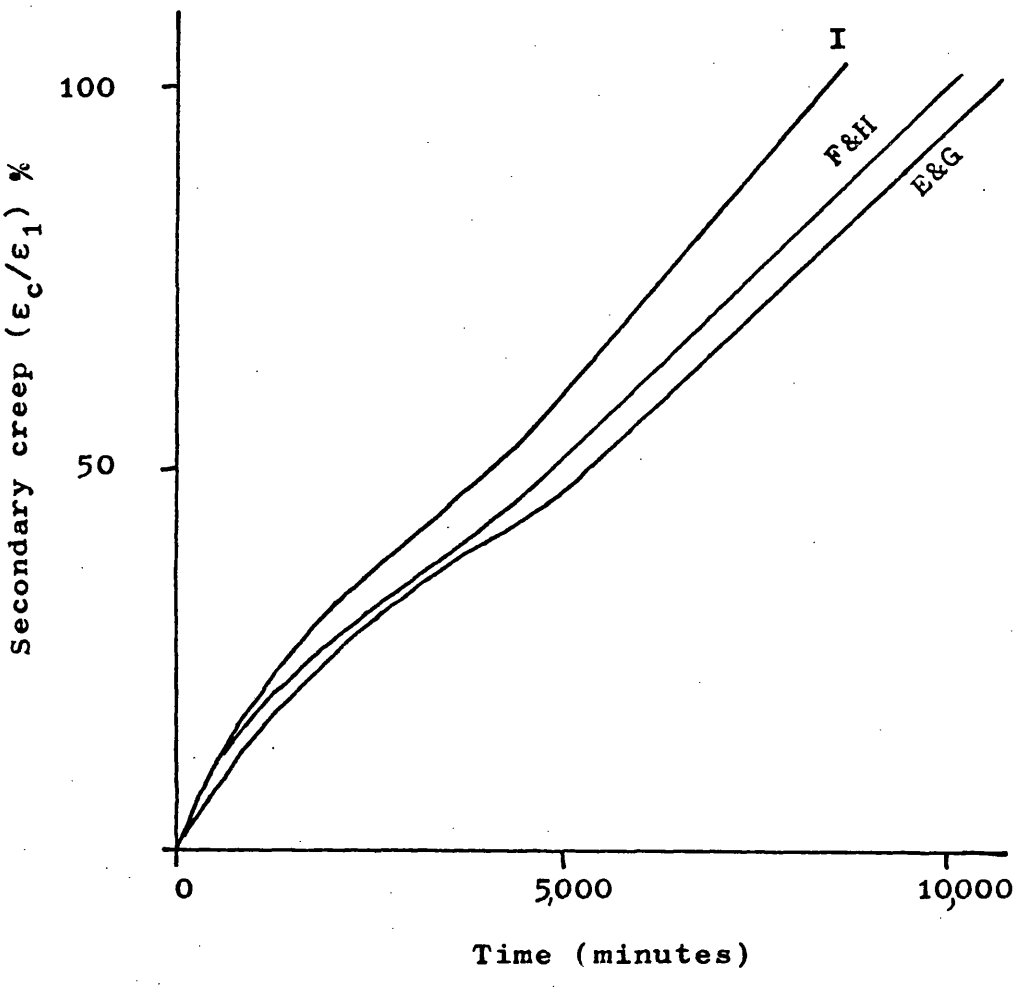

Figure 4.17 Secondary creep of filled vulcanizates E, F, G, H and I at 80°C and oven humidity.

independant of black additions. This implies that filler reinforcement is unaffected, over a wide range of creep strain, by network changes in the gum phase around individual carbon black particles. Although reinforcement markedly decreases with increasing temperature, it cannot be significantly affected by ageing. The influence of fillers on total creep response must therefore be predominantly viscoelastic in origin. Antioxidant and pro-oxidant influences of carbon blacks are subject to debate [17] but it would seem that they have negligible effect, in the temperature region of present interest, when compounded in a mix containing commercial anti-oxidant.

A more detailed discussion of the influence of carbon blacks on creep will be presented in Chapter 6.

4.5 The Influence of Temperature

Slopes 'K' for the linear portions of creep curves obtained for vulcanizate 'A' are indicated in Figure 4.18 as a function of initial elongation. As a first observation it will be noted that at the three lower temperatures these have general characteristics indicated by Figure 4.6 and a maximum is observed for strains in the region of unity. At 100°C, however, the creep rate continues to increase with increasing strains above 1.0 and this may reflect a stress activated process similar to that proposed by Kusano and Murakami [8] to explain stress relaxation behaviour at temperatures in this region. Further, it can be seen that unlike the decelerating initial response, linear creep rates 'K' are unaff-

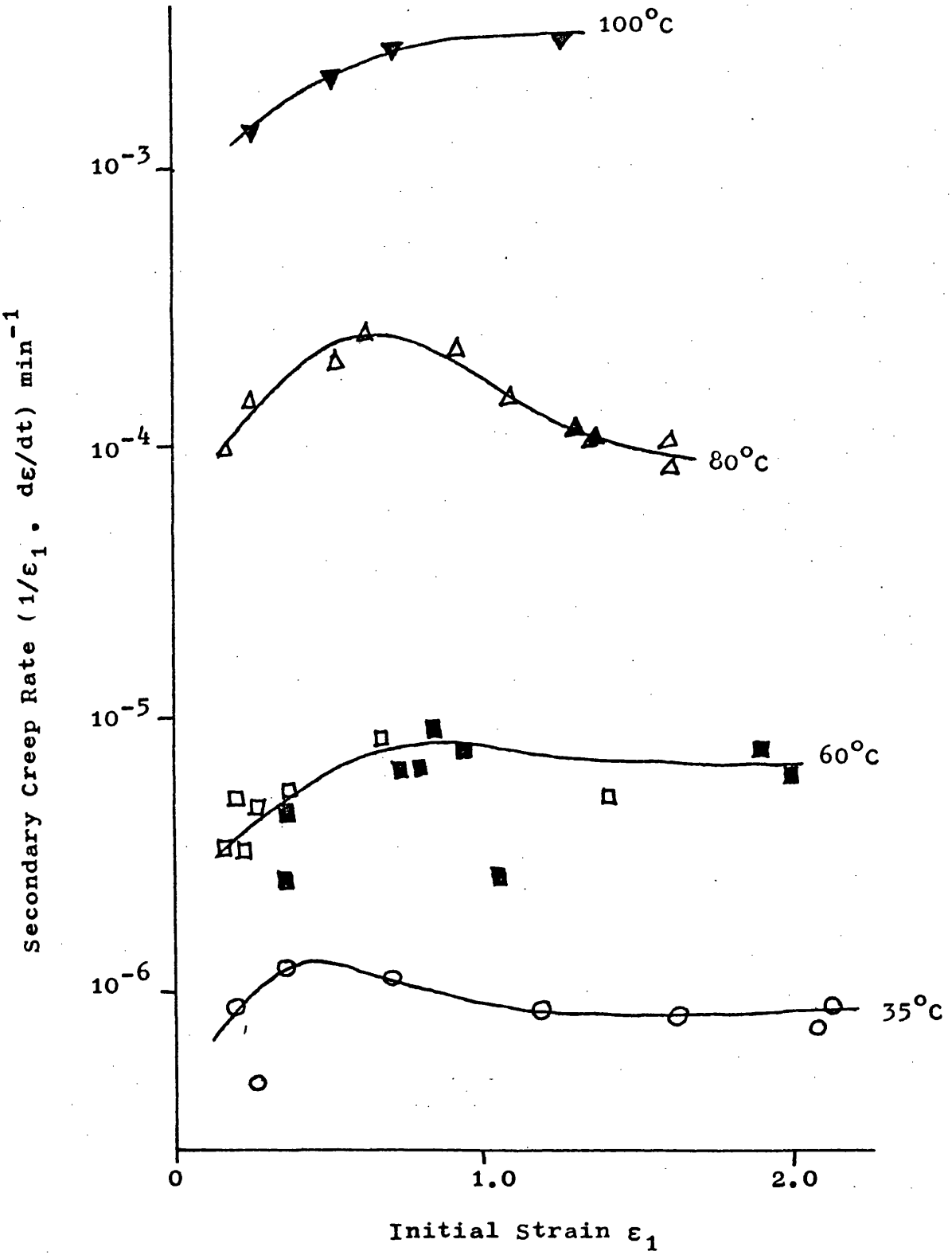

Figure 4.18 Experimental data for secondary creep rates of vulcanizate 'A' as a function of Initial Strain. Open symbols represent results at 40% relative humidity; filled symbols "oven humidity".

ected within experimental error by variations in relative humidity.

An Arrhenius plot for linear creep rates 'K' is shown in Figure 4.19 for both gum and filled vulcanizates. Good agreement is observed between present and published data [16] for vulcanizate 'A' and this is dispite differences in specimen thickness; 1.8 mm and 1.0 mm respectively. This lends support to the conclusion presented in Chapter 3 that creep rates in the present work were not limited by restricted oxygen infusion resulting from overlarge specimen cross section. An activation energy for the secondary creep process of 129 KJ mol^{-1} can be derived from Figure 4.19 and this contrasts with 74 KJ mol^{-1} for the oxygen rubber reaction. (see Chapter 3). These relative temperature dependences are in agreement with the fact that scission efficiences, determined from stress relaxation experiments, increase with decreasing temperature since creep rates decrease more rapidly with decreasing temperature than do ageing rates. This indicates that the secondary creep process for vulcanizates based on 'A' cannot be accounted for in terms of a simple oxidation mechanism. Nevertheless Derham et al [16] found that omission of antioxidant from vulcanizate 'A' increased the creep rate by a factor of 2.6 although the activation energy was unaltered. Oxidative ageing cannot therefore be neglected as a contributory factor in the creep process as observed in air atmosphere.

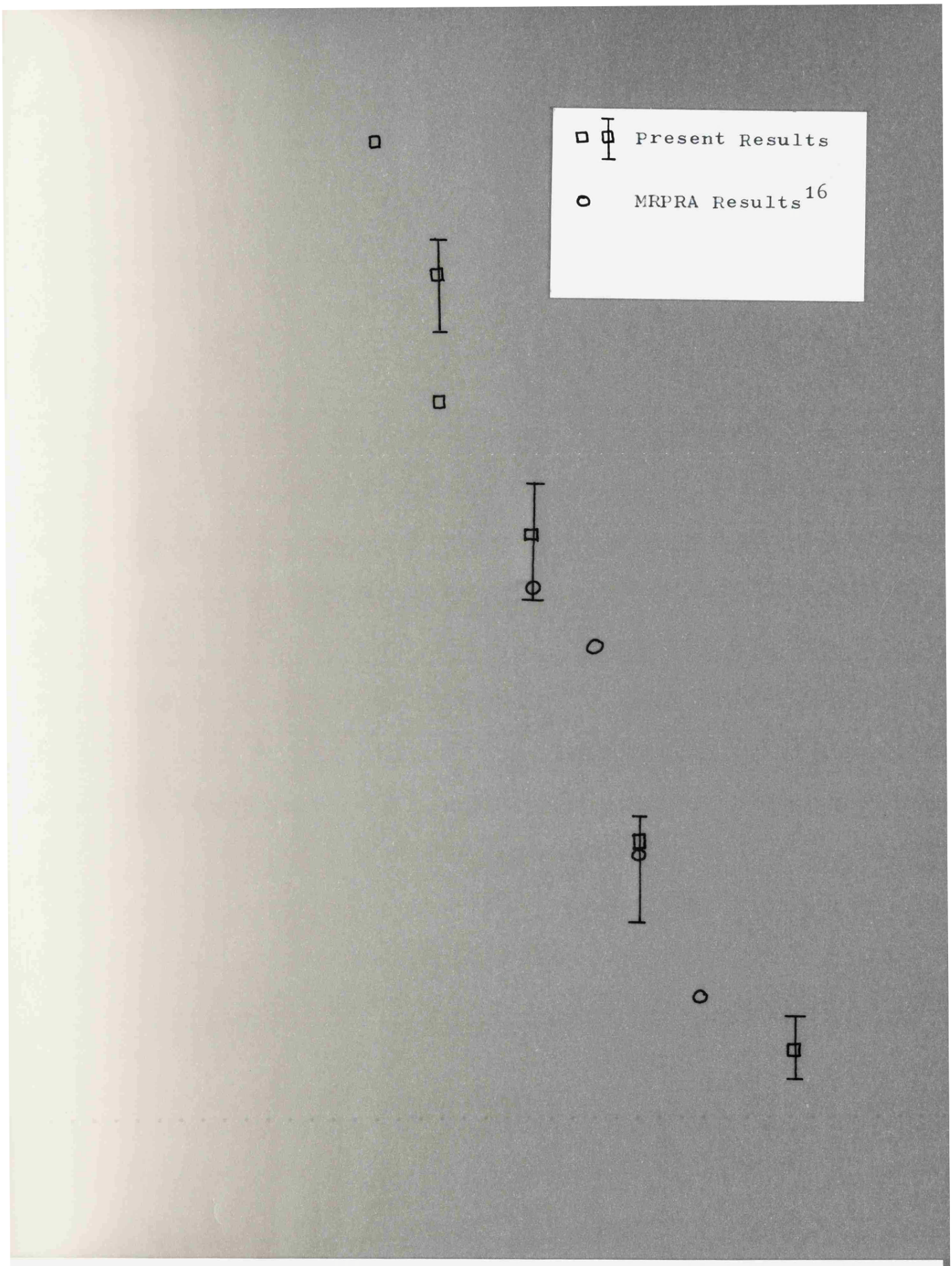

Figure 4.19a Creep data for vulcanizate 'A'.

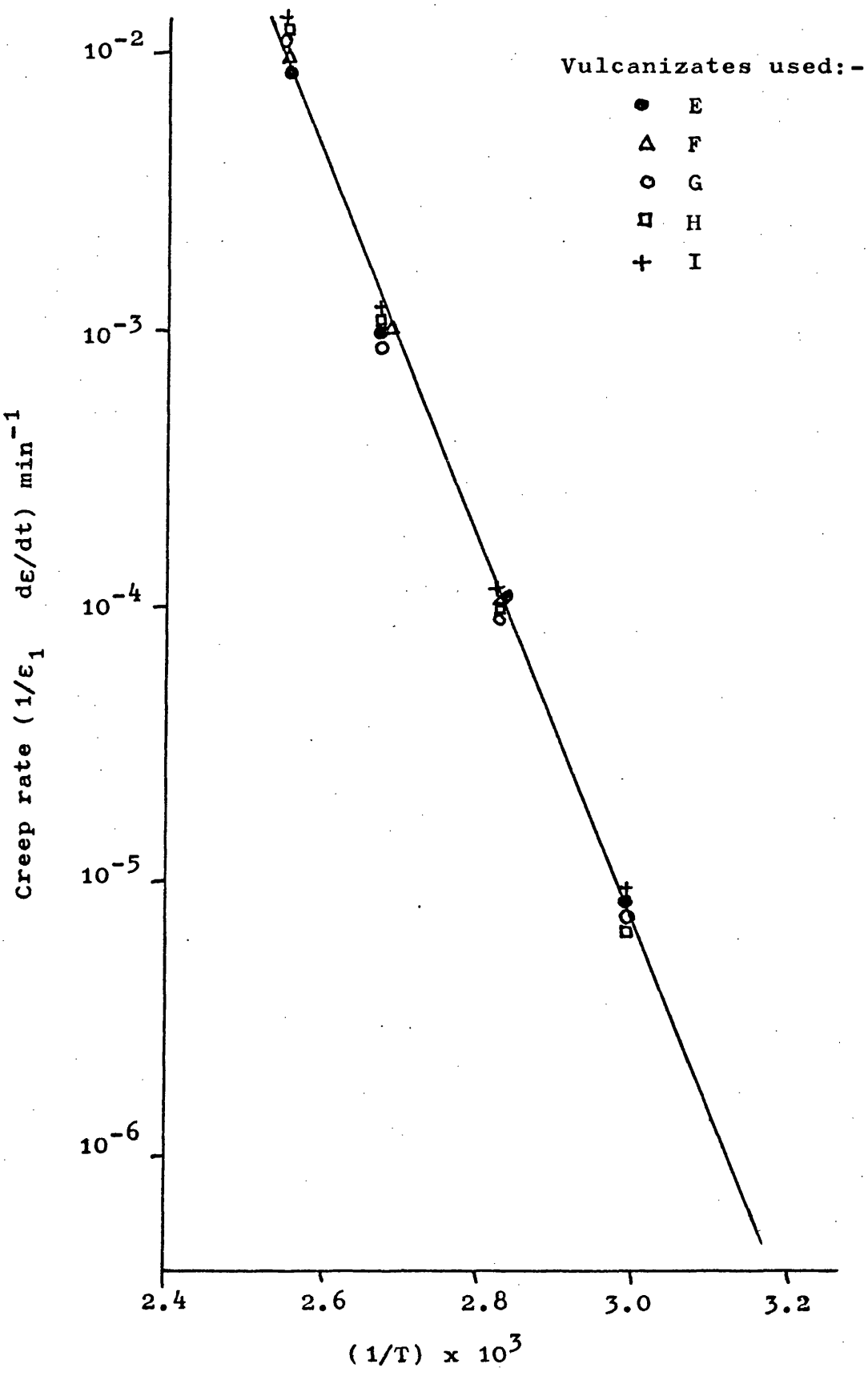

Figure 4.19b Creep data for vulcanizate 'A' with 30 pphr carbon black additions.

The increases in network modulus observed during the secondary creep of vulcanizate 'A' suggests that a continuation of the vulcanization process could have an influence on creep deformation. It should be noted, however, that the activation energy of vulcanization for compounds similar to 'A', 'F' and 'G' is known to be in the order of 87 to 95 KJ mol^{-1} [19]. Again this does not compare with the activation energy for creep.

The activation energy for diffusion of free sulphur in unvulcanized natural rubber in the absence of oxygen has been reported as 30 KJ mol^{-1} [18, 20]. By comparison, in the presence of oxygen a value of approximately 70 KJ mol^{-1} has been observed [21, 22]. On the other hand Bresler et al [23] have examined the diffusion of sulphur in vulcanized natural rubber, in the absence of oxygen, and have also observed a value of approximately 70 KJ mol^{-1}. They took the precaution to remove free sulphur from their samples by acetone extraction subsequent to vulcanization. This suggests that the presence of oxygen in the uncured samples using free sulphur [21, 22] caused a crosslinking process to occur, thus bonding the diffusing sulphur into the network. The observed activation energy would therefore equal that for a vulcanized system. This is of particular relevance to the secondary creep process since the diffusion of bound sulphur in a crosslinked network is equivalent to the envisaged sulphur bond lability mechanism for network reorganisation. Bresler et al [23] have proposed a simple mechanism to account for the difference between the

activation energy of diffusion of free and bound sulphur. They suggest that some of the bound sulphur is dissociated from the network and that only this is free to diffuse. Using the idea of a dissociation constant

$$R\,S_x \xrightarrow{K_d} R\bullet + S_x\bullet$$

and using the Gibbs-Helmoltz equation [24] they showed that the proportion of free to bound sulphur 'P' would be given by

$$P = \text{const} \sqrt{\text{Exp} - \frac{\Delta H_f}{RT}}$$

where ΔH_f is the enthalpy of formation of the S - S bond. Further, they showed that the activation energy of diffusion for bound sulphur Q_D' would be given by

$$Q_D' = Q_D + \frac{\Delta H_f}{2}$$

where Q_D is the activation energy for free sulphur diffusion. This follows from their proposal that $D' = PD$. Hence, using $\Delta H_f \sim 110$ KJ mol^{-1} [25] this gives

$$Q_D' \simeq 30 + \frac{110}{2} \simeq 85 \text{ KJ mol}^{-1}$$

which is in reasonable agreement with their observed value of 70 to 75 KJ mol^{-1}.

The facts outlined in the previous paragraph suggest a tentative explanation for the observed activation energy for secondary creep. The concept of sulphur bond dissociation and mobility and the idea that the presence of oxygen promotes crossliking of these bonds implies that creep occurs by a combined process of dissociation and oxygen favoured re-combination.

The high activation energy observed for creep of vulcanizate 'A' may be explained if it is assumed that the rate limiting process is determined by the scission of polysulphide crosslinks. This would follow if the processes by which radicals are removed from the system are relatively rapid; possible processes are:-

a) Recombination of radicals.

b) Reaction with adjacent network chains by means of a cross-linking reaction, with or without the aid of oxygen.

c) Interchange with other polysulphide bonds.

d) Termination by reaction with active groups.

It is implicitly assumed therefore that the rate of oxygen induced scission of network chains, as occurs in DCP vulcanizates, may be neglected in comparison to the activity of sulphur based groups. Consider a hypothetical energy potential profile for the process of bond scission:-

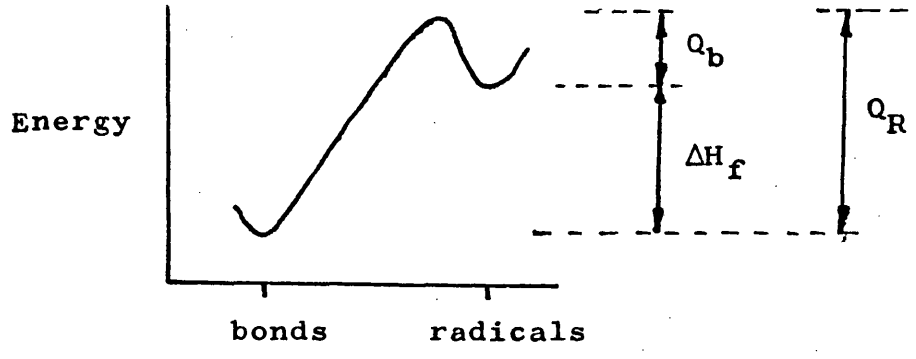

Q_R represents the activation energy for radical formation and therefore the activation energy for creep. Clearly, Q_R exceeds ΔH_f, i.e. $Q_R = 110 + Q_b$ KJ mol^{-1}. Q_b, the activation energy for removal of radicals from the system

would depend on their mechanism of removal; in case a) above for example Q_b would be determined by diffusion criteria since bond re-combination depends on the kinetics which govern the rate at which radical terminated chains "find" each other. By comparison case c) would depend on the mechanism of reaction. In practice the dominating process of radical removal may depend on a number of factors such as network structure, crosslink density, the presence of oxygen and the influence of antioxidants. This would explain the scatter of observed activation energies which have been observed for stress-relaxation, see Section 1.11. To illustrate this a simple model is presented in Appendix 4A which suggests that radical recombination according to case a) is not likely to be relevant to vulcanizate 'A' although it may occur in vulcanizates of very low crosslink density at high temperatures, $>130^{o}C$.

In conclusion, therefore, it is suggested that the creep mechanisms which occur in vulcanizate 'A' are dominated by polysulphide crosslink scission followed by radical elimination by means of processes b, c and d above; oxidative crosslinking may be important in determining this.

4.6 Concluding Remarks

The initial decelerating response observed in the creep behaviour of vulcanizate 'A' and the dependance of the creep rate on temperature may be explained tentatively in terms of a creep mechanism involving both

sulphur diffusion and oxidative crosslinking. The linear relationship observed between creep deformation and time under load for vulcanizates 'A' and 'B' over long periods of time cannot, however, be explained in terms of established stress-relaxation theory.

Rapidly accelerating creep at long times analagous to tertiary creep in metals and other materials did not occur except at the highest temperatures and stresses. No evidence for creep instability by necking in the gauge length was observed and this is illustrated by Figure 4.20 which shows crept specimens tested under conditions indicated. The sample tested at 100°C shows extensive permanent set in the absence of necking. This could be accounted for by a 'creep hardening' process in which loss of cross section is compensated by a corresponding increase in network integrity. This is in agreement with the observed increases in apparent modulus with creep.

Extrapolation of Figure 4.19 indicates a value for the linear creep rate at 15°C of about 5×10^{-8} min^{-1}. Assuming a typical logarithmic creep rate for vulcanizate 'A' of 2.5% per decade, this indicates that at room temperatures the secondary process begins to dominate after about 400 days (1 year) under load. This must, however, be regarded as an order of magnitude calculation only because of uncertainty in the importance of initial decelerating creep response at room temperatures.

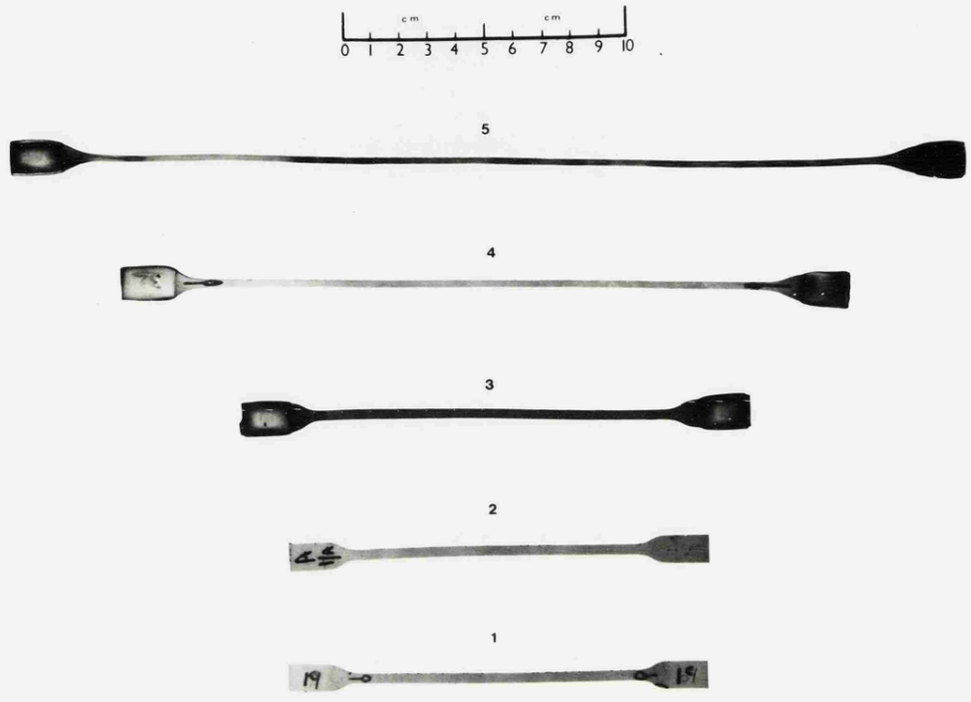

Fig 4.20 Vulcanizate 'A' specimens after various creep histories :-

	Temp.	Stress	Time	Rel. Humidity
1)	10 C.	0·32 GPa	11300 Mins.	40 %
2)	Virgin sample			
3)	60	1·17	10025	40
4)	80	1·53	11500	40
5)	100	1·43	400	Oven humidity

APPENDIX 4A

Bond Reformation by Radical-Radical Reaction

The removal of free radicals by mutual recombination is to be considered. It will be assumed that an equilibrium concentration of radicals is generated by S-S bond decomposition. Creep extension from this process may only occur when the radical concentration is sufficiently high so that each radical is close enough to an adjacent radical, other than the one from which it was originally scissioned, to react with it.

The equilibrium concentration of free radicals is given by

$$N_R = (n_s - 1)\ No\ Exp - \frac{\Delta H_f}{2RT}$$

see text

where N_R = conc of free radicals

n_s = no of S atoms in the cross-links

i.e. $(n_s - 1)$ = no of S-S bonds per cross-link

N_o = crosslink concentration

≃ network chain density

ΔH_f = enthalpy of formation of the S-S bond.

For simplicity it will be assumed that the fixed ends of radical terminated chains are arranged in a regular cubic array in space so that the typical separation

distance between them is $(1/N_R)^{1/3}$.

i.e. $$\left[\frac{1}{N_o\ (n_s - 1)}\right]^{1/3} \text{Exp} + \frac{\Delta H_f}{6RT}$$

Clearly, for mutual elimination of radicals by recombination this separation distance must be less than twice the contour length of radical terminated chains.

i.e. $$\left[\frac{1}{N_R}\right]^{1/3} < 2\, l_c$$

l_c - network chain length.

A value for l_c may be deduced if it is assumed that all chains have the same length.

Then $N_o\ l_c\ w = \rho$

w = mass of a network chain per unit length.

ρ = density of rubber.

i.e. $$l_c \simeq \frac{\rho}{N_o\ w}$$

Hence, for reaction to occur

$$\left[\frac{1}{(n_s - 1)N_o}\right]^{1/3} \text{Exp} + \frac{\Delta H_f}{6RT} < \frac{2\rho}{N_o\ w}$$

OR $$\text{Exp}\ \frac{\Delta H_f}{4RT} < \left[\frac{2\rho}{w}\right]^{3/2} \frac{(n_s - 1)^{1/2}}{N_o}$$

4A.1

For gum natural rubber $\rho \simeq 1000$ kg m^{-3} and w may be determined from the monomer mass and its repeat distance:-

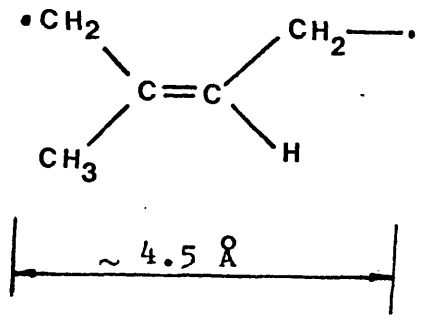

wt = 68 g mol^{-1}

= 1.13 x 10^{-25} kg per monomer

i.e. $w \approx \frac{1.13 \times 10^{-25}}{4.5 \times 10^{-10}}$ kg m^{-1}

$\approx 2.51 \times 10^{-16}$ kg m^{-1}

Hence $\frac{2\rho}{w} \approx \frac{2 \times 10^{3}}{2.51 \times 10^{-16}} \approx 8 \times 10^{18}$ m^{-2}

Substituting this into equation 4A.1 and taking $\Delta H_f \sim 110$ KJ mol^{-1} gives:-

$$\text{Exp } \frac{3300}{T} < (2.25 \times 10^{28}) \frac{(n_s - 1)^{1/2}}{N_o} \qquad 4A.2$$

According to the model the possibility of crosslink elimination by mutual recombination is favoured by high temperatures, low crosslink densities and by the presence of long polysulphide crosslinks. In the case of vulcanizate 'A' for example N_o is about 1.2 x 10^{-26} m^{-3} and n_s may be in the order of 1, 2, 3, 4 ....

Taking $n_s = 2$ gives

$$\text{Exp } \frac{3300}{T} < 187$$

i.e. $T > 360^{\circ}C$.

It is suggested therefore that radical-radical recombination does not play an important role in the creep of vulcanizate 'A'.

REFERENCES; CHAPTER 4

1. A. N. Gent J. App Polym Sci 6 (22), pp 442-8 (1962).

2. M. Mooney, W. E. Wohlstenholme and D. S. Villars J. App Phys 15, pp 324-37 (1944).

3. A. V. Tobolsky "Properties and Structure of Polymers." Ch. 5. Pub. Wiley, N. Y. (1962).

4. C. S. Kim Rubb Chem and Technol 42 (4) pp 1095-1121 (1969).

5. P. Thirion and R. Chasset Rubb Chem and Technol 37, pp 617-626 (1964).

6. G. Steiner and A. V. Tobolsky Rubb Chem and Technol 43 (5), pp 1036-39 (1970).

7. A. V. Tobolsky, I. B. Prettyman and J. H. Dillon J. App Phys 15 (4), pp 380-95 (1944).

8. T. Kusano and K. Murakami J. Polym Sci, Polym Chem Edn. 10, pp 2823-31 (1972).

9. M. S. Green and A. V. Tobolsky J. Chem Phys 14 (2), pp 80-92 (1946).

10. A. V. Tobolsky and A. Mercurio J. App Polym Sci 2 (5), pp 186-88 (1959).

11. M. L. Studebaker and J. R. Beatty Rubb Chem and Technol 45 (2), pp 450-66 (1972).

12. L. J. Maisey and J. Scanlon J. App Polym Sci 7, pp 1147-52 (1963).

13. K. Murakami and S. Tamura J. Polym Sci, Polym Letters Edn. 11 (5), pp 317-21 (1973).

14. A. V. Tobolsky, Y. Takahashi and S. Naganuma Polymer J. 3 (1), pp 60-66 (1972).

15. C. S. Kim Trans Soc Rheol 17 (3), pp 425-47 (1972).

16. C. J. Derham, E. Southern and A. G. Thomas N.R. Technology. Rubb Dev Supp No. 7 (1970).

17. W. L. Hawkins and F. H. Winslow
"Reinforcement In Elastomers." Ch. 17
Ed. G. Kraus
Pub. Interscience, N. Y. (1965).

18. G. J. Van Amerongen
Rubb Chem and Technol 37 (5), pp 1065-1152
(1964).

19. L. R. Barker J. Inst Rubb Indust 7 (3),
pp 121-23 (1973).

20. S. E. Bresler, V. I. Pryadilova and V. Ya. Khainman
Rubb Chem and Technol 29 (3), pp 946-79 (1956).

21. M. Ikeda, T. Yamamoto, S. Yoshiharu, N. Wada and
Y. Kaneko
Radioisotopes 22 (10), pp 556-60 (1973).

22. I. Auerbach and S. D. Gehman
Ind Eng Chem, Anal Edn.
26 (4), pp 685-90 (1954).

23. S. E. Bresler, V. P. Kushnev and S. M. Saminskii
Rubb Chem and Technol 29 (3), pp 980-98
(1956).

24. F. Daniels and R. A. Alberty
"Physical Chemistry." 3rd End Ch. 3.
Pub. Wiley, N. Y. (1966).

25. R. E. Powell and H. Eyring
J. Am Chem Soc. 65, pp 648-54 (1943).

CHAPTER 5

LOGARITHMIC CREEP

5.1 General Considerations

There is no doubt that in the rubbery plateau region creep follows closely to a logarithmic law over extensive time periods in the absence of chemical changes. This is illustrated in Figure 5.1 which shows some creep curves obtained in the vicinity of room temperature. Logarithmic creep is associated with physical processes occuring as a result of applied stress and is therefore a manifestation of viscoelastic response which in turn is associated with the versatility of movement of threadlike macromolecules. At the time of writing the mechanisms of logarithmic creep are uncertain but the process must represent a progression of the rubbery network towards equilibrium. Network restraints which prevent an immediate adoption of equilibrium conditions are therefore responsible for subsequent creep. Ferry [1, 2] has pointed out that the logarithmic relationship implies a very slow response to applied stress since it persists to very long times and that this cannot be accounted for by classical viscoelastic theory based on the kinetics of single molecular chains. Instead he has proposed that the behaviour may be ascribed to co-operative long range motions of the network extending through large regions of three dimensional structure. This is supported by

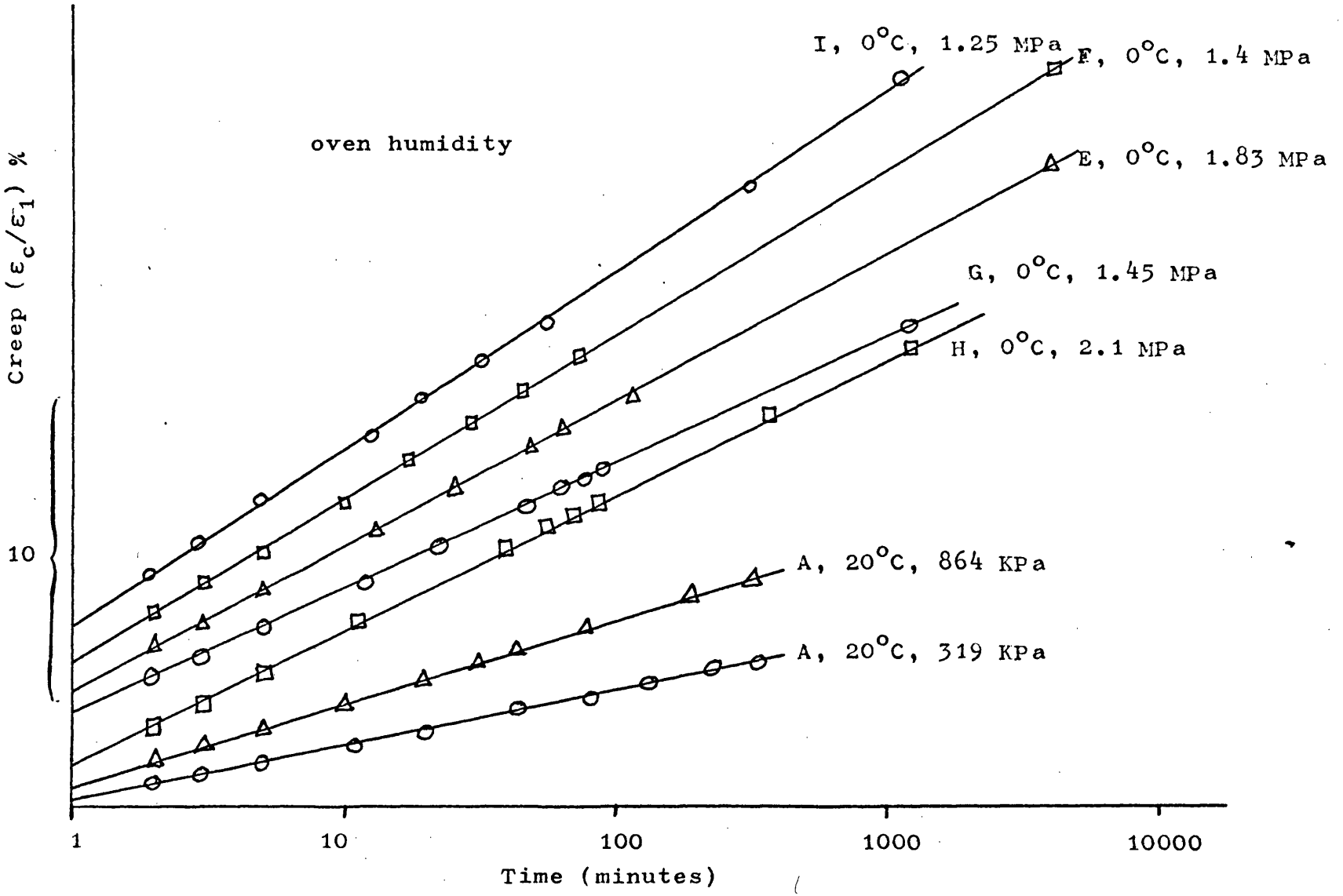

Figure 5.1 Logarithmic creep curves for a number of vulcanizates at the temperatures and stresses shown. Curves shown offset vertically for clarity.

Smith [4]. It implies that the volume of network associated with the creep mechanism may be many times that of a single chain and this idea will feature prominantly in the present chapter. A tentative theory for logarithmic creep based on activation energy ideas is to be presented.

5.2 The Influence of Temperature

In Chapter 2, Figures 19 and 20, it was shown that logarithmic creep rates for vulcanizates 'A' and 'B' were identical, within experimental error, over a range of temperature. Furthermore, the rate constant increased with decreasing temperature in the range $+15^{o}C$ to $-30^{o}C$ which is in fact the lower half of the rubbery plateau region for natural rubber. This behaviour is in agreement with general viscoelasticity theory presented in Chapter 1 since reductions of temperature below room temperature represent a shift towards the transition region. It would be useful to present creep data in the form of time-temperature transition mastercurves but the reduced modulus E_R is not strongly affected by temperature within the rubbery plateau. In practice it is not possible, in this region, to establish a clear quantitative picture of the influence of temperature on reduced modulus due to the inherent variability between individual test pieces and also because of the difficulty of measuring test piece cross-section with great accuracy. Indeed, a variation of specimen thickness along the gauge length of 2% is

permissible for creep samples according to BS 903 [5]. An empirical approach to the influence of temperature will now be described.

The logarithmic time relationship is not peculiar to elastomers and has been observed for metals at lower temperatures in the creep range and also for plastics. For metals a number of explanations have been considered including a distribution of activation energies for dislocation flow [6] and a distribution of activation stresses [7]. Whilst neither of these is disimilar to a distribution of relaxation times, the conventional approach to polymer viscoelasticity, it turns out that the activation energy concept has a simple mathematical interpretation. It can be shown that, for logarithmic creep, the activation energy for flow may be considered to increase linearly with the extent of prior creep.

Consider equation 1.4

$$\varepsilon = \varepsilon_1 + C\varepsilon_1 \log_{10} t \qquad 5.1$$

or

$$\varepsilon_c = C\varepsilon_1 \log_{10} t \qquad 5.2$$

where ε_c is the amount of creep strain observed in the time interval '1.0' to 't'.

i.e.

$$\varepsilon_c = \frac{C\varepsilon_1}{2.3} \ln t \qquad 5.3$$

and differentiating with respect to time gives:-

$$\frac{d\varepsilon_c}{dt} = \frac{C\varepsilon_1}{2.3t} \qquad 5.4$$

But from equation 5.3, $t = \text{Exp}\ (2.3\ \varepsilon_c/C\varepsilon_1)$

Hence

$$\frac{d\varepsilon_c}{dt} = \frac{C\varepsilon_1}{2.3}\ \text{Exp} - \frac{(2.3\ \varepsilon_c)}{(C\varepsilon_1)} \qquad 5.5$$

Equation 5.5 is analagous to the Arrhenius activation function

$$\text{Rate} = A \text{ Exp} - (Q/RT)$$

A = Constant

Q = Activation energy

R = Gas constant

T = Temperature

assuming that 'Q' increases linearly with the extent of creep 'ε_c'. This suggests that equation 5.5 might be re-written

$$\frac{d\varepsilon_c}{dt} = A \text{ Exp} - \frac{Q_1 + \beta\varepsilon_c}{RT}$$

$$\text{OR} \quad \frac{d\varepsilon_c}{dt} = B_1 \text{ Exp} - \frac{\beta\varepsilon_c}{RT} \qquad 5.6$$

β and B_1 are constants.

'Q_1' is the apparent activation energy at one minute under load. In the present work 'ε_c' is arbitrally taken as zero at 't' = 1 minute but in fact the creep strain could be measured from any other datum point in time and equation 5.6 would still hold, with relevant modification to the constant 'B'

$$\text{i.e.} \quad B_t = B_1 \text{ Exp} - \frac{\beta (\varepsilon_t - \varepsilon_1)}{RT}$$

ε_t = strain at time 't'

ε_1 = strain at time '1'

and time 't' would then be the datum point.

$$\text{i.e. In general} \quad \frac{d\varepsilon}{dt} = B_t \text{ Exp} - \frac{\beta (\varepsilon - \varepsilon_t)}{RT}$$

It should however be noted that these relationships cannot hold for very short times as an examination of equations 5.1 and 5.4 will show. At 't' = 0 the strain

is predicted to be minus infinity and the creep rate infinite. Nevertheless the logarithmic law agrees well with experimental data for times in excess of about 30 seconds. Equation 5.6 suggests that the activation energy is ever increasing and this implies zero creep recovery.

Equation 5.6 could possibly be used to analyse creep data at different temperatures were it not for the fact that the pre-exponential factor B_1 must itself be temperature sensitive. Consider two identical samples tested at two temperatures. After one minute under load the sample tested at the higher temperature will be closer to equilibrium than the other. This may be interpreted in two ways: the higher temperature sample may be considered to have already crept further during the first minute or alternatively it may be considered to contain fewer of the network restraints which prevent the immediate adoption of an equilibrium position. In either case the factor 'B_1' will be smaller. This in itself is sufficient to describe qualitatively the effect of temperature on creep rate. Despite this non constancy of 'B_1' it was decided to plot data for vulcanizates 'A' and 'B' at temperatures below 15°C in a fashion suggested by equation 5.6. Figure 5.2 shows experimentally observed logarithmic creep rates over a range of initial strain and for temperatures below 20°C. Values of the logarithmic creep rate 'C' can be taken from this figure for each temperature and for any given initial elongation 'ε_1'. Actual rates of creep ($d\varepsilon/dt$)

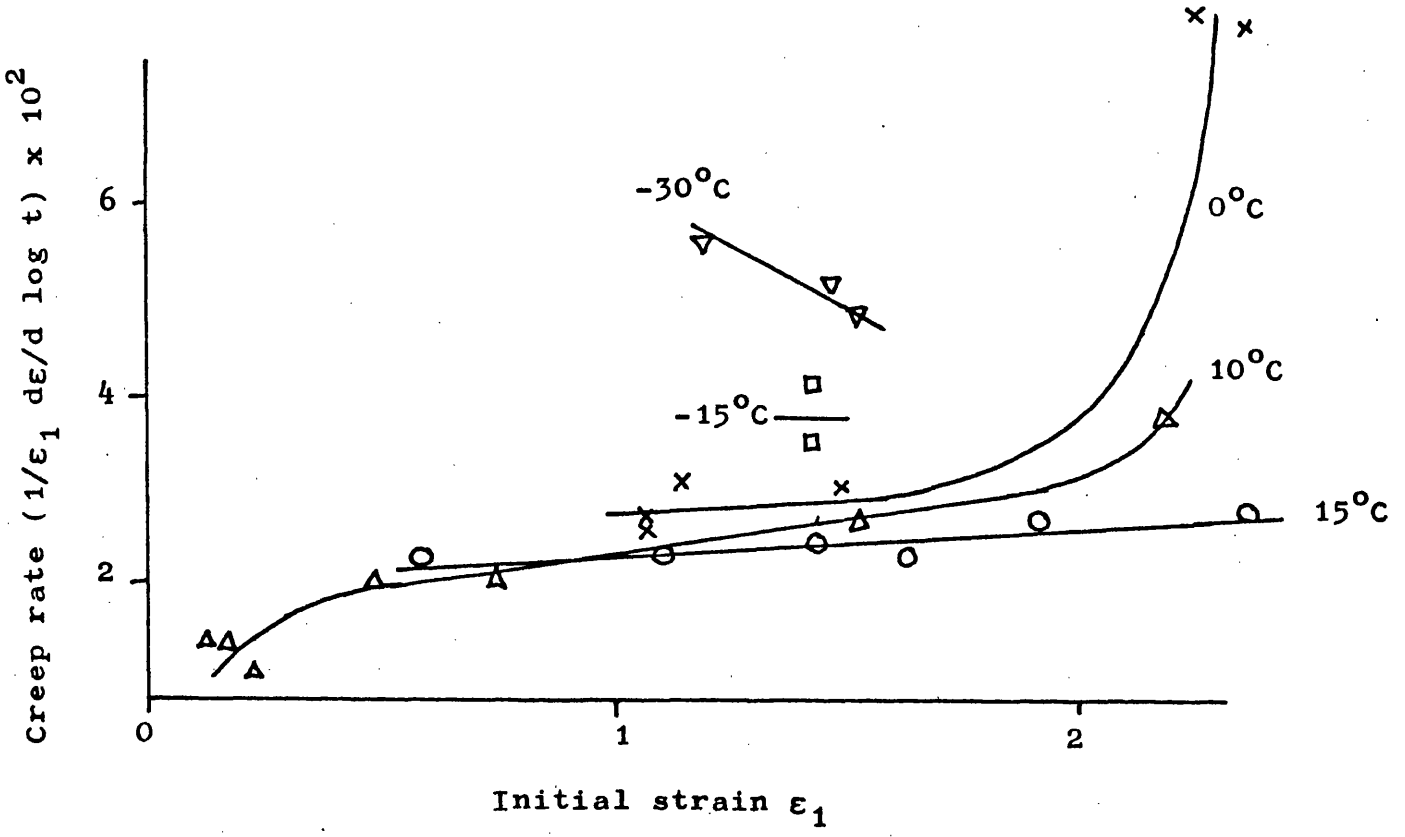

Figure 5.2 Logarithmic creep rates for vulcanizates 'A' and 'B' as a function of initial strain.

can then be calculated using equation 5.5:-

$$\ln \frac{d\varepsilon_c}{dt} = \ln \frac{C\varepsilon_1}{2.3} - \frac{2.3\,\varepsilon_c}{c\varepsilon_1} \qquad 5.7$$

or:-

$$\log_{10} \frac{d\varepsilon_c}{dt} = \log_{10} \frac{c\varepsilon_1}{2.3} - \frac{\varepsilon_c}{c\varepsilon_1} \qquad 5.7a$$

Figure 5.3 shows Arrhenius - like plots of the logarithm of the creep rate, so calculated, as a function of reciprocal temperature for an initial strain 'ε_1' of 1.5. Each line represents the creep rate after a given amount of prior creep 'ε_c' as indicated. Straight line relationships are observed. The positive slope is not unexpected since in this temperature region the creep rate decreases with increasing temperature and this in fact represents the effect of the pre-exponential factor 'B_1' on the creep rate as discussed above. It can however be seen that the plot yields an empirical relationship for the influence of temperature on creep rate since it is possible to draw the lines at different amounts of prior creep to intersect at a common point. Further, the slopes of these lines should vary linearly with the extent of prior creep. This is illustrated in Figure 5.4 where measured slopes are shown plotted against 'ε_c' together with similar data for other initial elongations. Remarkably it shows a linear relationship passing approximately through the origin. Assuming that the slopes of Figure 5.3 are given by ($\beta\varepsilon_c/2.3R$) then the slope of Figure 5.4 represents ($\beta/2.3R$) and a value for 'β' may therefore be evaluated; in this case 'β' is approximately 510 KJ mol^{-1} per unit strain.

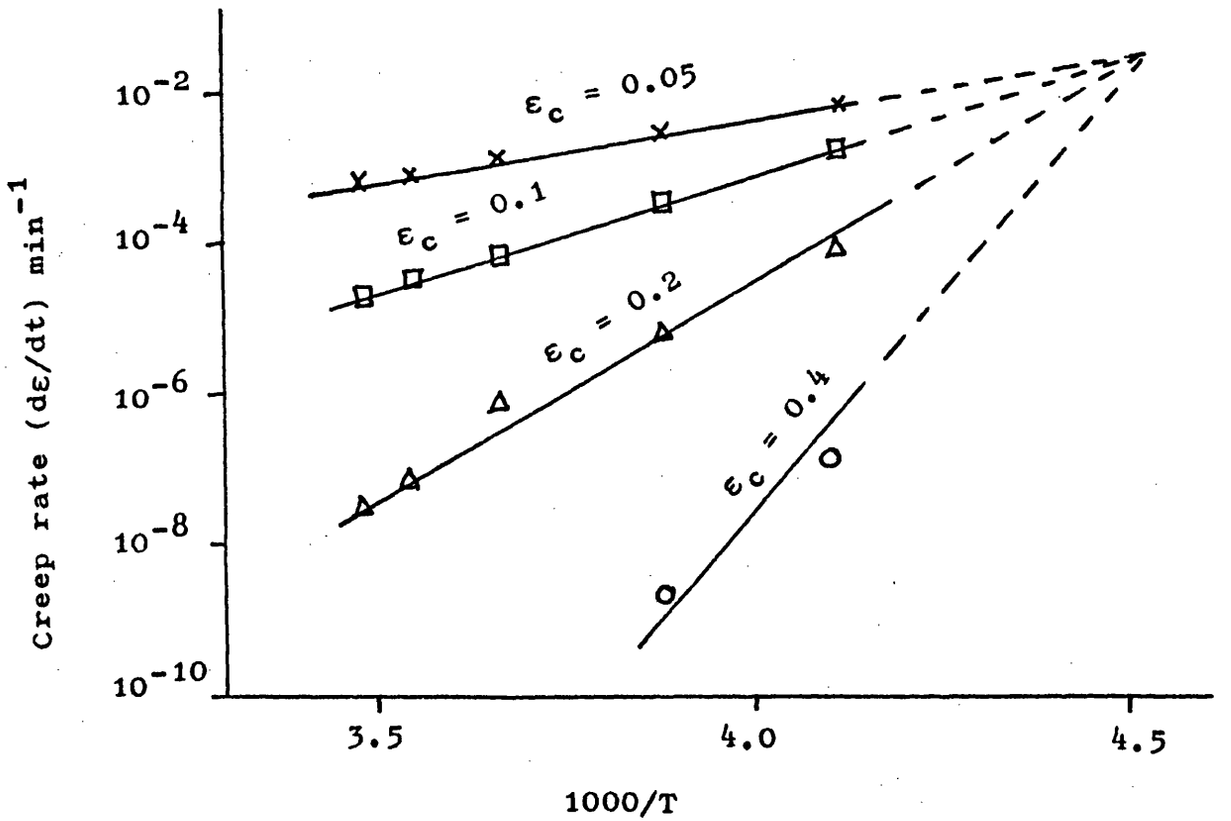

Figure 5.3 Creep rates of vulcanizates 'A' and 'B' as a function of temperature after various amounts of prior creep as indicated.

$\varepsilon_1 = 1.5$

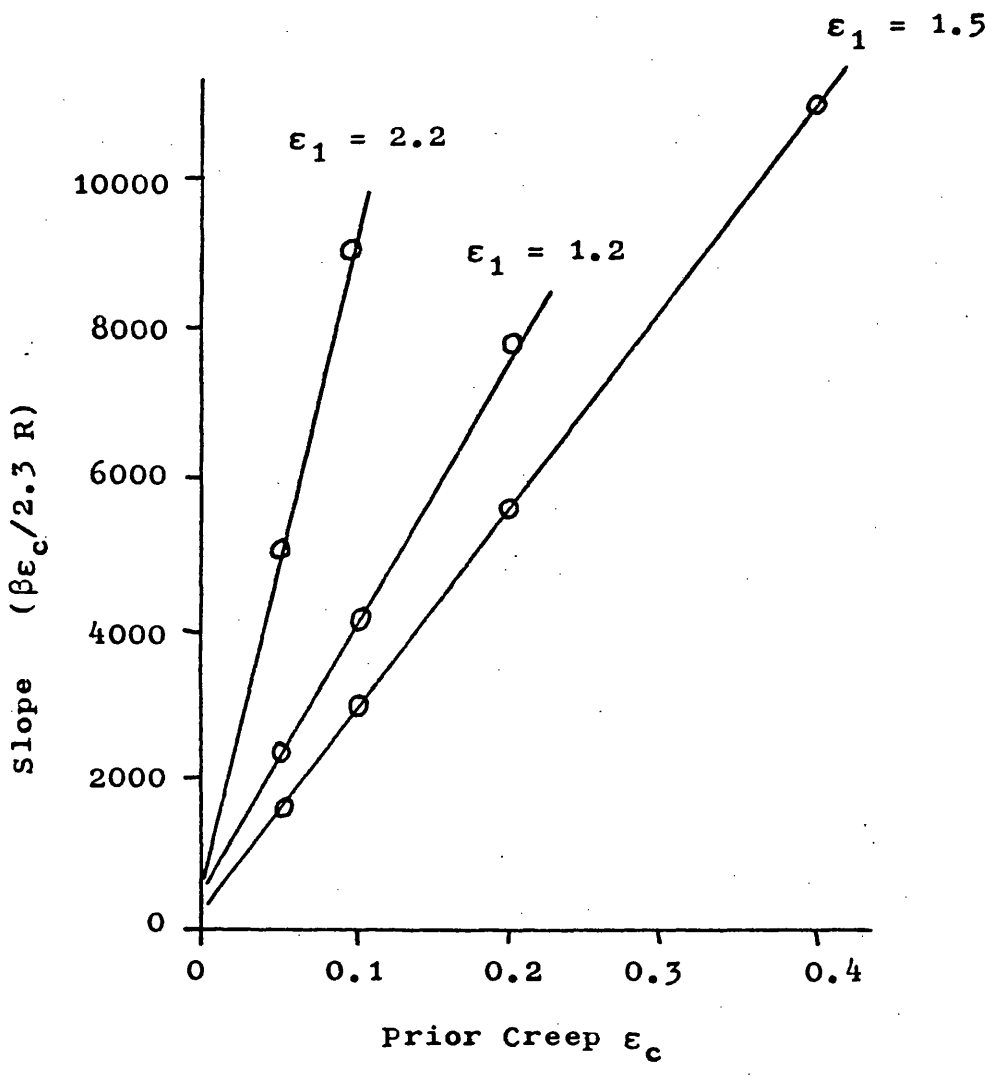

Figure 5.4 Slopes of the Arrhenius-like logarithmic creep plots as a function of prior creep. Data for vulcanizates 'A' and 'B'.

ε_1	β
1.2	670 KJ mol^{-1} $strain^{-1}$
1.5	510 KJ mol^{-1} $strain^{-1}$
2.2	1680 KJ mol^{-1} $strain^{-1}$

Using the above results the rate of creep, for a given initial strain, may be expressed in the form

$$\ln \frac{d\varepsilon}{dt} = A - \frac{\beta \varepsilon_c}{R} \left[\frac{1}{To} - \frac{1}{T} \right] \qquad 5.8$$

where the constants 'A' and 'To' are determined by the point of intersection as shown in Figure 5.3. This may be manipulated to give

$$\frac{d\varepsilon}{dt} = A \, Exp - \frac{\beta \varepsilon_c}{RTo} \cdot Exp + \frac{\beta \varepsilon_c}{RT} \qquad 5.8b$$

The first exponential term is associated with the increase of activation energy with continuing creep whilst the second term represents the greater ease of movement of the macromolecular network with increasing temperature. This second term is in fact analagous with the viscosity equation

$$n = no \, Exp + \frac{\Delta H}{RT}$$

n = viscosity

ΔH = activation energy for viscous flow.

It is well known that the Doolittle equation [3] is more suitable for the examination of the influence of temperature on the viscosity of polymers. This topic will not be pursued here however and equation 5.8 will be left as an empirical statement of observed results.

Creep data for vulcanizates 'A' and 'B' at two other initial elongations, plotted in the proposed Arrhenius fashion, are indicated in Figures 5.5 and 5.6. Again a single point of intersection can be drawn in each case. Gradients and derived values for 'β' are

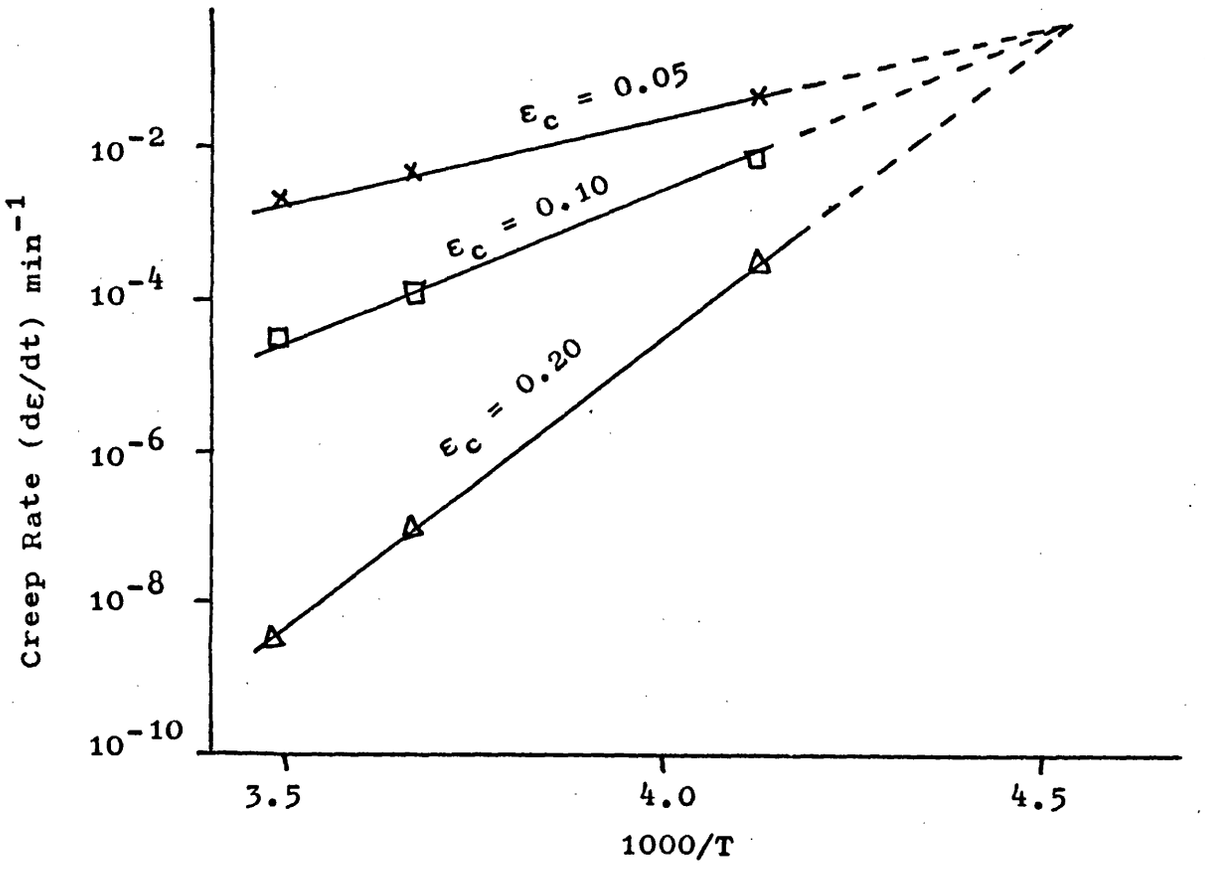

Figure 5.5 Creep rates of vulcanizates 'A' and 'B' as a function of temperature after various amount of prior creep.

ε_1 = 1.2

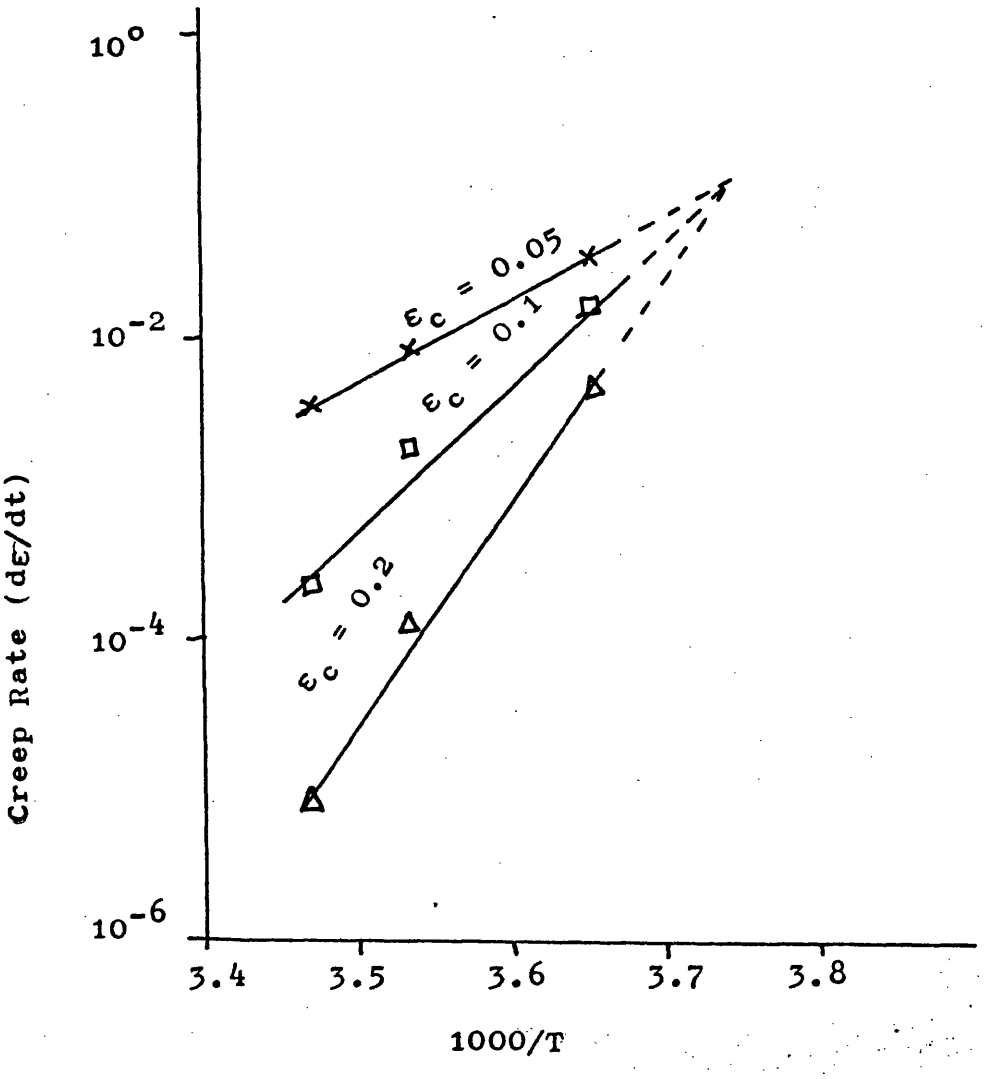

Figure 5.6 Creep rates for vulcanizates 'A' and 'B' as a function of temperature after various amounts of prior creep. $\varepsilon_1 = 2.2$

shown in Figure 5.4. It is of interest to point out that 'T_o' is approximately -53°C for initial strains of 1.2 and 1.5 whilst the corresponding temperature for an initial strain of 2.2 is only just below room temperature. In Chapter 2 it was mentioned that the high creep rates observed at high elongations may be associated with crystallisation. This would account for the large differences in 'β' and 'To' between results at $\varepsilon_1 = 2.2$ and results at moderate strains. The significance of 'T_o' is not understood but it is of interest to point out that viscosity and diffusion in elastomers are much influenced by the glass transition temperature [3]. Johnston and Shen [9] have recently shown that the glass transition for natural rubber is unaffected, within experimental error by extension; they obtained a value of $T_g = -69°C \pm 1/2°C$. It would seem therefore that a variation of 'T_o' with elongation cannot be attributed to changes in the glass transition temperature.

Above 35°C the logarithmic creep of vulcanizates 'A' and 'B' is relatively independent of temperature (see Chapter 2 Figures 19 and 20) and the temperature region 15°C to 30°C is marked by a transition in behaviour. An analysis of the time-temperature relationship in the above fashion for results obtained at temperatures above 15°C is not therefore possible. Nevertheless it is suggested that the mechanisms of creep in this region may be similar to those below 15°C and a more quantitative description will follow later. The proposed empirical relationship has been tested using other vulcanizates. Figure 5.7, for

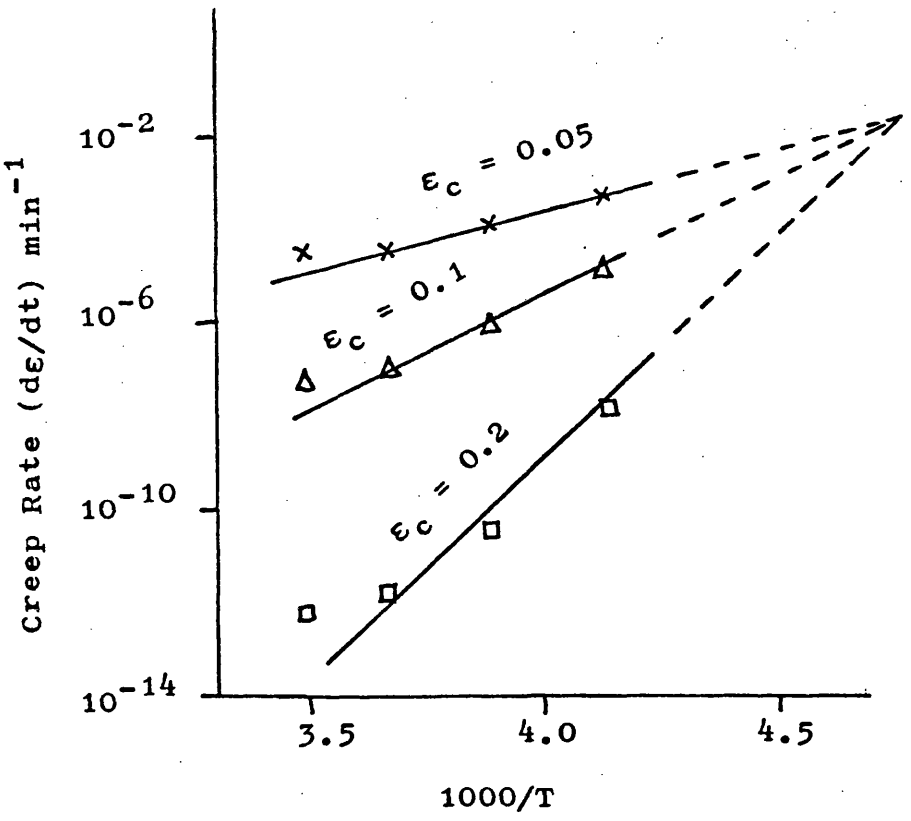

(a)

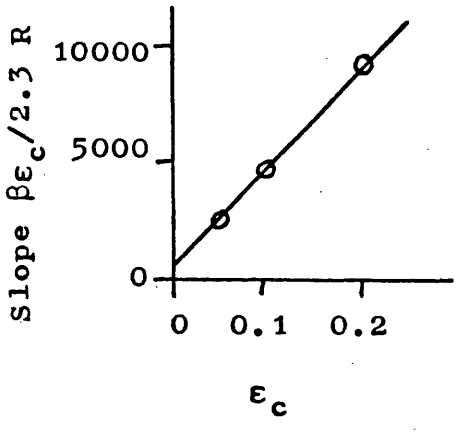

(b)

Figure 5.7 a) Creep rates as a function of temperature for a filled, commercial vulcanizate after various amounts of prior creep.

b) Slopes of the curves in (a) as a function of prior creep. β = 840 KJ mol^{-1} $strain^{-1}$

example, shows data for a commercial sulphur based mix containing carbon black and blending oil at an initial strain of 0.55. Again similar trends are observed. Two batches of vulcanizate 'C' were prepared which gave completely different behaviour despite almost identical moduli. These are referred to in Figure 2.1 as vulcanizates C and C2. C gave rates of creep somewhat lower than for 'A' and 'B' and displayed logarithmic behaviour over long time periods. By comparison C2 crept rapidly at first but showed a deceleration from logarithmic kinetics after about 100 minutes under load. Initial logarithmic data for C2 is shown in Figure 5.8 and associated rate-temperature plots in Figures 5.9-5.12. Good agreement with the empirical approach is observed considering the scatter of experimental results indicated in Figure 5.8. Similar data for vulcanizate 'D' is shown in Figure 5.13. The temperature scale for the Arrhenius - like plots of these peroxide based vulcanizates extends from 0°C to 50°C. It was not possible to carry out creep experiments below 0°C because of the dominating influence of crystallisation, see Section 2.6, and indeed the creep rates at 0°C were evaluated from results at short times before the onset of the crystallisation accelerated response. Note that, unlike the sulphur based vulcanizates, these materials do not show a transition in creep behaviour in the vicinity of room temperature.

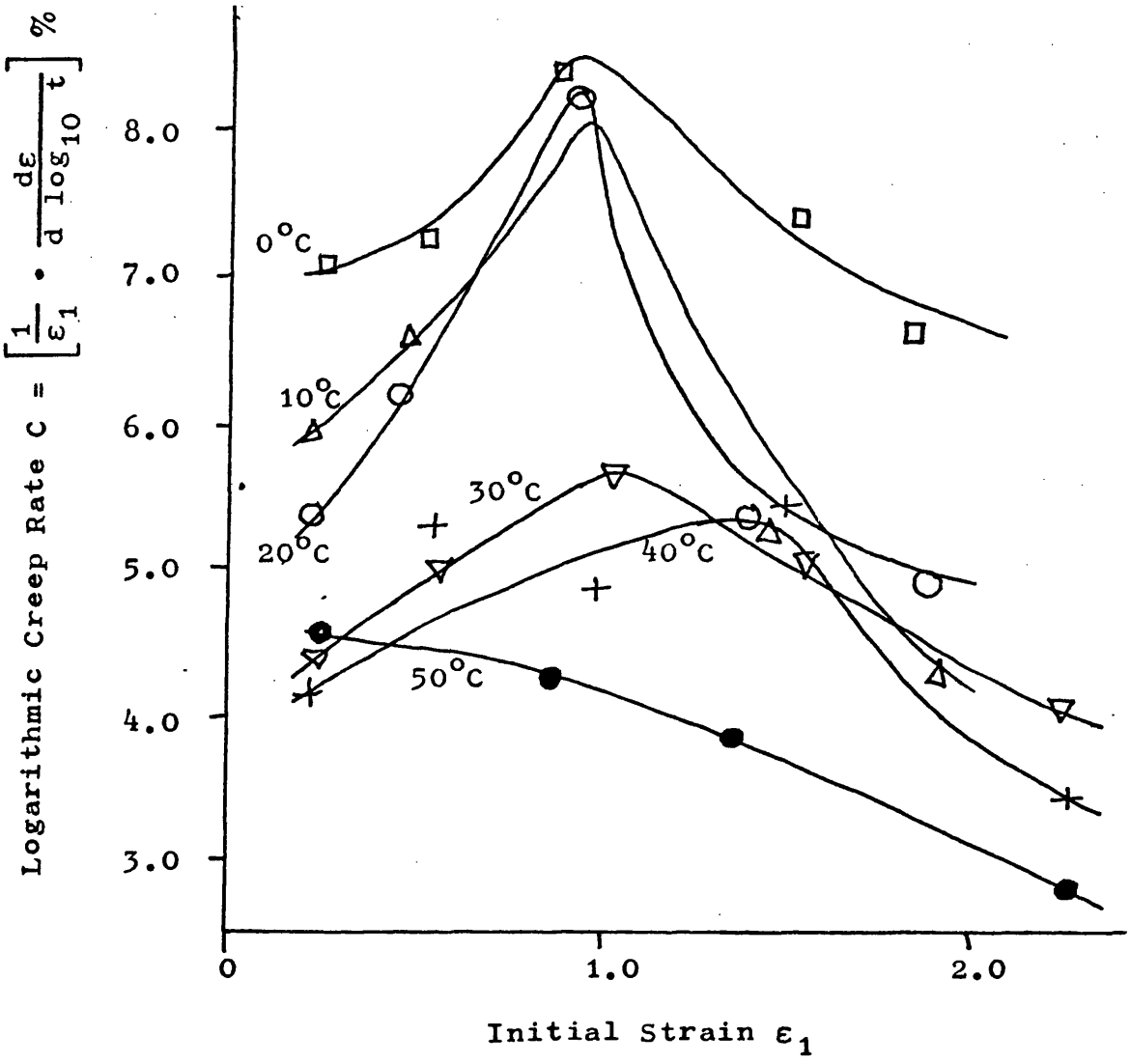

Figure 5.8 Logarithmic creep data for vulcanizate C2 as a function of initial strain.

□ 0°C
△ 10°C
○ 20°C
▽ 30°C
\+ 40°C
● 50°C

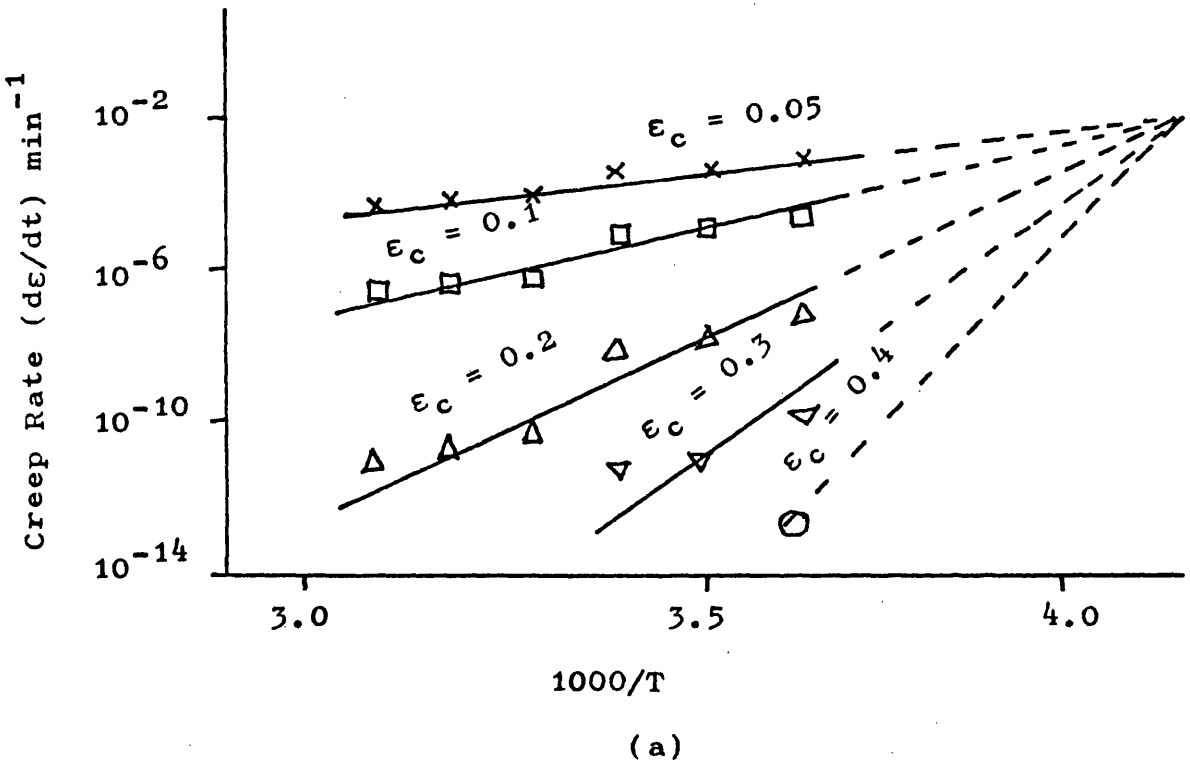

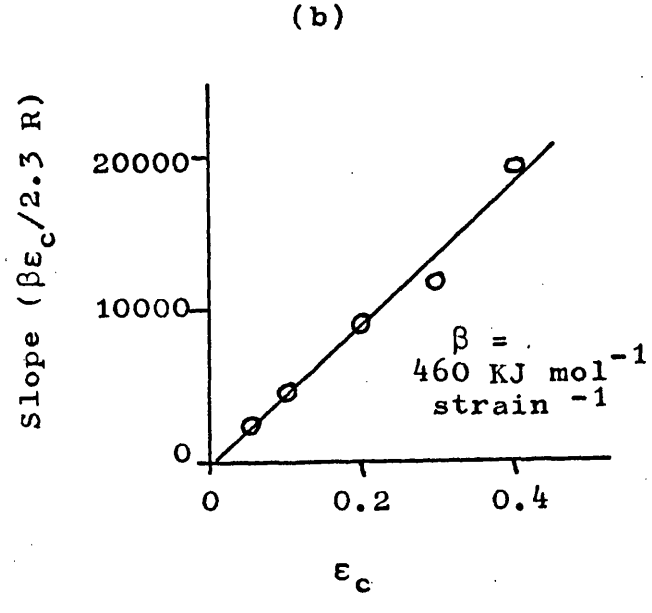

Figure 5.9 a) Rates of creep for the DCP vulcanizate C2 as a function of temperature after various amounts of prior creep.

b) Slopes of the Arrhenius-like plots in (a) as a function of prior creep. Initial Strain $\varepsilon_1 = 0.50$ $\beta \sim 460$ KJ mol^{-1} strain^{-1}

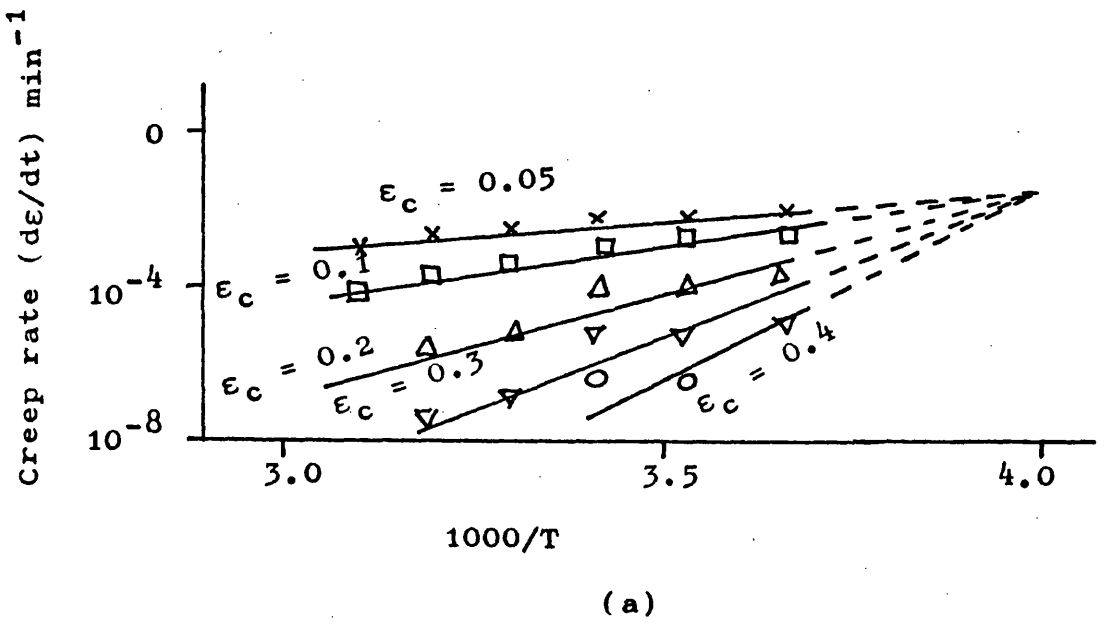

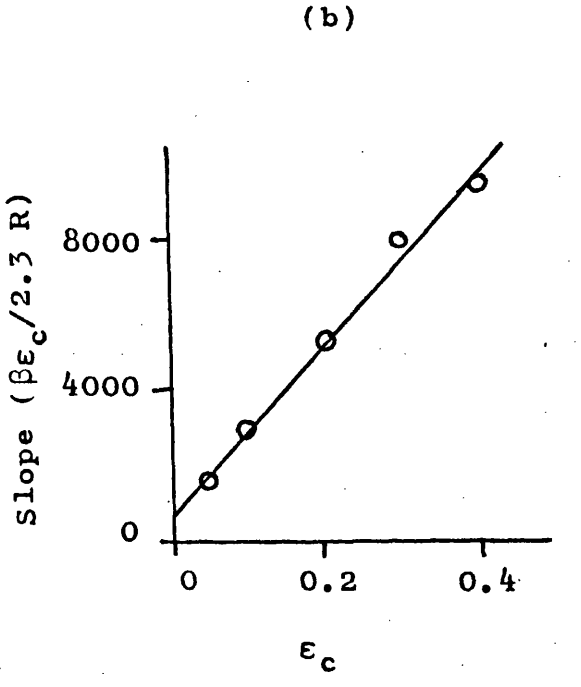

Figure 5.10 a) Rates of creep for the DCP vulcanizate C2 as a function of temperature after various amounts of prior creep.

b) Slopes of the Arrhenius-like plots in (a) as a function of prior creep.

Initial strain $\varepsilon_1 = 1.0$ $\beta \sim 400$ KJ mol^{-1} $strain^{-1}$

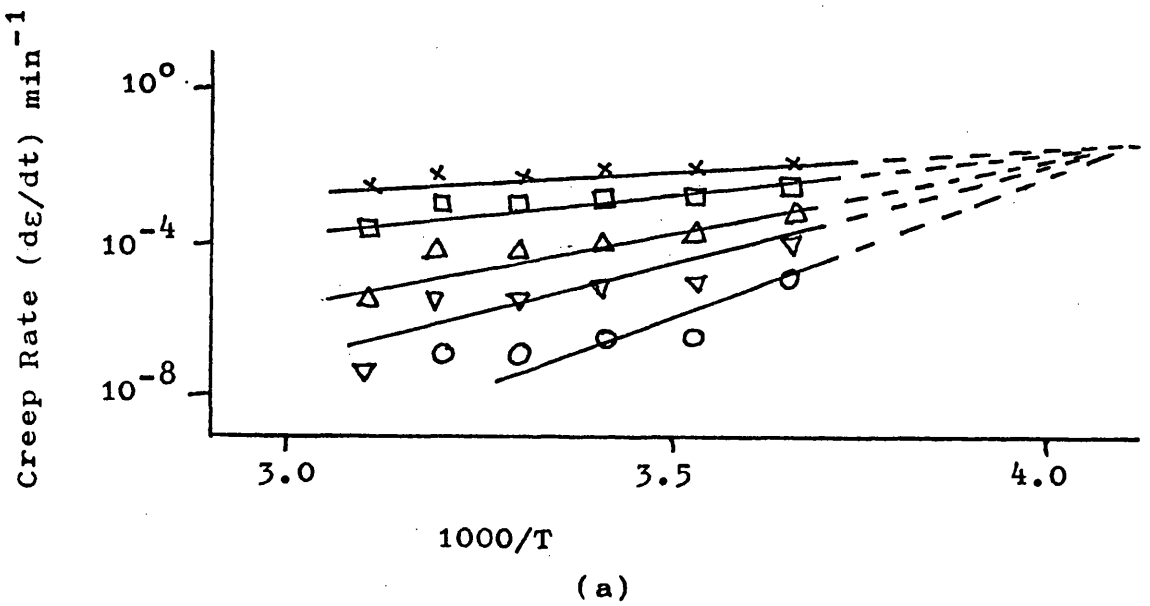

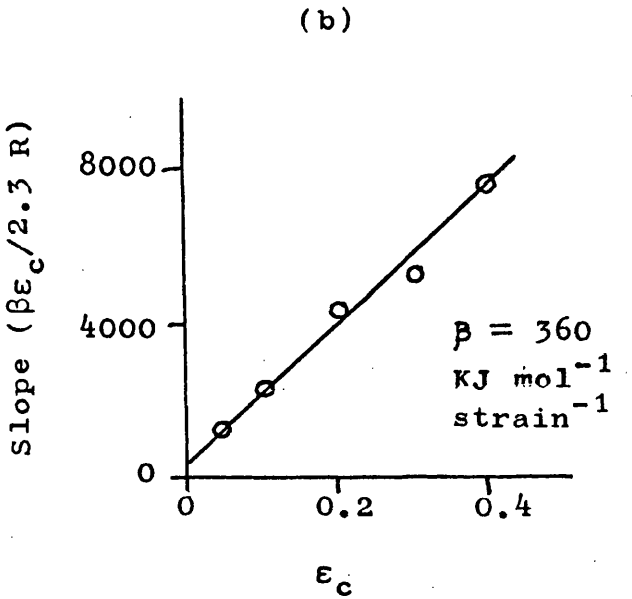

Figure 5.11 a) Rates of creep for the DCP vulcanizate C2 as a function of temperature after various amounts of prior creep.

b) Slopes of the Arrhenius-like plots in (a) as a function of prior creep.

Initial Strain $\varepsilon_1 = 1.5$ $\beta = 360$ KJ mol^{-1} strain^{-1}

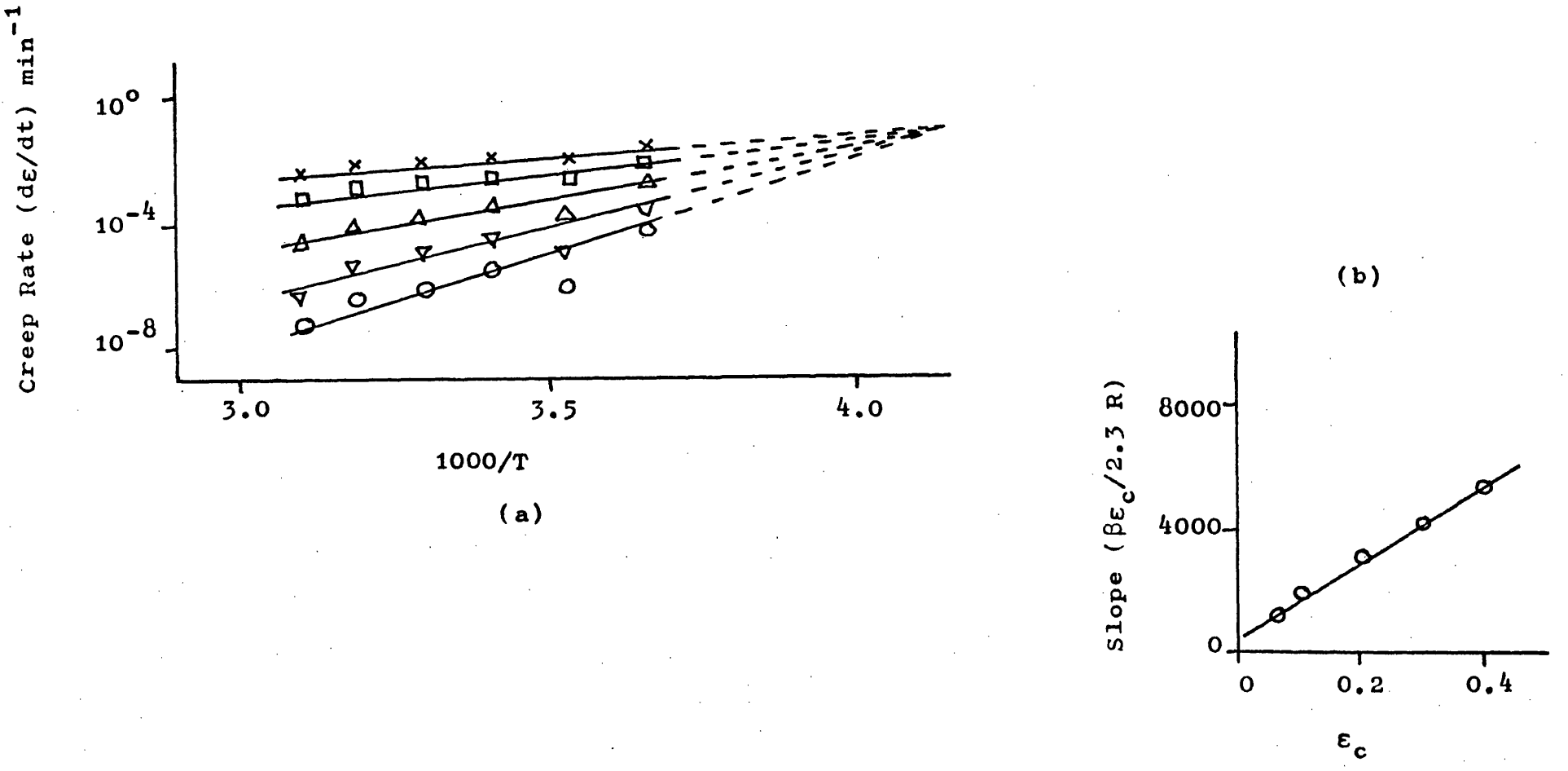

Figure 5.12 a) Rates of creep for the DCP vulcanizate C2 as a function of temperature after various amounts of prior creep.

b) Slopes of the Arrhenius-like plots in (A) as a function of prior creep.

Initial Strain ε_1 = 2.0 β = 230 KJ mol^{-1} strain^{-1}

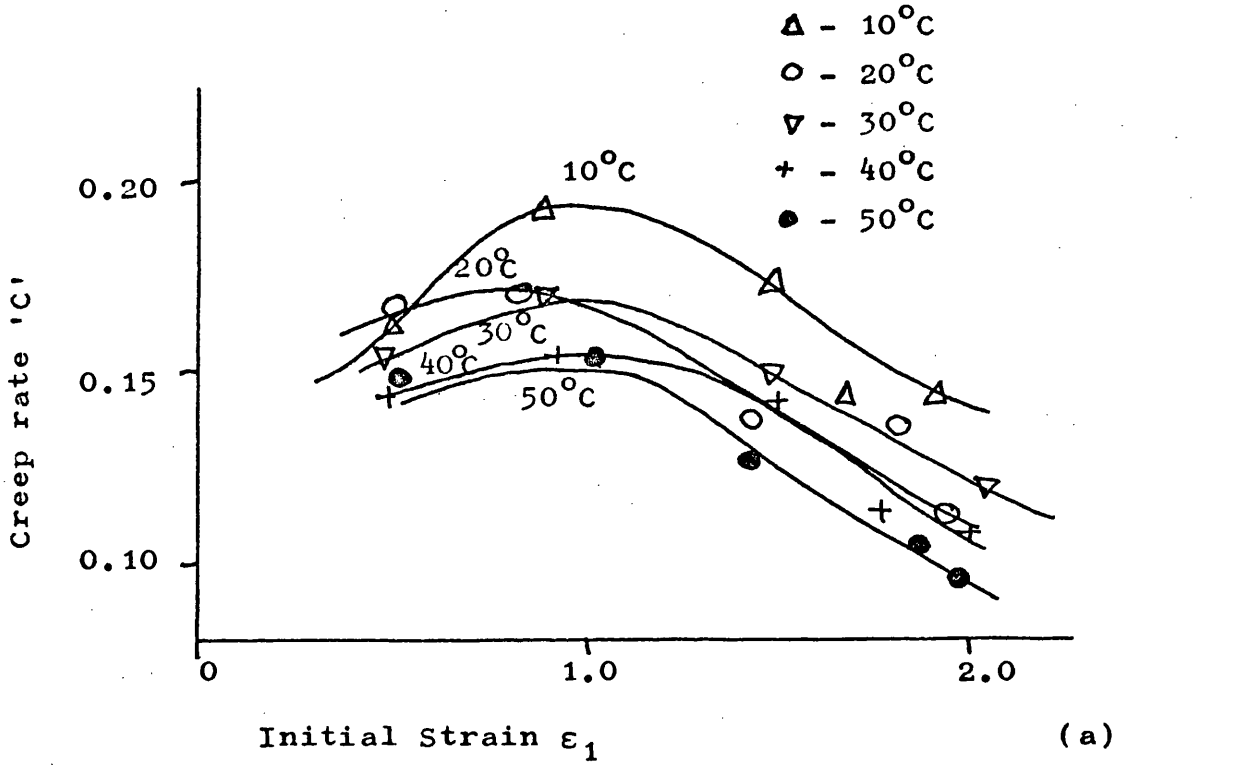

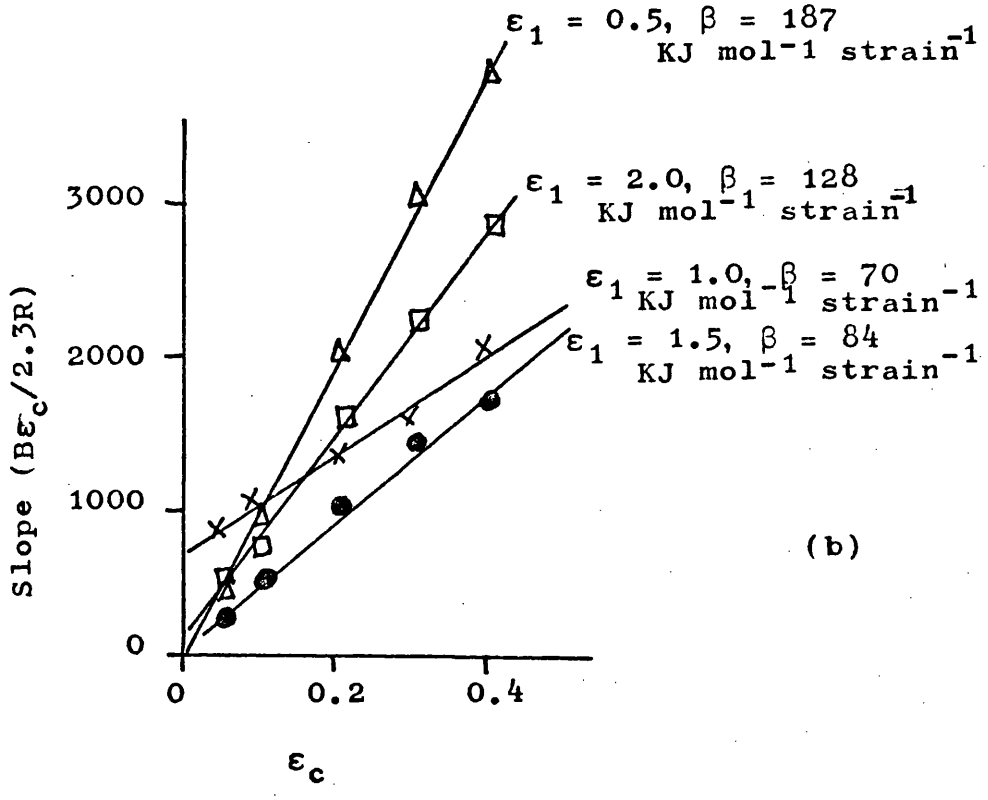

Figure 5.13 a) Experimentally observed logarithmic creep rates for vulcanizate 'D' as a function of initial strain.

b) Slopes of derived Arrhenius plots (not shown) of the rates of creep as a function of temperature.

5.3 Discussion

It is of interest to compare the activation energy approach outlined above with the time-temperature superposition principle. It has already been pointed out that the WLF technique is of limited value in the rubbery plateau region because of the relative independence of reduced modulus on temperature. Furthermore, for logarithmic creep, separate creep curves cannot be superposed since the intersection of two straight lines cannot be accomplished at similar values of strain and gradient simultaneously. Consider, however, a relative translation of two curves, Figure 5.14a some distance log a_T along the logarithmic time axis to give an intersection at equal amounts of creep strain. From geometry the required shift is clearly proportional to 'ε_c'. Similar reasoning would hold for the same results plotted in terms of creep modulus since:-

$$E_R(t) = \frac{\text{stress}}{\text{strain}} = \frac{\sigma}{\varepsilon_1 (1 + c \log_{10} t)}$$

This is idealised in Figure 5.14b. Again any horizontal translation of the curves to give superposition must depend on the value of $E_r(t)$ and in fact the shift will be exactly the same as that indicated in Figure 5.14a. The idea of plotting time shifts, log a_T, against reciprocal temperature is well established and has been discussed in Chapter 1. It is merely an extension of the WLF technique for the special case where a straight line relationship results and Ferry for example [3] considers that the log a_T shifts are synonymous with ΔH, the activation energy for flow. Ke [10, 11] has applied this

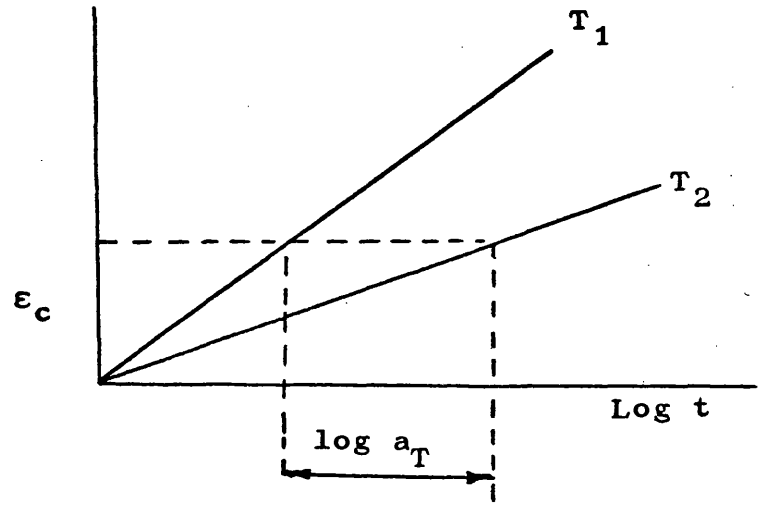

Figure 5.14a Schematic representation of two creep curves at temperatures T_1 and T_2, $T_2 > T_1$. The shift function log a_T is proportional to the extent of prior creep 'ε_c'.

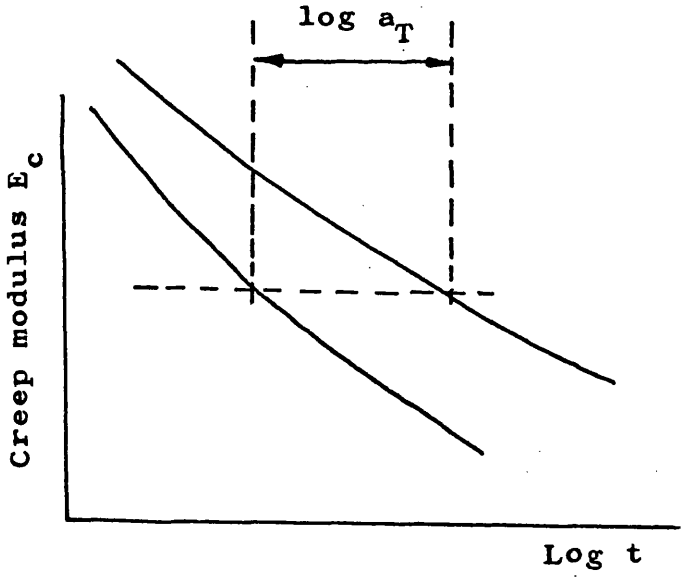

Figure 5.14b Schematic representation of the curves of Figure 14a plotted in terms of creep modulus. Again the 'log a_T shift depends on the extent of prior creep.

approach to the logarithmic creep of metals by plotting log a_T for the transpositions of $(\varepsilon_c/\varepsilon_1)$ versus log t curves against 1/T. He did not justify his somewhat arbitrary use of the ratio $(\varepsilon_c/\varepsilon_1)$ instead of for example observing the times for equal deflections but it is clearly an attempt to eliminate from the derived activation energy any effect due to the temperature dependencies of the limiting moduli. McCrum and Morris [12] have used a similar technique to analyse the β-relaxation in polymethyl-methacrylate. In the present work, however, it was decided to use the creep rate as the basis for deriving a temperature relationship. This is conceptually clearer in that the Arrhenius law and the viscosity - temperature equation which follows from it are framed in terms of rates. It is of interest to point out that if the parameter $\log_{10} (1/\varepsilon_1 \quad d\varepsilon/dt)$ is plotted against reciprocal temperature, instead of $\log_{10}$ $(d\varepsilon/dt)$, exactly the same curves are obtained but shifted downwards an amount $\log_{10} \varepsilon_1$. Log $(d\varepsilon/dt)$ has been used, however, since it is less confusing for the purpose of comparison.

The proposed empirical relationship for the influence of temperature on logarithmic creep has been based on a comparison of creep curves which start from equal initial strains and the comparison is made after equal amounts of creep. This is in fact almost synonymous, in this temperature range, with a comparison based on equal reduced stresses. More philosophically, however, it may be considered that the molecular network will be in the

same "condition" after stretching to an initial elongation 'ε_1' and subsequent creep 'ε_c' irrespective of the temperature and stress. This follows if the mechanism of creep is the same at all temperatures within the range being compared. Hence it may be more fundamentally valid to work in terms of strain. Activation energies for creep in polypropylene and polyethylene have been deduced from similar arguments [13].

In summary, it has been shown by two separate approaches that the activation energy for logarithmic creep may be considered to increase linearly with the extent of prior creep i.e. From the creep-time relationship and from the creep-rate - temperature relationship.

5.4 The Influence of Prior Creep on the Creep Rate

The empirical rate - temperature relationship described above is indicative of a temperature activated process in which the creep response is determined by the applied stress and a material viscosity factor. The fact that the apparent activation energy increases in proportion to the prior creep may be explained in terms of various assumptions based on the breakdown of structural units. The "exhaustion" theory for example assumes that a material contains a number of points of stress concentration having a linear distribution of activation energies [6] or activation stresses [7]. By comparison the "hardening" theory [14] assumes that the elastic retraction stress in the specimen increases with creep elongation and that this brings about a reduction in the creep rate. Logarithmic creep behaviour may be deduced from any of

these concepts. Further, they all predict stress softening and mechanical hysterisis phenomena [15]. In this section, logarithmic behaviour will be treated in terms of the "hardening" theory.

Saunders and Treloar [16] have examined the influence of temperature on the viscosity of unvulcanized natural rubber. Using a modified Mooney viscometer they were able to show that the shear rate was related to temperature in an Arrhenius fashion for any given value of applied stress.

i.e. shear rate = $f(\sigma)$ Exp - H/RT

'H' was in the order of 34 KJ mol^{-1}. It is suggested that creep in vulcanized rubber may be described in a similar fashion if account is taken of the elastic retraction stress developed in the cross-linked network as a result of the applied extension. Consider a rubber testpiece extended by a constant applied load. It is proposed that some of this load is supported by a viscous-like friction between adjacent structural units in the macromolecular lattice. The applied stress is therefore assumed to exceed the elastic network stress by an amount ($\sigma - \sigma i$) where 'σ' is the applied stress and 'σi' the internal elastic stress. The kinetic theory of rubber elasticity, see Section 1.4, is based on the assumption that internal and applied stresses are equal and should therefore predict 'σi' as a function of extention.

i.e. $\sigma_i = E_o (\lambda - \lambda^{-2})$ 5.9

Eo = a modulus term synonymous with 'nKT' of equation 1.1.

The 'excess stress' ($\sigma - \sigma i$) is assumed to be supported by internal friction within the structure and the temperature activation of friction points is manifested by creep. As creep proceeds however, 'σi' increases in accordance with equation 5.9 as a result of the increased network extension. Consequently the excess stress, ($\sigma - \sigma_i$), decreases and the rate of creep decreases. Conrad [14] has used this concept to examine logarithmic creep in copper at low temperatures and has proposed:-

$$\frac{d\varepsilon}{dt} = A \text{ Exp} - \frac{Q - \gamma (\sigma - \sigma_i)}{RT} \qquad 5.10$$

γ = A constant with the dimensions of volume.

A = A constant.

This is based on the assumption that the apparent activation energy for the creep process is reduced in proportion to the excess stress. Figure 5.15, representing a hypothetical energy barrier for the creep mechanism, indicates why this might be so [17]. For zero applied stress the rate of forward and backward reactions accross the energy barrier are equal and the net creep rate is zero. On introduction of an excess stress ($\sigma - \sigma_i$) however, a modification of the activation plot is assumed and the rate of the forward reaction exceeds that of the backward reaction. Hence the net creep rate is given by:-

$$\text{net creep rate} = A \text{ Exp} - \frac{Q - W_1}{RT} - A \text{ Exp} - \frac{Q + W_2}{RT}$$

W_1 and W_2 being the changes in activation energy for forward and backward reactions respectively. For

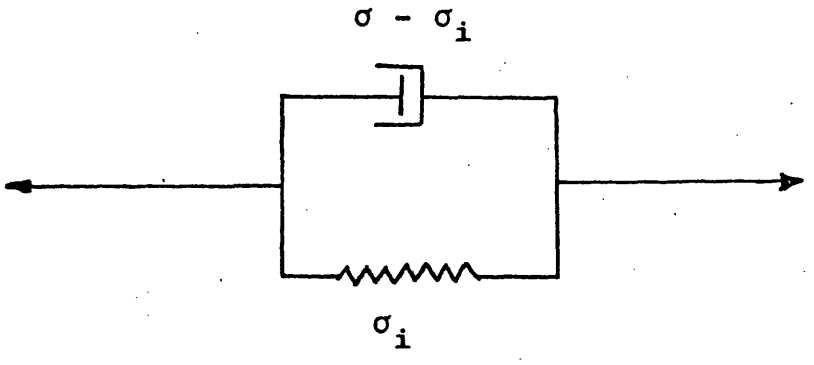

Figure 5.15a A hypothetical dashpot and spring model to represent logarithmic creep. The dashpot is assumed to flow under the action of an 'excess' stress $(\sigma - \sigma_i)$, aided by thermal fluctuations. An Arrhenius type law is assumed to apply directly to the dashpot response.

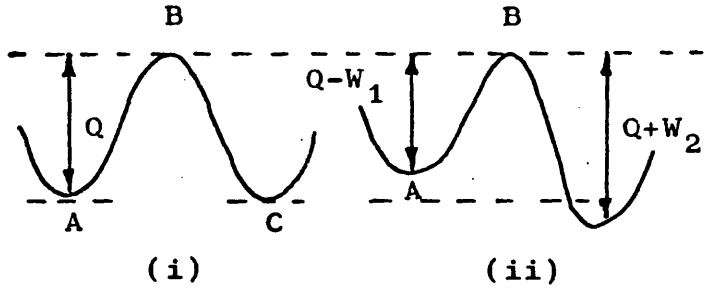

Figure 5.15b A hypothetical energy barrier for deformation of the dashpot shown in (a) above; (i) no applied stress (ii) applied stress = $(\sigma - \sigma_i)$. The excess stress $(\sigma - \sigma_i)$, supported by the dashpot, is assumed to influence the shape of the energy barrier as shown. The rate of flow A→C and C→A are equal in case (i) but in the stressed state the rate A→C exceeds that of C→A.

sufficiently high values of W_1 and W_2 however, the backward reaction may be neglected in comparison to the forward reaction. Further, if it is assumed that W_1 is proportional to the excess stress, i.e. $W_1 = \gamma (\sigma - \sigma_i)$, then equation 5.10 is derived.

Activation energy ideas leading to equations similar to 5.10 have been applied to the logarithmic creep and stress-relaxation of paper [18]. Zhurkov [19] has proposed a similar equation to explain creep rupture in a variety of materials and his theory has been applied to the creep-rupture behaviour of polybutadiene at ambient temperatures [20]. He considered the excitation and breakage of bonds by thermal fluctuations under the action of stress. By comparison, Bartenev [21] has proposed the equation.

$$\tau = \tau_o \text{ Exp } + \left[\frac{H - \gamma\sigma}{RT} \right]$$

to explain viscoelastic behaviour. Here 'τ' is a relaxation time and 'γ' is again an activation volume. He suggested that under experimental conditions 'τ' must approximate to the time of measurement 't' since all mechanisms with $\tau < t$ would be expired prior to the instant of measurement. Similarly, mechanisms for which $\tau > t$ would not contribute significantly to the viscoelastic process at time 't'. Putting $t = \tau$ therefore and re-arranging this equation gives

$$\sigma = \frac{H}{\gamma} - \frac{RT}{\gamma} \ln \frac{t}{\tau_o}$$

This Equation can be used to interpret logarithmic stress-relaxation at constant strain and may also be applied to the influence of strain rate on the stress-strain curve.

In the latter case, the time 't' to obtain a given elongation is inversely proportional to the strain rate '$\dot{\varepsilon}$' and hence the stress obtained at a particular elongation depends on '$\dot{\varepsilon}$'. From derived values of activation volume 'γ' Bartenev suggested that the structure of rubbery polymers consists of microregions of ordered "supramolecular" structure surrounded by a matrix of free chains and segments. The ordered microvolumes may be related to regions of short range order of the type associated with liquids and in the present analysis they will represent viscous-like behaviour. Free chains represent purely elastic behaviour. Chains and segments contained in the micro-blocks are considered by Bartenev to be bound and a state of dynamic equilibrium is envisaged between free and bound chains. The detachment of bound chains under the action of stress and thermal fluctuation leads to creep at constant stress or stress-relaxation at constant elongation. Simultaneously, free chains in equilibrium with the applied stress may attach themselves and this leads to the decay, growth and extinction of pre-existing microblocks together with the nucleation and growth of new microblocks. The concept of supramolecular microblocks has also been used to explain the elastic behaviour of rubbers [22,31,32,41,42] whilst a 'domain' structure has been postulated to explain various other properties such as heats of solution and ease of crystallisation [23]. Activation volume ideas have been applied to the logarithmic creep and stress-relaxation

of cement [24], to the yield and flow of polymers [25-27] and to yield in epoxy resin [28-30].

5.5 Application of the Model to Creep

The interpretation of equation 5.10 to the case of a creeping rubber network is to be considered. Since creep experiments are performed at constant applied stress, the 'σ' of equation 5.10 may be regarded as constant. Rearrangement then gives:-

$$\frac{d\varepsilon}{dt} = A \, Exp - \frac{Q}{RT} \; Exp + \left[\frac{\gamma \, (\sigma - \sigma_i)_1}{RT}\right] Exp - \left[\frac{\gamma \, \Delta\sigma_i}{RT}\right] \qquad 5.11$$

where $(\sigma - \sigma_i)_1$ = magnitude of the 'excess' stress at a time of 1.0 minutes under load.

$\Delta\sigma_i$ = change in the internal stress subsequent to 't' = 1.0.

The first three factors of equation 5.11 are constants for any given creep experiment and hence:-

$$\frac{d\varepsilon}{dt} = M \quad Exp - \frac{\gamma \, \Delta\sigma_i}{RT} \qquad 5.12$$

$$M = \text{constant.}$$

Furthermore, 'σ_i' is given by equation 5.9 and hence

$$\Delta\sigma_i = E_o \; \Delta \, (\lambda - \lambda^{-2})$$

where $\Delta \, (\lambda - \lambda^{-2})$ is the change in the function $(\lambda - \lambda^{-2})$ subsequent to $t = 1.0$.

This gives:-

$$\frac{d\varepsilon}{dt} = M \, Exp - \left[\frac{\gamma \, E_o \, \Delta \, (\lambda - \lambda^{-2})}{RT}\right] \qquad 5.13$$

OR, for small amounts of creep '$\Delta\sigma_i$' will be given approximately by the product of the tangent modulus and

the creep strain 'ε_c'

$$\text{i.e.} \quad \Delta\sigma_i \sim E\varepsilon_c$$

E = tangent modulus

and differentiating equation 5.9 gives

$$E = \frac{d\sigma}{d\lambda} = \frac{d\sigma}{d\varepsilon} = E_o\,(1 + 2\lambda^{-3}) \approx E_o\,(1+ 2\,\lambda_1^{-3})$$

where λ_1 = extension ratio at 't' = 1.0.

Hence, equation 5.13 can be re-written:-

$$\frac{d\varepsilon}{dt} \simeq M\,\text{Exp} - \frac{\gamma E_o\,(1 + 2\lambda_1^{-3})\,\varepsilon_c}{RT}$$

$$= M\,\text{Exp} - \frac{\gamma\, E\varepsilon_c}{RT} \qquad 5.14$$

which yields:-

$$\ln \frac{d\varepsilon}{dt} = \ln M - \frac{\gamma\, E\, \varepsilon_c}{RT} \qquad 5.15$$

Note that equation 5.15 is synonymous with equations 5.6 and 5.7 and is therefore representative of logarithmic creep.

Figure 5.16 shows creep data for vulcanizate 'A' at 20°C plotted in terms of equation 5.13. Individual experimental points have been evaluated graphically from plots of 'ε_c' against 't' and each line represents data for a single testpiece. Note that each sample obeys equation 5.13 throughout its creep history although the gradient $-\gamma E_o/2.3\,RT$ decreases with increasing applied stress, i.e. with increasing test elongation. This implies that 'γ' decreases with increasing initial elongation since E_o, R and T are constants. These gradii ($\gamma\, E_o/2.3\,RT$) are in fact shown in Figure 5.17 as a

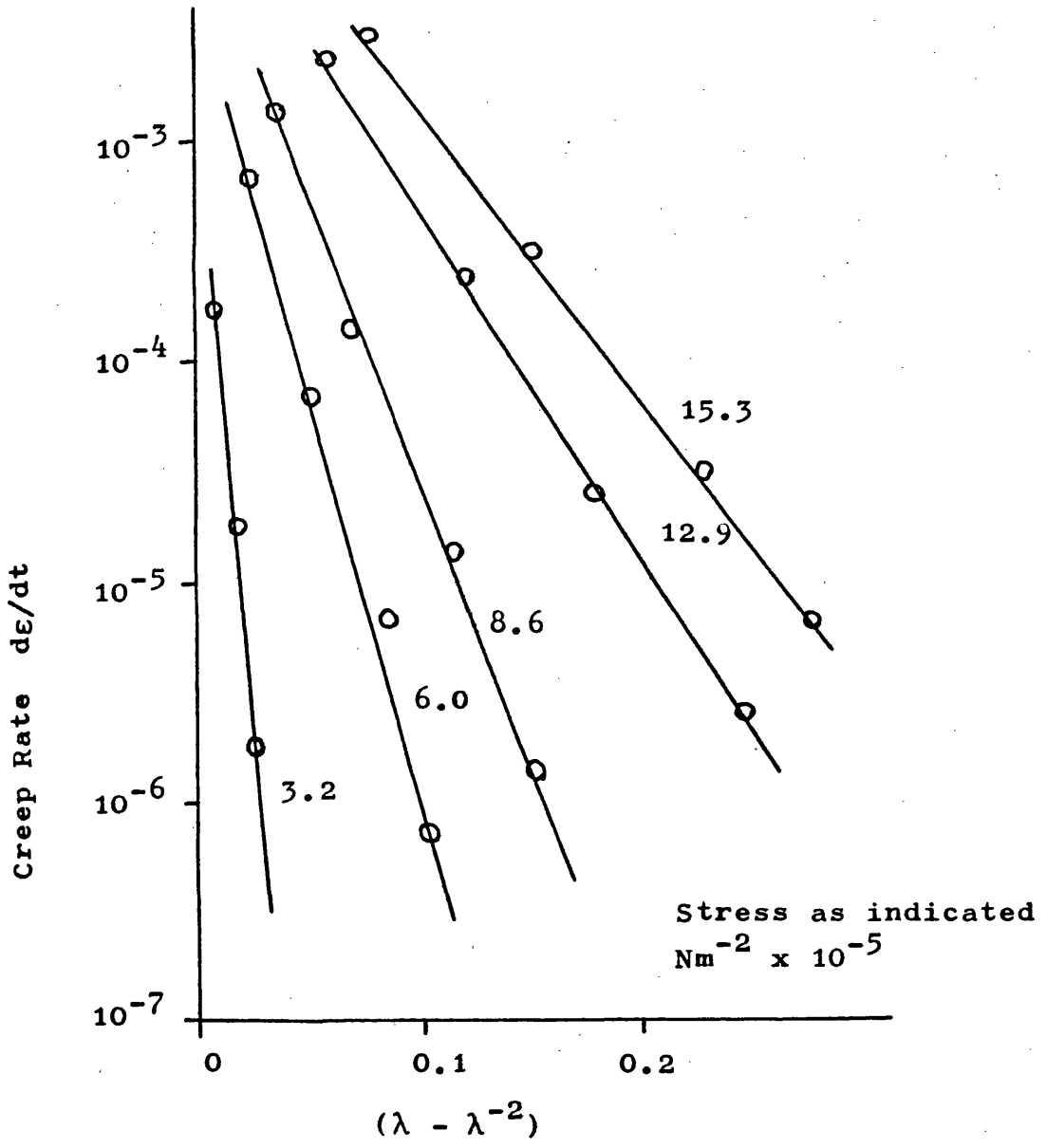

Figure 5.16 Creep rate as a function of the change in excess stress i.e. $\Delta\sigma_i = E_o . \Delta(\lambda - \lambda^{-2})$. Vulcanizate 'A' samples at 20°C. Note that the slope ($- \gamma Eo/2.3$ RT) depends on the applied stress (elongation).

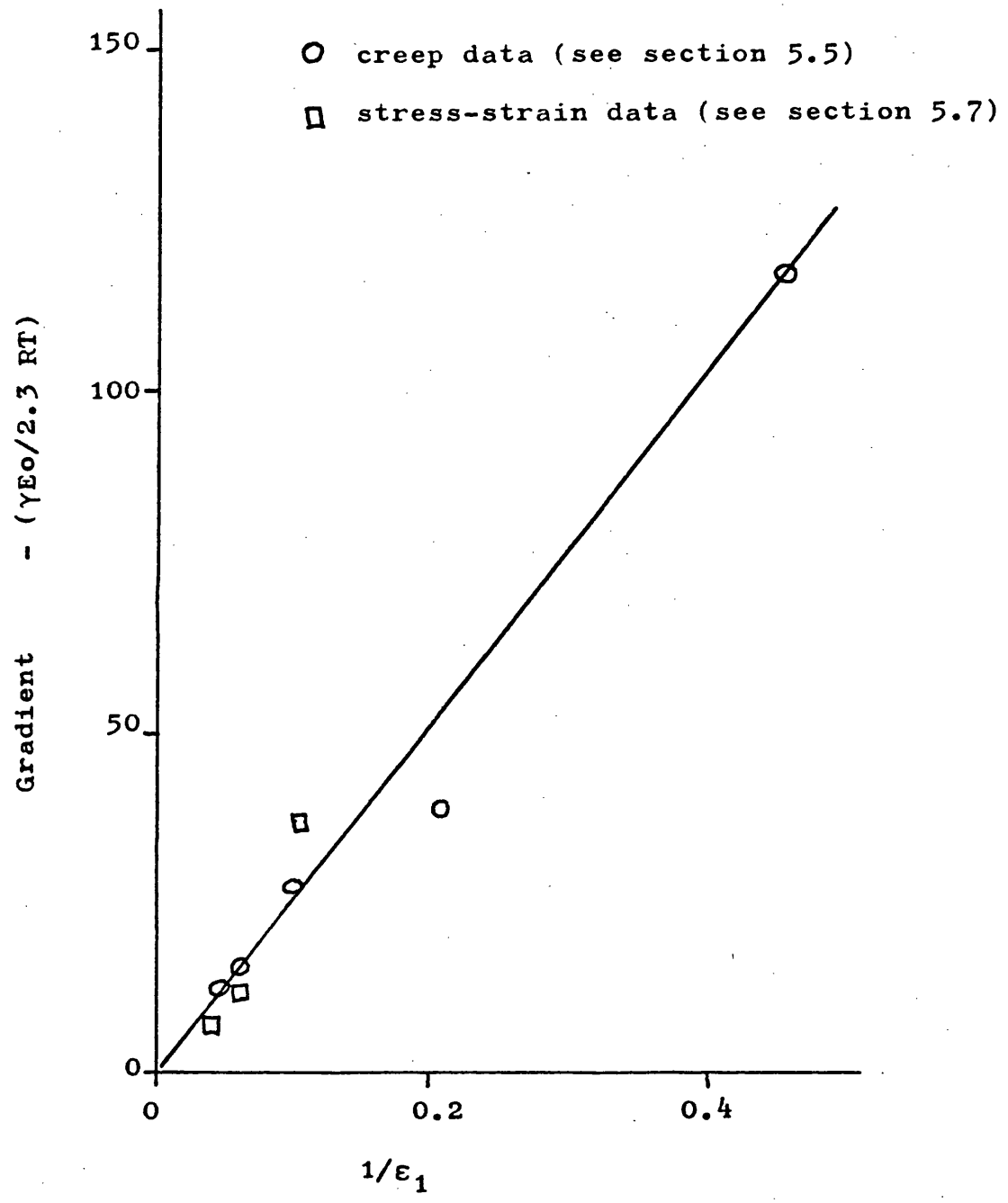

Figure 5.17 Influence of Initial strain on the function ($\gamma Eo/2.3\ RT$). Since Eo, R and T are constants this reflects the dependence of γ on initial strain. Results were obtained for vulcanizates 'A' and 'B' at room temperature.

function of the strain at one minute under load, 'ε_1'. Inspection shows that 'γ' is inversely proportional to 'ε_1'.

$$\text{i.e. } \gamma = \frac{2.3\ a\ RT}{E_o\ \varepsilon_1} \qquad 5.16$$

where 'a' = slope of the line in Figure 5.18. A tentative explanation for this behaviour may be derived if the activation volume is assumed to be synonymous with the size of supramolecular microblocks having properties described earlier. Consider that each microblock becomes a point of stress concentration as the network is extended to the initial test strain. This follows from the fact that the molecular chains bound within each microblock are connected directly or indirectly to the surrounding elastic matrix. The applied stress is therefore transmitted to the microblock along individual attached chains and this causes microblock decay. Simultaneously, other chains in equilibrium with the applied stress may attach themselves. The size of microblocks contributing to the creep deformation depends therefore on the extent of the initial implied elongation. Temperature and initial strain rate may also be important.

Equation 5.16 has been derived from creep results at room temperature and for relatively rapid rates of load application; it may not be valid under other conditions. It is of interest to point out in this connection that equation 5.10 may be interpreted slightly differently to give a different dependence of activation volume on initial strain. In the present analysis the

'excess' stress is based on the original unstrained specimen cross-section. By working in terms of the instantaneous cross-section true values for the change in excess stress with creep may be determined and this leads to a smaller derived dependence of 'γ' on initial strain. Nevertheless, in the present work all calculations will be based, for simplicity, on the original cross-section.

In practice 'γ' may be calculated, without the necessity to draw graphs, from a comparison of equations 5.14 or 5.15 with equation 5.5. If ln ($d\varepsilon/dt$) is plotted against 'ε_c', similar to Figure 5.16. the slope of the resulting curve may be interpreted from either of these equations and this leads to

$$\gamma = \frac{2.3\ RT}{C\varepsilon_1 E_o\ (1 + 2\lambda^{-3})} \qquad \text{per mol} \qquad 5.17a$$

$$\text{i.e. } \gamma = \frac{2.3\ kT}{C\varepsilon_1 E_o\ (1 + 2\lambda_1^{-3})} \qquad \text{per unit mechanism} \qquad 5.17b$$

k = Boltzmanns constant.

But, from equation 5.11 $E_o = nkT$, and hence:-

$$\gamma \approx \frac{2.3}{nc\varepsilon_1\ (1 + 2\lambda_1^{-3})} \qquad 5.18$$

per unit mechanism.

Values of the activation volume, so calculated, are shown in Figure 5.18 for vulcanizates 'A' and 'B' over a range of temperatures and initial strains. Clearly, initial strain is the major factor in determining activation volume rather than test temperature.

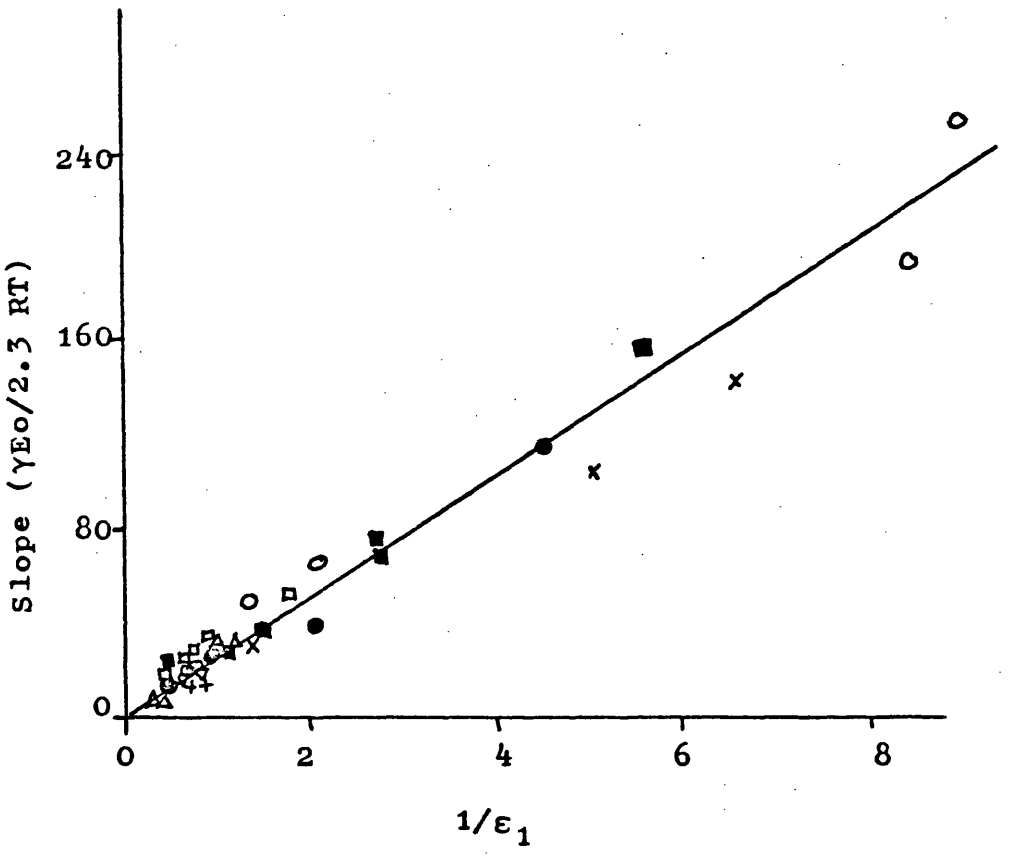

Figure 5.18 Values of (γEo/2.3 RT) for vulcanizates 'A' and 'B' as a function of initial strain. Obtained from creep data over a range of temperatures:-

+ -30°C
▽ -15°C
△ 0°C
o 10°C
□ 15°C
● 20°C
× 35°C
■ 60°C

The modulus term 'E_o' for vulcanizates 'A' and 'B' is approximately 500 KPa at 20°C. This gives experimentally derived values for 'γ' in the range 1.5×10^{-24} m ^{3} to 6×10^{-26} m^3 for results at the lowest and highest strains respectively. Assuming 'γ' to represent the size of spherical supramolecular domains, then these would be in the size range 200 Å diameter down to about 50 Å diameter. This is in reasonable agreement with the 10^{-24} to 10^{-25} m^3 observed by Bartenev at low strains and agrees with his suggestion that at least one dimension of a domain would not be less than 50 Å.

In summary it has been shown that equation 5.10, as proposed by Conrad, may be applied to the logarithmic creep of elastomers. An activation volume 'γ' is then associated with the flow process and may represent the size of supramolecular domains as envisaged by Bartenev.

5.6 The Influence of Modulus on Creep

The influence of crosslink density on creep and stress-relaxation rates has already been mentioned in section 1.7. Whilst the type of crosslink and associated network 'cleanliness' are known to be important [33-35], it is now well accepted that creep rates are smaller for samples of higher modulus [33-40]. Figure 5-19, for example, indicates some of the more relevant MRPRA data on the subject. In the present section it is intended to explain the general shape of these curves from considerations of the 'hardening' theory presented above.

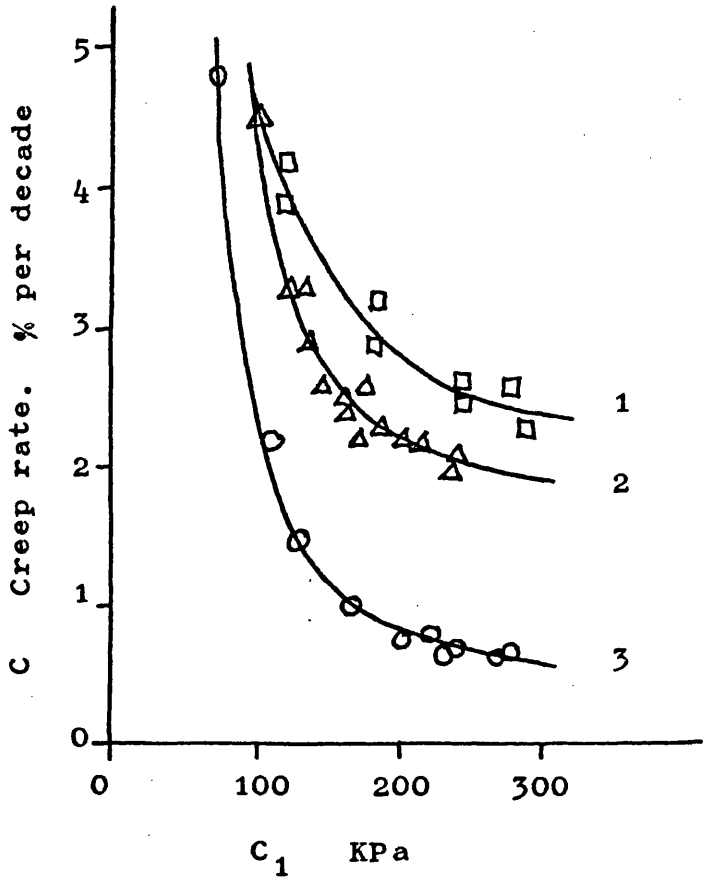

Figure 5.19 Influence of network modulus on creep rate. After Farlie [33].

1. EV vulcanizates.
2. Conventional sulphur vulcanizates.
3. Peroxide vulcanizates.

C_1 represents the Mooney-Rivlin modulus constant.

The 'hardening' concept involves the idea that creep is related to an 'excess' stress over and above that associated with the elastic retraction stress. This 'excess' stress diminishes as creep proceeds as a result of increasing network extension; i.e. because of the increase in elastically supported stress. Clearly therefore, the rate of decrease of excess stress with creep strain will be directly proportional to the network modulus. Consequently the deceleration in creep rate resulting from a given creep strain will be greater in a high modulus network than in a low modulus network. Assuming that the general structure of rubber is relatively unaffected by crosslink density this may be described in a semi-quantitative manner. If the logarithm of the creep rate were to be plotted against creep strain, analogously to Figure 5.16, the gradients of the resulting straight lines could be interpreted in terms of either equation 5.7 or equation 5.12. This implies therefore that:-

$$-\frac{\gamma E}{RT} = -\frac{2.3}{c\varepsilon_1}$$

$$\text{or that } c \alpha \frac{1}{\gamma E \varepsilon_1} \qquad 5.19a$$

E = tangent modulus.

In section 5.5 however, it was shown that for vulcanizate 'A' over a range of temperatures 'γ' tends to be inversely proportional to the initial strain. All other things being equal therefore:-

$$C \alpha 1/E \qquad 5.19b$$

i.e. The logarithmic creep rate should vary as the inverse of the network modulus. It is of interest to point out

however that this deduction assumes 'γ' to be unaffected by crosslink density and in practice this may not be so. Thirion and Chasset [40] for example have considered the influence of crosslink density on creep from a chain entanglement viewpoint. They suggested that long range entanglements are less likely to occur at high cross-link densities and that this results in a reduction of the relaxation mechanisms causing creep. By comparison, the present analysis assumes that 'γ' and therefore by implication the network structure are insensitive to crosslink density. Nevertheless, the qualitative argument leading to equation 5.19 remains valid and furthermore the result is supported by general trends in the experimental evidence as is exemplified by Figure 5.19.

5.7 Application of the Model to Tensile Tests

It is well known that the stress-strain curves of rubbery polymers are shifted to higher values of stress with increasing strain rate. Within the range of moderate to slow strain rates the full tensile test occupies some few minutes to several hours of experimental time and this implies that the behaviour may be attributed to slow but persistent mechanisms. It is proposed that within the rubbery plateau region the mechanisms most influencing the strain rate dependency of tensile response may be the same as those which cause creep within the same experimental time scale. This suggests that logarithmic creep and the strain rate sensitivity of tensile data may be interelated and it is intended to interpret this in

terms of equation 5.10.

The internal elastic network stress 'σ_i' is independent of time under load, being a function of elongation only in accordance with equation 5.9. If several test pieces were to be tensile tested at different strain rates, therefore, the elastic stresses 'σ_i' developed in each would be identical when compared at any particular value of strain. Further, the size of supramolecular domains in each sample would be identical if it is assumed that 'γ' depends only on strain as suggested in section 5.5. The observed stresses for each sample, corresponding to a particular strain, may therefore be related to the imposed strain rate using equation 5.10, expansion of which gives:-

$$\ln \frac{d\varepsilon}{dt} = \ln A - \frac{Q}{RT} - \frac{\gamma\sigma_i}{RT} + \frac{\gamma\sigma}{RT}$$

Hence, for a comparison of stress-strain data at a fixed value of strain and therefore of 'σ_i' :-

$$\sigma = \frac{RT}{\gamma} \ln \frac{d\varepsilon}{dt} + \text{constant} \qquad 5.20$$

This suggests that a straight line with gradient RT / γ may be obtained by plotting the stresses developed in a number of samples, at a particular value of strain, against the logarithm of the applied strain rate. To substantiate this, experimental stress-strain curves were obtained by subjecting standard dumbell creep samples, see Figure 2.2, to tensile tests over a range of cross-head speeds. An Instron floor model TT-DM tensile testing machine was used having a selection of cross head speeds in the range 500 mm min^{-1} down to

10^{-1} mm min^{-1}. This provided charts of load against cross-head displacement. Loads were converted to stress using individual micrometer thickness measurements for each sample and assuming all samples to be 4 mm wide. Cross-head displacements were converted to strain by assuming that these were directly proportional to each other. The proportionality constant was evaluated for each individual sample from separate measurements of strain at the end of each tensile test. This was achieved by stopping the machine cross-head and measuring the distance separating two bench marks scribed on each sample gauge length prior to testing. The tests were carried out under ambient room conditions in the temperature range 18°C to 20°C. Temperature variations were a problem with low strain rate tests which took up to two days to complete and this led to several results being discarded.

Figure 5.20 shows experimental stress-strain data for vulcanizate 'B' plotted in terms of equation 5.20 and indicates good agreement with theory. The scatter of results is considered good bearing in mind possible errors from sample cross-section measurement, from strain measurement and from temperature variations. The three lines indicate results at three different values of strain, namely ε = 1.0, 2.0 and 3.0. Derived slopes, $(2.3RT/\gamma)$ increase with increasing strain and this indicates that 'γ' must decrease with increasing strain. This reflects the dependence of 'γ' on initial elongation as was observed for creep data, see section 5.5, and lends support to the

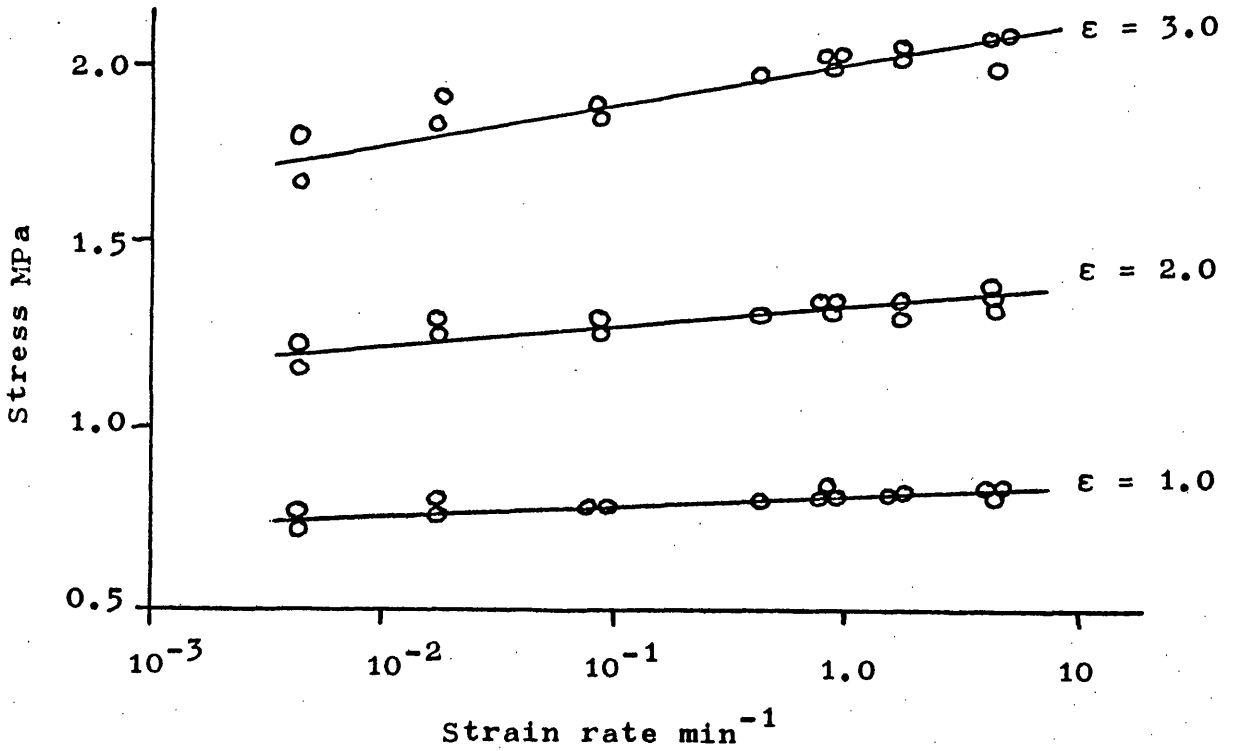

Figure 5.20 Stress-strain data for vulcanizate 'B' at room temperature as a function of strain rate.

ε	1.0	2.0	3.0	
slope	29	52	116	KPa dec^{-1}

idea that activation volumes decrease with imposed extension. Further, the gradii obtained in Figure 5.20 have been used to calculate values of the function ($\gamma E_o/2.3RT$) as was derived for creep data and the results are shown in Figure 5.17. Good agreement is observed between creep and stress-strain results. A typical value for 'E_o' of 500 KPa was estimated from 'slow' stress-strain data obtained by incremental loading.

The influence of strain rate on tensile data for the filled vulcanizates 'E', 'F' and 'I' are shown in figures 5.21 to 5.23. Again, good agreement with equation 5.20 is indicated. By comparison, figure 5.24, for the peroxide vulcanizate 'D', shows inflections in the curves at a strain rate of about 1.0 min^{-1}. Vulcanizate 'D' appears to have two relaxation characteristics, each of which dominate in different regions of its response. This reflects the peculiarities observed in the creep behaviour of vulcanizate 'D' as was discussed in section 5.2; the dual response may correspond to the deceleration of creep which occurs some 20 to 100 minutes after loading.

Activation volumes 'γ' have been calculated for vulcanizates A, B, E, F, H and I and the results are indicated in Figure 5.25 as a function of applied strain. Values derived from creep data agree reasonably well with those derived from stress-strain data, all things considered. The plots lend further support to the suggestion made in section 5.5 that 'γ' tends to decrease in inverse proportion to the strain. Activation volumes for the

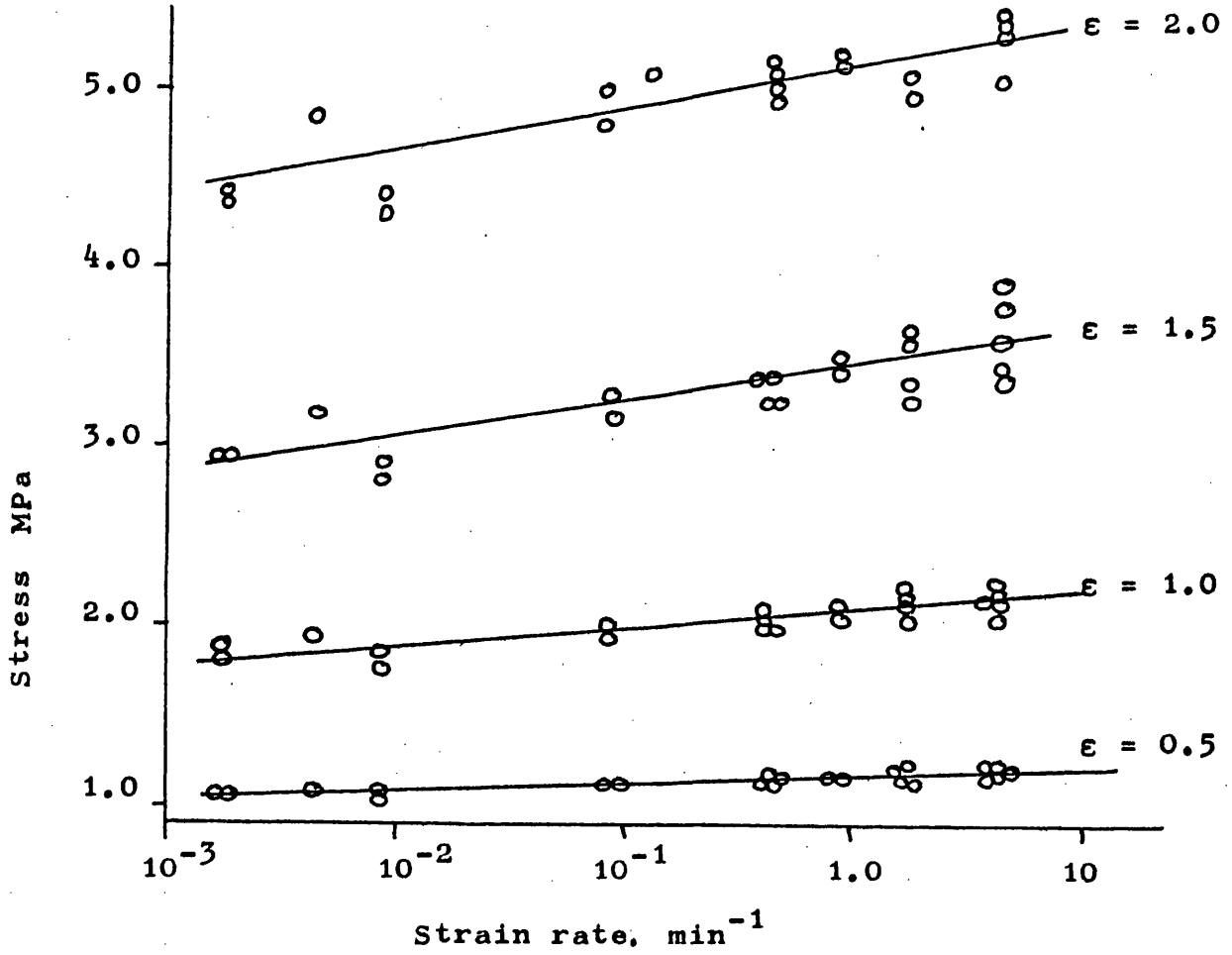

Figure 5.21 Stress-strain data for vulcanizate 'E' as a function of strain rate.

strain ε	0.5	1.0	1.5	2.0	
gradient	48	116	203	238	KPa dec^{-1}

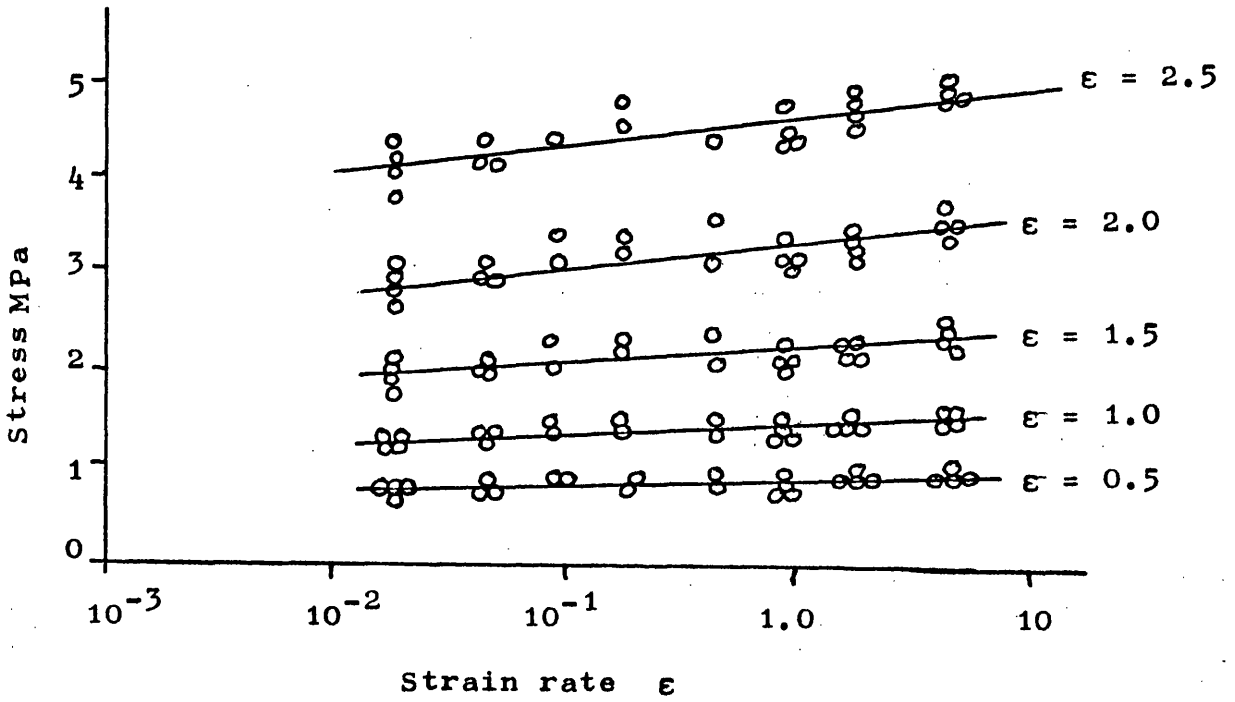

Figure 5.22 Stress-strain data for vulcanizate 'F' as a function of strain rate.

strain ε	0.5	1.0	1.5	2.0	2.5	
slope	43	118	169	282	341	KPa dec^{-1}

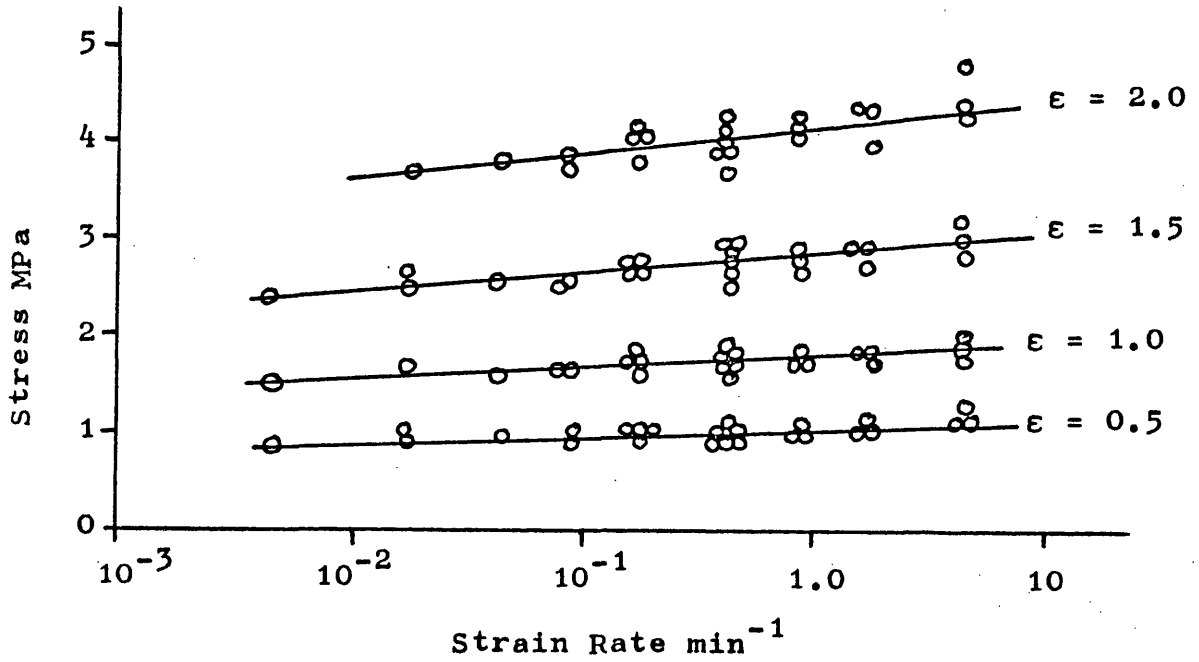

Figure 5.23 Stress-strain data for vulcanizate 'I' as a function of strain rate.

strain ε	0.5	1.0	1.5	2.0	
slope	87	135	202	270	KPa dec^{-1}

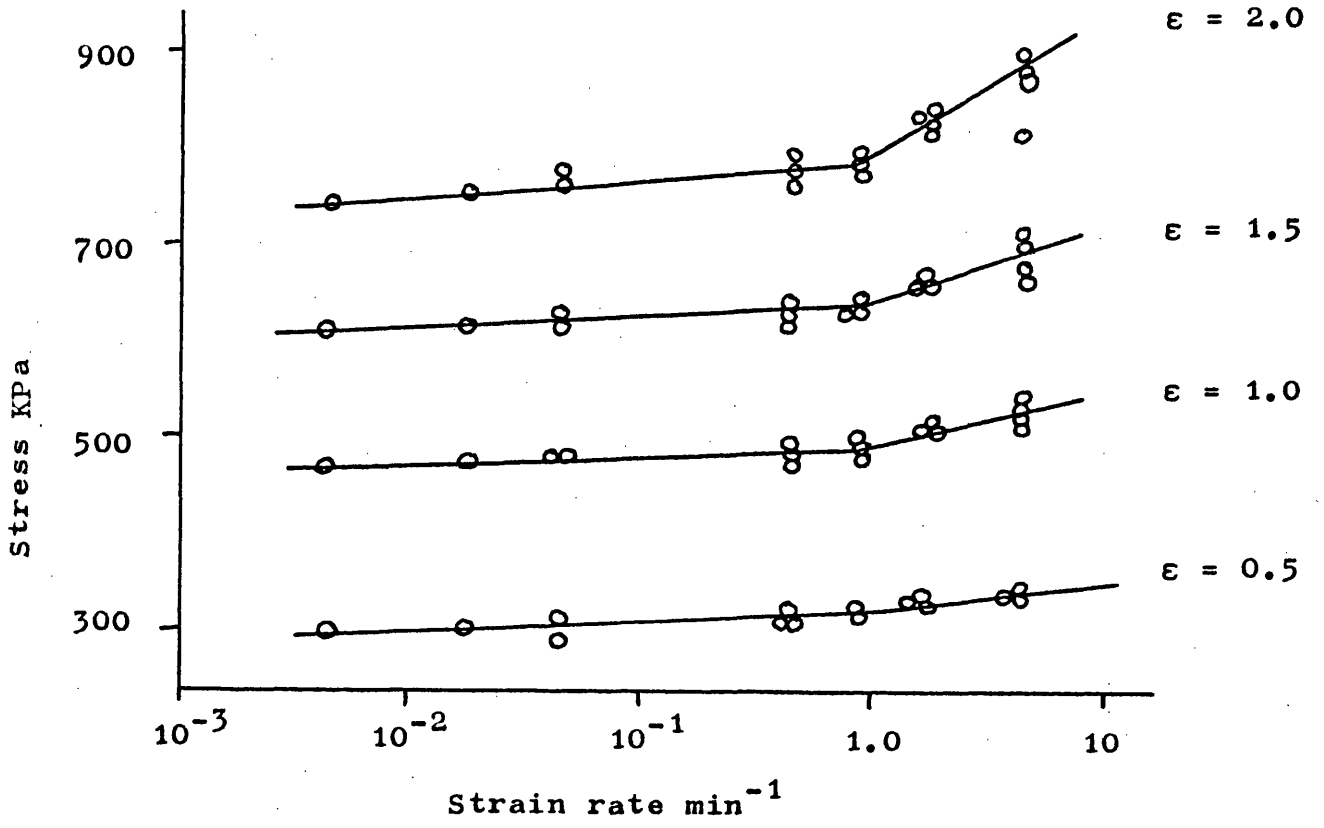

Figure 5.24 Stress-strain data for vulcanizate 'D' as a function of strain rate.

Strain	ε	0.5	1.0	1.5	2.0	
gradii	1	21	14	11	12	) KPa dec^{-1}
	11	154	82	58	27	)

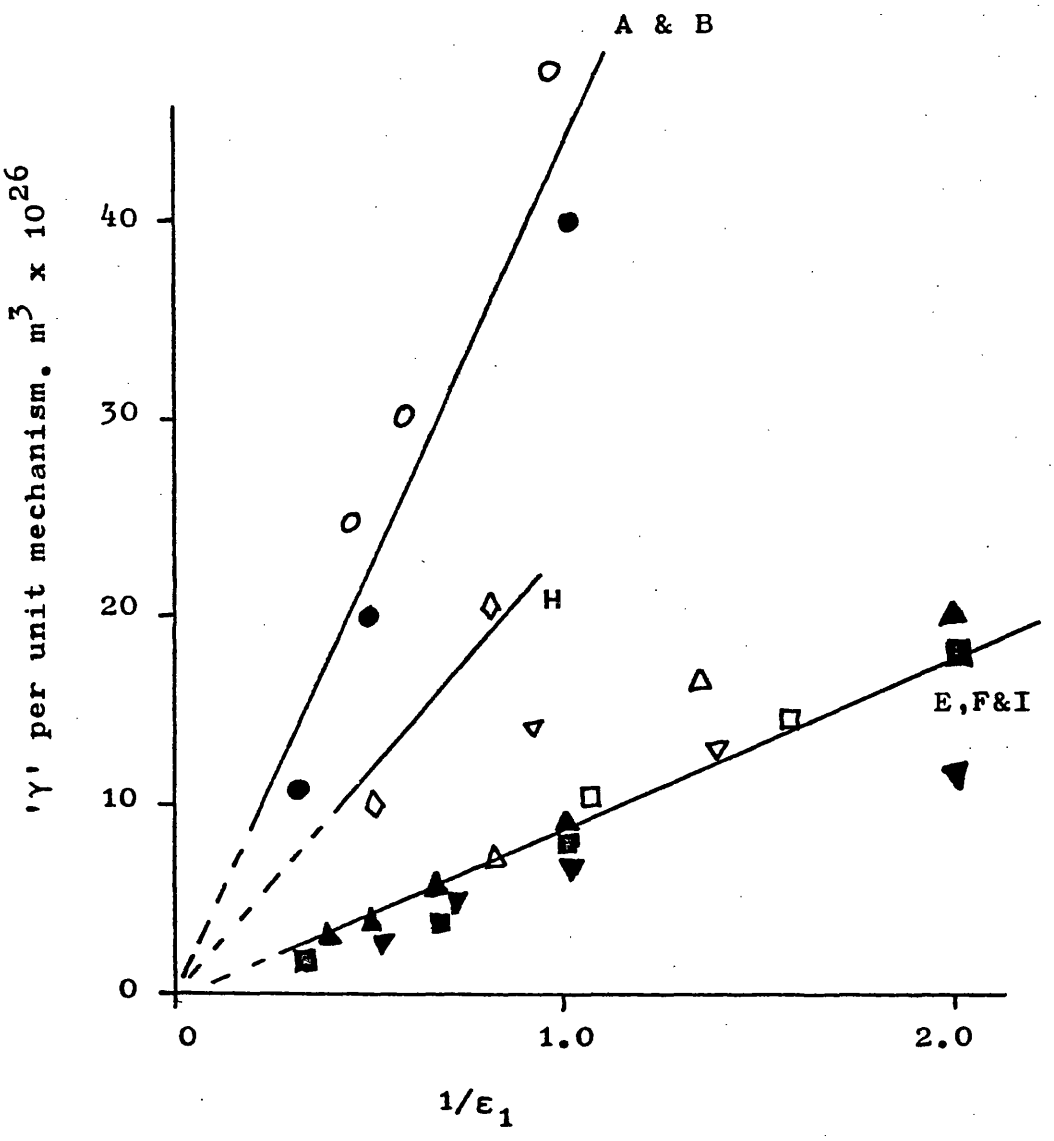

Figure 5.25 Activation volumes 'γ' calculated from creep data (open symbols) and stress strain data (filled symbols).

Vulcanizates:- ○ A & B
□ E
△ F
▽ I
◇ H

filled vulcanizates E, F and I are a factor of about four smaller than the gum equivalent. This may be explained in terms of the supramolecular domain concept if one assumes that the size of the domains is limited by the presence of carbon black particles. These three particular vulcanizates, for example, contain black particles of approximately 260 Å diameter ('E', 'F') and 200 Å diameter ('I') which at a 30 pphr loading (see Figure 2.1 indicates an average particle separation of about 300 Å. Clearly, the development of large supramolecular, semi-ordered structures would be prohibited. It is of further interest, in this respect, that values for 'γ' obtained for the three vulcanizates 'E', 'F' and 'I' are approximately the same within the observed scatter of results and this may follow from the fact that the black particle sizes are about equal. By comparison, activation volumes calculated for vulcanizate 'H' containing 30 pphr of a large diameter thermal black, 800 Å to 1500 Å, are about half way between those of vulcanizates 'E', 'F' and 'I' and that of the gum rubber.

5.8 Comments on the Model

The hardening theory presented above provides a tentative explanation of slow but persistent relaxation as is observed in the rubbery plateau, whilst the concept successfully interelates creep and stress-strain data in terms of the activation volume 'γ', it also contains a number of apparent contradictions which will now be discussed. Indeed, the most serious objection concerns

the physical interpretation of 'γ' and in particular the derived relationship between 'γ' and the logarithmic creep rate; considering equation 5.17 it is clear that large values of 'γ' correspond to low creep rates and vice versa, all other things being equal. This is atfirst sight contrary to the supramolecular domain concept since the presence of large domains, which would presumably be more effective in inhibiting the rapid attainment of elastic equilibrium, might be expected to cause rapid creep. This dilemma is not, however, peculiar to the 'hardening' theory and equations similar to 5.17 may be derived from alternative models based on the 'exhaustion' theory or even from hybrid concepts involving both hardening and exhaustion. Plausible modifications to either the mathematics or the models of these concepts do not yield satisfactory relationships which eliminate the derived γ-creep rate observation; nor can the derived strain dependency of 'γ' be removed by mathematical manipulation. Fundamentally, this arises from the fact that re-arrangement of activation-type equations usually results in multi-component equations in which the creep rate is determined by a front factor in addition to an exponential factor from which 'γ' may be deduced. In fact, closer examination shows that the exponential factor e.g. Equation 5.15

$$\frac{d\varepsilon}{dt} = M \, Exp - \frac{\gamma E \varepsilon_c}{RT}$$

does not define the actual creep rate but only its dependency on prior creep; indeed the pre-exponential

factor is usually a function of 'γ' also. One could modify equation 5.10, for example, by proposing that the increment in creep strain resulting from a specific activation event should be proportional to the initial strain, e.g.

$$\frac{d\varepsilon}{dt} = A\,\varepsilon_1 \quad \text{Exp} - \left[\frac{Q - \gamma\,(\sigma-\sigma i)}{RT}\right]$$

This follows from the fact that 'A' represents the product of a frequency factor, a proportionality constant relating the rate of 'events' to the rate of creep and a concentration factor determined by the number of potential mechanisms available. Nevertheless, an 'initial strain' modification does not influence the conclusions derived from an analysis of experimental data. In view of this it is appropriate to examine an alternative explanation of the γ-creep rate relationship and to accept the idea that domains decrease in size with increasing imposed strain as already discussed. Consider that, in the unstretched state, unit volume of rubber contains υ domains each of volume γ_o such that the volume fraction of domain material V_f is given by $V_f = \upsilon\,\gamma_o$, or $\upsilon = V_f/\gamma_o$. The constant 'A' of equation 5.10 must contain a domain concentration factor and should therefore be proportional to υ or to V_f/γ_o. Further, if V_f is determined by thermodynamic equilibrium considerations (see later) then, in general, large values of γ_o correspond to low domain concentrations and therefore to low creep rates. i.e. The pre-exponential factor of equation 5.10 should increase with decreasing domain size.

By comparison the exponential part of equation 5.10 is not a strong function of 'γ' at short times under load since the excess stress developed during initial stretching is limited by the ease of activation of the relaxation mechanisms. i.e. In the present theory, large domains would be more easily activated and this would inhibit the development of high excess stress. This is consistent with the suggestion that inherently large domains decrease in size with applied strain more readily than inherently small domains - see Figure 2.25.

By assuming that the equilibrium concentration of domain material in unstrained rubber is determined by thermodynamic criteria it is possible to obtain a qualitative insight into the influence of temperature on creep. Consideration of the reaction

amorphous rubber $\longrightarrow$ domains

suggests that an equilibrium constant, K, may be defined such that

$$K = \frac{[\text{domains}]}{[\text{amorphous rubber}]}$$

and assuming that the proportion of domain material is small this suggests

$$K \simeq [\text{domains}] = V_f$$

The influence of temperature may then be evaluated using the thermodynamic identity[8]

$$K = V_f = \text{Exp} - \frac{\Delta G^o}{RT}$$

where ΔG^o is the Gibbs free energy change associated with the transformation. Since ΔG^o is almost certainly negative this indicates that the proportion of domain

material increases with decreasing temperature. This means that with decreasing temperature there are increasing numbers of domains, assuming 'γ' to be relatively temperature insensitive as is suggested in Figure 5.18, but each domain will respond more sluggishly to applied stress. Indeed, a function such as

$$\frac{d\varepsilon}{dt} = B \, Exp - \frac{Q}{RT} \, Exp + \frac{\gamma \, (\sigma-\sigma_i)_1}{RT} \left[Exp + \frac{-\Delta G^o}{RT} \, Exp - \frac{\gamma E \varepsilon_c}{RT} \right]$$

may apply, other things being equal. Here, the penultimate exponential represents the temperature dependence of domain concentration whilst the other exponentials reflect the temperature dependence of domain activity. The portion in square brackets is very similar to the observed emprical function of equation 5.8b but a fundamental interelationship has not been found.

An alternative interpretation of activation volume may be suggested if 'γ' is assumed to be that volume of rubber which is associated with a single relaxation mechanism. In this case the mechanism may be any obstacle which inhibits a progression towards elastic equilibrium, e.g. chain entanglements, weak physical bonds between adjacent network chains, strain induced and pre-existing crystallites and so on. If it is assumed that many of these mechanisms are generated during initial straining then the volume available to each one would decrease with increasing strain; i.e. the activation volume would decrease with applied strain. Whilst such a concept may explain the large values of 'γ'

derived from results at low strains it also introduces other serious difficulties. This is best illustrated by examining a number of inherent advantages of the supramolecular domain theory:-

a) Influence of scragging.

It is well known that a rubber testpiece subjected to repeated strain cycles prior to creep testing will show improved creep resistance. This is known as scragging. Optimum creep resistance is obtained by pre-straining to the intended creep test extension[34] and each successive strain cycle produces a progressively smaller improvement[43]. This may be explained in terms of the domain theory if it is assumed that the domains are broken down by the rapid molecular network pertubations which accompany scragging.

b) Temperature cycling during creep.

In a recent paper Derham[43] has examined the influence of temperature changes on the creep response. In particular, he found that an imposed temperature rise during the duration of a creep test causes a sudden and rapid increase in specimen elongation. Again, this may be explained in terms of the domain theory since the domain concentration would reduce with increasing temperature and the remaining domains would be more active. The influence of further temperature cycles as described by Derham are however more difficult to explain.

c) Rubber elasticity.

The elastic response of rubbery networks would obviously be affected by the presence of domains which

inhibited the approach to elastic equilibrium. According to the present theory their prominence in this respect should decrease with increasing strain since their size is assumed to decrease with strain. This is interesting in that the stress-strain behaviour of real elastomers show negative stress deviations from ideal behaviour at strains in excess of about 80%[44] and it is possible that non equilibrium effects may play some part in this. Indeed, a good approximation to real rubbery stress-strain behaviour is given by the Mooney-Rivlin equation (see Section 1.4) in which the fraction of the total stress contributed by the C_2 term, namely $C_2/(C_1 \lambda + C_2)$, decreases with increasing elongation. That C_2 is influenced by non-equilibrium activity of domain origin cannot be ruled out, particularly at low and moderate temperatures where domain concentrations are thought to be high. Furthermore, factors known to affect C_2 would also fit in with this, e.g. the fact that C_2 decreases with swelling could be explained by assuming that domains are opened up by the ingress of solvent.

d) Dynamic testing.

It is well known that the in phase modulus of crosslinked rubbers decreases with increasing strain amplitude[45]. Again this is in agreement with a labile domain concept assuming that applied strain has a dominating influence on domain breakdown.

The above facts, together with the references given in section 5.4 support the idea of a domain/activation energy theory of logarithmic creep.

REFERENCES; CHAPTER 5

1. J. D. Ferry "Viscoelastic Properties of Polymers." Wiley & Son. N. Y. & London (1961). Ch. 10 'Molecular Theory'.

2. Ibid Ch. 13 'The Rubbery State'.

3. Ibid Ch. 11 'Dependence of viscoelastic behaviour on temperature.'

4. T. L. Smith "Mechanical Behaviour of Materials." Proc of the Int Conference on the Mechanical Behaviour of Materials. Kyoto, Japan (1971). Vol. III pp 431-442 Pub. Soc of Materials Sci, Japan (1972).

5. B. S. 903 part A15 (1958).

6. N. F. Mott and F. R. N. Nabarro "Report of a conference on the strength of solids." Bristol (1947). pp 1-19 Pub. The Physical Society (1948).

7. A. H. Cottrell J. Mechs and phys of solids 1, pp 53-63 (1952).

8. F. Daniels and R. A. Alberty "Physical Chemistry." Ch. 6 3rd Ed. Wiley, N. Y. (1966).

9. W. V. Johnston and M. Shen Polymer pre-prints American chem soc. Div of polym chemistry 11 (1), pp 154-7 (1970).

10. T. S. Ke Physical Review 71 (8), pp 733-46 (1947).

11. T. S. Ke Physical Review 72 (1), pp 41-46 (1947).

12. N. G. McRum and E. L. Morris Proc Roy Soc A281, p 258 (1964).

13. J. E. Sinclair and J. W. Edgemond J. App polymer Sci 13, pp 999-1012 (1969).

14. H. Conrad Acta Metallurgica 6, pp 339-50 (1958).

15. R. L. Woolley Report of a conference on the strength of solids, Bristol (1947) pp 51-56. Pub. The Physical Soc (1948).

16. D. W. Saunders and L. R. G. Treloar
Trans inst rubb indust 24, pp 92-100 (1948).

17. R. E. Reed-Hill "Physical Metallurgy Principles" Ch. 19. Pub. D. Van Nostrand Co., Princeton (1967).

18. J. Kubat "Rheology" Vol. 5. Ch 10
Ed. F. R. Eirich
Pub. Academic Press. N. Y. and London (1965).

19. S. N. Zhurkov J. Fracture Mechs 1, pp 311-23 (1965).

20. C. S. Kim Rubb Chem and Technol 42 (4), p 1095-1121 (1969).

21. G. M. Bartenev J. Polym Sci A2 9, pp 1371-78, (1971).

22. F. De Candia and L. Amelino
J. Macromol Sci-phys B9 (3), pp 435-45 (1974).

23. S. M. Ahoroni J. Macromol Sci-phys B7 (1), pp 73-103 (1973).

24. P. Klug and F. Whittman Materials Sci and Engineering 15, pp 63-66 (1974).

25. C. A. Pampillo and L. A. Davis
J. App phys 43 (11), pp 4277-85 (1972).

26. L. A. Davis and C. A. Pampillo
J. App phys 43 (11), pp 4285-93 (1972).

27. I. M. Ward J. Mater Sci 6, pp 1397-17, (1971).

28. E. Pink and J. D. Campbell
J. Mater Sci 9, pp 658-64 (1974).

29. E. Pink and J. D. Campbell
J. Mater Sci 9, pp 665-72 (1974).

30. E. Pink and J. D. Campbell
Materials Sci and Engineering 15, pp 187-94 (1974).

31. R. Blockland and W. Prins
J. Polym Sci A2 7, pp 1595-1618 (1969).

32. K. Dusek and W. Prins
Adv Polym Sci 6, p 1 (1969).

33. E. D. Farlie J. App Polym Sci 14, pp 1127-41 (1970).

34. C. J. Derham, E. Southern and A. G. Thomas
N.R. Technol. Rubb Dev Supp No. 7 (1970).

35. C. J. Derham, E. Southern and A. G. Thomas
Int Rubb Conf Moscow (1969).

36. D. J. Plazek J. Polym Sci A2 4, pp 745-63 (1966).

37. L. A. Wood Rubb Chem and Technol 43, pp 1482-90 (1970).

38. L. A. Wood and G. W. Bullman
J. Polym Sci A2 10, pp 43-50 (1972).

39. L. A. Wood, G. W. Bullman and G. E. Decker
Rubb Chem and Technol 45 (5), pp 1388-402 (1972).

40. P. Thirion and R. Chasset
Rubb Chem and Technol 44 (5), pp 1256-72 (1971).

41. M. Ilavsky and W. Prins
Macromol 3 (4), pp 415-25 (1970).

42. M. Ilavsky and W. Prins
Macromol 3 (4), p 425 (1970).

43. C. J. Derham J. Mater Sci 8, pp 1023-29 (1973).

44. L. R. G. Treloar "The Physics of Rubber Elasticity." Ch. 5
Oxford, Clarendon Press (1949).

45. A. R. Payne "Reinforcement of Elastomers." Ch 3
Ed. G. Kraus
Wiley, N. Y. and London (1965).

CHAPTER 6

THE INFLUENCE OF CARBON BLACKS ON PHYSICAL CREEP

6.1 Introduction

The inclusion of reinforcing pigments, especially carbon blacks, in engineering rubbers to obtain improved modulus, hardness and tensile strength is the rule rather than the exception. Only limited information about the effect of such fillers on creep has been published and the situation is exacerbated by the large number of pigment types in common use. It has already been shown in Chapter 4 that the secondary creep of vulcanizate 'A' is unaffected by the inclusion of various types of carbon black in the mix and it was therefore suggested that such additional types of microstructural pertubation as may be possible in a filled system do not contribute to the secondary process. By comparison however, logarithmic creep rates are very sensitive to the amount and type of carbon black added to the mix and this is to be discussed in the present chapter.

Gent[1], Derham et al[2-7] and Cooper[8] have examined the logarithmic creep of black filled vulcanizates and have observed creep rates which exceed those of the pure unfilled gum equivalents by a factor of two or more. Similarly, stress-relaxation rates of filled rubbers

exceed those of their gum equivalents [9-11]. This may be attributed either to the enhanced activity of those relaxation mechanisms which occur in gum rubber or to the activity of additional mechanisms peculiar to the filler-rubber interaction. The time dependency of such mechanisms is of prime importance in determining their influence on creep. Mechanisms which are easily activated, during initial extension to the test elongation or at very short times under load, merely contribute to the initial strain and not to the subsequent creep. On the other hand potential mechanisms which are very stable at the applied stress and temperature of test may never be activated. Indeed, only those mechanisms having "relaxation times" within the experimental or design time scale are likely to determine creep response.

The mechanisms of reinforcement of rubber by carbon blacks are of obvious relevance to creep since any slow but persistent instability in reinforcement would lead to additional creep extension. Gent[1], for example, found that a HAF (high abrasion furnace) black reinforced SBR vulcanizate showed a higher rate of creep than its gum equivalent and he suggested that this was in part due to the progressive failure of gum-carbon black interfaces followed by subsequent vacuole formation. By comparison, in HAF reinforced natural rubber he found no evidence for such cavitation but still observed enhanced creep activity. In this case he proposed that

the creep rate of the filled system was determined in part by enhanced crystallisation in areas of high strain concentration between filler particles. Lyalina and Bartenev[9] suggested that the enhanced stress-relaxation which they observed in filled vulcanizates was caused by the slow breakdown and reorganisation of immobilised "shells" of absorbed rubber on the surfaces of carbon black particles. This is essentially similar to Cotton and Boonstra[12] who proposed that this assumed immobile shell around each filler particle contributes an additional number of network chain entanglements or effective crosslinks to the polymer network and that subsequent instability of these entanglements under stress leads to creep. In more qualitative terms this shell breakdown concept is analagous to a slow progressive breakdown of "hard zones" of the type envisaged by Mullins and Tobin[13] to account for reinforcement and stress-softening in filled rubbers (see later).

It is clear from the above discussion that the mechanisms of creep and of reinforcement in filled elastomer systems may be interelated. Extensive reviews of the theories of reinforcement are available[14-16]. Reinforcement is determined primarily by pigment particle size[17] and to a lesser extent by specific physical and chemical interactions between filler and rubber:-

The increase in modulus brought about by the addition of carbon black to a rubber mix almost always exceeds that which would be predicted by simple consideration of the

volume loading of black. Since carbon black is almost completely inextensible in comparison to gum rubber it may safely be assumed that all the deformation in a filled vulcanizate takes place in the gum phase only. Consequently, the deformations of the gum, in the absence of cavitation, always exceeds that of the macroscopically observed strain by a factor:-

$$\overline{\varepsilon}_g = \varepsilon/(1-V_f) \qquad 6.1$$

where $\overline{\varepsilon}_g$ = Average strain in the gum phase

ε = Macroscopically measured strain

V_f = Volume fraction of filler.

As a result the modulus of a filled rubber should exceed that of its gum counterpart in accordance with the difference in gum extensions when the two are compared at equal measured strains. To explain the enhancement of modulus over and above this level Mullins and Tobin[13] proposed the existance of inextensible hard zones in filled rubbers. In this theory the gum phase is assumed to have duplex character in which some regions respond to stress similarly to unfilled gum whilst other regions are considered hard and immobile. In this case Equation 6.1 could be modified to read

$$\overline{\varepsilon}_g = \varepsilon/(1 - V_f - V_h) \qquad 6.2$$

where V_h = volume fraction of hard zones.

The concept of "bound rubber shells" around filler particles lends a physical interpretation to the hard zone hypothesis. It has long been known that insoluble

gels are formed when carbon black loaded uncured gums are milled. W. F. Watson[18] suggested that rubber molecules may be broken by the high shear stresses generated during the milling process and that the free radicals so formed are then chemisorbed onto carbon black surfaces. This insoluble gel is known as "bound rubber". Experiments have shown that the amount of bound rubber absorbed by unit weight of black depends primarily on the surface area of black[14,15], on its surface activity and on its structure[19]. Since these factors are also important in determining the reinforcement potential of carbon blacks it is not surprising that the bound rubber forming ability of blacks is related to their reinforcement potential[20,21]. This may be explained if it is assumed that bound rubber relates to immobile shells around filler particles or to the hard zones of the Mullins and Tobin theory. More recently Medalia[22] has suggested another contribution to immobile or "hard" rubber. Together with Heckman[23,24] he examined the structure of carbon blacks in vulcanized rubbers and found that many unit pigment particles were agglomerated together into chains and more complex three dimensional arrangements as are in fact found in as received blacks prior to milling into rubber. He suggested therefore that those regions of rubber which were occluded within or close to these rigid black structures would be protected from externally applied stress and would not contribute to deformation.

Other physical theories of reinforcement are based on the distribution of strains in the rubber matrix around filler particles. The hard zone concept implies that a sharp boundary should exist between deformed and undeformed regions and in practice this may not be so. An elastic deformation theory may be derived by assuming a gradual transition from constrained to unconstrained response of the rubber phase with increasing distance from the black surface[25]. Assuming spherical particles this gives rise to the Einstein - Guth - Gold Equation[26]:-

$$E = E_o (1 + 2.5 V_f + 14.1 V_f^2) \qquad 6.3$$

where E = modulus of filled rubber

E_o = modulus of unfilled equivalent

V_f = volume fraction of filler.

The observed moduli of filled rubbers are however generally in excess of those suggested by Equation 6.3 and a number of modifications have been suggested to account for this. Again by assuming the existance of a thin immobile zone around filler particles V_f may be replaced by a term which equals the sum of the volume fractions of hard rubber and of particles[27]. Alternatively a shape factor may be introduced to take account of the fact that the true shape of reinforcing agglomerates are generally not spherical[28].

The idea that rubber molecules react with carbon black surfaces gives rise to the so called chemical theories of reinforcement. Here, surface reactivity is considered to be all important; reactivity is considered

to increase with decreasing particle size since small particle sized blacks show higher bound rubber absorption. A. M. Bueche[29] suggested that the chemisorption of molecules is equivalent to an increase in the concentration of crosslinks in the network which in turn corresponds to an increase in network modulus. In this case bound rubber formation represents the propensity of cross-link formation at the black-rubber interface. By comparison, F. Bueche[30,31] considered that certain lengths of network chain would be crosslinked at both ends to adjacent carbon black particles. On stretching the rubber some of these would approach their limiting extension at only moderate applied strains and would therefore contribute disproportionately to the induced stress.

From the above it is clear that good creep resistance in filled vulcanizates depends not only on the inherent properties of the base polymer but also on the long term stability of the reinforcing mechanisms. It is well known, however, that these mechanisms are by no means stable as is exemplified by the fact that filled vulcanizates show greatly enhanced stress-softening. When an as received rubber sample is stretched to a given strain and then relaxed, subsequent extensions to the same or lower strain require lower applied stress than on the first cycle. Most of this "softening" occurs during the first deformation cycle and after a few cycles a steady state is achieved. This effect is known as stress-softening and it is far more prominent in filled

systems. Various theories have been proposed to account for the additional softening observed in filled systems; Mullins and Tobin[13] suggested the breakdown of hard zones as described earlier for example. By comparison Harwood et al[33,34], Mullins and Tobin[35] and Meluch[36] have proposed that stress-softening is related only to the polymer phase rather than to polymer-filler interactions and that the extra softening observed in reinforced systems may be accounted for by a strain amplification factor synonymous with Equation 6.1. Bueche[31] and Nakane[37] have attributed stress-softening to the breakage of highly stressed network chains between adjacent filler particles. Bueche considered that some chains would be bonded at both ends to filler particles and that these would fracture when the interparticle separation exceeded their limiting extension. Boonstra[27] and Dannenberg[38] on the other hand have suggested that such highly stressed chains would not break but that they would "slip" at their points of bonding and they proposed this as an alternative stress-softening mechanism. Kraus et al[39] have suggested the stress induced breakdown of pigment agglomerates as a contributory factor whilst Smith[40] has attributed stress softening in black filled SBR-polybutadiene blends to filler polymer interfacial failure and subsequent vacuole formation. This latter proposal corresponds to Gents view[1] that the creep of a similar reinforced SBR rubber was due to vacuole formation.

Derham et al[2-5, 41] have shown that when a filled rubber is pre-strained or momentarily overextended and then relaxed it shows improved creep resistance in subsequent tests. This may be related to the stress-softening phenomenon if it is assumed that the mechanisms of softening, i.e. of reinforcement instability, and of creep are interelated. The implication is that a proportion of the decrease in modulus E (t) which represents creep or stress-relaxation may be brought about by a prior strain cycle. In industrial terms this phenomenon represents the scragging process in which finished components are pre-loaded to just above their design stress in order to improve their in-service creep or stress-relaxation performance. Furthermore, the influence of scragging may be interpreted in terms of the hardening theory described in Chapter 5 since pre-strained samples show greater initial elongation when subjected to a particular stress than do as-received samples and they are therefore closer to equilibrium from the first instant of loading. The effectiveness of scragging increases with the extent of filler loading[3], gum rubbers being only slightly affected, and this is in agreement with the fact that stress-softening is more prominent in highly filled systems.

The present chapter is devoted to a study of the influence of various types of carbon black on creep together with a brief discussion of some possible mechanisms.

6.2 Description of Filled Rubbers

Vulcanizates E, F, G, H and I (see Figure 2.1) were used to determine the influence of black reinforcement on creep. Each of these was based on vulcanizate 'A' but with 30 pphr carbon black addition. Vulcanizates 'E' and 'F' contained high structure and low structure high abrasion furnace blacks (HAF) respectively both of which have equal pigment particle sizes in the range ~ 260Å to 300Å diameter. Because of its tendency towards higher agglomeration and to long chain structure formation the high structure black imparts a slightly higher modulus than its low structure counterpart when compared at the same volume loading. It is intended therefore that a comparison of vulcanizates 'E' and 'F' should indicate the influence of black structure on creep. Vulcanizates G, H, and I were compounded with low structure super abrasion furnace (SRF) black, 600Å diameter, low structure furnace thermal (FT) black, 800 - 1500Å diameter, and normal structure super abrasive furnace (SAF) black, 200Å diameter, respectively. Comparison of all five vulcanizates should therefore indicate the influence of pigment particle size on creep. Additional vulcanizates J, K, L and M were also prepared from the largest and smallest particle size blacks at loadings of 10 and 50 pphr, see Figure 2.1, although these were not used in creep work.

Bearing in mind the proposed theories of reinforcement it is clear that the surface area of carbon blacks should

be important in determining their reinforcing potential. Whether reinforcement occurs by hard zone formation around black particles or by specific chemical interactions between black and matrix, the extent of the effect should depend, other things being equal, on the interfacial area available. It is not surprising, therefore, that general correlations may be established between specific surface area, i.e. area per unit weight, of black and its reinforcement value. This is illustrated in Figure 6.1 which shows modulus results taken from stress-strain data for all the black filled vulcanizates and for vulcanizate 'A' at 20°C. The ordinate represents modulus at 100% strain whilst the abscissa indicates surface areas estimated from the volume loading of black and its nominal particle diameter. Good general agreement is observed despite the fact that the area calculation wrongly assumes that black particles are broken down into unit spheres during processing. The lower curve for scragged samples represents data for samples which were stretched to 200% strain and relaxed prior to tensile testing. The amount of stress-softening brought about by this pre-stressing cycle clearly depends on the level of initial reinforcement, being small for the gum vulcanizate 'A' for example and quite substantial for vulcanizates 'I' and 'M'.

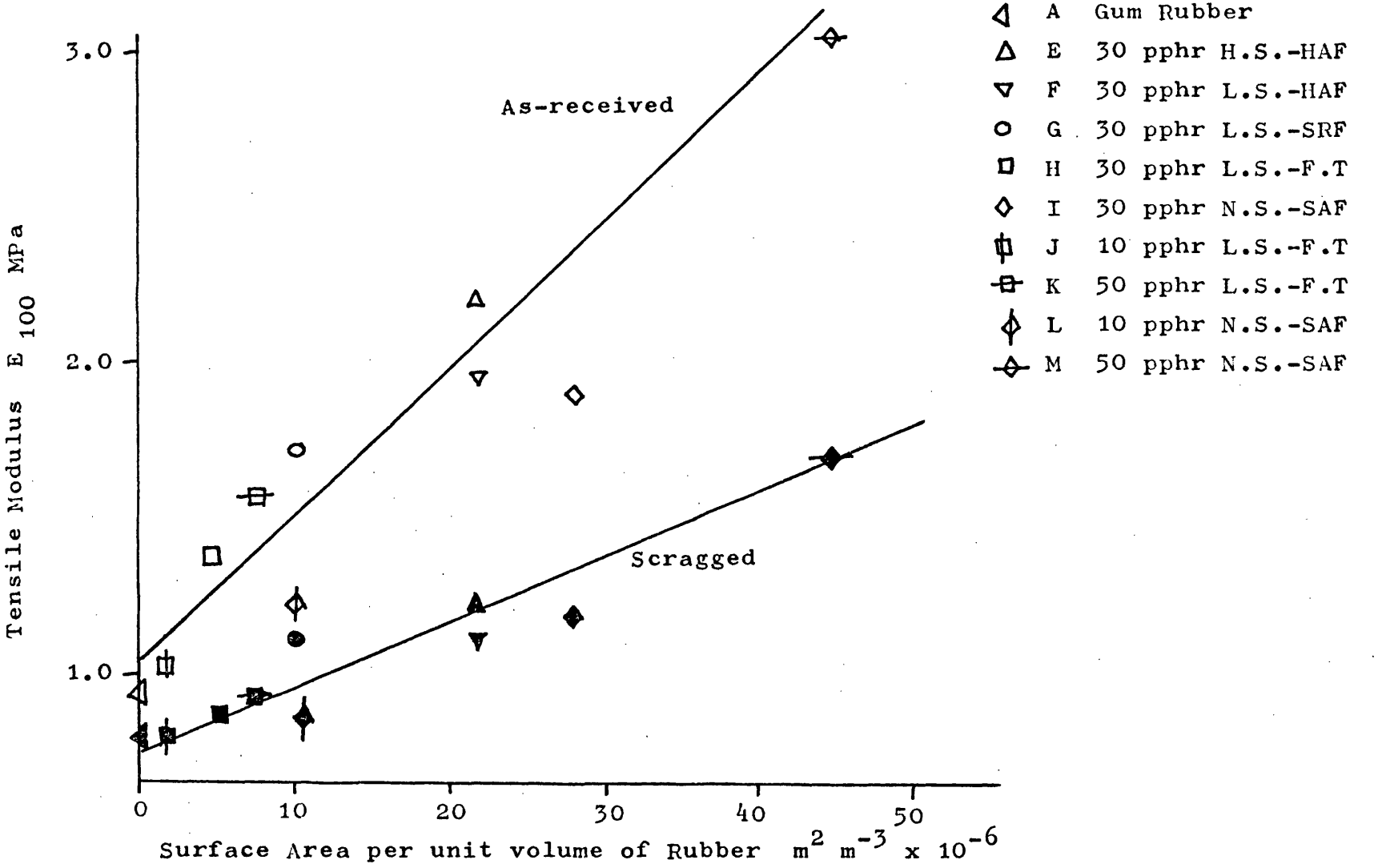

Figure 6.1 The influence of specific surface area on reinforcement. Scragged samples were pre-strained to 200% strain.

6.3 Creep Results

Typical creep plots for the black reinforced vulcanizates at 20°C and "oven humidity" are shown in Figure 6.2. Each curve has been displaced vertically for clarity and in fact the intercepts with the vertical axis at t = 1.0 represent zero measured creep. Two factors distinguish these curves from those of vulcanizate 'A'; not only are their initial logarithmic creep rates somewhat greater but they also show an accelerating response after roughly 10^3 to 10^4 minutes under load.

Accelerating creep, as shown in Figure 6.2, has not been observed in vulcanizate 'A' when tested at similar initial strains and stresses and this suggests that such behaviour does not correspond to secondary creep of the type discussed in Chapter 4. Analysis of the curves in Figure 6.2 indicates that the discrepancy between the observed response and a semi-logarithmic extrapolation is not proportional to time under load but rather to $\sim t^{0.5}$. Furthermore, the expected secondary creep rate at 20°C, obtained by extrapolating Figure 4.19b, would be $\sim 10^{-7}$ min^{-1}, i.e. 10^{-5}% min^{-1}. This indicates that the total secondary contribution at 10^4 and 10^5 minutes under load should be in the order of 0.1% and 1.0% respectively whereas the breakaway contributions shown in Figure 6.2 greatly exceed this amount. Alternatively, it may be considered that the accelerating response corresponds to the early stages of a slow

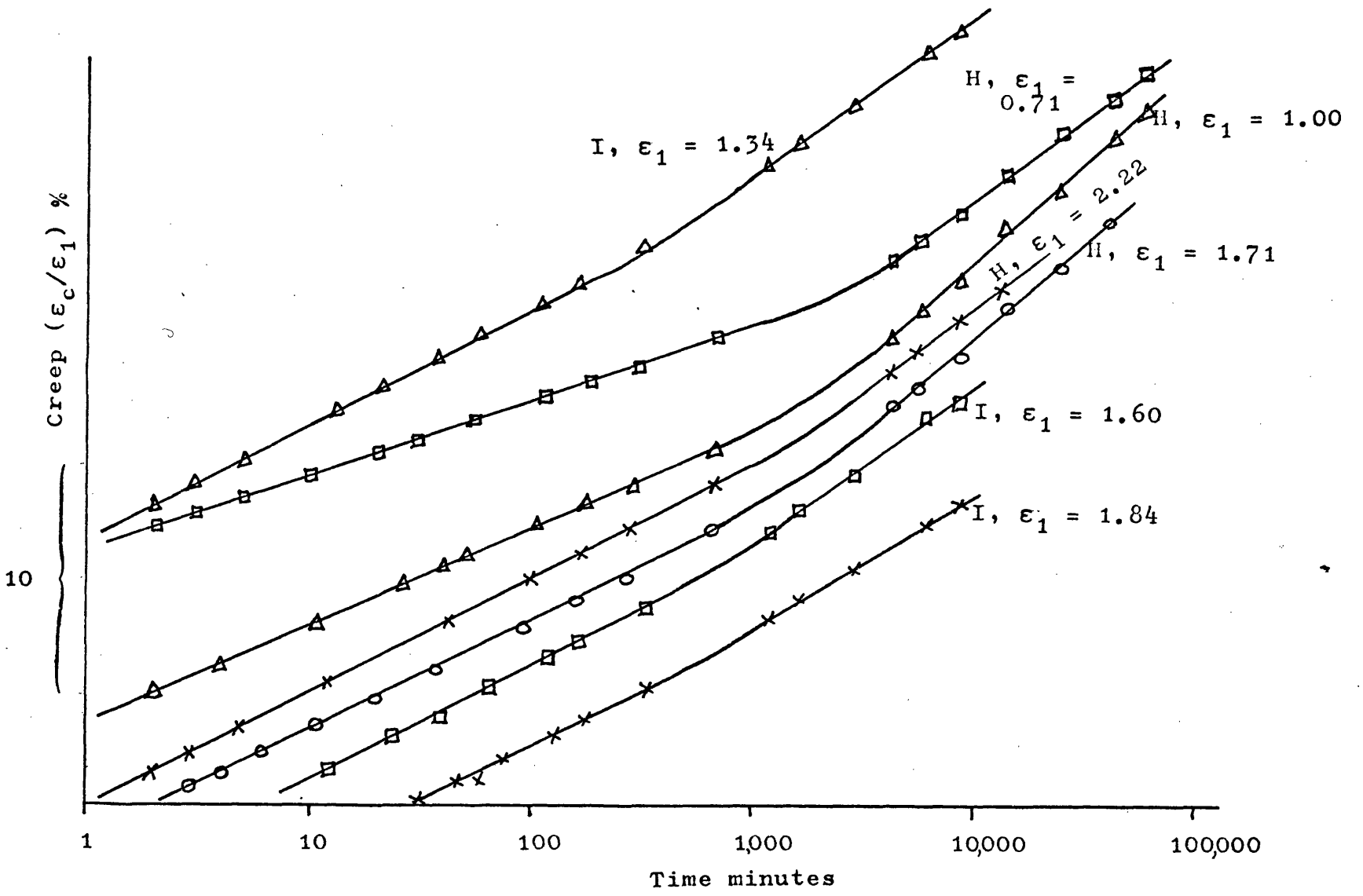

Figure 6.2 Semi-logarithmic plots for the creep of filled samples at 20°C and oven humidity. The curves are displaced vertically for clarity.

crystallisation process in regions of high strain in the rubber phase between filler particles; the curves of Figure 6.2 are not unlike those for the crystallisation accelerated creep of vulcanizate 'C' shown in Figure 2.21 for example. If this were the case, however, then Gents suggestion[1] that enhanced logarithmic creep, i.e. the first part of the curves in Figure 6.2, is caused by crystallisation may be in some doubt. In the present work no explanation of this accelerating response is to be offered except to say that it may result from crystallisation, from a breakdown in filler-rubber interaction over and above that causing logarithmic creep or from enhanced viscoelastic processes in the gum phase. From the engineering design viewpoint, however, the onset of such a breakaway process is of obvious importance and Figure 6.3 indicates how it may be accounted for. This shows the same results plotted on log-log scales as suggested in Figure 2.4, and in this case a straight line relationship is obtained from $t \sim 100$ minutes onwards. Design extrapolations based on log-log plots suggest creep deflections which exceed those based on semi-log plots by a factor of about 3/2 to 5/2 after 10 to 20 years under load.

The onset of breakaway creep, as described above, throws some doubt on the real effectiveness of scragging as a means of mitigating in-service creep and to investigate this a number of long term creep tests were conducted on scragged samples. Each sample was scragged by repeatedly loading and unloading, $\sim$ 10 times, to the

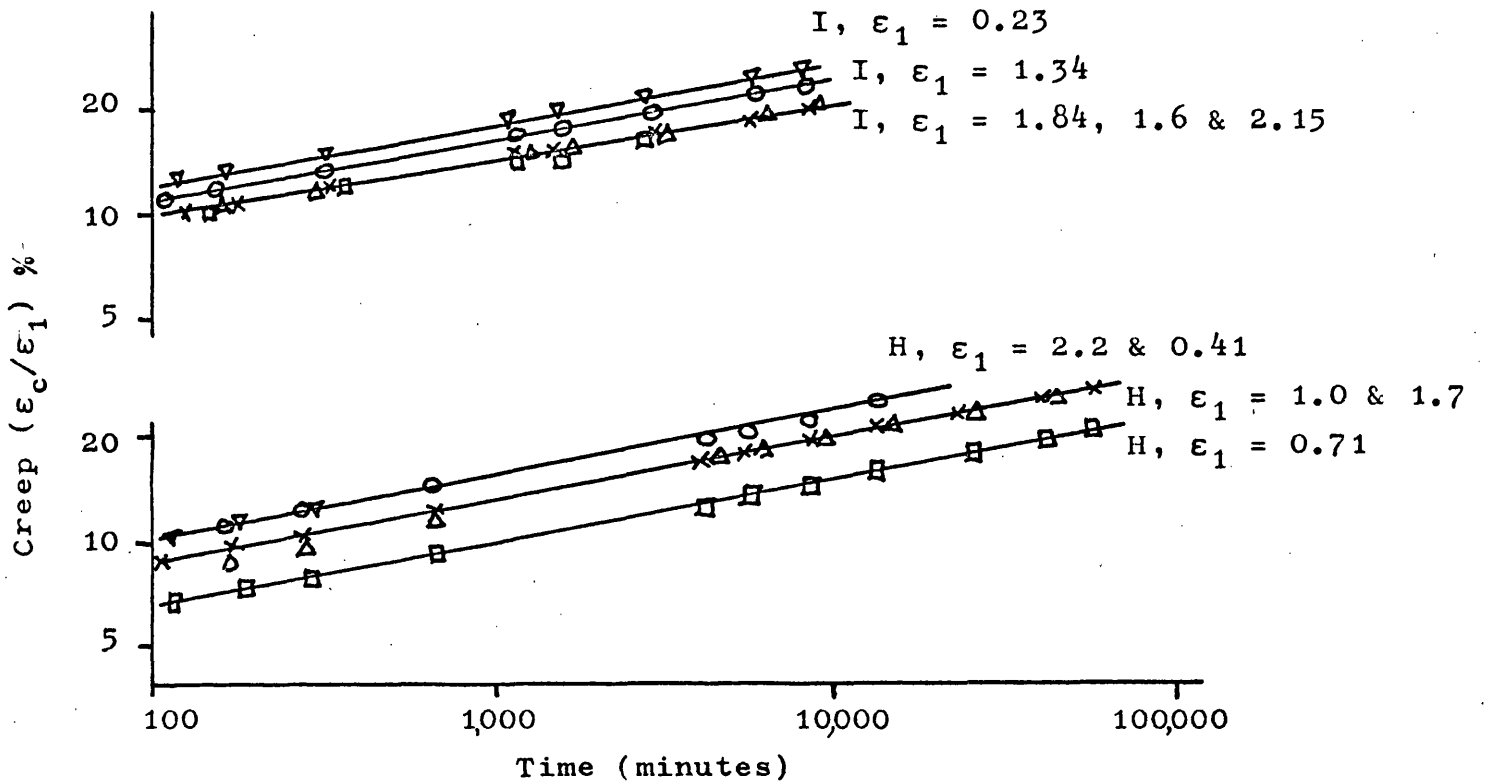

Figure 6.3 Log-Log plots for the creep of filled samples at 20°C and oven humidity.

same stress as that at which it was to be creep tested. One day was then allowed for recovery. Figure 6.4 shows the semi-logarithmic plots so obtained and again they show accelerating behaviour, this time somewhat earlier in the creep history at $\sim 10^2$ to 10^3 minutes under load. Log-log plots for the same results are shown in Figure 6.5 which again indicates straight line relationships from about 10^2 minutes onwards. Figure 6.6 shows a comparison of the creep response of as-received and scragged samples in terms of the log-log analysis. As the initial portions of log-log plots are always concave downwards, see Section 2.4, the creep elongation which occurs at short times of less than 10^2 minutes or so is not reflected in the log-log creep rate. Figure 6.6 therefore shows the extent of creep at an arbitrary time under load within the log-log region, in this case 1000 minutes, to indicate the influence of the transient response. The results show that the gradients of log-log creep curves are only slightly influenced by initial elongation (applied stress) but that the "transient" creep tends to decrease with increasing elongation. Comparison of data for as-received and scragged samples of vulcanizates 'H' and 'I', containing the largest and smallest particle size blacks respectively, at the same stress or same initial elongation shows that the "transient" creep contribution is much reduced by prior scragging. By comparison scragging has no mitigating effect, within experimental error, on observed log-log gradients. On this basis, therefore, scragging

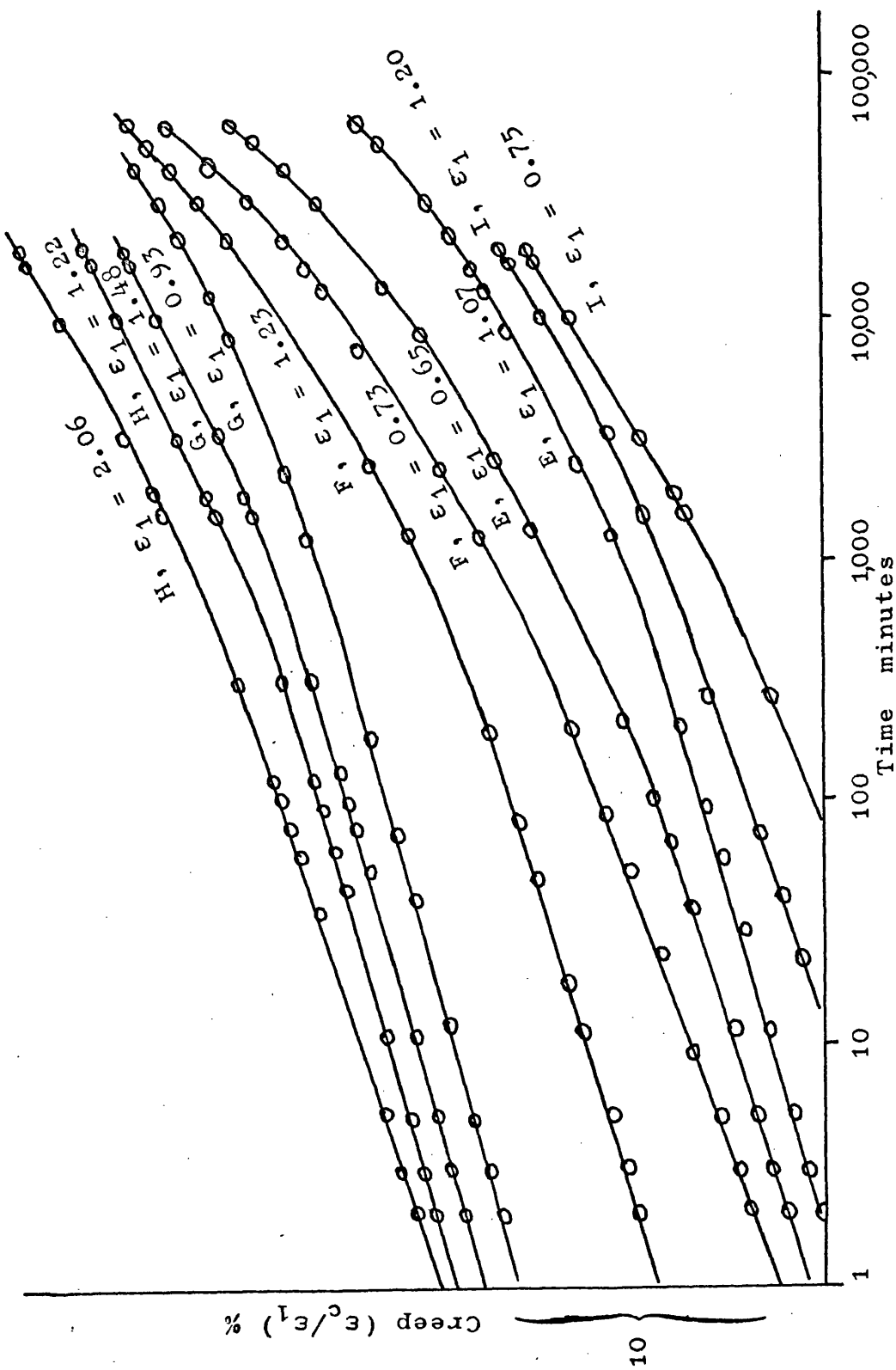

Figure 6.4 Semi-Log plots for the creep of scragged, filled vulcanizates at 20°C and oven humidity scragged by pre-straining to the creep stress ~ 10 times. One day was allowed for recovery before the start of creep testing. Curves are displaced vertically for clarity.

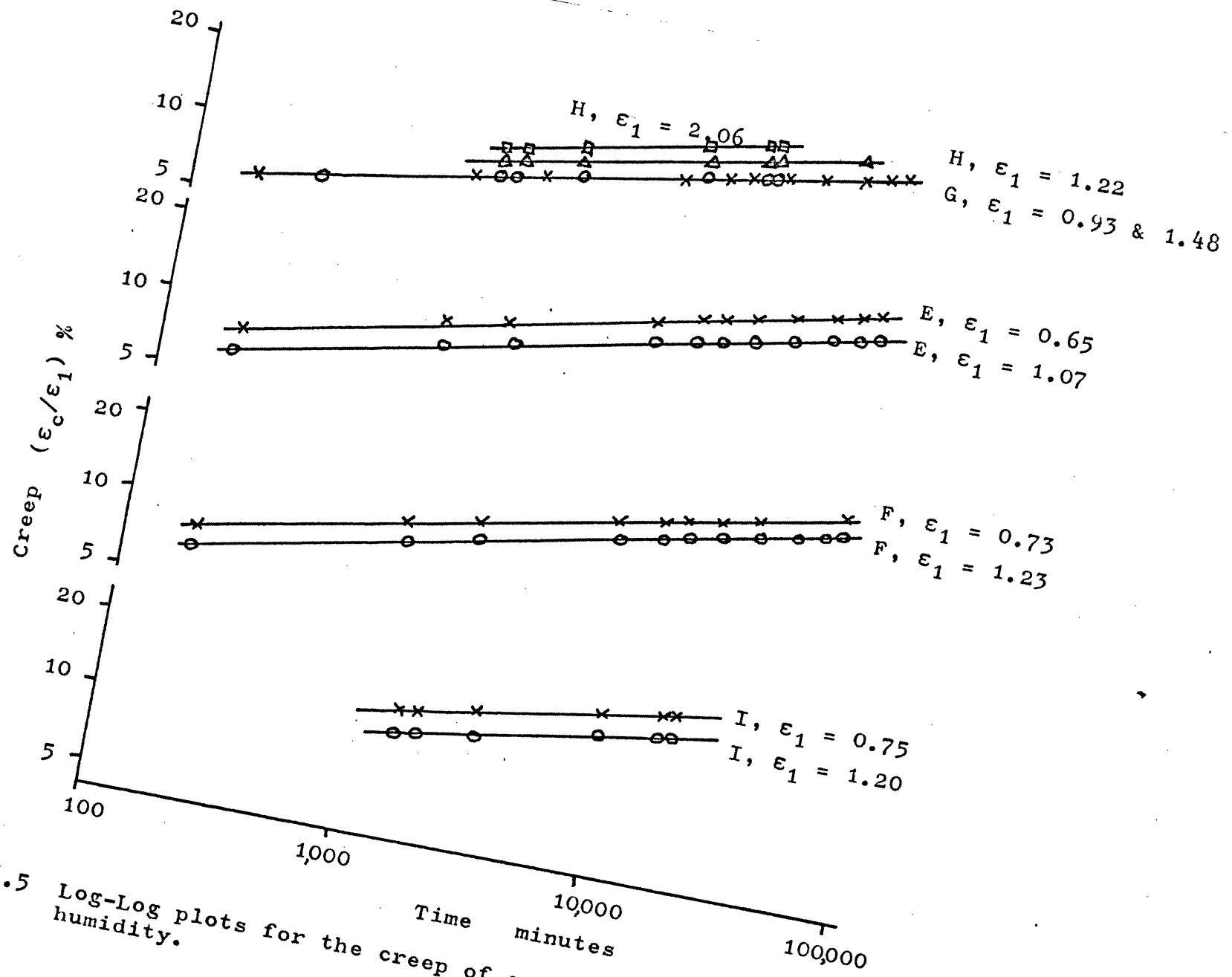

Figure 6.5 Log-Log plots for the creep of scragged samples at 20°C and oven humidity.

Vulcanizate		ε_1	Stress MPa	Gradient	Creep at t = 1000 mins $(\varepsilon_c/\varepsilon_1)$ %
H	As-received	0.41	0.71	0.18	15.6
H		1.00	1.26	0.18	13.2
H		1.71	1.88	0.18	13.2
H		2.22	2.54	0.195	10.0
H		2.41	2.76	0.195	10.0
I		0.23	0.66	0.175	18.4
I		1.34	2.31	0.175	16.5
I		1.60	2.85	0.16	14.5
I		1.84	3.44	0.16	14.5
I		2.15	4.4	0.16	14.5
E	Scragged	0.65	1.26	0.20	10.5
E		1.07	1.82	0.20	8.5
F		0.73	1.28	0.195	11.0
F		1.23	1.88	0.20	9.2
G		0.93	1.37	0.175	8.1
G		1.48	1.94	0.175	8.1
H		0.75	1.30	0.18	12.0
H		1.20	1.91	0.175	9.8
I		1.22	1.48	0.16	10.1
I		2.06	2.23	0.15	8.5

Figure 6.6 Log-log creep analysis results for as-received and scragged samples at 20°C and oven humidity. Gradient = $d.\log_{10}[(\varepsilon_c/\varepsilon_1)\%] / d.\log_{10} t$. Creep at 1000 minutes indicates the influence of creep at short times prior to the establishment of steady state log-log behaviour.

may be considered particularly beneficial since the deformation of a scragged sample always lags a decade or so of time behind that of an as-received sample and the difference between them progressively increases with increasing time under load. Finally, Figure 6.6 shows that with the exception of 'I' there were no significant differences between the various vulcanizates when compared on a log-log basis. Vulcanizate 'I', however, showed both a low gradient and low transient creep, either in the as-received or scragged condition.

6.4 Logarithmic Creep Rates

Despite the onset of breakaway creep as described above there is no doubt that creep at short times follows an essentially semi-logarithmic law of the type discussed in Chapter 5. It is of interest therefore to examine the influence of various types of carbon black on this type of response. Figure 6.7 indicates observed logarithmic creep rates for the filled vulcanizates and for vulcanizate 'A' at 20°C and oven humidity as a function of initial strain. Note that applied strain (stress) has different influences on different filler systems and that there is no logical interelationship between filler type, its particle diameter, structure or reinforcing ability and the influence of strain. This suggests that different creep mechanisms may dominate in different systems. In all cases the creep rates for the filled vulcanizates exceed those for the gum equivalent 'A' and this is in accordance with the work of Gent and Derham as discussed earlier in Section 6.1. Further examination of Figure 6.7 indicates

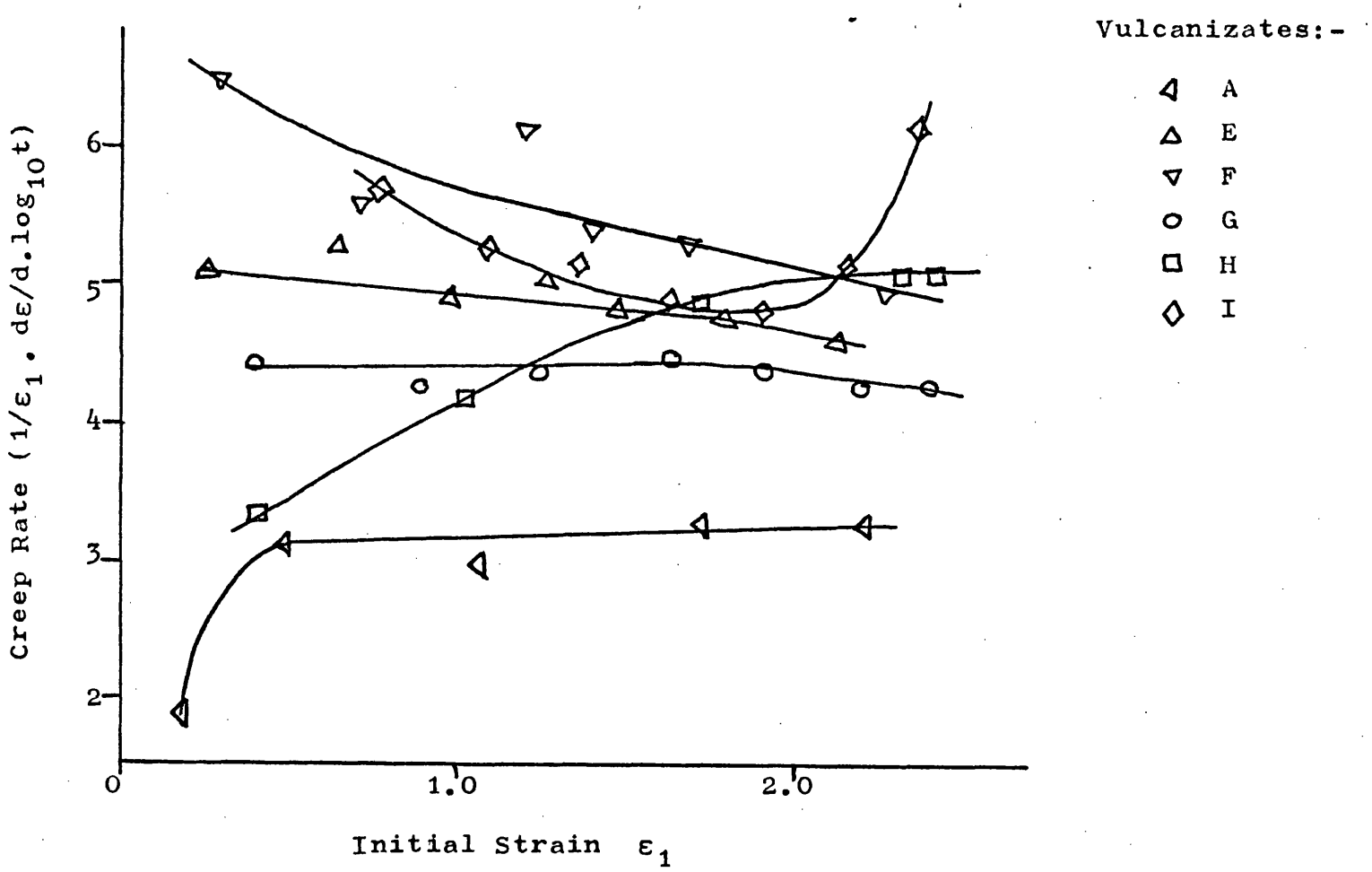

Figure 6.7 Logarithmic creep rates for as-received samples at 20°C and oven humidity.

that the more highly reinforced systems show the greatest creep rates, particularly in the range of strain most relevant to engineering design, i.e. $\varepsilon_1 < 100\%$. This is illustrated more clearly in Figure 6.8 which indicates creep rates for both as-received and scragged samples at 100% initial strain as a function of their 100% modulus. The plotted points have been derived by interpolation of Figure 6.7 and similar graphs. The 100% modulus used in plotting Figure 6.8 was based on measurements from as-received samples; nevertheless the moduli of scragged samples would have been similar since they were pre-stressed (scragged) to the same stress as that to which they were subsequently subjected to in creep. This is illustrated more clearly in Figure 6.9 which shows a schematic illustration of stress-strain curves for both loading and unloading of an as-received sample and for a successive stress cycle. The strain increment $\Delta\varepsilon$, shown, caused by stress-softening in the first cycle is generally small in comparison to the total strain ε_b when compared at the same stress as the pre-stress i.e. σ_b. Consequently the modulus of scragged creep samples at their creep extension would not be significantly different to as-received samples. By comparison, the modulus of scragged samples is very much reduced for all strains below the pre-strain; at a strain ε_a (Figure 6.9) for example the modulus loss would be determined by $\Delta\sigma$ and in general this would be a significant proportion of σ_a. In Figure 6.1, for example,

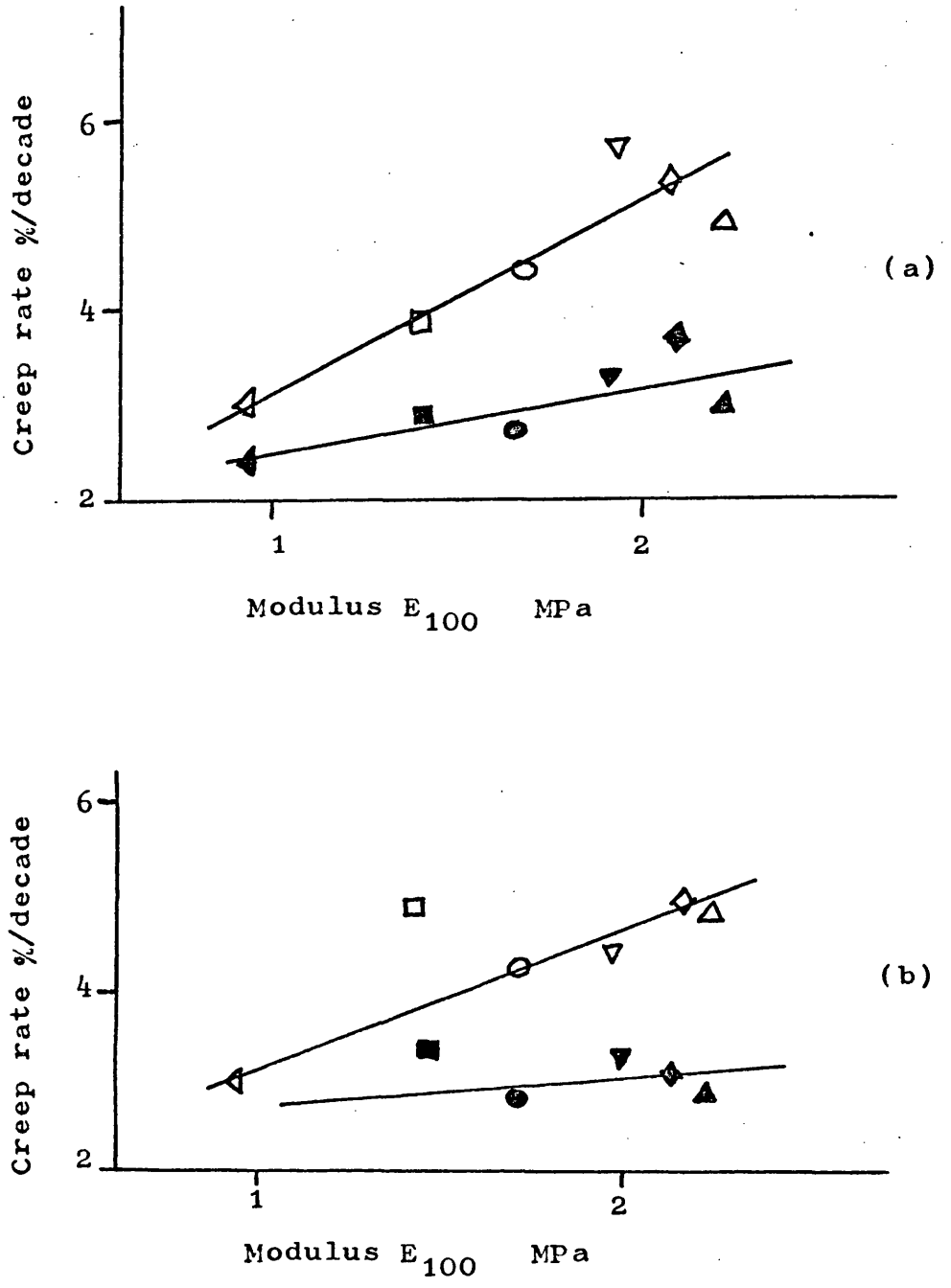

Figure 6.8 Logarithmic creep rates for filled samples at a) 20°C and b) 0°C as a function of 100% modulus. Symbols are as on Figures 6.1 or 6.7.

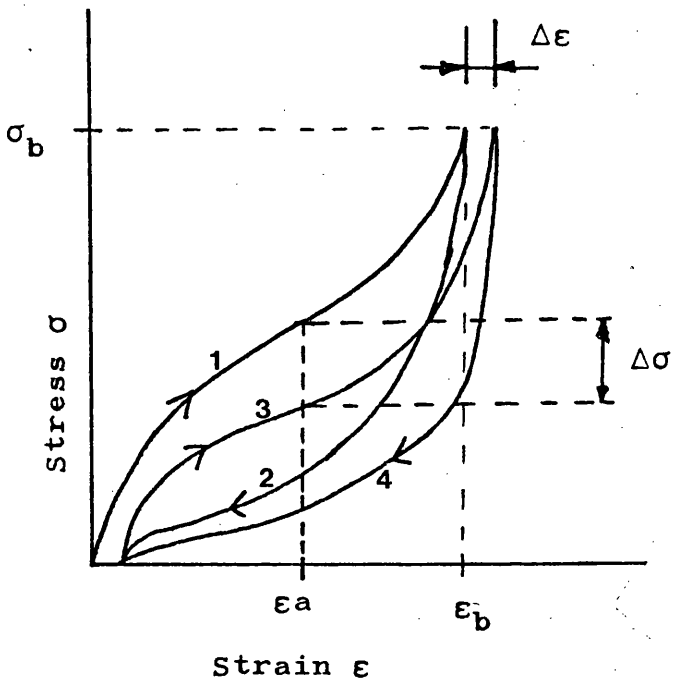

Figure 6.9 Schematic illustration of the loading and unloading curves for an as-received sample (1&2) and for a second subsequent cycle (3 and 4).

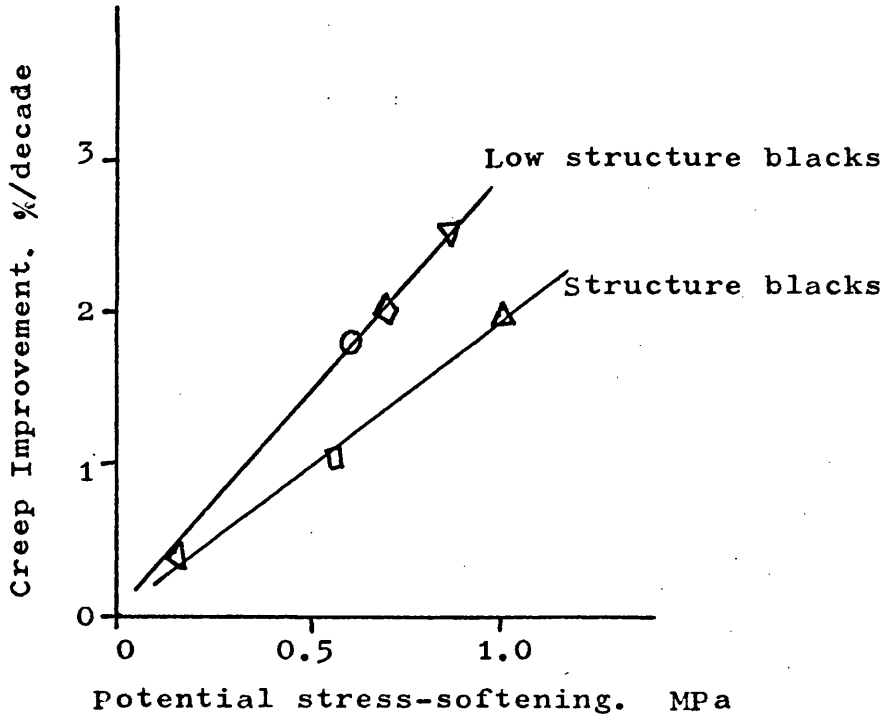

Figure 6.10 Improvement in logarithmic creep rate at 100% strain due to prior scragging. Symbols are as on Figures 6.1, 6.7 and 6.8.

the 100% moduli of scragged samples is much less than those of as-received samples and this follows from the fact that they were pre-strained to ~ 200%.

The interelationship between logarithmic creep rates and compound modulus, as shown in Figure 6.8, is in agreement with the idea presented in Section 6.1 that the creep of filled systems is determined by instability of reinforcement. Indeed, when many of the less stable reinforcing mechanisms are broken down by prior scragging the observed logarithmic creep is reduced to almost that of the unfilled gum. To further illustrate this point Figure 6.10 shows a comparison of the influence of scragging on each vulcanizate with its stress-softening behaviour as indicated arbitrarily by its stress loss at 100% strain due to a pre-strain of 200%. The general agreement so obtained suggests that the mitigation of creep by scragging and therefore the high creep of as-received samples is related to reinforcement instability. Furthermore, the influence of scragging may also be interpreted in terms of the "hardening" theory of Chapter 5 since the initial elongation of scragged samples is always slightly greater, see Figure 6.9, than that of as-received samples at the same applied stress; consequently scragged samples may be considered to be closer to equilibrium from the moment of initial loading. The hardening theory may also be useful in explaining some observations by Derham et al[2,4,5,41] that the optimum improvement in logarithmic creep is

obtained by scragging to exactly the same strain as that to be imposed in creep testing. At first sight this is contrary to the reinforcement instability concept of creep enhancement in filled systems since the spectrum of reinforcing mechanisms remaining after scragging should be increasingly stable with increasing strain of scragging. In practice, however, the removal of increasingly stable reinforcing mechanisms with increasing pre-strain has two mutually opposing effects due to the elimination of both their creep and strain hardening potentials i.e. The stress-softening caused by scragging to excessive strains reduces the sample modulus at its intended creep strain and therefore brings about an increase in the creep extension required to compensate for a given amount of structural pertubation whilst under load. Consequently those creep mechanisms which are little affected by prior scragging, reversible physical creep of the type described by Gent[42] for example, may appear more prominent as the scragging strain is increased.

6.5 The Influence of Filler-Matrix Bonding on Creep

The results described in the two preceeding sections show that the physical creep of the carbon black filled vulcanizates exceeds that of their gum equivalent by a factor of about two. The fact that this can be mitigated by prior scragging together with a consideration of the theories of reinforcement and of stress-softening indicate that this may be attributed in part to the long

term instability of the reinforcing mechanisms. High interfacial bond strength between reinforcing particles and rubber matrix is a pre-requisite to modulus enhancement at the level imparted by carbon blacks and it is not surprising therefore that both the physical and chemical theories of reinforcement implicitly assume good bonding. The chemical theories for example assume the existence of strong chemical bonds at the molecular level between filler and rubber whilst physical theories based on hard zone or immobile shell concepts must pre-suppose the existence of interfacial tractions and therefore of close interfacial contact indicative of bonding. It may be imagined that activation of the various plausible creep mechanisms may have a deleterious effect on this interfacial bonding which in extreme cases might lead to interfacial failure; slow but progressive physical or chemical pertubations in the matrix adjacent to or at the surface of filler particles may lead to eventual debonding. Subsequent separation of the rubber and filler interfaces would then lead to micro-vacuole formation and consequently to corresponding further creep extension.

Unlike most materials such as metals or rigid polymers, gum vulcanizates show almost no volume change when stretched. Christensen and Hoeve[43] measured the dilation with strain of a series of peroxide cured natural rubber vulcanizates for example, and observed dilations in the order of only 0.01% at an elongation ratio of 2. By comparison, vulcanizates containing

large sized particles of non-reinforcing fillers often show extensive dilation as a result of filler/matrix debonding and subsequent vacuole formation[44-46]. Sekhar and Van Der Hoff[47] have examined the cavitation process in more detail and have shown that the initial dilation rate is very rapid but that the process slows down with time; after about one minute under load dilation was proportional to the logarithm of time. They suggested that this behaviour could be explained if it is assumed that the growth of cavities is determined by the rate at which dissolved gasses in the rubber matrix can diffuse into them and so favour their expansion. Such dilation kinetics would clearly lead to a logarithmic creep contribution. In contrast to rubbers containing non-reinforcing fillers, carbon black loaded vulcanizates generally show very little cavitation at short times under load (the long term response has not been investigated). Mullins and Tobin[48], for example, used a densitometric technique to examine the dilation of black filled rubbers as a function of strain. They observed maximum dilations of only 0.03% to 0.05% at strains in the range of 1 to 2. At higher strains a contraction was observed and this was attributed to crystallisation in the rubber phase. At strains of ~ 2 the net dilation was roughly zero since at this point dilation and crystallisation effects were about equal. They concluded that most of the initial dilation could be accounted for by vacuole formation around zinc oxide pigment particles in the mix and that cavitation

did not occur around pigment particles. More recently, however, Shinomura and Takahashi[49] have observed dilations in the order of 1% to 2% in carbon black loaded butyl rubber and SBR; note that these are non crystallising. Various other workers[50-52] have observed cavitation around black particles, particularly in butyl and SBR rubbers, by electron microscopy using both direct and replica techniques. The prevalence of debonding increases with increasing particle or agglomerate size and in general there is usually a minimum extension below which no debonding occurs at all. Gent[53] has proposed a simple explanation for these observations by considering the energy balance situation during debonding; the decrease in stored elastic energy in the matrix must equal or exceed that required to produce new surfaces. Such an analysis suggests that interfacial bond stability increases with decreasing particle size.

Such fundamental physical or chemical pertubations in the matrix as may lead to eventual debonding or to enhanced creep in the absence of debonding would be extremely difficult if not impossible to detect directly. By comparison, the occurence of debonding with subsequent vacuole formation may be determined by simple densitometric or dilatometric techniques whilst some indication of interfacial bond strength may be obtained by electron microscopy. Various attempts have been made to elucidate these factors in the present work and these are to be described.

a) Simple Volume Assessments of Creep Samples

The volumes of certain creep samples were calculated from gauge length and thickness measurements obtained using a cathetometer and micrometer respectively. The volumes of samples after extensive creep at elevated temperatures measured whilst still under load were then compared with as-received volumes. Figure 6.11 indicates the results obtained. Clearly this is a very approximate technique but within experimental error there was no detectable dilation of any of the vulcanizates during creep.

b) Densitometric Determinations

Attempts were made to compare the densities of as-received and crept samples by densitometry. Samples were weighed in air and in a liquid of known density. Glycerine was chosen as the prefered liquid since it has a volume thermal expansion coefficient fairly close to that of the vulcanizates examined and it was hoped that this would compensate for temperature differences between one density determination and another. In practice, however, the vulcanizates slowly absorbed glycerine during the weight determinations and a great deal of time was required to obtain constant weight. The technique was therefore abandoned since its accuracy was no better than that of a simple flotation method which will now be described.

Vulcanizate	Test Temperature °C	ε_1	Total Creep ($\varepsilon_c/\varepsilon_1$) %	V/V_o
E	80	0.65	125	0.97
E	100	0.59	155	0.98
E	120	0.63	180	1.02
F	80	0.82	130	1.05
F	100	0.76	170	0.91
F	120	0.71	190	0.97
G	80	0.81	125	0.80
G	100	0.83	147	0.98
G	120	0.80	200	0.99
H	80	0.98	125	0.95
H	100	0.96	165	1.00
H	120	0.94	200	1.04
I	80	0.66	175	0.97
I	100	0.64	220	1.06
I	120	0.64	230	1.05

Figure 6.11 Dilation of filled vulcanizates during creep. Comparison of unstretched, as-received volume, V_o, with volume after creep and whilst still under load. Data based on simple volume estimates calculated from sample thickness and length measurements. All samples were tested at ~1.5 MPa stress. Test durations were ~ 10,000 mins at 80°C, 1000 mins at 100°C and 175 mins at 120°C.

c) Flotation Technique

In this method two small pieces of unstretched rubber ~ 2 mm x 4 mm x 4 mm were cut, using a razor blade, one from the centre section of an as-received sample and one from a crept sample. They were then placed in a 100 ml capacity measuring cylinder containing ~70 ccs of potassium chloride solution of concentration such that the samples just floated (Density ~1.074 grms/cc). This was titrated with distilled water (Density 1.0 grms/cc) until one and then the other sample began to sink. The difference in titre values for the two "end points" was used to calculate the difference in salt concentration and hence the difference in solution densities required to support the two samples. This method overcomes the problem of solution absorption by the samples during the experimental duration if it is assumed that both the as-received and crept sample absorb at the same rate. Flotation determinations were always carried out immediately after the end of each creep experiment so as to minimise the decay by air diffusion of any vacuole pockets in the crept samples. The salt solution was stirred inbetween additions of distilled water to ensure a homogeneous mix. A small amount of "Decon Concentrate", a proprietary non-foaming detergent, was added to the salt solution to ensure good wetting of the rubber samples and to prevent air bubbles from adhering to them.

Figure 6.12 shows the relationship between salt concentration and solution density at 20°C obtained using a hydrometer; the line is in excellent agreement with literature values[54]. An estimate for the method sensitivity may be derived as follows:-

Density change is given by, see Figure 6.12,

$$\Delta\rho = 6.7 \times 10^{-3} \Delta C_w$$

where $\Delta\rho$ = density difference

ΔC_w = difference in % wt concentration.

Assuming a typical density of 1.074 gcm^{-3} for the rubber, then $C_w \sim 11.0\%$. Assume that the measuring cylinder contains $\sim$ 70 ccs of solution and that the end-point may be ascertained to within 0.2 cc.

Then

$$\Delta C_w \approx \frac{70}{70 + 0.2} \times 11.0 \quad \%$$

$$3.1 \times 10^{-2} \%$$

$$\text{and } \Delta\rho \approx 3.1 \times 10^{-2} \times 6.7 \times 10^{-3}$$

$$\sim 2.1 \times 10^{-4} \text{ grms/cc}$$

i.e. The sensitivity was limited to about $\pm 10^{-4}$ grms cm^{-3} but in fact this was less than the variation between one as received sample and another. In practice, therefore, accuracy was limited by the inherent variability of as-received material and in general this was in the range 10^{-4} to 4×10^{-4} grms cm^{-3}.

Differences in density between crept and as-received rubber were generally about an order of magnitude greater than the method sensitivity and 2 to 3 times greater than the inherent variability between samples. Results are

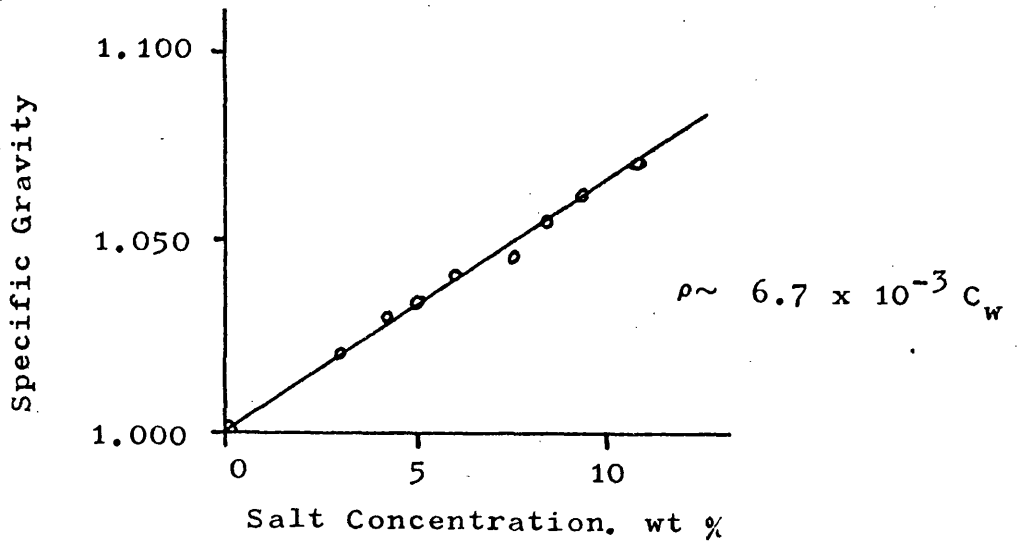

Figure 6.12 Specific gravity of aqueous potassium chloride solutions as a function of concentration.

Vulcanizate	ε_1	Time under load (mins)	$\Delta\rho \times 10^3$
E	0.65	61,000	- 1.7
	1.07		- 1.01
F	0.73	61,000	- 1.33
	1.23		- 1.68
G	1.37	61,000	- 0.94
	1.48	18,500	- 1.34
H	1.22	18,500	- 1.0
	2.06		- 0.5
I	0.75	18,500	- 0.8
	1.20		- 1.14

Figure 6.13 Density differences between crept and as received samples as determined by the flotation method. (Crept at 20°C).

shown in Figure 6.13. Whilst the results are not sufficiently accurate to allow a comparison of the various vulcanizates it is clear that density changes are so small as to be insignificant in terms of creep contribution. Even if the actual dilation in the stretched state was an order of magnitude greater than that measured, as described here for relaxed rubber immediately after creep, the creep contribution would still be small $\sim 1\%$ creep in 50,000 minutes say. Indeed, the lack of a general trend between different vulcanizates suggests that cavitation may occur only around zinc oxide/stearate particles and not around carbon black particles - as was proposed by Mullins and Tobin[48].

Differences in density between scragged and as-received samples were too small to be measured since in general such differences were less that the inherent variability of as-received samples. This suggests, therefore, that density changes develop slowly over a period of time under load and this lends support to the gas diffusion theory of Sekhar and Van Der Hoff[47].

d) Dilatometry

An attempt to measure cavitation in stretched samples was carried out using a dilatometer, see Figures 6.14 and 6.15. This works by the transfer of mercury from a reservoir A to a bucket B; the weight of mercury in the bucket strains the sample from which it is supported. The whole apparatus is filled with

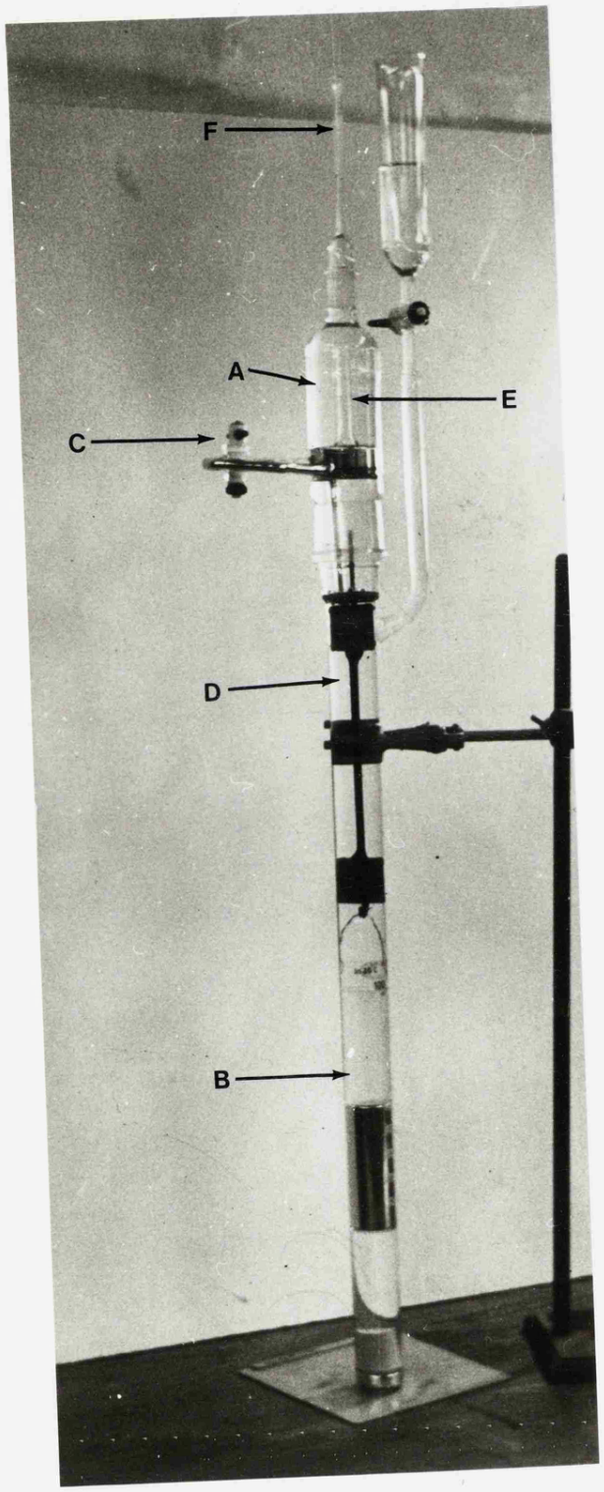

Fig. 6.14 Photograph of Dilatometer

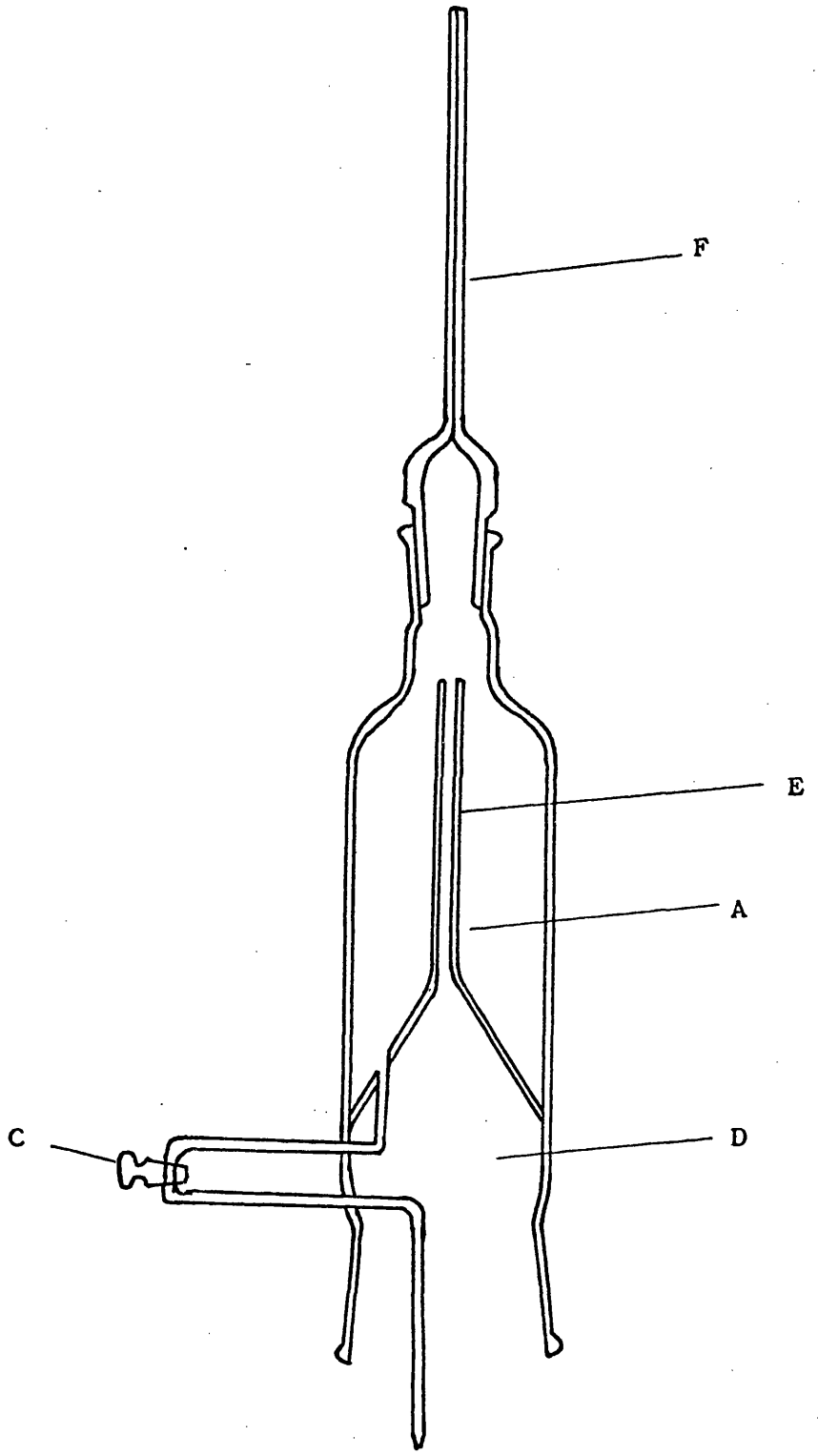

Figure 6.15 The Dilatometer. Detail of mercury reservoir and tap control arrangement.

A - Mercury reservoir
C - Tap
D - Top of working chamber
E - Reservoir/chamber separator
F - Capillary (0.5 mm).

water/Decon mix. As mercury runs out of the reservoir through the tube and tap C, an equivalent amount of water is transferred through the inverted "filter funnel" separater E into A to take its place. i.e. This represents an interchange of mercury from A with water from D. Volume changes in the rubber sample due to stretching are registered in the 0.5 mm diameter capillary F. The dilatometer was designed so that it could be assembled in such a way that air bubbles could be elliminated at each stage. In use the complete equipment was immersed in a water bath containing ~ 50 litres of water at room temperature. Even then utmost care was required to ensure adequate thermal stability. The equipment was loaded and then left for at least 12 hours to equilibriate. The equipment was kept in a small room in the centre of a large building (no outside walls and no windows). Best results were obtained in the early hours of the morning when temperature variations due to sunshine and central heating conditions were at their minimum.

Unfortunately only limited data was collected from this equipment. Nevertheless, a few results are shown in Figure 6.16. The top curves indicate the response of vulcanizate 'K' (50 pphr L.S-F.T) at $\varepsilon \sim 0.7$ and ~ 0.95. In each case a rapid dilation occurred during initial loading but this subsequently decayed and the net volume change after 20 minutes or so was zero. It is suggested that the initial volume increase was due

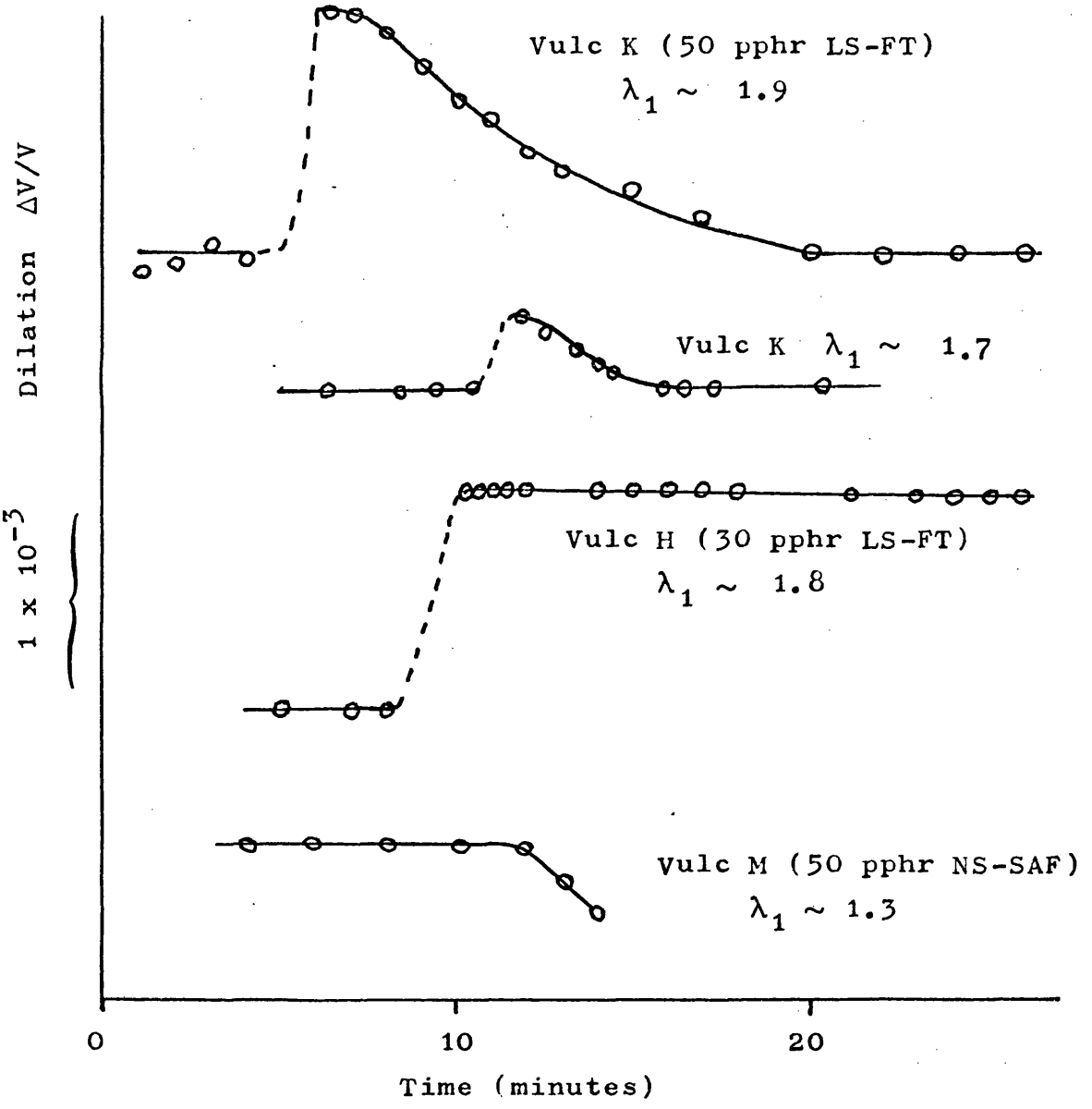

Figure 6.16 Dilation time curves obtained using the dilatometric technique. The discontinuity in each curve corresponds to the point of loading.

to cavitation and that the subsequent decrease was due to crystallisation in the rubber phase. The zero net volume change at equilibrium is in agreement with the data of Mullins and Tobin[48]. Other results for vulcanizates H and M are not so clear and repeated runs were not carried out. Dilations in excess of 2×10^{-3} were not observed and it is clear, therefore, that specimen volume change under load is not a significant contributory factor in logarithmic creep. These results are in agreement with those obtained by the flotation method.

e) Electron Microscopy

Replicas were taken from the fracture cross-sections of samples broken by bending in liquid nitrogen as described in Section 2.4. Typical micrographs are shown in figures 6.17 to 6.19. In the case of large particle sized blacks, e.g. the L.S-F.T of diameter 800 - 3000 Å, many black agglomerates were extracted onto the replica as is shown by the black features in Figures 6.17 and 6.18. Sites of unextracted black are indicated by the ring features. The proportion of black extracted may be used as a measure of black-rubber adhesion[50]; high levels of extraction indicate poor adhesion and vice versa. Negligible extraction was observed for the small particle sized blacks, Figure 6.19. To illustrate this more clearly, Figure 6.20 shows the proportion of extracted black as a function of agglomerate size for results obtained from vulcanizate 'H' specimens; clearly agglomerates of < 1000 Å are difficult to extract and

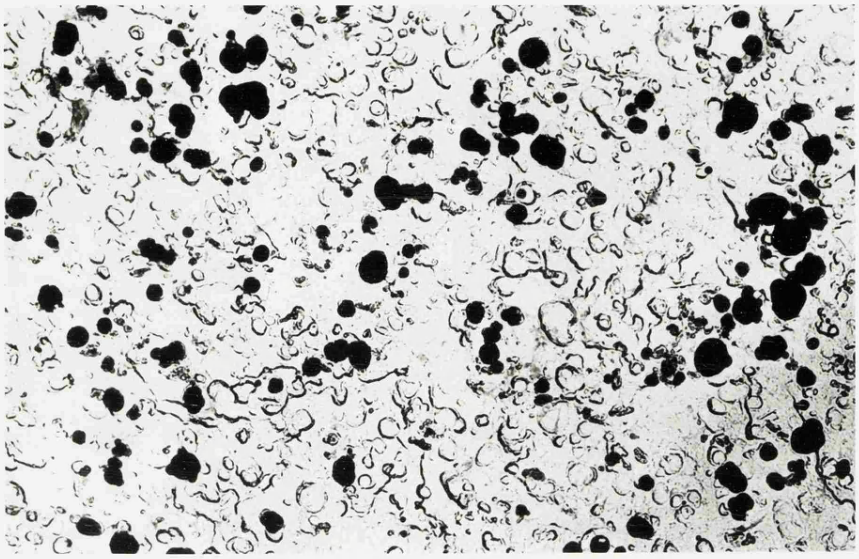

x 8K

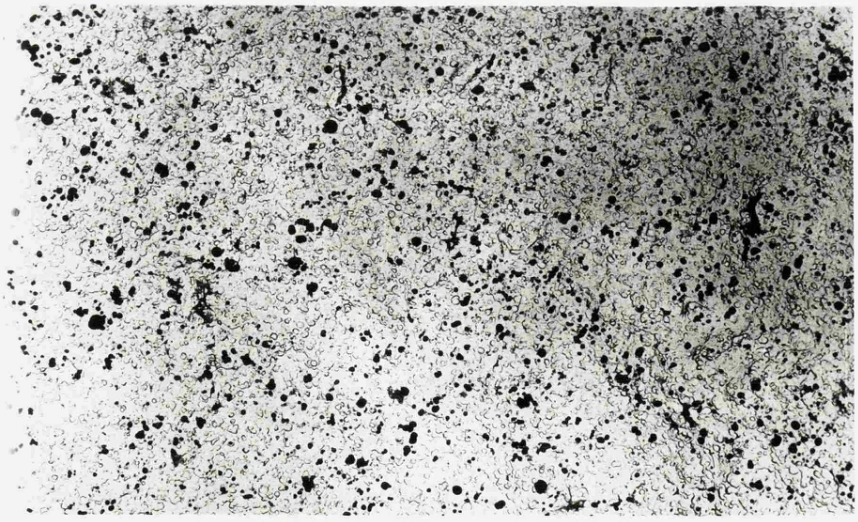

x 1.9K

Fig. 6.17 Replicas taken from liquid nitrogen fractured cross sections of Vulcanizate H. As received.

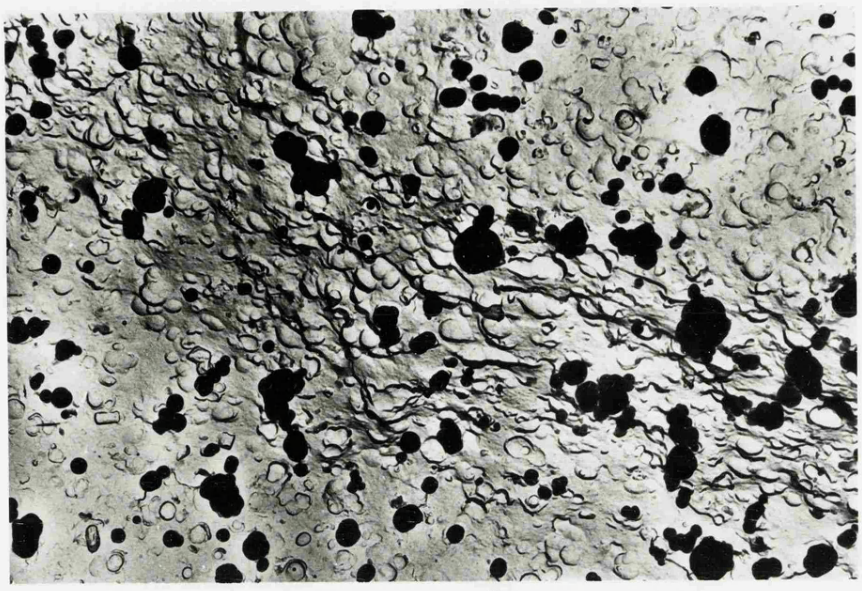

a x 8K

b x 3K

Fig. 6.18 Replicas taken from liquid nitrogen fractured cross sections of Vulcanizate H.

a) As received, showing fracture striation

b) After - 17 000 minutes creep at 20°C

a X 8K

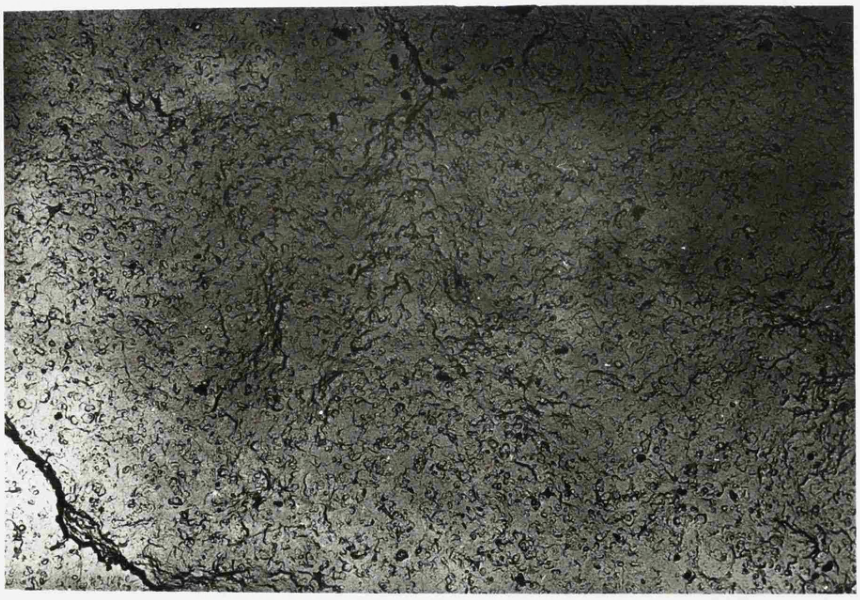

b X 30K

Fig. 6.19 Replicas taken from liquid nitrogen fractured cross sections of Vulcanizates, as received a) Vulcanizate G

b) " "

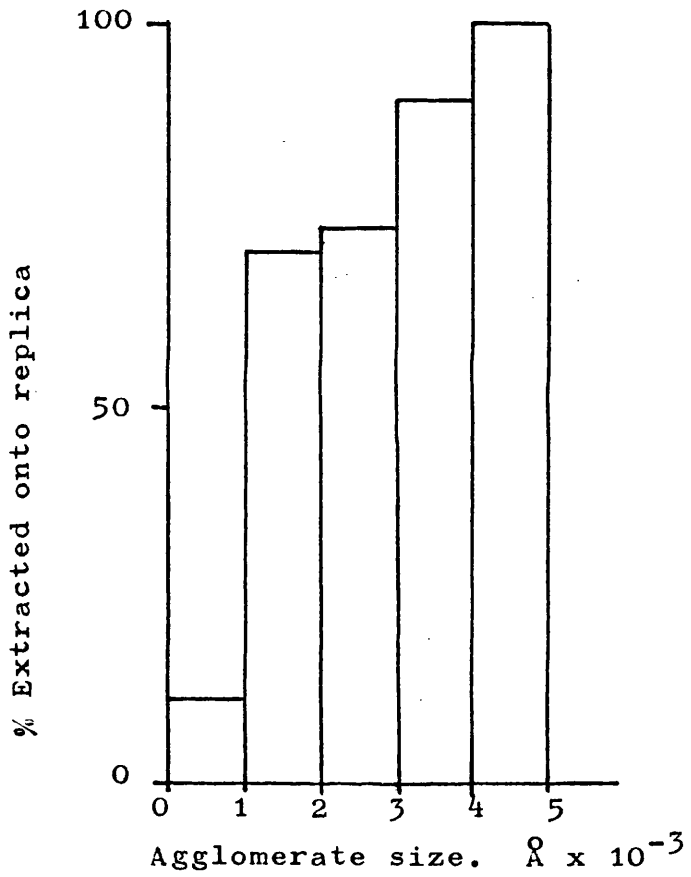

Figure 6.20 Ease of black extraction as a function of agglomerate size. Data obtained from vulcanizate 'H'.

this is in agreement with the low levels of extraction observed for vulcanizates G (600 Å) and H (200 Å). Note that allowance has been made, in calculating the proportion extracted for the fact that only half of the black particles are present on any one replica face i.e. Actual % extracted ~ twice that observed. The observed results are in accordance with the brief literature review presented earlier.

Figure 6.18a shows a fracture striation on a vulcanizate 'H' fracture section. But for the black particles it is very similar in appearance to the fracture striations observed in vulcanizate 'A', see Section 2.4.

Measurable agglomerate/particle extraction was not observed for blacks of particle size $\ll$600 Å, either in the as-received condition or after exposure to creep loading. No conclusions can be drawn therefore regarding the influence of creep on black/matrix adhesion. In the case of vulcanizate 'H' however, a number of micro-photographs were examined statistically and the results showed that only ~47% of agglomerates were extractable after 17000 minutes creep exposure (20°C, ε_1~ 1.6 - 2.0) whereas ~69% were extractable in the as-received condition. i.e. (487/2065) x 2 as compared to (778/2260) x 2. Creep exposure appears therefore to improve adhesion, not reduce it. Accepting the accuracy of the results, there are two possible explanations for this behaviour:-

a) Molecular reorganisation around carbon black particles due to applied stress causes an increase in adhesion,

possibly by reducing internal contraction stresses developed when the vulcanizate is cooled from the cure temperature, for example, or by reducing the thickness of constrained immobile layers around particles. Alternatively, b) it may be considered that the adhesion is so worsened by creep exposure that some black particles debond and are lost during the liquid nitrogen fracture process. In this case there would be fewer agglomerates to extract from the fracture cross-section and a spurious result would ensue. Further study would be required to elucidate this point; use of shadowing techniques or scanning electron microscopy would indicate which ring features on surfaces such as Figure 6.18 were caused by adhering particles and which by 'craters' left behind by particles. For the present, however, it is suggested that explanation a) is more likely since examination of Figure 6.18 and similar micrographs shows that the proportion of large particles extracted is approximately 100%; i.e. number of large agglomerates/number of large rings $\sim$1/1. This suggests that there was no loss of large agglomerates during sample preparation and since these should have the poorest adhesion, then it is likely that no agglomerates of any size were lost.

The microstructural studies outlined above have not indicated any evidence for poor matrix/black adhesion nor any evidence that adhesion is reduced by creep exposure. This is in agreement with the dilatometric and flotation results and indicates that

cavitation does not contribute to creep within the time scale examined. Macromolecular pertubations may occur around black particles during creep or initial loading however, and this may lead to improved adhesion.

6.6 Conclusions

Physical creep processes are always more prominent in carbon black loaded rubbers than in their gum equivalents when compared at similar initial elongations. This may, however, be mitigated by scragging. The scragging process may be related to stress-softening and therefore to instability of reinforcement.

Black loaded rubbers do not obey simple semi-logarithmic creep-time behaviour at times $>10{,}000$ minutes under load; instead they follow a log-log relationship.

Significant matrix/black interfacial debonding has not been observed within the experimental time scale.

REFERENCES; CHAPTER 6

1. A. N. Gent — Rubb Chem and Technol 36 (3), pp 697-708 (1963).

2. C. J. Derham, E. Southern and A. G. Thomas
N. R. Technology. Rubb Dev Supp No. 7 (1970).

3. C. J. Derham — J. Mater Sci 8, pp 1023-29 (1973).

4. C. J. Derham, E. Southern and A. G. Thomas
Int Rubb Conf, Moscow (1969).

5. C. J. Derham, G. J. Lake and A. G. Thomas
J. Rubb Inst Malaya 22 (2), pp 191-200 (1969).

6. C. J. Derham — MRPRA 3rd Rubb in Engineering Conference
London (1973). Paper F.

7. C. J. Derham — Rubber India 26 (10), pp 16-20 (1974).

8. D. H. Cooper — Ind Eng Chem 43, pp 365-73 (1951)

9. N. M. Lyalina and G. M. Bartenev
Colloid Journal 34 (3), pp 307-312 (1972).

10. A. Voet, F. R. Cook and A. K. Sircar
Rubb Chem and Technol 44 (1), pp 175-84 (1971).

11. A. K. Sircar, A. Voet and F. R. Cook
Rubb Chem and Technol 44 (1), pp 185-198 (1971).

12. G. R. Cotton and B. B. Boonstra
J. App Polym Sci 9, pp 3395-3408 (1965).

13. L. Mullins and N. R. Tobin
Proc 3rd Rubb Technol Conference
London (1954) pp 397-412.

14. G. Kraus — Rubb Chem and Technol 38 (5), pp 1070-1114 (1965).

15. G. Kraus — "Reinforcement of Elastomers."
Pub Wiley and Son. Interscience.
N.Y. (1965).

16. L. Mullins — "The Chemistry and Physics of Rubberlike Substances." Ch. 11.
Ed L. Bateman.
Pub McLaren & Son, London.
Wiley, N.Y. (1963).

17. J. B. Donnet, B. Bariou, J. Schultz, Y. Schwob and J. Gossot
J. Inst Rubb Indust 6 (3), pages 119, 120, 127 (1972).

18. W. F. Watson Proc 3rd Rubb Technol Conf. London (1954) pp 553-564.

19. J. J. Brennan, T. E. Jermyn and B. B. Boonstra
J. App Polym Sci 8 (6), pp 2687-706 (1964).

20. I. Pliskin and N. Tokita J. App Polym Sci 16, pp 473-92 (1972).

21. J. J. Brennan and T. E. Jermyn
J. App Polym Sci 9, pp 2249-62 (1965).

22. A. I. Medalia Rubb Chem and Technol 45 (5), pp 1171-94 (1972).

23. F. A. Heckman and A. I. Medalia
J. Inst Rubb Indust 3 (2), pp 66-71 (1969).

24. A. I. Medalia and F. A. Heckman
Carbon 7, pp 567-82 (1969).

25. J. Rehner Rubb Chem and Technol 17, pp 865-74 (1944).

26. E. Guth J. App Phys. 16, pp 20-25 (1945).

27. B. B. Boonstra "Reinforcement of Elastomers." Ch. 16
Ed. G. Kraus. Pub Wiley, Interscience N.Y. (1965).

28. E. Guth and R. Simha Kolloid-Z 74, p 266 (1936).
or see for example
L. Mullins Rubb Chem and Technol 42 (1), pp 339-362 (Ref 32) (1969).

29. A. M. Bueche J. Polym Sci 25, pp 139-149 (1957).

30. F. Bueche J. App Polym Sci 5 (15), pp 271-281 (1961).

31. F. Bueche J. App Polym Sci 4 (10), pp 107-114 (1960).

32. L. Mullins Rubb Chem and Technol 42 (1), pp 339-62 (1969).

33. J. A. C. Harwood, A. R. Payne and R. E. Whittaker
J. Macromol Sci B5 (2), pp 473-486 (1971).

34. J. A. C. Harwood, L. Mullins and A. R. Payne
J. App Polym Sci 9, pp 3011-21 (1965).

35. L. Mullins and N. R. Tobin
J. App Polym Sci 9, pp 2993-3009 (1965).

36. W. C. Meluch J. App Polym Sci 13, pp 1309-18 (1969).

37. R. Nakane Reports on Prog in Polym Phys, Japan. 13, pp 317-20 (1970).

38. E. M. Dannenberg Trans Inst Rubb Indust 42, pp T26-T42 (1966).

39. G. Kraus, C. W. Childers and K. W. Rollman
J. App Polym Sci 10, pp 229-244 (1966).

40. R. W. Smith Rubb Chem and Technol 40 (2), pp 350-8 (1967).

41. C. J. Derham and A. G. Thomas
Nature 218 (5136), p 81 (1968).

42. A. N. Gent J. App Polym Sci 6 (22), pp 433-441 (1962).

43. R. G. Christensen and C. A. J. Hoeve
J. Polym Sci A1 8, pp 1503-12 (1970).

44. A. E. Oberth and R. S. Bruenner
Trans Soc Rheology 9 (2), pp 165-185 (1965).

45. T. L. Smith Trans Soc Rheology 3, pp 113-136 (1959).

46. R. J. Farris Trans Soc Rheology 12 (2), pp 303-314 (1968).

47. N. Sekhar and B. M. E. Van Der Hoff
J. App Polym Sci 15, pp 169-182 (1971).

48. L. Mullins and N. R. Tobin Trans Inst Rubb Indust 33 (1), pp 2-10 (1957).

49. T. Shinomura and M. Takahashi
Rubb Chem and Technol 43 (5), pp 1025-35 (1970).

50. E. H. Andrews J. Polym Sci 33, pp 39-52 (1958).

51. W. M. Hess "Reinforcement of Elastomers"
Chapter 6. Ed. G. Kraus
Pub. Wiley, Interscience. N.Y. (1965).

52. T. Shinomura and M. Takahashi
Rubb Chem and Technol 43 (5), pp 1015-25 (1970).

53. A. N. Gent and D. A. Tompkins
J. Polym Sci, A2. 7, pp 1483-88 (1969).

54. N. A. Lange and G. M. Forker
"Handbook of Chemistry." p 1163
Pub. McGraw Hill (1961).

CHAPTER 7

SUMMARY

7.1 Creep Data Extrapolation

The creep response at various temperatures of elastomers based on vulcanizate 'A' have been described in Chapters 2, 4, 5 and 6.

At steady state, chemical creep (Chapter 4) followed a generally linear law except at short times where a decelerating response was observed. The prediction of long term secondary creep from accelerated tests at elevated temperatures is therefore uncertain; whilst a steady state rate of $\sim 10^{-5}\%$ min^{-1} of the initial strain would be expected at 20°C for example, the importance of the initial decelerating contribution is at present obscure. Nevertheless, this transient response is complete at relatively short times and bearing in mind that it has not been observed to exceed ~5% of the initial strain, then it is suggested that it may be accounted for in engineering design calculations simply by adding say 5% to the creep equation. The penetration of oxygen into rubber was discussed in Chapter 3 and it was shown that maximum penetration depths at "room temperature" would not exceed ~10 mm. The expected chemical creep rate of large components such as suspension blocks and bridge bearings should therefore be less than predicted in Chapter 4. In view of the

present uncertainty of the relative importance of oxidative and non-oxidative contributions to chemical creep, however, it is suggested that the results of Chapter 4 or similar data should be used in design calculations. This would then leave a safety factor, albeit of unknown magnitude.

The results of Chapters 2 and 6 indicate that a log-log prediction of physical creep may be more appropriate than the hitherto accepted semi-logarithmic (logarithmic creep) approach. Although the deviations from semi-logarithmic behaviour observed for reinforced vulcanizates (Chapter 6) may represent a slow crystallisation process, in which case they would not continue indefinitely, it is considered that the log-log extrapolation procedure may be more reliable and again could provide a safety factor of unknown magnitude.

The above discussion suggests that long term predictions of creep may be derived using an equation of the type:-

$$\text{creep} = A + Bt + ct^n \qquad 7.1$$

where A represents decelerating transient chemical creep. Typically 5% say.

B represents steady state chemical creep.

C and n determine physical creep.

7.2 Mechanisms of Deformation in Elastomers

Not only is the slow physical creep response of rubber vulcanizates difficult to reconcile with relaxation mechanism concepts[1] but it is clearly at variance with elastic behaviour. The stress-strain response of vulcanized rubbers follows fairly closely to kinetic theory and this suggests that internal friction between adjacent molecules in the network structure is minimal; indeed the lack of a yield point indicates that the mechanisms of deformation on the molecular scale of size must occur with rapidity and ease. Assuming that gum vulcanizates are homogenious it is difficult to imagine a deformation process which would require almost zero activation stress (no yield point) during initial straining but which could then continue to operate at constant load.

Before discussing possible mechanisms for physical creep it is pertinent to examine what specific processes, if any, operate during simple straining. There is no reason why estimates of ideal shear strength, as calculated for crystalline solids[2,3], should not be applied to amorphous materials such as rubbers. If one assumes that deformation occurs by the simultaneous shear of imaginary sections through a rubber block, one over the other, then one would expect a yield point in the order of E/10 to E/2 say. The lack of such a discontinuity in the stress-strain response indicates that deformation occurs either heterogeneously or by the operation of many individual mechanisms in rapid

succession. Within the rubbery plateau region of temperature, elastomeric networks are envisaged to exist in dynamic equilibrium with applied stress and this suggests that individual network chains may be considered to be in rapid kinetic motion, not unlike the atoms of an ideal gas. The vibration and oscillation of individual chains relative to each other may therefore explain the observed ease of deformation of the network. Two types of relative chain displacement are necessary:- a) longitudinal translation of parts of each chain through the surrounding "matrix" of other network chains and b) transverse motion. This may be understood from consideration of Figure 7.1 which shows a network chain passing through a section normal to the direction of applied stress. The network chain is assumed to be sufficiently long so that it contains sub-sections or segments of all orientations and the mean orientation is random (in practice this will not be achieved in a single network chain although it would apply to a collection of many chains). On imposing a strain in the XX' direction the rubber will become longer in that direction and correspondingly narrower in the two normal directions. Consequently, those chain segments at small angles, θ, to the XX' axis will not be sufficiently long to fill their place in the matrix whilst segments at high angles of θ will be too long. Matrix lengths at a critical angle, θ_{crit}, inbetween these two extremes should remain unchanged in length.

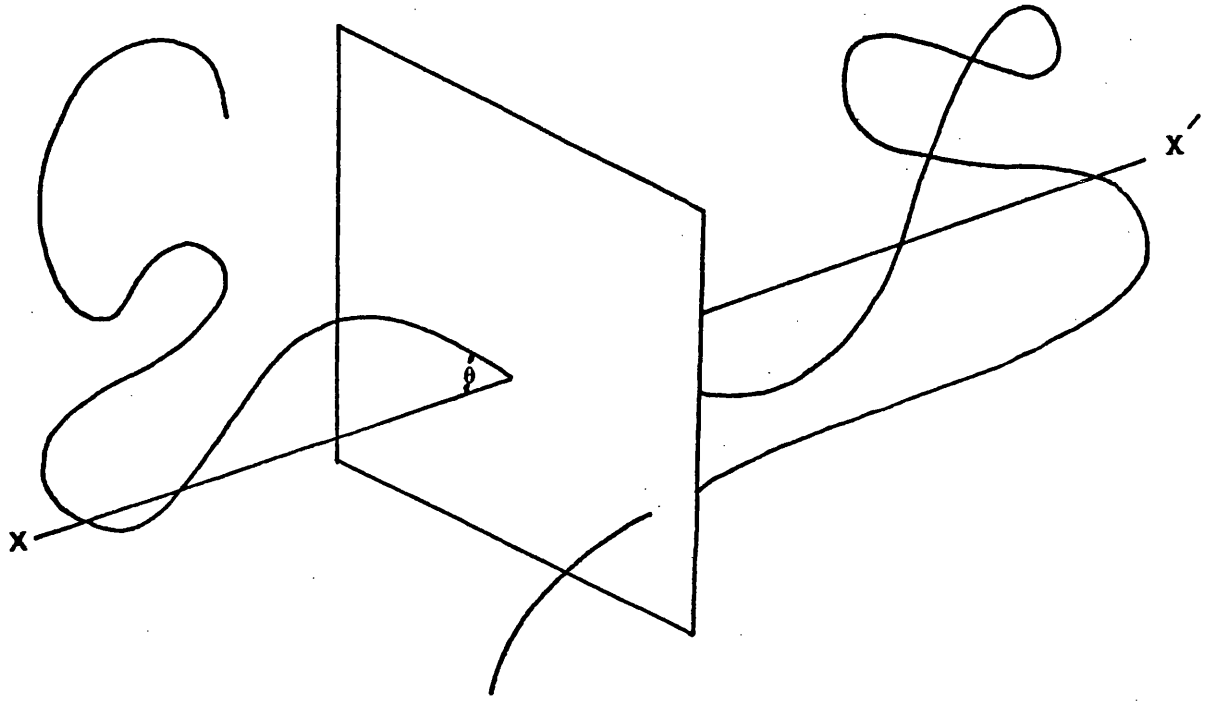

Figure 7.1 A cross-section normal to the strain direction XX′. A random chain is illustrated at an angle θ to the XX′ axis at the point of the section.

$$\theta crit = \cos^{-1} \left[\frac{\lambda - 1}{\lambda^3 - 1} \right]^{1/2}$$

It may be envisaged therefore that the ideal random chain could translate longitudinally during straining in such a way that the surplus lengths of segments at high angles of θ compensate for deficiencies at low angles. This could occur provided no net change in total length of network chain was required. To illustrate this Figure 7.2a represents a length of rubber matrix, δR, occupied by a segment of network chain at an angle θ to the XX' axis. Figure 7.2b indicates the same "matrix space" after straining to an elongation ratio λ. Assuming affine deformation this causes a change in the length of matrix space to $\delta R'$ as indicated where:-

$$\delta R' = \delta R \left[\lambda^2 \cos^2\theta + \frac{1}{\lambda} \sin^2\theta \right]^{1/2} \qquad 7.2$$

Consequently, the total length of network chain required to fill the matrix after straining would be:-

$$\frac{L}{L_o} = \sum_{\theta=0}^{\pi/2} \frac{\delta R'}{\delta R}$$

where L_o = chain contour length at zero strain

L = chain contour length at an elongation ratio λ.

N.B. This assumes zero sideways translation of the network chain through the matrix.

i.e. $$\frac{L}{L_o} = \sum_{\theta=0}^{\pi/2} P(\theta) \left[\lambda^2 \cos^2\theta + \frac{1}{\lambda} \sin^2\theta \right]^{1/2}$$

where $P(\theta)$ = Probability of an individual segment being at an angle θ.

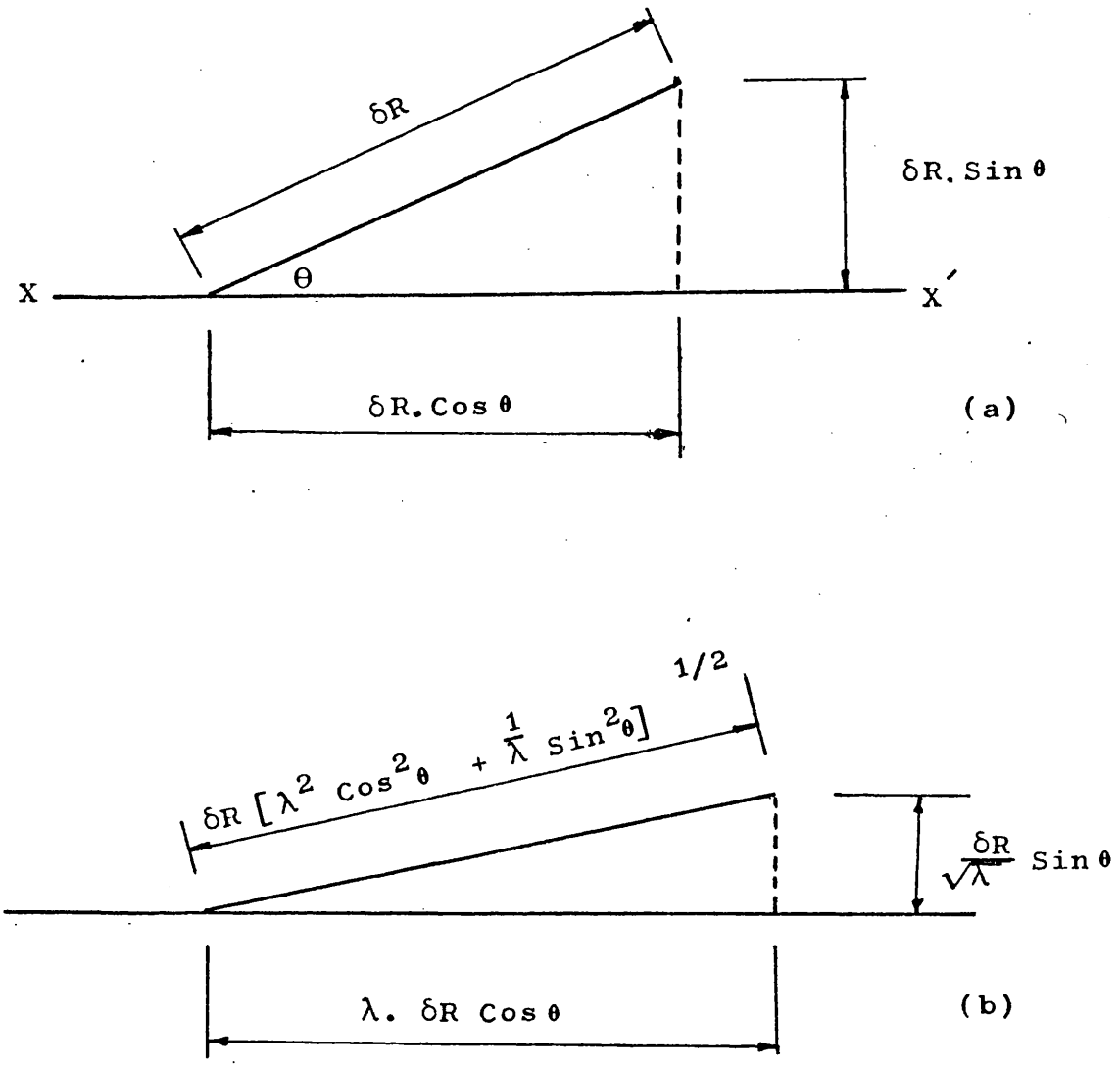

Figure 7.2 Schematic illustration of a length of rubber matrix occupied by a network chain.

(a) zero strain
(b) after stretching to an elongation ratio λ.

Assuming an initially random distribution of θ's, $P(\theta)$ is given by the well known spherical distribution:-

$$P(\theta) = \sin\theta$$

$$\text{Hence } \frac{L}{L_o} = \int_0^{\pi/2} \sin\theta \cdot \left[\lambda^2 \cos^2\theta + \frac{1}{\lambda} \sin^2\theta \right]^{1/2} \cdot d\theta \qquad 7.3$$

This is solved in Appendix 7A and the result is shown plotted in Figure 7.3 as a function of λ. Clearly, it would be possible for an ideal rubber, as described, to deform to small strains with very little sideways translation of its molecules. i.e. when $L/L_o \simeq 1.0$ for longitudinal translation only. At higher values of strain however, and certainly for highly crosslinked rubbers with chain lengths too short to contain a random distribution of segment orientations, transverse chain motion would be essential to deformation in the absence of structural breakdown.

The above model suggests that rubber deformation depends on at least two mechanisms; the longitudinal and transverse displacement of segments of network chains. The ease by which this is accomplished however indicates that each process may occur by a series of small displacements rather than by single, rapid and simultaneous motions of whole chains. Amerongen[4] for example, has discussed the diffusion of the homologous series of n-paraffins in vulcanizates of natural rubber. The diffusion coefficient decreases, as expected, with increasing values of n, the number of carbon atoms in the paraffin chain but only up to $n \sim 5$. Increases in

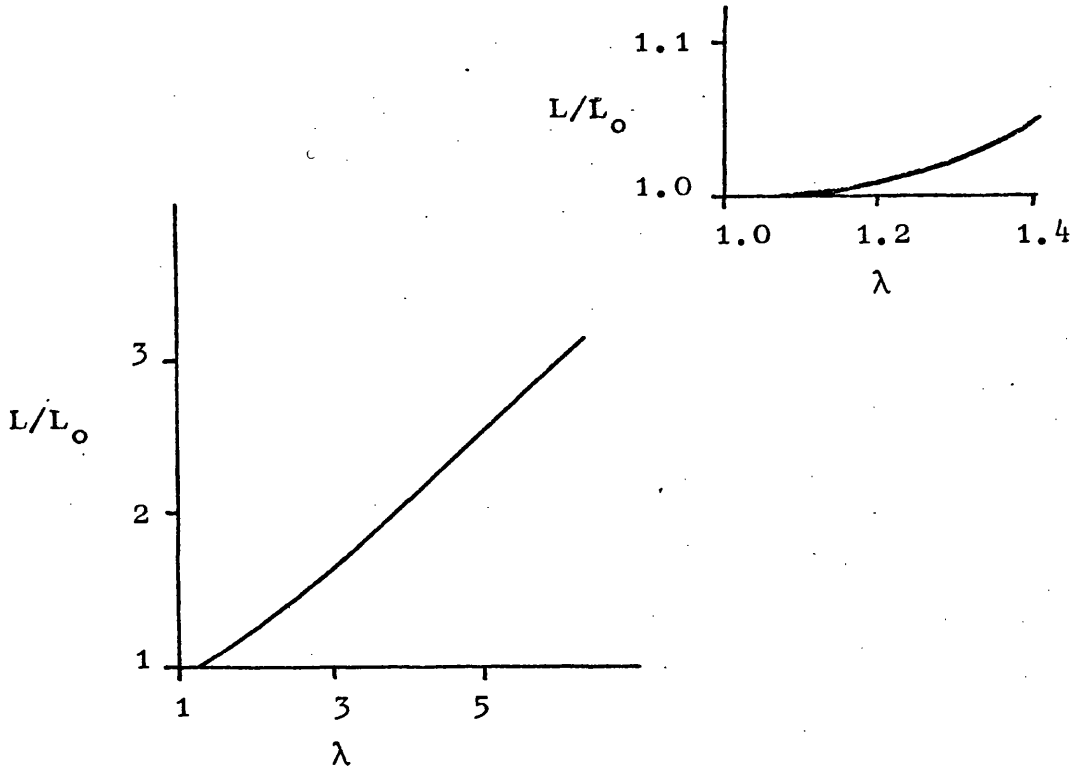

Figure 7.3 L/L_o as a function of λ as calculated from Equation 7.3.

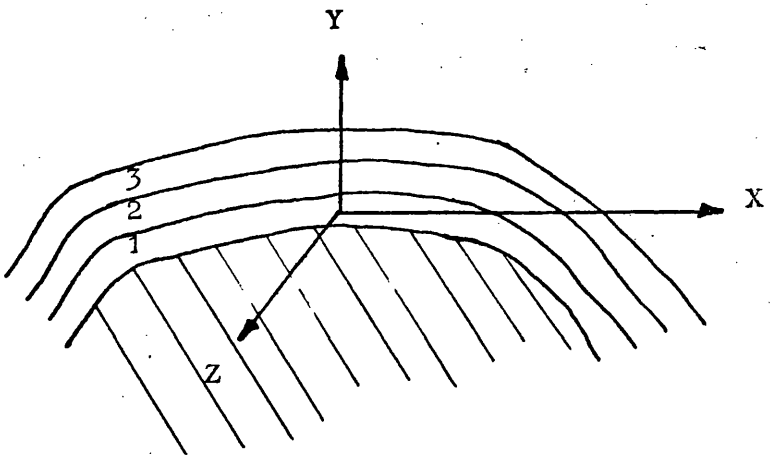

Figure 7.4 Schematic illustration of parallel infinitesimal layers of rubber at the surface of a filler particle.

paraffin chain length above this do not influence diffusion and it has been suggested that the motion of such hydrocarbons through a rubber network occurs preferentially in their length direction by a series of discrete "jumps" involving only ~5 segments of chain at a time. This possibly occurs by the penetration of a length of ~5 atoms long into a hole or vacancy in the network "lattice", followed by subsequent lengths as thermal fluctuations allow. This is equivalent to a dislocation-like mechanism of longitudinal translation in which only a small section of molecule moves at a time. Alternatively, if one considers the kinetic vibration of network chains, it may be envisaged that pertubation of the network structure initiates travelling waves in the chains and that these bring about molecular translation. This too would result in a heterogenious deformation process in which small lengths of chain are translated at a time.

The sideways motion of chains across imaginary planes (lateral displacement) may also be eased by the operation of heterogeneous deformation processes. Much recent discussion has been devoted to the concept of dislocation-like mechanisms in amorphous structures and indeed Gilman[5] considers that any inhomogeneous shear process involving the nucleation and growth of shear regions may be considered as a dislocation process. Bowden and Raha[6] have actually calculated burgers vectors for dislocations in glassy polymers whilst

Lavengood et al[7,8] claim to have observed dislocations in glass by the use of etching techniques. Marsh[9] has proposed a dislocation theory to account for deformation in glass. Nevertheless, it is difficult to imagine a dislocation-like discontinuity in an amorphous solid since the structure immediately before, behind and in the vicinity of the shear line would all be identical and this has been pointed out by Hillig and Charles[10]. The ease of tranverse molecular chain motion in rubbers may in any case be accounted for by the random thermal fluctuations of individual network chains.

The addition of fillers to rubber adds another conceptual difficulty to the understanding of deformation. Figure 7.4 illustrates a section through a filler particle/matrix interface; the rubber is divided into imaginary infinitesimal layers parallel to the filler surface. The layer adjacent to the interface, 1, is unable to deform due to the constraining influence of the rigid surface and consequently induced strains in the x and z directions, shown, due to the application of external load should always be zero. Furthermore, the fact that poissons ratio for gum rubber is almost exactly 0.5 (zero volume change) implies that the strain in the y direction should also be zero. As a result, layer 1 appears to be totally immobilised and rigid. The same argument may therefore be applied to layer 2 because of the restraining influence of layer 1 and then to layer 3 and so on. Even allowing for the fact that poissons ratio for gum rubbers is slightly less

than 0.5 it is clear that an easier mechanism of deformation must operate than is suggested by this model. In practice deformation of the apparently immobilised shell of rubber must take place by the translations of individual molecular chains through the rubber matrix rather than by the shear and tensile displacements of infinitesimal "unit cubes" as is envisaged in classical elasticity mechanics. This gives vise to a "ball of wool" concept in which individual protruding chains are pulled out of the ball during deformation; consequently the ball may be considered to decay with increasing strain.

The ball of wool concept, above, emphasises the ease of motion of individual and groups of molecular chains in the network lattice of elastomers and suggests a further contributory mechanism to general deformation. It may be considered that discrete regions or deformation centres may exist even in gum rubbers, perhaps with impurity phases (by-products of vulcanization) crystallites or zones of short range order at their cores. Each region would deform by the "ball of wool" process. This gives rise to the idea of supramolecular zones as was described in greater detail in Chapter 5 and is in agreement with the observation that the apparent size of such zones decreases with increasing applied strain.

7.3 Mechanisms of Physical Creep

Each of the mechanisms of deformation described above suggests a corresponding creep mechanism. The high elasticity of rubbers however, implies that general deformation occurs with such ease that many of the fundamental contributory processes would not continue to operate at constant stress, certainly not for long periods of time as is observed in creep. This eliminates such processes as dislocation-type motions from further consideration; creep deformation results only from the operation of relatively stable mechanisms requiring thermal activation.

The lateral chain displacements required for rubber deformation, as described earlier, unlike longitudinal chain pertubations, may cause the development of chain entanglements of which the least stable could provide sites of potential creep mechanisms. Indeed, the high extension of some individual chains resulting from multiple entanglement may provide sites of subsequent chain rupture during creep; such chain rupture by thermal fluctuation has been described by Bartenev.[11]

An alternative molecular model for creep may be derived by considering the slow breakdown of weak cross-links as are believed to exist between adjacent chains, Van Der Waals bonds for example. Consideration of the time dependency of the physical creep response suggests, however, that structures rather larger than individual molecular chains are involved. See Chapter 5. Whilst molecular processes, as described above, may be involved

in the operation of such larger mechanisms, it is suggested that they do not control the creep-time interelationship. The supramolecular domain concept of Chapter 5 overcomes many of these philosophical difficulties and suggests that rubber may be considered as a heterogeneous solid in which the "matrix" responds readily and elastically to applied stress. The slower response of supramolecular domains then explains slow long term creep.

7.4 Suggestions for Further Work

The creep data presented in Chapters 4 and 6 casts uncertainty on present extrapolation procedures used to predict the long term stress response of engineering components. It would be useful, therefore, to carry out creep experiments over long time periods; several years, at 20°C say and perhaps one year or more at slightly elevated temperatures up to about 35°C. This should also be augmented by further study of the fundamental processes contributing to creep extension, particularly the influence of oxygen, water vapour and sulphur diffusion. The alternative proposed mechanisms of water aggravation of creep, vis a vis osmotic or interchain interaction, could be resolved for example as described in Section 2.5. Similarly, the proposed model for oxygen diffusion presented in Chapter 4 could be evaluated experimentally. This could be achieved by measuring the distribution of oxygen across a section through an aged block using electron microprobe analysis for example. Alternatively, a thick sandwich of

individual rubber sheets could be aged; subsequent mechanical tests on each sheet would then give an indication of oxygen penetration. Having obtained experimental confirmation (or otherwise) that oxygen does not penetrate great distances into rubber it would be pertinent to examine the creep response in the absence of oxygen as this would have more relevance to the engineering design of large components. Further consideration of labile sulphur bond interchange, as may be deduced from diffusion studies, could be relevant to non-oxidative chemical creep and in particular may offer a more complete explanation of observed activation energies.

Further work on the proposed model for physical creep, Chapter 5, could be carried out by cycling the temperature as did Derham[12] or the stress during the duration of creep tests. Tensile stress-strain curves with rapid changes of strain rate during the loading cycle could also be examined in terms of the proposed model.

APPENDIX 7A

Integral Solution

$$L/L_o = \int_o^{\pi/2} \text{Sin}\,\theta \left[\lambda^2 \text{Cos}^2\theta + \frac{1}{\lambda} \text{Sin}^2\theta \right]^{1/2} d\theta$$

$$= \int_o^{\pi/2} \text{Sin}\,\theta \left[\lambda^2 + \frac{1}{\lambda} (1 - \text{Cos}^2\theta) \right]^{1/2} d\theta$$

$$= \int_o^{\pi/2} \text{Sin}\theta \left[(\lambda^2 - \frac{1}{\lambda}) \text{Cos}^2\theta + \frac{1}{\lambda} \right]^{1/2} d\theta$$

$$= \int_o^{\pi/2} \text{Sin}\theta \left[(\lambda^2 - \frac{1}{\lambda}) (\text{Cos}^2\theta + B^2) \right]^{1/2} d\theta$$

where $B^2 = \dfrac{\frac{1}{\lambda}}{\lambda^2 - \frac{1}{\lambda}} = \dfrac{1}{\lambda^3 - 1}$

Hence $L/L_o =$

$$(\lambda^2 - \frac{1}{\lambda})^{1/2} \cdot \int_o^{\pi/2} \text{Sin}\theta \left[\text{Cos}^2\theta + B^2 \right]^{1/2} d\theta$$

Put $\text{Cos}\,\theta = B\,\text{Sinh}\,\phi$

and $-\text{Sin}\theta\, d\theta = B\,\text{Cosh}\phi\; d\phi$

Gives:-

$$L/L_o = -\left[\frac{\lambda^3 - 1}{\lambda}\right]^{1/2} \int_{\text{Sinh}^{-1}\,1/B}^{\text{Sinh}^{-1}\,0} B\,\text{Cosh}\phi \left[B^2 + B^2\,\text{Sinh}^2\phi\right]^{1/2} d\phi$$

$$L/L_o = \left[\frac{\lambda^3 - 1}{\lambda}\right]^{1/2} \int_{\text{Sinh}^{-1}\,0}^{\text{Sinh}^{-1}\,1/B} B^2\,\text{Cosh}^2\phi \; d\phi$$

$$L/L_o = B^2 \left[\frac{\lambda^3 - 1}{\lambda}\right]^{1/2} \int_{\text{Sinh}^{-1}\,0}^{\text{Sinh}^{-1}\,1/B} \text{Cosh}^2\phi \; d\phi$$

$$= \frac{1}{2} \left[\frac{1}{\lambda\,(\lambda^3 - 1)}\right]^{1/2} \left[\text{Cosh}\phi\;\text{Sinh}\phi + \phi\right]_{\text{Sinh}^{-1}\,0}^{\text{Sinh}^{-1}\,(\lambda^3 - 1)^{1/2}}$$

REFERENCES; CHAPTER 7

1. J. D. Ferry "Viscoelastic Properties of Polymers." Wiley & Son. NY & London (1961).

2. A. Kelly "Strong Solids." Ch 1 Clarendon Press, Oxford (1973).

3. R. E. Reed Hill "Physical Metallurgy Principles." Ch 4 D. Van Nostrand Co., Inc. N.Y. (1964).

4. G. J. Van Amerongen Rubb Chem and Technol 37 (5), pp 1065-1152 (1964).

5. J. J. Gilman "Physics of Strength and Plasticity." Ch 1 Ed A. S. Argon MIT Press. Massachusetts (1969).

6. P. B. Bowden and S. Raha Philosophical Mag 29 (1), pp 149-166 (1974).

7. W. C. Levengood J. Fract Mechs 2, pp 400-12 (1966).

8. W. C. Levengood and T. S. Vong J. App Phys 31 (8), pp 1416-21 (1960).

9. D. M. Marsh Proc Roy Soc, London A279, p 420 (1964) A282, p 33 (1964)

10. W. B. Hillig and R. J. Charles J. App Phys 32 (1), pp 123-4 (1961).

11. G. M. Bartenev and Yu S. Zelenev "Strength and Failure of Viscoelastic Materials." Pergamon Press, Oxford (1968).

12. C. J. Derham J. Mater Sci 8 (7), pp 1023-9 (1973).